ACS OMEGA

Open Access

http://pubs.acs.org/journal/acsodf

Review

Sensing the Future—Frontiers in Biosensors: Exploring Classifications, Principles, and Recent Advances

Sumitha Manoharan Nair Sudha Kumari* and Xavier Thankappan Suryabai*

Cite This: *ACS Omega* 2024, 9, 48918−48987

Read Online

ACCESS | Metrics & More | Article Recommendations

ABSTRACT: Biosensors are transforming healthcare by delivering swift, precise, and economical diagnostic solutions. These analytical instruments combine biological indicators with physical transducers to identify and quantify biomarkers, thereby improving illness detection, management, and patient surveillance. Biosensors are widely utilized in healthcare for the diagnosis of chronic and infectious diseases, tailored treatment, and real-time health monitoring. This thorough overview examines several categories of biosensors and their uses in the detection of numerous biomarkers, including glucose, proteins, nucleic acids, and infections. Biosensors are commonly classified based on the type of transducer employed or the specific biorecognition element utilized. This review introduces a novel classification based on substrate morphology, offering a comprehensive perspective on biosensor categorization. Considerable emphasis is placed on the advancement of point-of-care biosensors, facilitating decentralized diagnostics and alleviating the strain on centralized healthcare systems. Recent advancements in nanotechnology have significantly improved the sensitivity, selectivity, and downsizing of biosensors, rendering them more efficient and accessible. The study examines problems such as stability, reproducibility, and regulatory approval that must be addressed to enable the widespread implementation of biosensors in clinical environments. The study examines the amalgamation of biosensors with wearable devices and smartphones, emphasizing the prospects for ongoing health surveillance and individualized medical care. This viewpoint clarifies the distinct types of biosensors and their particular roles, together with recent developments in the "smart biosensor" sector, facilitated by artificial intelligence and the Internet of Medical Things (IoMT). This novel approach seeks to deliver a comprehensive evaluation of the present condition of biosensor technology in healthcare, recent developments, and prospective paths, emphasizing their significance in influencing the future of medical diagnostics and patient care.

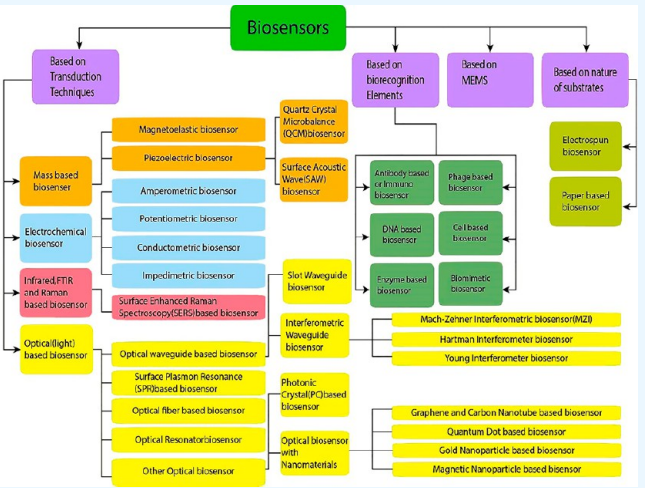

1. INTRODUCTION

Biosensors have emerged as transformative tools in healthcare, uniting biology, chemistry, physics, and engineering to address various diagnostic and monitoring needs.[1] A biosensor is an analytical device that combines a biological sensing element, such as enzymes, antibodies, or nucleic acids, with a physicochemical detector to convert biological interactions into measurable signals.[2,3] The healthcare sector has widely embraced biosensors for their ability to detect and monitor biomarkers associated with diseases, including infectious agents and chronic conditions such as Parkinson's disease and cancer.[4−7] The glucose biosensor represents a notable progression in diabetes therapy by enabling continuous, noninvasive monitoring of blood glucose levels.[8,9] Biosensors offer several advantages over traditional diagnostic methods, including rapid reaction times, increased sensitivity, portability, and the capacity for real-time, point-of-care (POC) applications, hence facilitating prompt clinical decision-making by healthcare professionals.[10,11]

There is a current need in the medical and analytical sensing industries for telemedicine, healthcare monitoring, and mobile e-health services, and technological advancements have hastened their expansion. Improvements in the design of biosensing devices have spurred large areas of study, leading to the creation of new sensing technologies. Innovative biosensors utilizing nanoparticles are evolving as analytical tools for diverse

Received: September 4, 2024
Revised: October 29, 2024
Accepted: November 18, 2024
Published: December 6, 2024

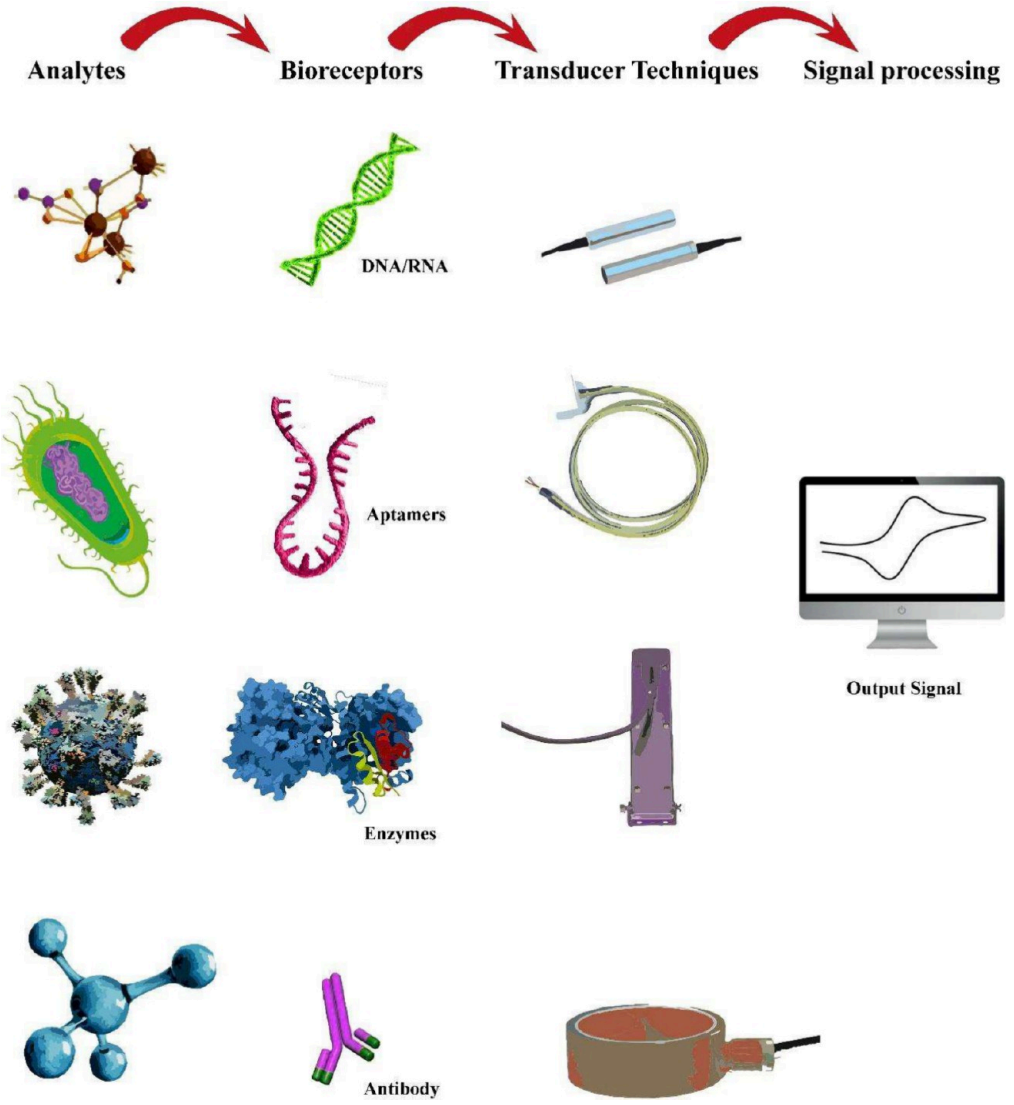

Figure 1. Illustration of the different components of a biosensor.

biomolecules, highlighting the crucial role of nanomaterials in this context.[12] The incorporation of nanotechnology into biosensor development has significantly enhanced their functionality. Nanomaterials, such as nanoparticles, and graphene are employed to increase the surface area of sensors, thereby improving their sensitivity and detection limits.[13] This has been particularly important in the detection of low-abundance biomarkers, such as certain cancer markers, enabling earlier diagnosis and more effective treatment plans.[14] Significant progress in biosensor technology may be achievable through the thorough exploration and systematic development of metal oxide-based nanomaterials, such as nanowires (NWs), nanorods (NRs), carbon nanotubes (CNTs), quantum dots (QDs), and nanocomposite dendrimers. An analysis of the design and fabrication of these nanoparticles reveals new opportunities for enhancing biosensor detection efficacy. The exceptional platform offered by these nanomaterials for manipulation and customization allows researchers to accurately alter their characteristics to satisfy the requirements of diverse biosensing applications.[15] This precise engineering improves the sensitivity of biosensors while enabling the adjustment of their selectivity and overall effectiveness.

A biosensor can detect an enzyme or nucleic acid by utilizing a biological interaction to ascertain the concentration of the substance.[16] The integration of mechanical contact with the unique adhesion, affinity, and mobility of biological components facilitates the assessment of molecular or subcellular variations in mass, displacement, and other parameters.[17] The primary mechanism via which biosensors operate is signal transduction. Heat sterilization is not feasible for these devices due to the denatured characteristics of biological components.[18] Effective early detection and diagnosis can diminish future healthcare expenditures. Diagnostic tools are proteins located on the surfaces of bacterial and viral cells. Among the various biosensors employed in medical diagnostics, a glucose sensor is particularly notable. The enzyme glucose oxidase on the sampling strip biochemically interacts with the glucose in the blood sample, enabling the calculation of glucose concentration.[19] Molecular interactions among biomolecules or faulty genes have been linked to numerous diseases, including cancer, Alzheimer's, Parkinson's, autoimmune disorders, and AIDS, among others.[20−24] Currently, biosensors employing electrochemical, optical, and piezoelectric principles can identify a diverse range of analytes, such as lactate, glucose, cholesterol, and specific DNA sequences. Moreover, miniaturization and

https://doi.org/10.1021/acsomega.4c07991
ACS Omega 2024, 9, 48918−48987

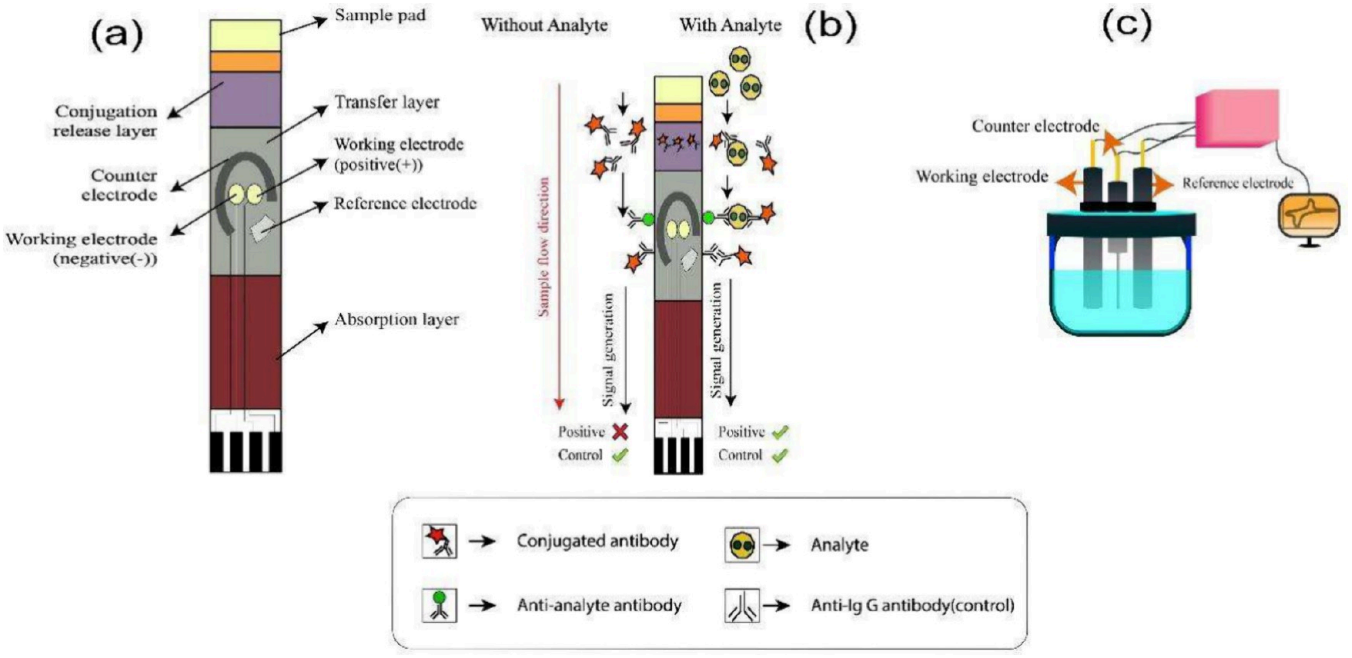

Figure 2. Schematic representation of (a) the main components of a screen-printed electrode, (b) the detection mechanism of the bioanalyte, and (c) an electrochemical cell.

progress in microfabrication have facilitated the creation of portable biosensors that may be seamlessly incorporated into wearable devices. This facilitates ongoing surveillance of patients' physiological metrics, enhancing personalized therapy and improving outcomes, particularly for individuals with chronic conditions necessitating prolonged monitoring.

This comprehensive overview analyses the many categories of biosensors and their main uses in identifying biomarkers, including glucose, proteins, nucleic acids, and infections. Biosensors are traditionally grouped based on the transducer type (electrochemical, optical, piezoelectric, or thermal) or the biorecognition element (enzymes, antibodies, aptamers, nucleic acids, etc.) employed for object detection. Optical biosensors are employed for the detection of proteins and nucleic acids in cancer diagnostics, while electrochemical biosensors are predominantly utilized for glucose monitoring in diabetes management. Furthermore, due to their capacity to identify subtle variations in mass, piezoelectric sensors are advantageous for illness detection. This overview presents a novel framework for categorizing biosensors based on the morphology of the substrate, enhancing prior classifications. The structural characteristics of diverse substrates, including paper and electrospun fiber mats (or thin films), are examined concerning their influence on the sensitivity, stability, and selectivity of biosensors. This substrate-based classification elucidates biosensor technologies, highlighting the significance of material morphology in augmenting detection efficacy. This comprehensive method facilitates a deeper understanding of biosensor functionality and enhances the development of next-generation medical biosensors with more efficiency.

2. BIOSENSORS

Biosensors can quantify analytes or evaluate the degree of biochemical interactions by integrating a biochemical transducer with a biological recognition element. The preliminary phase of the operational principle requires the biological component—such as an antibody, nucleic acid, aptamer, or enzyme—to selectively attach to the target analyte. A biological change, such as the production of electrons, a shift in optical properties, or a shift in mass, can be induced by this contact. After this change occurs in the body, the physicochemical transducer turns it into a measurable signal like a voltage, light intensity, or sound wave.[25−27] Electrochemical biosensors work by detecting currents generated by oxidation or reduction reactions induced by analytes and enzymes, respectively. Optical biosensors detect changes in light intensity due to changes in the refractive index or fluorescence caused by analyte binding. To accurately identify the connection and transform it into a measurable signal, the bioreceptor, transducer, and signal processor all work together as part of a biosensor.[28,29] Blood glucose concentration or pathogen detection are examples of understandable outputs that can be produced by a signal processor after it has been amplified and processed by the transducer, which ensures high specificity by identifying only the target analyte. Biosensors deliver sensitive, quick, and precise measurements across various medical applications due to the seamless integration of biological and physicochemical elements. Figure 1 depicts the different components of a biosensor as an illustration, while Figure 2 provides a simplified schematic diagram of (a) a screen-printed electrode, (b) the detection mechanism of a bioanalyte, and (c) an electrochemical cell.

2.1. Principle and Working of a Biosensor. Traditional approaches, such as membrane encapsulation, physical adsorption, covalent or noncovalent binding, etc., are used to immobilize a bioreceptor on a suitable substrate, making it the sensor's main component.[30] When the sample's analyte binds to the sensing platform's bioreceptor, a biomolecular interaction occurs, eliciting an optical, electrical, or chemical response. Sometimes, a new product will be formed during the interaction, and byproducts like ions, gases, heat, light, etc. will be released. These surface responses from the transducer are then transformed into electrical or optical signals, which may be read with the help of an amplifier. The differential gap between the sample

https://doi.org/10.1021/acsomega.4c07991
ACS Omega 2024, 9, 48918−48987

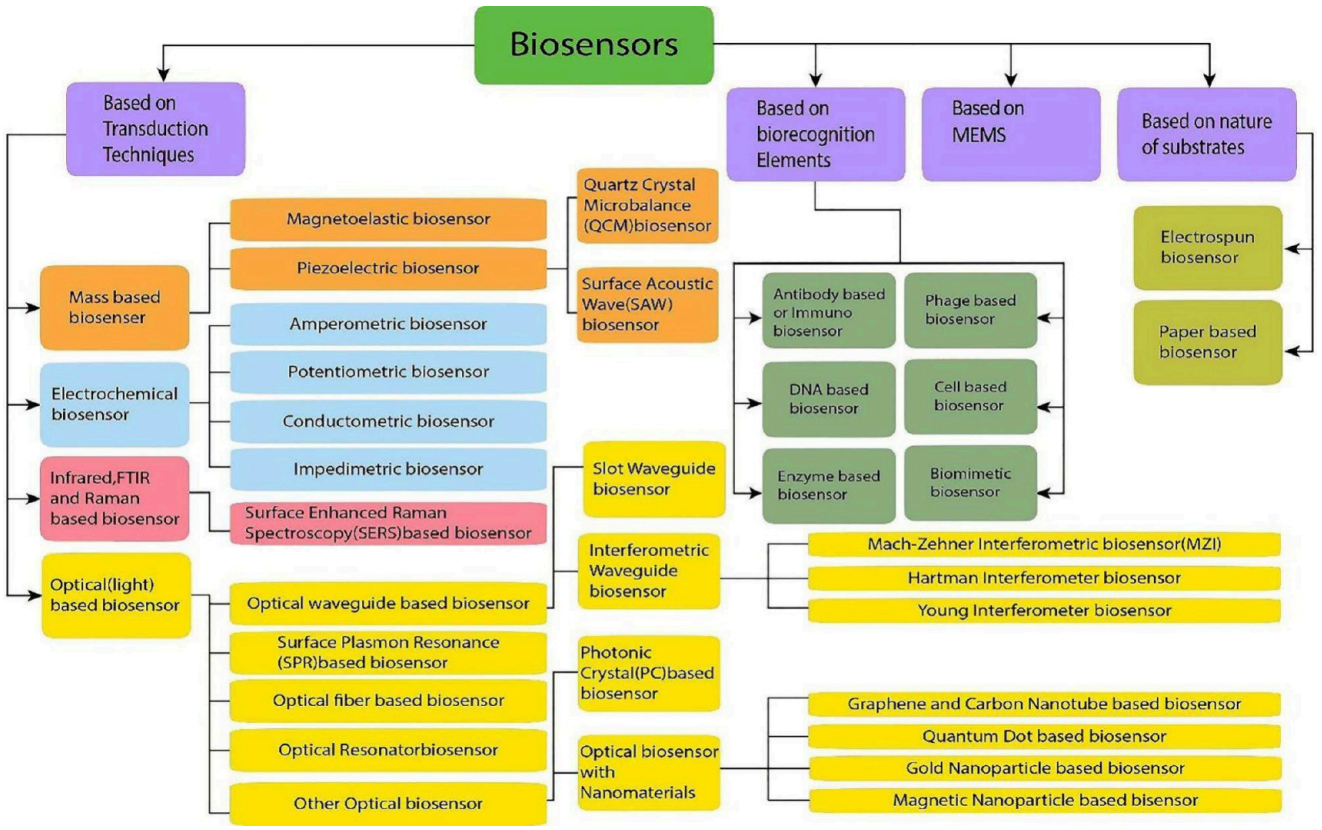

Figure 3. Classification of biosensors based on the transducer element, biorecognition element, MEMS, and nature of the substrate.

signal and the reference signal is amplified typically in the signal processing stage. The microprocessor unit receives the digital signal and processes, calibrates, and displays the data in the chosen units.

Essential to a biosensor's performance are its sensitivity, selectivity, and stability. The biosensor has what is called a "working range", or a range of concentrations of the bioanalyte in which it is effective. Precancer diagnostic biomarker detection requires a biosensor sensitive enough to pick up on even trace concentrations of the analyte. Graphene was described by M. Pumera et al. to be a promising material for detecting the target particle at concentrations as low as ppm or ppb.[31] Graphene's low noise and strong electrical conductivity allow for its extraordinary sensitivity.[32] Researchers have also shown that graphene and reduced graphene oxide's sensitivity and specific affinity can be greatly enhanced through functionalization[33−35]

Having the biosensor properly identify the biomarker molecule is a crucial step in the process. Different proteins or antigens may be present in the target blood sample. However, even in this case, the biosensor should react solely to the target biomolecule and no extraneous substances. Higher and improved sensitivity can be achieved thanks to the lock-and-key mechanism disclosed by antigen−antibody interaction.[36] To detect the cancer biomarkers carcinoembryonic antigen (CEA), CA 125, and Her-2/Neu, Jokerst and his colleagues created a semiconductor QD-based biosensor that can do all three at once. They found that it was far more sensitive than the standard ELISA (Enzyme-based Immunosorbent assay) test.[37] Researchers have used MWCNTs on the electrodes of the immunosensor's scaffolds to detect several antibodies, including TGF-beta 1 cytokine, thanks to the material's high conductivity and electro-catalytic characteristics.[38,39]

The accuracy of the measurement is crucial for any machine performing quantitative analysis. The signal strength was more affected by the concentration of the analyte. Maintaining a consistent signal is essential for accurate readings. It is also important for a biosensor to have a quick response time, as this is essential for real-time monitoring. It has been stated that a submicron-sized glucose sensor implanted under the skin can provide results in under a millisecond.[40] The biosensor's durability is determined by several elements, including the accuracy with which the transducer electronics are tuned, the bioreceptor's affinity, and the bioreceptor's degradation time or rate, among others.[41]

2.2. Types of Biosensors. The biorecognition elements, sensor substrate, and sensing methods used in biosensors all contribute to the devices' unique classifications. Figure 3 is a high-level overview diagram of the several kinds of biosensors now in use in the field of biomedicine. The classification of biosensors in healthcare, as shown in diagram 3, is structured into several categories based on their transduction techniques, biorecognition elements, microelectromechanical systems (MEMS), and the nature of substrates. Under the transduction techniques category, biosensors are divided into mass-based, electrochemical, and optical biosensors. Mass-based biosensors include types like magnetoelastic, piezoelectric, and quartz crystal microbalance (QCM) biosensors, which measure changes in mass or mechanical properties. Electrochemical biosensors are further classified into amperometric, potentiometric, conductometric, and impedimetric types, all of which convert biochemical interactions into electrical signals. Optical biosensors utilize light-based phenomena and include surface plasmon resonance (SPR), optical fiber-based, and surface-enhanced Raman spectroscopy (SERS) biosensors.

https://doi.org/10.1021/acsomega.4c07991
ACS Omega 2024, 9, 48918−48987

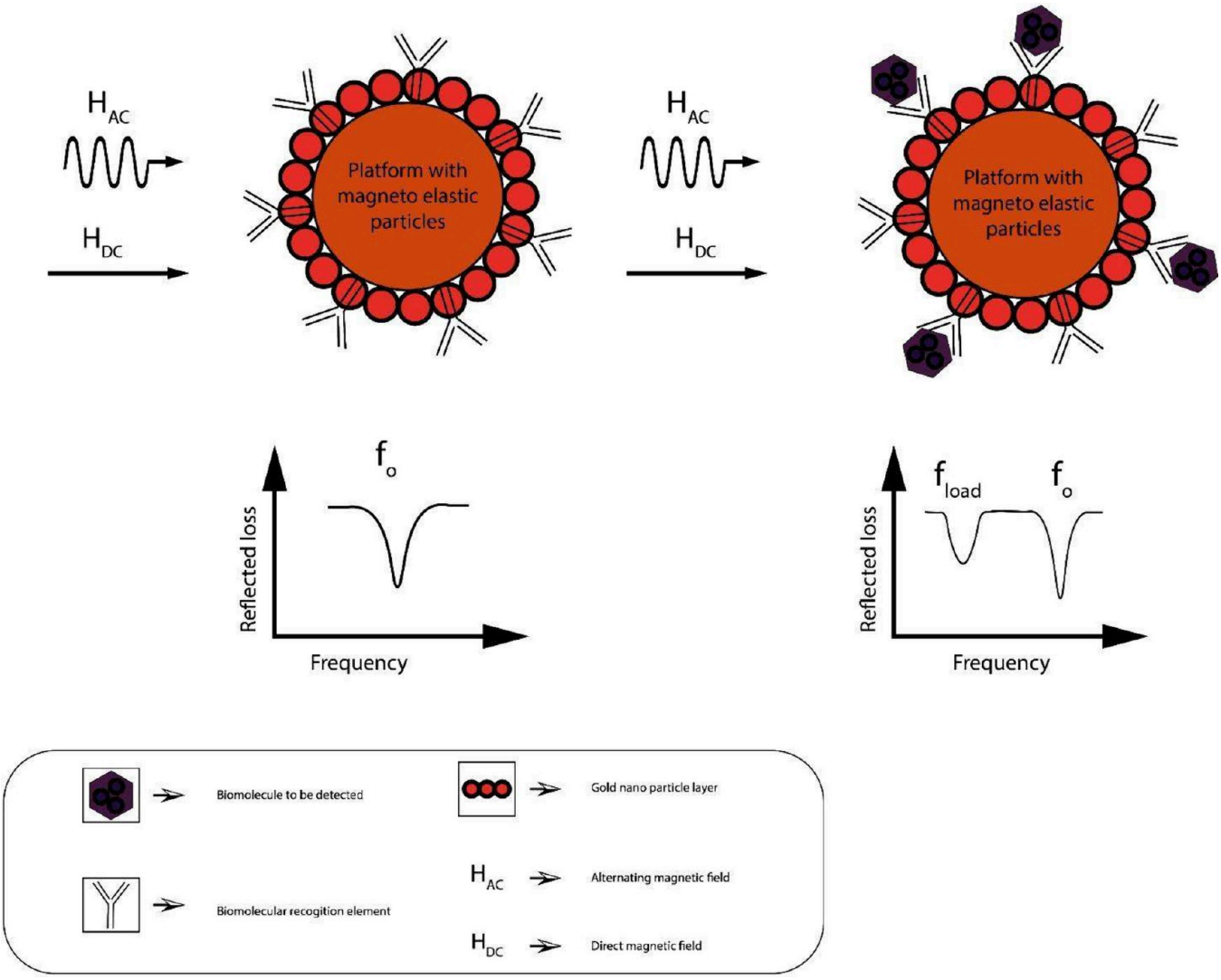

Figure 4. Schematic working of a magnetoelastic biosensor.

In terms of biorecognition elements, biosensors can be classified based on the biological material used, such as antibodies, DNA, enzymes, or phages. These bioreceptors selectively bind to their target analytes, enabling the detection of specific biomolecules. MEMS-based biosensors, leverage advanced miniaturization technology to improve precision and sensitivity.

Finally, the classification also includes biosensors based on the nature of the substrate, such as those using electrospun materials, and paper. These various biosensors offer various benefits, including enhanced surface area for improved sensitivity, biocompatibility, and the ability to fabricate flexible, wearable biosensors. This diverse classification framework reflects the wide range of biosensor technologies available for healthcare applications, each designed to meet specific diagnostic or monitoring needs. Biomolecules can take many forms, including enzymes, cells, antibodies, DNA, and many others. Physicochemical interactions between the biorecognition component and the sample's target molecule are crucial to the signal transduction process and various types are discussed below.

2.2.1. Transduction Techniques. It is possible to carry out transduction in several methods. Mass, electrochemical interactions, and optical phenomena serve as the primary dividing lines. There are countless potential transductions because each class contains several subclasses.[42] The following sections examine the major biosensor classifications based on the transducing techniques used.

2.2.1.1. Mass-Based Biosensors. 2.2.1.1.1. *Magnetoelastic Biosensors.* Many different types of sensors, such as biosensors used to detect *Bacillus anthracis*, *Salmonella typhimurium*, etc., are built using the magnetoelastic phenomena.[43−52] It is based on magnetostriction that magnetoelastic sensors function. Some ferromagnetic materials undergo morphological transformations when their magnetization is altered. We all know that when a system is operating at its resonant frequency, the amplitude of its vibrations is maximized. Mechanical resonance in magnetostrictive materials can be explained as having a magnetic source. External mechanical strain is caused by a vibrating magnetic field. Any change in magnetic field strength is translated into a change in strain by the ferromagnetic material. As a result of the strain reaching its maximum value at resonance, the magnetic values similarly peak at their highest level.[53] Therefore, the magnetoelastic biosensor is a product of both magnetic and mechanical resonance, as suggested by the name.

https://doi.org/10.1021/acsomega.4c07991
ACS Omega 2024, 9, 48918−48987

Various detecting methods, such as optical, acoustic, magnetic, etc., are available for the operation of a magnetoelastic sensor strip.[54] Magnetostrictive materials exhibit a linear strain when subjected to a magnetic field. Magnetoelastic sensors can detect in both the frequency and time domains.[55−57] Frequency mode enables effective wireless real-time monitoring by continuously exciting the sensor over a frequency range to determine its resonance frequency. The resonance frequency was determined by Zeng et al.,[58,59] who employed multiple cycles at a specified frequency. Sensors with a larger collecting area benefit from time-domain detection, whereas those with a smaller footprint should use the frequency mode. Due to background noise, the output detection signal from tiny sensors operating in liquid media may not be particularly reliable. Better detection was achieved by Wen et al. time's domain approach using a pulse-initiated magnetic field rather than a biased magnetic field since the sensitivity is DC-dependent.[60]

Vibrations at the resonant frequencies will occur when a magnetic field is applied in an alternating fashion. For a material with length L, Elasticity E, and density, the frequency-density relation is:[61]

$$\mathbf{f} = (\mathbf{1}/\mathbf{2}L)\sqrt{(\mathbf{E}/\rho)} \quad (1)$$

which is also valid for the vibrational frequency of a ribbon-like thick film sensor with these same parameters. When a biorecognition element, such as a bacterium or an enzyme, is captured on the sensor platform, its mass will increase relative to the reference, causing the resonant frequency to drop.[60,62] The operation of a magnetoelastic biosensor is depicted in a simplified diagrammatic form in Figure 4.

The equation[61]

$$\Delta f = -\mathbf{f_0}[\Delta m/\mathbf{2m_s}] \quad (2)$$

describes the change in resonant frequency when an additional mass Δm is attached to a magnetoelastic sensor with an initial resonant frequency f_0 and initial mass m_s. To detect the *Bacillus anthracis* bacteriophage, Johnson et al. reported fabricating an effective gold-coated magnetoelastic sensor platform utilizing photolithography and sputtering.[63] To detect swine fever virus E2 antibody at a cheap cost and with high throughput, Guo and colleagues created a magnetoelastic biosensor.[64]

2.2.1.1.2. *Piezoelectric Biosensor*. By applying mechanical stress, piezoelectric materials can produce electrical current. Some substances also display the opposite of the piezoelectric effect, known as the inverse piezoelectric effect, in which mechanical strain is generated in response to an electrical current. Quartz, Rochelle salt, zinc oxide, aluminum phosphate and nitrides, topaz crystal, lead titanate, polyvinylidene fluoride, etc. are examples of anisotropic materials that are more likely to exhibit piezoelectricity.[64−71] A mass attached to the sensor surface causes an oscillation shift, which is the basis for the piezoelectric biosensor's operation. Figure 5 is a simplified schematic depiction of this concept.

The following equation defines the frequency shift Δf, brought about by the bound mass, Δm on the piezoelectric crystal:

$$\Delta f = -[2.3^{*}\mathbf{10}^{\mathbf{6}}\mathbf{f_0}^{\mathbf{2}}\Delta m]/\mathbf{A} \quad (3)$$

where f_0 means the fundamental mode of the crystal oscillation in hertz and A is the piezoelectrically active area in centimeters.[72] Environmental conditions, as well as the equation related to viscosity reported by Kanazawa et al., are taken into account, even though equation 3 is employed for thin film adhered to the transducer surface.[73] There are several types of piezoelectric transducers on the market, but they may be broken down into two main categories: bulk acoustic wave (BAW) and surface acoustic wave (SAW).[74] Quartz crystal microbalances (QCM) are the most common type of BAW device, and they are made up of a large piezoelectric crystal (often quartz) and two conducting electrodes.[75]

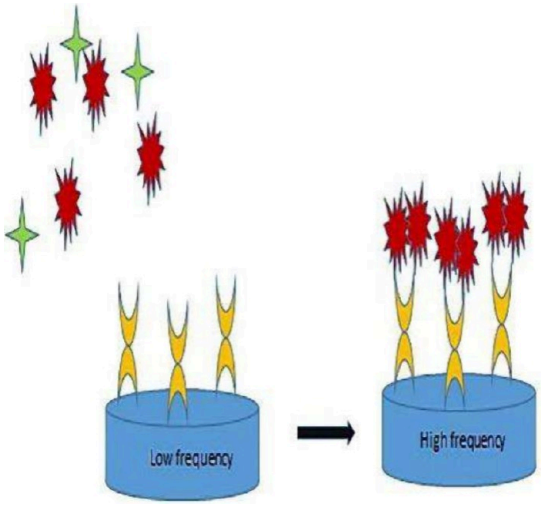

Figure 5. Simplified schematic illustration of the working of a piezoelectric sensor.

2.2.1.1.2.1. *Quartz Crystal Microbalance (QCM)*. In 1959, Sauerbrey established a connection between variations in resonant frequency and the mass density of the sensor surface. QCM sensors have subsequently been utilized for various applications. Figure 6 depicts a QCM.

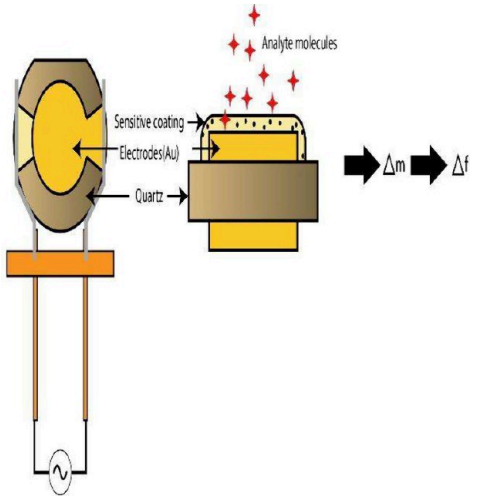

Figure 6. Schematic diagram of a QCM.

A QCM sensor has a quartz oscillator disc and circular electrodes. AC in these electrodes causes the quartz to vibrate. When an analyte molecule attaches to quartz, the mass changes, and the vibration frequency changes. Quartz signal transducer translates a nanogram shift in mass (67 Hz cm $^{-2}$ ng^{-1} sensitivity at 170 MHz) generated by biorecognition element and bioreceptor hybridization.[76] Using diverse bioreceptor surfaces increases QCM's adaptability.

https://doi.org/10.1021/acsomega.4c07991
ACS Omega 2024, 9, 48918−48987

There are piezoelectric QCM immunobiosensors.[77,78] Viruses and bacteria have unique cell surface proteins. Hemagglutinin and neuraminidase are H1N1 virus coat proteins. If these proteins are present, the sample contains the H1N1 Virus. Li et al. developed a QCM-based biosensor to detect H5N1.[79] Alzheimer's illness requires molecular peptide detection. M. K. Mustafa and his team utilized QCM and spectroscopic ellipsometry to detect -amyloid peptide (1−16) and amyloid precursor protein (APP770), enabling Alzheimer's disease early diagnosis.[80] Mannelli et al. reported direct DNA probe attachment for affinity biosensors.[81] Setyawan P Sakti and colleagues produced milk adulteration detection equipment with a 1 ppm detection limits.[82]

2.2.1.1.2.2. *Surface Acoustic Wave (SAW) Transducer-Based Biosensors.* Electroacoustic devices use piezoelectric crystals based on sound vibrations. BAW and SAW propagation transducers are common. Any change in the transducer's mass, viscoelasticity, or dielectric characteristics will affect the output. Bioaffinity membrane on piezoelectric substrate affects SAW phase velocity and propagation loss. SAW devices can detect very tiny vapor concentrations, making them electronic noses. Analyte changes in acoustic wave characteristics: due to their high sensitivity, they're commonly utilized in defense to detect TNT, RDX, and other explosives.[83,84] Several cancer cells release certain gas vapors which are specific to the type of cancer and can be treated as a biomarker for cancer. Hence, the gas/vapor detecting 'electronic bio nose' has significant importance in the present era. IDT (micrometallization patterns made of aluminum, gold, platinum (and its alloys), titanium, conducting ceramics, etc.),[74] piezoelectric substrates (quartz, Gallium Arsenide, etc.), and chemically active thin surfaces with affinity are the basic components of a SAW device. SAW biosensors can detect even a little change in mass or viscosity, which affects the acoustic wave's frequency response.[83] SAW devices have better sensitivity than QCM devices because their operating frequency range is a few MHz to GHz.[85] Figures 7 and 8 show the SAW sensor and two-port delay line with the sensing screen and analyte gas/vapor molecules.

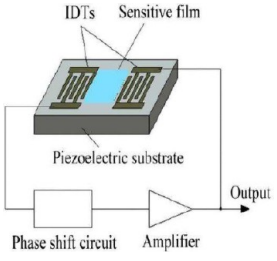

Figure 7. Schematic diagram of a SAW sensor.[86] [Reprinted with permission from Liu, J.; Lu, Y. Response Mechanism for Surface Acoustic Wave Gas Sensors Based on Surface-Adsorption. Sensors 2014, Vol. 14, Pages 6844−6853 2014, 14 (4), 6844−6853. 10.3390/S140406844]. Copyright [2014] [Liu et al. Licensee MDPI, Basel, Switzerland].

A brief consolidation of piezoelectric biosensor research over the years is shown in Table 1.

2.2.1.2. Electrochemical Biosensors. More than half a century has passed since the introduction of the first electrochemical sensor on the market.[99] The electrochemical biosensor takes advantage of electrical conductivity-dependent electrochemical interactions between electrodes and electrolytes.[100] Scopus data on biosensor publications from 2018 to

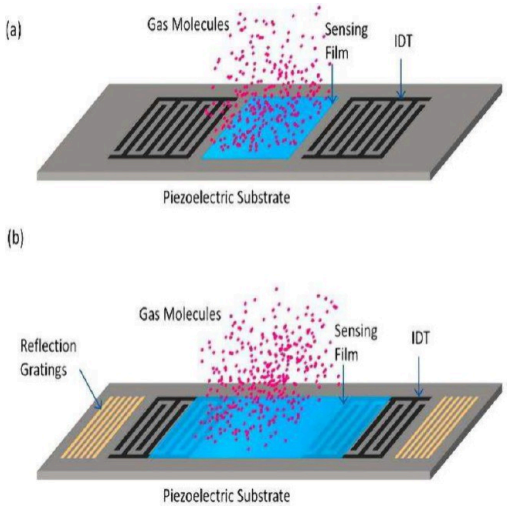

Figure 8. (a, b) Two-port delay line with analyte on the sensing film.[84] [Reprinted with permission from Devkota, J.; Ohodnicki, P. R.; Greve, D. W.; Luo, J.; Xuan, W.; Fu, R. Y. Q. SAW Sensors for Chemical Vapors and Gases. Sensors 2017, Vol. 17, Page 801 2017, 17 (4), 801. 10.3390/S17040801]. Copyright [2017] [Devkota et al. Licensee MDPI, Basel, Switzerland].

2024 February are shown in Figure 9 indicating a rise during the period of COVID-19.

In this recent pandemic scenario, the values are still rocketing. This popularity of electrochemical biosensors can be attributed to their high-sensitivity transducer qualities, low cost, and capacity to integrate with the next generation of downsizing technologies in the nano regime.[42] The electrochemical biosensor has multiple modes of operation, which are depicted in Figure 10.[101]

MXenes, a novel class of two-dimensional transition metal carbides, nitrides, and carbonitrides, exhibit exceptional electrochemical, mechanical, and catalytic properties, making them suitable for electrochemical sensor and biosensor applications. Mohanapriya et al. provided a comprehensive analysis of the synthesis, design, and engineering techniques utilized to enhance the unique properties of MXenes for the detection of environmentally and biologically significant analytes, including nitro and phenolic compounds, metal ions, biomolecules, and small molecules. Considerable focus is placed on the role of MXenes in point-of-care electrochemical detection systems, highlighting their potential for innovative and effective identification of pollutants and advantageous chemicals. This analysis reviews recent advancements and methodologies in MXene-based electrochemical sensing technologies to offer perspectives on future progress.[102] Wang et al. described the creation of a very sensitive nanonanosensor for detecting microRNA-21 (miR-21), a biomarker linked to colorectal cancer, utilizing electric field force to align multiwalled carbon nanotubes (MWCNTs) on the electrode surface. The independent MWCNT electrode, with enhanced active sites, demonstrates a 150-fold increase in peak current responsiveness compared to a bare electrode. The sensor has remarkable sensitivity (48.24 μA μm^{-1}), a broad detection range (0.01×10^{-15} to 100×10^{-12} m), and a low detection limit (1.2×10^{-18} m), making it an essential tool for the early diagnosis of colorectal cancer through miR-21 detection in human serum.[103]

Li et al. fabricated an ultrasensitive CNT-Pt composite electrochemical sensor with a printed wrinkled carbon nanotube

https://doi.org/10.1021/acsomega.4c07991
ACS Omega 2024, 9, 48918−48987

Table 1. Brief Survey of Piezoelectric Biosensor Research

Piezoelectric technique/ device used	Analyte	Bioreceptor	Sensitivity	Ref
8 μm thick lead magnesium niobite-lead titanate piezoelectric plates	DNA	DNA probe	10^{-19} mol/L in urine samples	87
SAW biochip	*Escherichia coli* l-asparaginase	Chip immobilized polyclonal antibody (pAb) as the bioreceptor	Method quantified *E. coli* l-ASNase.	88
SAW biochip	HIV	Functionalized (ink jet printing) dual-channel biochips were with capture coatings to detect either anti-p24 or anti-gp41 antibodies,	100% sensitivity (for anti-gp41) and 64.5% (for anti-p24)	89
ZnO based FBAR	Tumor marker Mucin (MUC1)	Streptavidin self-assembled gold electrode	4642.6 Hz/nM	90
Flexural Plate Wave (FPW) gravimetry	Mc5	Gold particles attached to a secondary Ab (Goat Anti-Mouse IgG) and NP5	3-fold higher at 5V, with 180 ° out of phase acoustic streaming IDTs, compared to no mixing.	91
SH-SAW (love mode)	Interleukin-6 (IL-6)	Immobilized monoclonal IL-6 antibody	Could detect even in the fg range	92
Lead zirconate-lead titanate glass piezoelectric microcantilever sensor	Marker of cancer Her2	Antibody	0.06 nmol/L	93
QCM	Drug melphalan	Molecularly Imprinted Polymer from electropolymerized 3-thiophene acetic acid	5.40 ng/mL	94
QCM	Taurine	Electrochemically polymerized l-methionine with molecularly imprinted taurine	0.12 μmol/L	95
Piezoelectric PVDF platform	COVID-19 virus	polyvinylidene fluoride (PVDF) unsmooth nanofibers-based MEMS	Fempto molar sensitivity, introduced a mathematical model	96
Piezoelectric biosensor	immunoglobulin Y	carboxymethyl chitosan (CMCS)+ antibody matrix	270 ng/mL	97
Piezoelectric biosensor	Identifying anomalies related to a thrombus in cardiovascular grafts	$NaNbO_3$ fibers) in elastomeric matrix	130 mV m N^{1-}	98

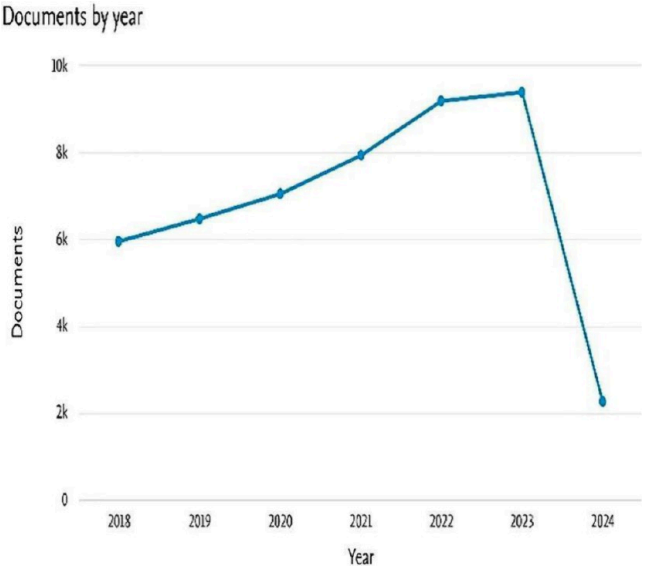

Figure 9. Scopus data from 2018 to 2024 February on biosensor publications.

(CNT) nanostructure for the concurrent detection of dopamine (DA) and uric acid (UA). The sensor, designed to emulate the architecture of taste buds, features a biomimetic wrinkled CNT layer with nanoscale Pt electrodes, enhancing sensitivity by around 40% relative to traditional Pt sensors. The distinctive wrinkled structure and hydrophilicity of the CNT sheet improve detection precision, significantly minimizing interference from ascorbic acid (AA). The sensor exhibits significant promise for electrochemical analysis, especially in the diagnosis of metabolic illnesses by the measurement of DA and UA.[104]

The generation or consumption of charged particles, which can be detected by a voltage change or a current change, is a defining feature of the electrolyte solution upon the interaction between the immobilized biomolecules and the analyte molecules in the sample.[105,106] A variety of electrochemical biosensor approaches for detecting a wide range of analyte molecules are reviewed here.

2.2.1.2.1. *Amperometric Biosensor*. In amperometry, the oxidation or reduction that occurs at the electrode as a result of the interaction between the analyte and the biorecognition element is measured at a constant or variable voltage. It is possible to use the electric current produced to determine the concentration of the analyte.[106] The current in Clark's amperometric glucose detector is first determined by the oxygen concentration at the oxygen electrodes. Figure 11 shows a schematic representation of a first-generation glucose sensor.

The KCl solution is placed between a Pt (Platinum) cathode and an Ag (silver) anode electrode. Gluconic acid and hydrogen peroxide are byproducts of the oxidation of glucose, which enters the cell through the bottom membrane. H_2O_2 and gluconic acid are produced when glucose is exposed to oxygen. The result is less oxygen at the cathode and a smaller amount of electricity flowing through the circuit. It is also feasible to use a relative potential of + 0.68 V to cause the following reactions without having to measure current in terms of oxygen concentration:

$$H_2O_2 \rightarrow O_2 + 2H^+ + 2e \quad \text{(at the Pt anode)}$$

https://doi.org/10.1021/acsomega.4c07991
ACS Omega 2024, 9, 48918−48987

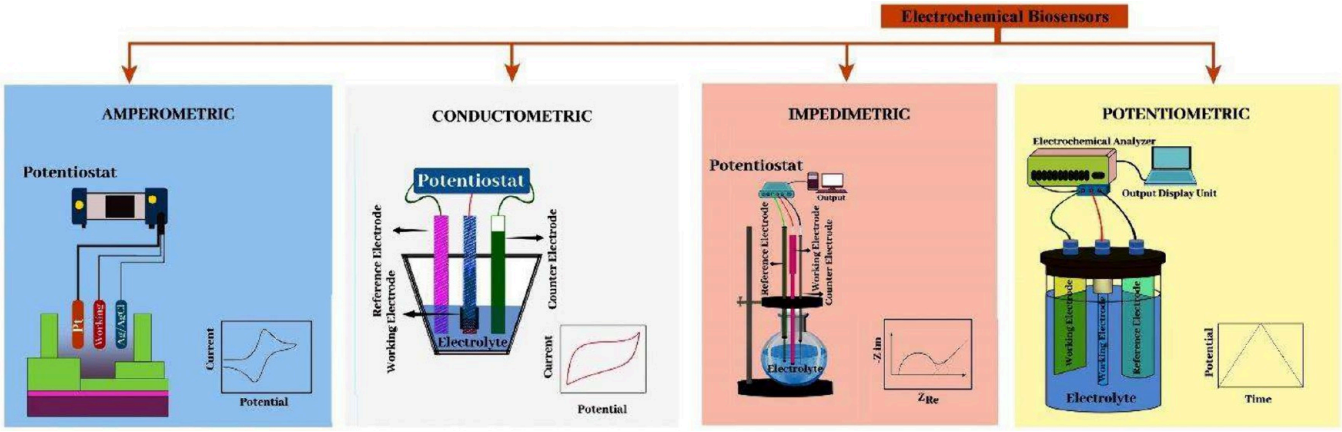

Figure 10. Schematic diagram of different working modalities of an electrochemical biosensor.[101] [Reprinted with permission from Sumitha, M. S.; Xavier, T. S. Recent Advances in Electrochemical Biosensors − A Brief Review. Hybrid Advances 2023, 2, 100023. 10.1016/j.hybadv.2023.100023]. Copyright [2023] [Sumitha M S, Xavier T S, Elsevier B.V.].

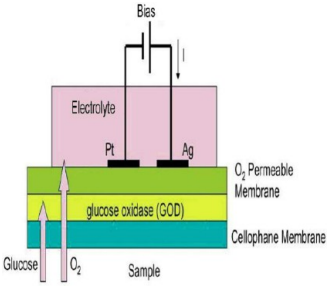

Figure 11. Schematic picture of the first-generation glucose sensor.

$$2AgCl + 2e \rightarrow 2AgO + 2Cl \quad \text{(at the Ag cathode)}$$

All commercially available glucometers have a disposable test strip where a small amount of blood is measured. Figure 12 depicts a typical glucometer and each strip includes electrodes, enzymes, and separators.

Figure 12. Photograph of a commercially available glucometer.

A blood-sugar level of 80−120 mg/dL, while fasting is considered normal. The ideal glucose sensor would be able to accurately detect both hypo and hyperglycemia.[107] The electrochemical biosensors have developed from this to artificial intelligence-assisted real-time monitoring nano biosensors and due to the recent developments in the biosensor business, we now have implantable, continuously monitoring sensors that can quantify the transfer of enzyme to electrode.[108] Numerous diseases, including cancer, Alzheimer's, Parkinson's, heart problems, premature aging, and others, have been linked to free radicals, also known as Reactive Oxygen Species (ROS).[109] In 2015, Mauro Tomassetti and colleagues created an amperometric sensor with the enzyme superoxide dismutase (SOD) and used it to detect the antioxidant capabilities of various mixed berries, comparing the results to those obtained using spectrophotometric and spectrofluorimetric methods.[110] Here, Pt serves as the anode, and Ag/AgCl/Cl serves as the cathode. Interest enzyme is immobilized in a Kappa-carrageenan gel sandwiched between a cellulose acetate and commercially available dialysis membrane (A-9777).[110] Changes in current due to hydrogen peroxide release were recorded by adding xanthine oxidase and xanthine solutions to the sensor's phosphate buffer solution at regular intervals and in optimized proportions. The xanthine concentration in both the control and test samples was plotted against the slope of the current fluctuation. The slope was found to be steeper for the one that lacked antioxidant properties.

Electrospun Cu/CNF electrodes are more sensitive than undoped electrospun CNF, suggesting that they may be a promising amperometric biosensing candidate for catechol, as reported by Jiapeng Fu et al. Cu/CNFs/Lac/Nafion/GCE was found to have a sensitivity of 33.1 A/mM.[111] Glass carbon electrode. GCE was utilized as the working electrode, Pt wire was employed as the counter electrode, and Ag/AgCl (saturated KCl) was used as the reference electrode in the amperometric experiments. At an operating potential of 0.5 V, the current−time curve of Cu/CNFs/Lac/Nafion/GCE is depicted in Figure 13. Calibrating the plot is included here as an insert (current Vs concentration).

Polymer films of the thiophenes (2,2′-BT) and (4,4′-bBT) were electrochemically polymerized by Maria Pilo and colleagues to entrap glucose oxidase. Real samples, such as pears, apricots, peaches, etc., had their glucose levels measured,

https://doi.org/10.1021/acsomega.4c07991
ACS Omega 2024, 9, 48918−48987

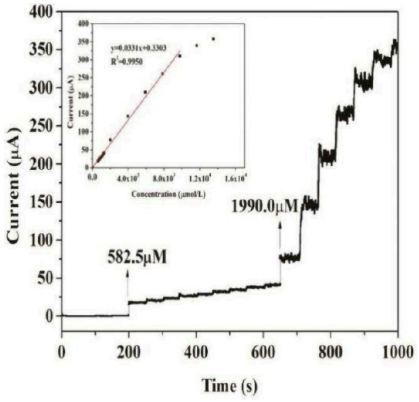

Figure 13. Amperometric reading for Cu/CNFs/Lac/Nafion/GCE electrode[111] [Reprinted with permission from [Fu, J.; Qiao, H.; Li, D.; Luo, L.; Chen, K.; Wei, Q. Laccase Biosensor Based on Electrospun Copper/Carbon Composite Nanofibers for Catechol Detection. Sensors 2014, Vol. 14, Pages 3543−3556 2014, 14 (2), 3543−3556. 10.3390/S140203543]. Copyright [2014] [Fu et al, Licensee MDPI, Basel, Switzerland].

and it was discovered that a thinner polymer layer generated at the electrode resulted in a lower detection threshold, which could have an impact on how well the enzyme attached to the electrode.[112] Some cationic metal complexes will bind to double-stranded DNA electrostatically in a process called Indirect DNA hybridization if they are present.[113] As a result of using a DNA intercalator called PIND-Ru, Gao and colleagues were able to speed up the oxidation of amines and detect DNA at a lower limit (1.5 pmol/L) at 0.65V (Ag/AgCl) in their studies.[114] An amperometric sensor electrode containing a biotin-streptavidin horseradish peroxide complex was utilized by Wang et al. to detect promyelocytic leukemia/retinoic acid receptor alpha fusion gene in a concentration range of 0.05 to 5.0 nmol/L.[115] To identify West Nile Virus (WNV), Lonescu, et al. created a femtogram (fg) sensitive DNA sensor.[116]

2.2.1.2.2. *Potentiometric Biosensor*. Variations in voltage are measured to deduce analyte concentrations, and hence voltammetry and potentiometry are likewise included among the electroanalytical techniques. The concentration of the biomolecule to be detected is proportional to the potential of the working electrode, which is determined by the difference between the reference and working electrodes when no current is flowing. The logarithmic format is commonly used to record the concentration vs potential difference data. Because of their sensitivity, portability, moderate cost, and real-time fast measurements[117] electrochemical sensors, particularly those using potentiometric characterization tools, are well established, and can be used to detect a wide range of organic or inorganic materials, including urea, sugar, neurotransmitters, biological entities, etc.[118] Several commercial potentiometric glucose sensors exist; these employ standard glass pH electrodes for their measurement. The pH will drop as a result of the electrochemical reaction with the glucose oxidase occurring at the electrode, and this will be measured. Between 2004 and 2007, Pusoschi et al. immobilized the reactive enzyme in several glucose sensors using membranes such as Nylon, cellophane, nitrocellulose, etc.[119−122] Enzyme entrapment on a platinum electrode has also been achieved with a polypyrrole sheet.[123] There are several commercially available methods for determining cell viability or toxicity, including dye exclusion (Trypan blue, eosin, Congo red, erythrosine B assays), colorimetric (MTT assay, MTS assay, XTT assay, WST-1 assay, WST-8 assay, LDH assay, SRB assay, NRU assay, and crystal violet assay), and fluorometric (Alamar Blue assay).[124] These traditional approaches typically rely on cellular metabolic activity, which does not lend itself to a rapid and precise measurement.[125] Potentiometric cell viability testing has the advantage of providing fast, real-time, continuous data for a variety of analytes, regardless of their potential concentration.[125,126] A negative potential is generated by the adherence of cells to the electrodes; this potential is then measured with a standard.[125,127−129] Tuberculosis (TB) can be detected in many ways, including the Tuberculin Skin Test (TST; DTH measurement),[130] IGRAs (interferon-gamma release assays; ELISA (QuantiFERON V R-TB), ELISpot (T-SPOTV -TB test),[130,131] Antigen Detection Assay (IDA; Immunochromatography),[132] PCR based nucleic acid amplification tests,[133−135] etc. Voltammetry can be carried out in several different ways; however, the most common and well-established methods are cyclic voltammetry (CV), square wave voltammetry (SWV), and differential pulse voltammetry (DPV), all of which show the current response as peaks that are proportional to the concentrations of the analyte being measured. The different sensor advancements for the detection of *Mycobacterium tuberculosis* and tuberculosis biomarkers are discussed in a 2019 review by Behrouz Golichenari et al.[136] The voltammetric biosensor created by Chi Hung Tzang et al. is highly sensitive to the detection of formate and glucose 6-phosphate.[137] Voltammetric responses at 100 mV/s for a 3,4-DHB modified GC electrode in 0.1 M phosphate buffer solution (pH 7.0) and different concentrations of NADH and NADPH and the lower detection limits for these compounds, respectively, are 2.5×10^{-5} M and 1.0×10^{-4} M. The toxicity to cells can be understood using potentiometric measures. Using a potentiometric assay, Ramya Kolli and colleagues determined how different electrodes affected cell survival.[125] The work of Yashas etal showcases the creation of a polyphenol oxidase (PPO) biosensor to detect catechol, utilizing a matrix of strontium copper oxide ($SrCuO_2$) and polypyrrole nanotubes (PPyNT). The manufactured sensor has a longer shelf life and great reproducibility. The wide linear range of 1−50 μM is where the suggested biosensor finds its use. Using the devised sensor, a real sample analysis of tap water, mineral water, and home wastewater revealed adequate recovery. Thus, the biosensor aims to be used in environmental protection and monitoring.[138]

Formaldehyde is produced in the human body and is found in food, animal products, and bodily fluids. To detect the presence of formaldehyde, Y.H. I. Korpan et al. developed an ion-selective field effective transistor. Using cells of the methylotrophic yeast Hansenula polymorpha, they were able to produce alcohol oxidase (AOX) with an enzyme-based sensor response time of one minute and a cell-based biosensor configuration response time of two minutes.[139] To detect urea in blood serum with a long shelf life of nearly five months, S. V. Marchenko and colleagues developed two pH-sensitive FETs, one with BSA (Bovine Serum Albumin) in PVA/SbQ photopolymer as the reference and the other with immobilized recombinant urease in the same photopolymer platform. Rapid responses of 60−120 s were achieved throughout a sensitive detection range of 0.5−40 mM.[140] To detect uric acid in real time, Juliana de Fa'tima Giarola et al. developed a platinum electrode and polypyrrole/uricase/graphene composite, (Pt-PPy/UOx/Grap) and measured a sensitivity of 0.541 nmol/L.[117]

https://doi.org/10.1021/acsomega.4c07991
ACS Omega 2024, 9, 48918−48987

2.2.1.2.3. *Conductometric Biosensors*. Like amperometric and potentiometric biosensors, conductometric biosensors benefit from a lack of a reference electrode, allowing them to function more effectively at lower alternating voltages by preventing Faraday processes at the electrodes. These biosensors also allow us to create compact, portable conductometric biosensors for use in point-of-care diagnostics.[141]

There was research into conductometric glucose sensors in the 1990s; Shul'ga et al. used thin film interdigitated metal electrodes, and the detection limit was in the 0.01 mM range.[142,143] Equations 6 and 7 outline the fundamental

$$(\beta\text{-D-glucose} + O_2) \rightarrow (\text{D-gluconolactone} + H_2O_2)$$

$$(\text{D-gluconic acid} + H_2O) \leftrightarrow (\text{acid residue} + H^+)$$

enzymatic processes:[141]Renal impairment may be indicated by a decreased urine urea level and an increased blood urea level.[144] An increase in positive and negative ions produced by the initial enzymatic reaction will cause a shift in the biosensors' membrane conductivity. In 2012, Saiapina and colleagues created a conductometric L-arginine detection biosensor based on an arginase-urease system.[145]

Conductometric biosensors have been used by Hnaien and others to detect *Escherichia coli* (*E. coli*),[146] protein denaturation,[147] and other phenomena. Compared to the original protein, the conductivity was found to be drastically different after protein denaturation (nearly a 3-fold difference).[147] Hnaien et al. also compared conductometric bienzymatic sensor action for the detection of myoglobin release with the UV/vis spectroscopy characterization technique.[148] It is possible to detect substances such as lactose,[149] maltose,[150] insecticides, and more with the use of a variety of conductometric biosensors. In 2007, Phuong and colleagues created a biosensor to identify GMO soybeans. DNA sensor sensitivity was measured to be 4.28 V /pM, and the reaction time was measured to be less than 60 s. Detection is achieved through a change in conductance brought about by the hybridization of matching DNA sequences.[151] Johne's illness is caused by *Mycobacterium avium* subsp. Paratuberculosis (MAP), and its source were identified. A conductometric biosensor developed by Okafor et al. has a rapid reaction time of 120 s for the IgG antibody.[152] The choice of electrodes for a conductometric sensor with an interdigitated transducer is crucial for optimizing its performance. Commonly used sensor electrode materials include platinum,[153,154] gold,[155−157] nickel/cobalt,[158] copper,[159] silver,[160] carbon,[161] titanium,[162] aluminum,[162] etc.

The relationship between membrane thickness and the active area of electrodes is crucial to the miniaturization of the conductometric transducer, which is easier to build than other electrochemical transducers. Photolithography, thick film printing technology, etc., are just a few of the main methods utilized to create conductometric transducers. Conductometric methods can also be used to determine the catalytic activity of enzymes. In the case of amidases, a change in conductivity results from the creation of ion groups, whereas in the cases of dehydrogenases and decarboxylases, it results from the separation of various charges. Researchers are working on different experimental approaches to address the potential drawbacks of conductometric sensors, such as a high signal-to-noise ratio, low specificity, and electrode polarization during enzyme activities. Glucose oxidase silicalite modified glutaraldehyde (GOxSME-GA) stainless steel electrode was developed by Oleksandr Ye Dudchenko et al., who also compared it to a nonmodified one (GOx-GA) and found that the silicalite modification improved enzyme entrapment on the electrodes, which improved the biosensor's signal reproducibility and storage stability.[163] Figure 14 shows the SEM image of an electrode from a conductometric transducer.

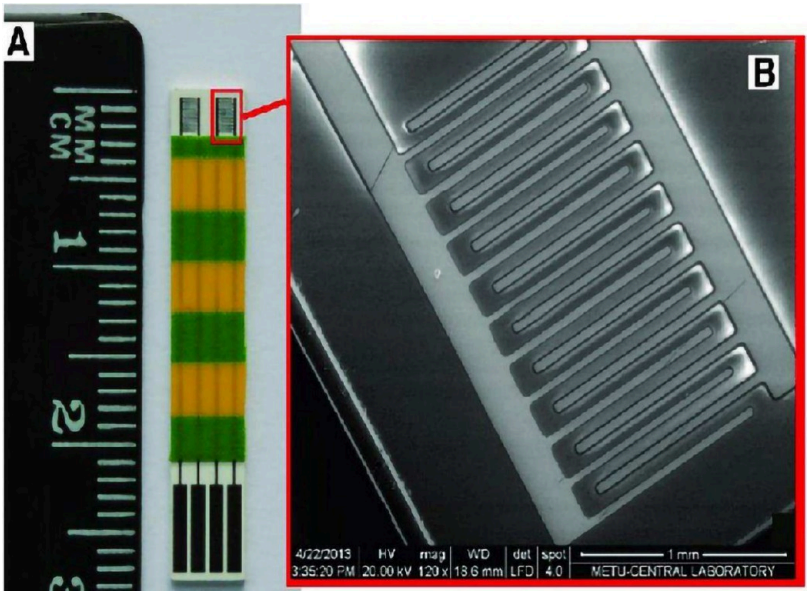

Figure 14. SEM picture of a (a) single set of electrodes and the (b) entire bare conductometric transducer zoomed portion[163] [Reprinted with permission from Dudchenko, O. Y.; Pyeshkova, V. M.; Soldatkin, O. O.; Akata, B.; Kasap, B. O.; Soldatkin, A. P.; Dzyadevych, S. V. Development of Silicalite/Glucose Oxidase-Based Biosensor and Its Application for Glucose Determination in Juices and Nectars. Nanoscale Res Lett 2016, 11 (1), 1−7. 10.1186/S11671-016-1275-2]. Copyright [2016] [Dudchenko et al. 2016, PMCID: PMC 4740475 PMID: 26842792].

https://doi.org/10.1021/acsomega.4c07991
ACS Omega 2024, 9, 48918−48987

2.2.1.2.4. *Impedimetric Biosensors*. Electrochemical impedance spectroscopy (EIS) is a technique for the sensitive detection of biomolecules that takes advantage of electrical changes at the modified electrode surface caused by biomolecular events such as the binding of receptors or proteins or cells, enzymatic activities, etc. Many types of immunosensors and aptasensors rely on impedimetric measurements to function. The key and basic mechanisms between antigen and antibody are utilized in immunosensors. The presence of an antigen can be understood through an increase in electron transfer resistance caused by the creation of an antigen−antibody complex. The impedance change serves as the basis for impedimetric aptasensors, which detect DNA damage, conformational changes, or the binding of a specific sequence.[164] In this way, the EIS can be thought of as a molecular fingerprinting technology. By connecting capacitors, resistors, and other electrical components in series or parallel, we can create electrical circuits that are equivalent to the various electrochemical reactions. The electrolyte resistance R_s; which depends upon solution conductivity and cell geometry, Charge-transfer resistance (R_{ct}) at the electrode/electrolyte interface, which can be thought of as the ratio of over potential to current in the absence of mass transfer limitation; double-layer capacitance (C_{dl}), which is a function of electrode area, nature, the electrolyte ionic strength, and permittivity and mass transfer resistance (R_{mt}) and Warburg impedance (W) are the characteristic features of impeimetric measurements.[164] Nyquist or Bode plots are used to show the frequency-related impedance spectra, where the straight line region in the low-frequency range represents the diffusion-limited process and the semicircle region in the high-frequency range accounts for the electron-transfer-limited process. For highly rapid electron transfer processes, only the straight line segments will be present, but for slower processes, a larger semicircular segment will be present. The diameter of the semicircle is a measure of electron transfer resistance.[165]

Using mercaptobenzoic acid (MBA) and cysteine-coated magnetic Fe_3O_4 NPs on gold electrodes as the DNA immobilization probe, Maurilia and co-workers have developed an impedimetric sensor for the detection of tuberculosis DNA. The use of electrochemical impedimetric sensors has benefits and drawbacks. The EIS is a nondestructive method that addresses disturbances of low amplitude from a steady state. Impedance measurements can be performed with or without the redox couple, making them either faradaic or nonfaradaic.[164] Important parameters that are vital in the selection of a redox probe include charge, hydrophilicity/hydrophobicity, redox couple size, electrode properties, etc.[169] The precision of the measuring instruments and the methods used are crucial in determining the accuracy of the impedance measurement, as stated by Yuan et al.[165]

Immunosensors, which employ antigen−antibody complex production with impedimetry as the detecting approach, have been the subject of increased study. Specific antigen binding to an antibody inhibits the Faradaic reaction of the redox pair, leading to a significant increase in electron transfer resistance relative to the initial state.[166] Epidermal growth factor receptor (EGFR) was identified as a cancer marker by Elshafey and colleagues. Anti-EGFR antibodies are more likely to bind to the electrode since it has been modified with G proteins.[167] There have been multiple reports of impedimetric immunosensors for human epidermal growth factor receptor-3 (HER-3),[168−170] PSA,[171] etc. Aptamers, which are merely synthetic DNA or RNA strands, outperform antibodies in terms of specificity and stability. Impedimetric techniques allow for three different kinds of detections to be made: by measuring changes in impedance, resistance, or current. Once the aptamer has bound to the target nucleic acid sequence, we can either detect it directly without a label or use a labeled redox active particle or nanoparticle to do so. When using signal probes, for example, we can also employ indirect labels.[172]

Researchers have reported using a wide variety of materials, including ZnO,[173] the core/shell structure of FePt/ZnS,[174] Thiol-modified DNA,[175] Streptavidin-modified DNA,[176] graphene oxide-modified Gold NPs,[177] etc., to boost the sensitivity of DNA hybridization and amplify changes in the charge transfer resistance (Rct) for improved impedimetric detections. The development of impedimetric biosensors based on enzymes is also actively being researched. Affinity-based attachments or self-assembled monolayer-based immobilization are being exploited for more selective linking of the target molecule.[178] A biosensor based on impedimetric measurements was developed by Reddy and colleagues to detect Creatinine. As little as 20 ng/mL was detected.[179] Using glucose oxidase, Shervedani et al. successfully commercialized a glucose impedimetric sensor with a detection limit of 15.6 μM.[180] Using the breakdown of glutamate oxidase as a catalyst, Maalouf et al. created a glutamate biosensor with a detection limit of 20 μM.[181] Detecting cells is vital in the medical field for identifying dangerous pathogens and cancerous cells. The phospholipid bilayer that makes up cell membranes provides the membrane with an insulating value of about 10^{-7} S/m[182] and keeps ions out until ion channels are opened.[183] In this analogy, each ion channel corresponds to a parallel resistor,[182] with the total resistance ranging from 105 to 1 M Ω μm.[2,184,185] An increase in impedance is measured and used for sensing when the desired cells adhere to a working electrode, thereby decreasing the available area. To detect ssDNAs, several research teams have reported using impedimetric biosensors that immobilize materials such as gold nanoparticles, graphene,[186] etc. Droplet evaporation on an electrode has been reported by Alam et al. to trigger osmoregulatory pathways, allowing for the detection of 104 living cells/mL and the discrimination between naturally occurring and genetically engineered *S. typhimurium*, as well as between the living and dead *E. coli* and *S. epidermidis*.[187]

Understanding how mammalian cells interact with artificial surfaces in real-time is made possible by EIS technology.[188] Also, impedimetric sensing is a breeze with the lab-on-a-chip method.[189] A microorganism-detecting impedimetric lab-on-a-chip with a total fluidic path volume of 30 nL was fabricated by Gomez and colleagues. By injecting a viable cell suspension of *Listeria innocua*, the impedance properties were altered according to the metabolic activities of the bacterium.[190] With the use of closed dielectrophoretic (DEP) cages, Medoro et al. created a parallel lab-on-a-chip impedimetric system. The prototype was based on commercially available printed circuit board technology, and particle presence was confirmed by a change in the electric field above the electrode location.[191]

In light of the current COVID-19 situation, it would be highly beneficial to increase the number of tests utilizing EIS, which can be used to analyze pulmonary edema, respiration rate, body temperature, and lung composition.[192] Results from a study using AD5933 to take bioimpedance measurements at a frequency range of 10 kHz to 100 kHz with a four-electrode interface indicated some encouraging trends.[193,194] Recent research by Minsoo Kim et al. produced an impedimetric biosensor for detecting vascular endothelial-derived growth

https://doi.org/10.1021/acsomega.4c07991
ACS Omega 2024, 9, 48918−48987

Table 2. A Brief Consolidated Electrochemical Biosensor Performance

Electrochemical detection technique	Disease or infectious agent	Sample/analyte/enzyme used for detection	Electrode/immobilization	Limit of detection	Ref
Amperometric	Glucose	Glucose oxidase	Polyimide-laser-engraved porous graphene (LEPG)/Pt NPs/Glucose oxidase	0.3 μM	196
Amperometric	Sarcosine (prostate cancer biomarker)	Sarcosine oxidase	GCE/Chitosan+Ti based MXene/SO	18 nM	197
Amperometric	Cancer marker L-fucose	The recombinant dehydrogenase domain (PQQ domain: residues 240−649) of *Coprinopsis cinerea* pyranose dehydrogenase (*Cc*PDH)	The isolated PQQ domain from *Cc*PDH /(AuNP)/SAM	13.6 μM	198
Amperometric	Uric acid	Uricase	Uricase+Boron nitride nanosheets/ Nafion	0.14 μM	199
Enzymatic Amperometric	Nitrite	Salivary nitrite	Cyanocobalamin (VB_{12}) bionic enzyme-assisted system	1 nM	200
Amperometric	miRNAs	(His-Tag-Zinc Finger Protein/ dsRNA)+ (biotin/ synthetic complementary RNA detector probe)+ streptavidin−horseradish peroxidase conjugate	SPE	0.91 nM	201
Amperometric	Catecholamine	Tyr (tyrosinase)/EDC(1-ethyl-3-(3-dimethyl aminopropyl)-carbodiimide)-NHS(N-hydroxysuccinimide)/ChitNPs nanocomposite	The screen-printed graphene electrode with ChitNPS+ Tyr enzyme	0.17 μM	202
Enzymatic Amperometric	Uric acid	Uricase	(AuNPs/TiS2 + Uricase/Nafion) SPE	0.18 μM	203
Amperometric	Glucose	Nonenzymatic	Nickel NPs + graphene	0.0152 μM	204
Cyclic voltammetry	Alicyclobacillus acidoterrestris	DNA	Reduced graphene oxide(rGO)/ a polymer derived from 3-hydroxybenzoic acid/a specific DNA probe sequence complementary with the genomic DNA of *A. acidoterrestris*	12 ng/mL	205
SWV	Saxitoxin (STX)	STX aptamer	Porous Pt NP's Round-type microgap electrode (RMGE)/aptamer	4.669 pg/mL	206
Potentiometric	Urea in sweat	Polyaniline ink, urease bioink, and a polyvinyl chloride membrane	Screen-printed carbon electrodes (SPCEs)	5 to 200 mM at pH 7	207
DPV	Mtb	DNA	AuNP/probe/Target DNA/probe/MP/SPCE	0.01 ng/mL	208
Label free voltametric aptasensor	Inflammatory response checker-Lipopolysaccharides (LPS)/ endotoxins	Au NP-thiol functionalized LPS binding Aptamer	The PEI-rGO-MoS_2 nanocomposite	3.01×10^{-5} ng/mL	209
Conductometric	*Salmonella* Enteritidis	monoclonal anti-*Salmonella* Enteritidis antibodies	polyaniline/zinc oxide (PANI/ZnO) nanocomposite film on a gold electrode	6.44 CFU/mL in 0.1% peptone water	210
Impedimetric	SARS-CoV-2	Spike (S) protein	secondary antibody-gold nanoparticle (AuNP) conjugates and target Abs/ IDEs (dielectrophoresis (DEP))	200 ng/mL (Au NP) and 2 μg/mL (DEP method)	211
Impedimetric	L-hydroxyproline (L-hyp)	3-aminophenylboronic acid (3-APBA)	3-APBA + o-phenylenediamine (OPD)/L-hyp/screen-printed electrode	0.13 μg/mL	212
Impedimetric	*Escherichia coli* O157:H7	Bacterial phage	AuNPS/multiwalled carbon nanotubes (MWCNTs)/tungsten oxide nanostructures (WO3)	3.0 CFU/mL	213
Impedimetric	SARS-CoV-2	angiotensin-converting enzyme 2 (ACE-2) transmembrane receptor	ACE-2/indium tin oxide electrode (ITO)	10.0 pg/mL (ITO-APTES-mVero) and 7.25 pg/mL(ITO-APTES-mCalu)	214
Impedimetric	-	Thrombin	Histidine-labeled thrombin-binding aptamers (TBA)/Cu2+/poly(pyrrole-nitrilotriacetic acid film	4.7×10^{-12}−5×10^{-10} mol/L	215
Impedimetric	caspase-9	-	zinc oxide and copper oxide at the electrode−solution interface	0.07 U/mL (0.032 μM)	216

https://doi.org/10.1021/acsomega.4c07991
ACS Omega 2024, 9, 48918−48987

factor (VEGF) with a detection limit of 0.5 pg/mL, making it a potentially useful tool in the clinical diagnosis of VEGF-related ocular illnesses.[195] A consolidated analysis of electrochemical biosensor performance is tabulated in Table 2.

2.2.1.3. Infrared and Raman Spectroscopy Facilitated Biosensors. Numerous health issues and early illness diagnostics rely on the detection of biofluids containing lipids, proteins, nucleic acids, etc. Due to the complexity of biomolecules, chemometrics, and other enhanced statistical approaches are being proposed as necessary for characterization studies of biomolecules using FTIR and Raman Spectroscopy.[217] The discipline of bio analyte detection relies heavily on vibrational spectroscopy, which consists of Infrared and Raman spectral series that complement each other and encompass a broad range of fingerprint molecule vibrational wavenumbers from 14,000 to 50 cm^{-1}.[218−220] The primary benefits of utilizing vibrational spectrometry as the biosensor detecting equipment are its blameless sensitivity with extremely low detection limit and its nondestructive susceptibility, which allows the samples to be reused for subsequent analytical procedures.[221] Compared to more traditional detection methods, vibrational spectroscopy excels due to its ability to precisely determine the molecular structure composition of an analyte. In addition to these benefits, it is considered a "green" analytical method because only a small amount of potentially polluting chemical reagents and solvents are used.[222] The FTIR spectrum is a plot of light intensity vs wavenumber that can be used to detect transmission or absorption.[217] Spectroscopy methods like Fourier transform infrared (FTIR) and Fourier transform infrared (FT-Raman) are currently widely utilized for the detection of a wide range of lipids, proteins, nucleic acids, etc.[223,224]

In recent years, the study of biomolecular spectroscopy has become increasingly interested in FTIR/Raman studies of the biological activities of specific chemical compounds and its halogen substitutions, such as 2-amino-5-flurobenzoic acid with Cl/Br substitution.[225] As the disease progresses, a noticeable shift in the lipid profile of RBCs will be present.[226] Lack of phospholipids and increased LDL cholesterol and triglyceride levels are described as depression indicators by researchers.[222,227] Additionally, elevated levels of immunoglobulin G (IgG) may be indicative of an infection or inflammatory response in the body, and corresponding alterations in nucleic acids may be indicative of malignancy.[228,229] When combined with chemometrics analysis, spectroscopic techniques like Fourier transform infrared (FTIR) and Raman spectroscopy can be utilized as a potent tool for detecting a wide range of biological components. Principal Component Analysis (PCA), Linear Discriminant Analysis (LDA), Partial Least Squares Discriminant Analysis (PLS-DA), Orthogonal Projection to Latent Structures Discriminant Analysis (OPLS-DA), Stepwise Multiple Linear Regression (SMLR), and Multiplicative Scattering Correction (MSC) are all examples of spectral processing techniques.[219,230,231] Because the amount of light absorbed is governed by the Beer−Lambert equation, FTIR and the attenuated total reflectance approach can be used to estimate biomolecular concentrations.[232] The studies conducted in the field of biosensors employing FTIR and Raman spectroscopy are summarized in Table 3.

Xie and colleagues used FTIR with PLSR and ATR techniques within a wavenumber range of 1600−900 cm^{-1} to efficiently detect glucose in the blood serum.[233] Albumin and immunoglobulin G (IgG) from serum can be detected by FTIR and PLSR in distinct wavenumber domains, as demonstrated by

Table 3. Recent Biosensing Research Works Using FTIR and Raman Spectroscopy

Sample	Analyte	Experimental conditions	Tool used	LOD/Y and R^2 values/ key features	Ref
Serum	Glucose	Wavenumber scanning in the 1800−400 cm^{-1}	PLSR	R = 0.86	293
Gaseous Sample	Formaldehyde	Range, 2.5mW 830nm diode laser	3-methyl-2-benzothiazolinone hydrazine (MBTH) patch (known as M-hydrogel patch)	1.46×10^{-8} mg/mL	294
Urine	Platelet-derived growth Factor (PDGF)-BB dimer, biomarker for Chronic Heart Disease and atherosclerosis	SiO_2-shelled AuAg alloy nanoparticles/agarose gel	SERS+PCA-LDA (Principal component analysis (PCA) combined with linear discriminant analysis (LDA))	87.9% sensitivity	295
Serum	MCF-7 tumor marker	Ag Np colloids	SERS	LOD 0.2 cells mL^{-1}	296
Liquid sample	Sunitinib malate (SM)	Gold nanowires	SERS	10^{-10} M	297
Liquid sample	carbendazim (CBZ) detection on apple peel	filter paper substrates/silver nanoparticles (AgNPs)	SERS	1.20 ng/cm^2	298
Serum	Nucleoside diphosphate kinase NM23-H2 (NDKB)	electrospun PVDF/CQDs film/ Au-Ag NPs	MIP-SERS	0.82 pg/mL	299
Liquid sample	Zika Virus	Au@Ag NPs	SERS	0.11 ng/mL	300
		silver nano islands			

https://doi.org/10.1021/acsomega.4c07991
ACS Omega 2024, 9, 48918−48987

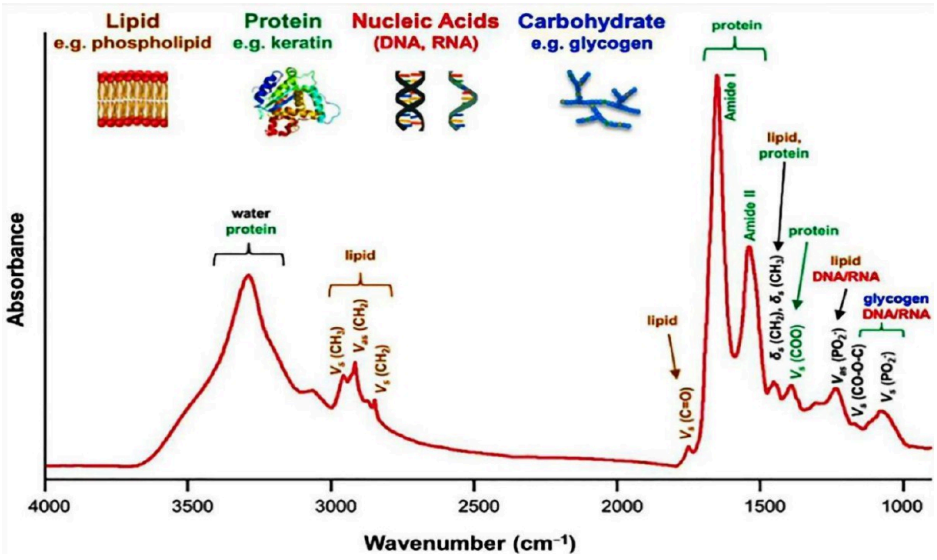

Figure 15. FTIR spectra of biomolecules[238] [Reprinted with permission from Wang, R.; Wang, Y. Fourier Transform Infrared Spectroscopy in Oral Cancer Diagnosis. Int J Mol Sci 2021, 22 (3). 10.3390/ijms22031206]. Copyright [2021] [Wang et al. Licensee MDPI, Basel, Switzerland].

the work of Perez Guaita et al.,[234] and Spalding et al.,[235] respectively. Using the principal component analysis (PCA) technique over a scan range of 4000−400 cm^{-1}, Gok and coresearchers distinguished between cancer cells and normal cells.[236] Similarly, Lima et al. used FTIR, PCA-LDA, and GA-LDA to identify ovarian cancer markers in plasma at a wavenumber range of 1800−900 cm^{-1}.[237]

Figure 15 shows the FTIR spectra of biofluids[238] (representing different lipids, nucleic acids, and amide bonds).

Based on the reviews of the literature, the absorption peaks of amide I, amide II, and amide III are located at 1648 cm^{-1}, 1544 cm^{-1}, and 1314 cm^{-1}, respectively.[224,239] Additionally, peaks at 1644 cm^{-1}, 1650−1658 cm^{-1}, 1640−1620 cm^{-1}, and 1695−1670 cm^{-1} are unmistakable vibrational identifiers of the random coil structure, -helic structure, and -sheet structures, respectively.[239] Absorption peaks at 2963 cm^{-1}, 2922 cm^{-1}, and 2850 cm^{-1} verify the existence of lipids in the biological sample by their corresponding asymmetric stretching vibrations of CH_3, CH_2, and symmetric vibrations of CH_2.[224] Additional evidence that phospholipids are present in the sample may be found at 1057 and 1249 cm^{-1}.[240,241] There was a significant difference between the serum samples of depressed and healthy individuals regarding the severity of absorption peaks in the lipid profile.[242] Proteins and immunoglobulins, which can serve as biomarkers for a wide range of disorders, can be analyzed quantitatively and qualitatively using ATR-FTIR spectroscopy.[243]

The molecular interactions between staphylococcal protein A (SpA) and anti-*Escherichia coli* immunoglobulin G (IgG) were investigated by Kengne et al. using Raman spectroscopy. Since they discovered that the tyrosine amino acid residue in the -helix structure of SpA is crucial for its interaction with IgG, this discovery paved the way for the rapid and simple application of Raman spectroscopy to the detection of disease-causing pathogens.[240] The vibrational analysis with Density functional theory calculations of stanozolol and oxandrolone molecules at the B3LYP/6−31G (d, p) basis set was performed by TibebeLemma and colleagues, and it will aid in the detection of a wide variety of steroids.[241] In Figure 16, the spectra of both living and dead cells are shown.[242]

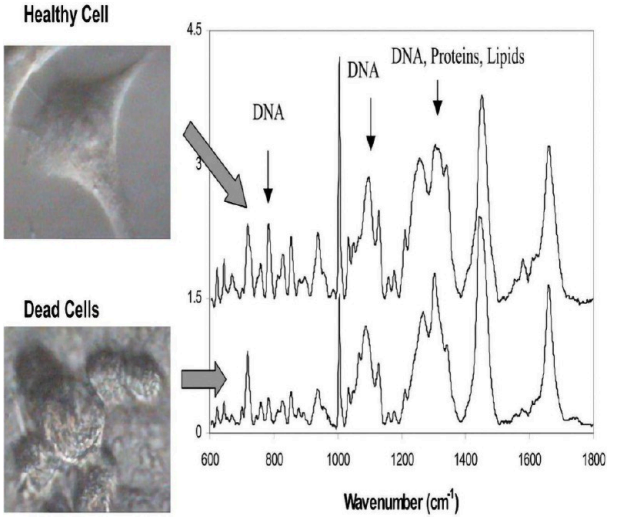

Figure 16. Comparison Raman spectrum of dead and viable cells[242] [Reprinted with permission from Notingher, I.; Verrier, S.; Haque, S. A.; Polak, J. M.; Hench, L. L. Spectroscopic Study of Human Lung Epithelial Cells (A549) in Culture: Living Cells versus Dead Cells. Biopolymers 2003, 72 4, 230−240]. Copyright [2003] [Wiley Periodicals, Inc.].

I. Notingher and colleagues studied and compared dead cells and healthy cells, derived from the A549 lung cell line, and understood the difference from viable cells through a decline in the various peak intensities, such as protein peaks at 1320 cm^{-1} and 1342 cm^{-1} and phenylalanine at 1005 cm^{-1} and also by the sharp dip at 788 cm^{-1} and 782 cm^{-1} indicating the breakdown of phospho diester bonds and DNA pairs, etc.; which can be used to get information.[242] As in Owen et al experimental work, which combined Raman with least-squares fitting for the quantitative detection of topoisomerase II inhibitor, several studies employ Raman spectroscopy to learn more about how medications interact with living cells.[243]

2.2.1.3.1. *Surface Enhanced Raman Spectroscopy (SERS).* Despite its many benefits, Raman spectroscopy has been spurred to find ways to boost the Raman signal, leading to the

https://doi.org/10.1021/acsomega.4c07991
ACS Omega 2024, 9, 48918−48987

development of Resonance Raman and Surface Enhanced Raman Spectroscopy.[244] Field studies have shown that a boost of roughly 10^{16} in the Raman signal can be obtained by combining the two approaches.[245] We have known about the SERS mechanism ever since Fleischmann first noticed it in 1974.[246] Because SERS may boost a signal by a factor of several, it has the potential to be used for single-molecule detection.[247−250] Using metal nanoparticles like gold, silver, or copper, SERS compensates for Raman's low cross-section by controlling the local electromagnetic field generated by the analyte biomolecule's adsorption to the nanoparticle.

SERS can be explained in terms of chemical enhancement due to polarizability or electromagnetic (EM) enhancement that can be attributed to an applied electric field.[251] The molecular orbital concepts of HOMO (Highest Occupied Molecular Orbit) and LUMO (Lowest Utilized Molecular Orbit) can be used to express chemical enhancement in three distinct ways.[252,253] The simplest and initial method involving non-covalent binding of the analyte with no charge transfer is ground-state chemical enhancement. Metallic contact alters the electrical charge distribution of the analyte, which in turn affects its polarizability. The second method involves the analyte molecule's covalent binding to the nanoparticle surface, either directly or indirectly, and results in an increase in Raman resonance. Because of these interactions, a new electronic state will be created at the surface, which could be in resonance with the laser, leading to an amplified Raman signal.[251] Charge transfer resonance, which is related to the transfer of charge between the analyte and the metal nanoparticle, is the third chemical enhancement mechanism. In this case, there is a resonance between Charge transfer transitions and excitation caused by the laser energy and the difference in energy level between the Fermi level of the metal and the HOMO or LUMO energy levels of the molecule. Chemical improvement has a smaller all-around effect than electromagnetic improvement[251]

Surface plasmon resonance (SPR), a unique phenomenon of metallic nanoparticles, has been linked to electromagnetic enhancement; this will be covered briefly here, while a comprehensive description will be given in the optical sensor section. The great sensitivity of SPR is due to the resonant response of the metallic nanoparticles' free electron charges to the wavelength of an external laser. Nanoparticles made of metal have a highly variable refractive index or dielectric constant. The diameter of the metallic nanoparticle, d, and the wavelength of the incident laser energy, determine the wavelength at which Localized Surface Plasmon Resonance (LSPR) occurs.[254] Field studies have revealed that the nature, size, and geometry of the metallic nanoparticle are the determining elements in SPR amplification. Different metal nanoparticles showed varying degrees of enhancement in various parts of the electromagnetic spectrum; for example, silver nanoparticles showed stronger enhancement than gold nanoparticles in the infrared area.[254] Because there will be a greater concentration of excited atoms in a bigger volume as a result of quantum confinement, the intensity of the electromagnetic field will be amplified, leading to an increase in the SERS effect. In the nano domain, for example, the SERS effect was amplified over one hundred times when the particle geometry changed from a sphere to a nanorod.[255] Enhancement was also observed to be greater for nanoparticles with sharper edges.[256] Surface roughness of metallic nanoparticles was found to affect the resonance frequency, and it was shown that an increase in roughness led to a boost in SERS because of increased scattering.[257,258]

Researchers Deepak et al. looked into how LPSR affected solar cells by fine-tuning metallic nanoparticles, and they discovered that the addition of plasmonic materials improved scattering cross sections and light absorption.[259,260] Tuan Vo-Dinh looked at silver-coated substrates in the 1990s to see if they may improve the Raman signal used to detect compounds in liquid or gaseous samples. Using SERS technology, a fiber optic sensor, and vapor dosimeter were used to detect and identify the chemicals.[261] SERS technology is commonly used for the nanomolar detection of neurotransmitters utilizing nanometals. Tiwari et al. used AgNPs for the detection of glutamate (10^{-7} M) and γ-amino butyric acid (GABA) (10^{-4} M), two amino acid neurotransmitters with a strong link to epilepsy.[262] The detection limits of 2 μM for choline, 4 μM for acetylcholine, 10 μM for dopamine, and 0.7 μM for epinephrine were achieved by Siek et al., who created a SERS substrate containing Ag NPs by electrodeposition.[263] Combining SERS with Spatially Offset Raman Spectroscopy (SESORS) allows for more accurate in vivo measurements at greater depths than is possible with either technique alone.[264] Here, the light needs to travel laterally when it is gathered from an off-center point before it can be scattered by the surface, making it an ideal candidate for below-ground surveillance.[265] Moody et al., used Surface-enhanced Spatially Offset Raman Spectroscopy (SESORS) with the use of Principal Component Analysis (PCA) and multivariate analysis to gain a detection limit of 100 μM for melatonin, serotonin, and epinephrine traces in a cat's skull.[266] Tian et al. employed SERS probes with biocompatible gold nanostars and Raman/FTIR imaging to track the in vivo transport of Mitoxantrone, a cancer medication that can be used in anti-inflammatory therapy for persons with cardiovascular illnesses.[267] SERS has been used in numerous studies to identify potential indicators of cardiovascular disease.[244] Pucetaite et al. used FT-Raman and SERS to detect uric acid, and their substrate of choice was colloidal Ag NPs.[268] Another promising measure for detecting chronic cardiovascular disease is C-reactive protein (CRP). Leucomalachite green (LMG) was reduced to malachite green (MG) by Guo and colleagues, and this transformation was used to detect CRP. Au-SERS substrates with antibody (Ab) adhesions corresponding to CRP, Horse Radish Peroxidase (HRP), and LMG were employed in the experiment.[269] Important cardiac marker N-terminal pro-brain natriuretic peptide (NT-proBNP) was detected by He et al. with a limit of detection (LOD) in the subfg mL^{-1} range using a SERS sandwich assay tool consisting of Au NPs, Toluidine, Blue reporter, and primary and secondary antibodies in conjunction with the magnetic compound of cobalt ($CoFe_2O_4$).[270]

To enhance the SERS sensitivity in molecule detection, Chahinez DAB et al. developed a plasmonic platform based on a cubic pattern of gold spheres. The COSMOL Multiphysics software was used for the simulation, which employed finite element methods. Using both 20 nm Large Plasmonic Nanostars (LPN) and 2 nm sized Small Plasmonic Nanostars (SPN), an 85% SERS boost in the intensity was reported, opening the door to potential future models for detecting biomolecules with a variety of structures.[271] Tip-Enhanced Raman Spectroscopy (TERS) is a newer SERS instrument that takes advantage of the imaging prowess of Scanning Probe Microscope (SPM) technology by using a metal-coated SPM tip that is placed on the substrate during mounting to produce a strong LSPR when irradiated with a laser.[272−274] This clever method, which may be used for single-molecule detection, allows for high-resolution SERS imaging with a short acquisition time because the tip

https://doi.org/10.1021/acsomega.4c07991
ACS Omega 2024, 9, 48918−48987

radius is lower than the diffraction-limited spot size. Another perk of TERS is that the analyte does not have to be in physical touch with the SERS substrate to generate a detectable surface-enhanced Raman signal.[275] Functionalizing the substrate with the right nanomaterials was found to increase its stability and affinity for analytes. By altering the AgFON (silver film over nanosphere) substrate with atomic layer deposition (ALD) of subnano level Alumina, Zhang et al. demonstrated an improved anthrax spore detection limit of 1400 from 2600.[276]

Since adenine has a larger Raman scattering cross section than any other DNA base pair, it can be used for single-molecule identification.[277,278] For DNA or aptamer detection, the employment of intrinsic SERS and TERS has become commonplace. In their SERS experiment, Halas and colleagues attributed the peak shift in vibrational bands at 729 cm^{-1} to the DNA base pair adenine, which they detected using biocompatible gold nanoshells encased in a glass substrate.[279] In the realm of cancer diagnosis and treatment, they also used the SERS tool's detection and imaging capabilities to track and analyze dsDNA's spectral shifts in response to chemotherapeutic agents like cisplatin and transplatin.[280] Multiple investigations have shown that TERS is an effective method for direct label-free detection of DNA and RNA, including viral detection.[281] Tobacco mosaic virus (TMV) was detected in a work conducted by Deckert and colleagues by taking advantage of the interaction between an Ag-coated AFM tip and the envelope protein.[282] When compared to semiconductor nanoparticles emitting in the NIR range, SERS imaging tags are superior for tumor recognition even in vivo. In their study, Qian et al. employed PEG/AuNP SERS substrates to successfully measure tumor locations at a depth of 2 cm below the skin.[283]

Numerous studies aimed at detecting cancer cells rely heavily on SERS. Twenty MCF-7 breast cancers were found by Zhang et al. Core−shell nanorod SERS substrates for tracking circulating tumor cells in a 1 mL blood serum-like liquid including a mixture of HeLa cells and Human Embryonic Kidney cells.[284] SERS (Scintillation Enhanced Recovery after Surgery) is the foundation for REMI (Raman Encoded Molecular Imaging), a technique that accurately pinpoints surgical margins during cancer therapies.[244] Epidermal growth factor receptor (EGFR) and programmed death ligand 1 (PGL1) were revealed to be part of a multiple tumor marker breast cancer screening tool discovered by Webb and colleagues.[285] It is possible to use photothermal therapy in conjunction with REMI to provide a more targeted surgical approach to cancer treatment.[244] Using Au nanoshell SERS substrates and the cancer cell lines H1299 and H522, Park et al. created a biosensor with a sensitivity of 97.3% for exosomes produced by malignant cells.[286] The detection of aldehydes using an electronic nose may be useful in the early detection of lung cancer. Qiao and colleagues' SERS active substrate including Au NPs formed into Au superparticles functionalized with 4-ATP and ZIF-8 metal−organic framework enabled the detection of aldehyde at a 10 ppb level.[287] Using Prostate Specific Antigen (PSA), Silica cores, and Raman-labeled Ag NPs, Chang and colleagues created a SERS sensor for prostate cancer with a 0.11 pg mL^{-1} detection limit.[282] Using an aptamer-based SERS sensor, Yang et al. were able to detect PSA at a level as low as 5 pg mL^{-1}.[288] These Au NPs were functionalized with 4,40-dipyridyl (DP) and a PSA complementary DNA strand, and they were attached to a magnetic NP in a new way.[288]

In this scenario involving the spread of COVID-19, the requirement for quick and accurate identification of the viral genome is of the utmost importance. For the identification of nucleoproteins like H1N1, Maneeprakorn et al. developed a SERS-based lateral Flow Immunochromatographic Assay. Detection was found to be possible down to 6.7 ng mL^{-1}.[289] A schematic illustration of the quantitative detection of human IgM using an SERS-based lateral flow immune assay is shown in Figure 17.[290]

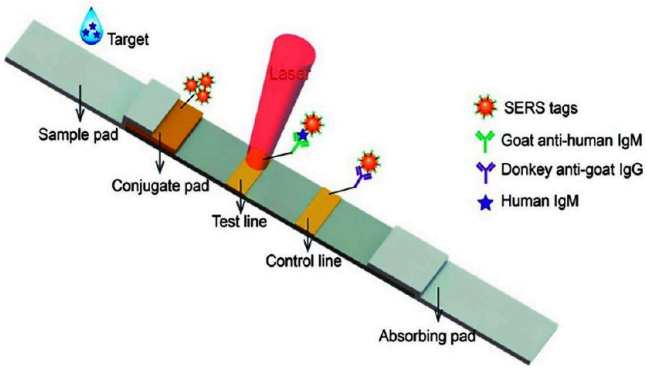

Figure 17. A schematic illustration of the quantitative detection of human IgM using an SERS-based lateral flow immune assay[290] [Reprinted with permission from Jia, X.; Wang, C.; Rong, Z.; Li, J.; Wang, K.; Qie, Z.; Xiao, R.; Wang, S. Dual Dye-Loaded Au@Ag Coupled to a Lateral Flow Immunoassay for the Accurate and Sensitive Detection of *Mycoplasma pneumoniae* Infection. RSC Adv 2018, 8, 21243−21251. 10.1039/C8RA03323D]. Copyright [2018] [The Royal Society of Chemistry].

Utilizing a head-flocked nanopillar SERS substrate, Woo Hyun Kim et al. created a label-free, ultrasensitive cancer diagnostic senor for the marker miRNA.[291] Reactive ion etching (RIE) with a 10.67 mW excitation at 785 nm was employed to create the nanopillars. Multiple tumor markers miR-10b, miR-21, and miR-373 all had LODs of 3.53 fM, 2.17 fM, and 2.16 fM, respectively, in this experiment.[292] Additionally, SERS has the potential to be employed for the detection of a wide range of bacteria.[292] Assigning distinctive peaks in bacterial SERS is difficult because of the potential for overlapping peaks of different lipids, proteins, carbohydrates, etc. The outer bacterial cell membrane will separate from the sample bacteria when it comes into touch with the capped plasmonic nanoparticles.[292] Consequently, SERS can prove why it is the gold standard in biosensing by offering a large range of analyte possibilities at an unrivaled sensitivity. A consolidated research work exploiting FTIR and Raman spectroscopy is shown in Table 3.

2.2.1.4. Optical Biosensors. As mentioned before, the physicochemical changes that take place upon engagement between the target molecule and the biorecognition element are crucial to the signal transduction process. Because optical signals are more sensitive, insensitive to noise, and stable than other physical signals,[301] biosensors that use the optical transduction technique have promising applications in the performance arena.[302] Corona virus pandemics are currently unfolding over the world, making timely diagnoses and ongoing monitoring of the virus's genome crucial for containing the outbreak.[303] There are several direct and indirect ways of detecting viruses, but they all have drawbacks, such as being time-consuming, having low sensitivity, and requiring access to specialized equipment.[303] We are reminded of the necessity for a commercially available truly quick sensitive and specific biosensor by the emergence of new viral strains around the world such as Nipah, Zika, COVID-19,

https://doi.org/10.1021/acsomega.4c07991
ACS Omega 2024, 9, 48918−48987

etc., which pose a grave threat to human survival. In this case, an optical biosensor would be ideal because it would solve the problem and provide the required data within no time. The next sections will go over the many categories of optical biosensors.

2.2.1.4.1. *Surface Plasmon Resonance (SPR)*. Biosensors based on surface plasmon resonance (SPR) have been available in the industry since the early 1980s[254] and have reached remarkable progress by overcoming the limitations in detecting low biomolecular concentrations through evolving innovative techniques and configurations.[304]

2.2.1.4.1.1. *Principle of SPR*. Delocalized electron oscillations at a metal-dielectric interface called surface plasmons are in resonance with incident radiation.[305] SPR, which is sensitive to the refractive index at the nanometallic border, amplifies the localized electromagnetic fields.[306,307] Thin film optical refractometers detect changes in refractive index brought on by biomolecular interactions.[308] The SERS section explains how electromagnetic or chemical enhancement can account for the functioning mechanisms. The localized surface plasmons are responsible for the broad frequency enhancement seen in electromagnetic enhancement, while in chemical enhancement we rely on the amplification of the Raman signals of biomolecules linked to SERS substrates.[308] Figure 18 is a schematic depiction of the SPR's operational mechanism.

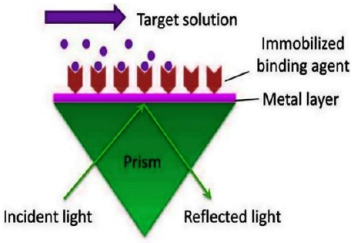

Figure 18. Schematic diagram of the SPR sensor operational mechanism[309] [Reprinted with permission from Murali, S.; Rustandi, R.; Zheng, X.; Payne, A.; Shang, L. Applications of Surface Plasmon Resonance and Biolayer Interferometry for Virus−Ligand Binding. Viruses 2022, 14, 717. 10.3390/v14040717]. Copyright [2022] [Murali et al. Licensee MDPI, Basel, Switzerland].

By undergoing total internal reflection at small reflecting angles, incident light generates an evanescent field at interface.[308] When p-polarized light shines on a metallic interface, it causes the creation of surface polaritons, leading to a dramatic decrease in the reflected light intensity at the angle where SPR waves are induced. This perpendicular electric field component is responsible for the near-surface amplification. Distance (d) over which the intensity decreases to 1/e of the original value is roughly estimated to be $\lambda/2$ in the sample buffer above the metallic surface.[310] When a bioanalyte binds to a functionalized metallic surface, it shifts the SPR angle, which in turn changes the refractive index of the interface; by calculating these shifts, we may determine the concentration of biomolecules at the surface. The biosensor has trouble detecting receptor−ligand interactions at distances greater than 600nm from the sensor chip, which is a key limitation of the SPR sensor. To our relief, however, the sensor's sensitivity may be adjusted by varying the affinity coatings on the metal surface and the buffer solutions.[308] Depending on the electromagnetic wave's propagation constant, the surface plasmon frequency can be calculated using the dispersion relation shown below:[308]

$$\beta_{sp} = (2\pi/\lambda)[(\varepsilon_m{}^{*}\varepsilon_d)/(\varepsilon_m + \varepsilon_d)]^{1/2} \quad (8)$$

where β_{sp} is the propagation constant of the surface plasmon on the interface, λ is the wavelength of incident light, and ε_m and ε_d are the permittivities of metal and dielectric, respectively.[311] Collectively oscillating surface plasmons in the excited state raise the field adjacent to the analyte−ligand interaction at resonance, resulting in a localized electromagnetic enhancement as these surface plasmons transform their energy into electromagnetic waves.[312] Localized surface plasmon resonance (LSPR) and propagating surface plasmon polariton (PSPP) sensors are the two most common varieties of SPR biosensors.[254] Figure 19 depicts the LSPR sensor mechanism.[313]

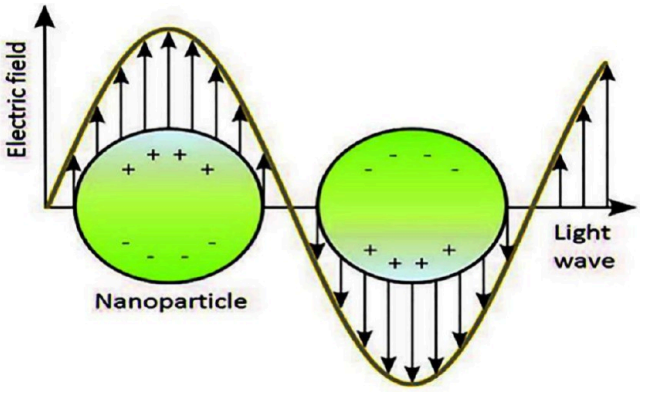

Figure 19. Schematic diagram of LSPR mechanism[313] [Reprinted with permissions from Unser, S.; Bruzas, I.; He, J.; Sagle, L. Localized Surface Plasmon Resonance Biosensing: Current Challenges and Approaches. Sensors 2015, 15 (7), 15684−15716. 10.3390/s150715684]. Copyright [2015] [Unser et al., licensee MDPI, Basel, Switzerland].

Quantum confinement effects of metallic nanoparticles are relied on to generate strong electromagnetic fields for use in the LSPR sensor.[308] Charge density oscillations are generated by incident light striking the nano metallic substrate surface, and LSPs are confined to the surface, giving rise to vertically attenuated electronic oscillations.[314] The resonant frequency is determined by extinction peaks, which are in turn determined by the refractive index, and the richer electromagnetic fields increase interactions at the interface.[308] Using PSPP sensors, in which excitation occurs via the coupling between SPs and photons at the interface, negates the drawbacks of interference and the damage created by direct irradiation of laser in sample.[315] Here the surface plasmon polaritons waves can travel along the interface.[308,315] Thin-film refractometer spectral extinction measurements of LSPR peak shifts are used for SPR sensor detection.[316] To properly interpret the findings, we need a firm grasp of how scattering spectra differ from ensemble extinction spectra of the metal nanoparticle.[317,318] In the lab, the shift and refractive index can be determined after locating the LPSR peak.[308] Direct, label-free biomolecular detection can be achieved via refractive index fluctuations, as seen by a shift in the sensogram proportionate to the amount of mass adsorbed on the SPR chip surface.[319]

SPR biosensor test for Epstein−Barr virus detection was developed by Riedel et al., and validated by detecting three antigens of the virus at the same time.[320] The SPR biosensor developed by Pimkova and colleagues detects VEGFR-1, the protein marker for myelodysplastic syndrome, with a sensitivity of 25 μg L $^{-1}$.[321] Arsenic (III) detector with a 1nM detection

https://doi.org/10.1021/acsomega.4c07991
ACS Omega 2024, 9, 48918−48987

level was the contribution of Choi and colleagues while study activities of Pennacchio et al. provided us with an immune-chemical SPR biosensor with a limit of detection of 0.1 nM for the mycotoxin; -patulin.[322,323] The SPR cancer detector developed by Altintas et al. involves immobilizing antibodies against a carcinoembryonic antigen on a gold nanoparticle-built sensor chip with the use of 11-mercaptoundecanoic acid functionalization.[324] When the refractive index of the environment changes, LPSR biosensors use this shift to their advantage, allowing them to detect changes in the spectral composition of the environment.[325] Computational studies reveal that bioligand binding affinities are characterized by association/dissociation features; for example, molecules with relatively low binding affinities or K_i values can be ascribed to strong target recognition.[326] About the HIV protease inhibitor molecule, Ha ma la inen et al. characterized almost 300 structurally distinct compounds.[327] A pharmaceutical firm in Sweden developed a biosensor design called BIAcore TM that uses surface plasmon resonance technology to detect atrazine in real time without using a label and with a detection limit of 0.05 μgL^{-1}.[328]

Recently, Kim et al. have made use of the harmless and selective sticking properties of M13 bacteriophage to fabricate a highly sensitive SPR sensor.[329] Recent years have seen the development of plasmon assisted microscopy of nano-objects (PAMONO) sensors for bioimaging, which are particularly useful for real-time viral quantifications, detection of extracellular vesicles, etc.[330] There are commercially accessible aptamer-based affinity-based SPR sensor platforms. Researchers from several institutions have created SPR-based aptamer sensors specific to diverse avian influenza virus strains and subtypes.[331,332] Despite the current worldwide viral pandemic, there is hope for the future of biomedicine with the development of SPR-aided vaccine designs (VSV-Ebola immunization).[333]

2.2.1.4.2. *Optical Waveguide*. An optical waveguide, as the name indicates is a structure that guides light energy; usually constructed on a thin substrate using glass or polymer.[334,335] The configuration in which light is confined in the transverse direction comes under the slab waveguide category and that in which light can travel only in the longitudinal direction comes under the stripe waveguide category. Figure 20 gives the schematic representation of the classifications of optical waveguide.[336]

Dimensions and nature of material intensely affect the decreasing electric field and its penetration depth. A good sensor candidate is one with a small optical waveguide having a significant difference in refractive index values between the core and cladding.[301] Two types of biosensors are discussed below whose sensor arm is generally a rib waveguide.

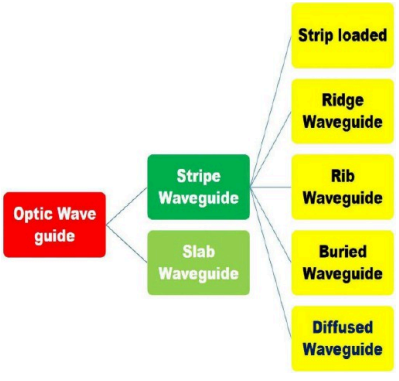

Figure 20. Schematic representation of a classification of the optical waveguide.

2.2.1.4.2.1. *Slot Waveguide Biosensor*. To create a slot biosensor, a low refractive index medium is sandwiched between two high refractive index slab waveguides.[337] The polarization charge generated by the dielectric discontinuity interacts with the plasma oscillations existing at the interface. Because of the break in the electric field (the normal component's), light is restricted in the low refractive index area.[338] Light energy can be stored in the slots with less propagation loss and an assumed optical capacitance in this waveguide design, which is compatible with Complementary Metal-Oxide-Semiconductor (CMOS) technology.[338] Resonance redshift calculations for the biosensor built by Barrios et al. using a slot waveguide with a microring resonator showed a sensitivity of 212 nm/RIU and a limit of detection of 2.3×10^{-4} RIU.[339]

2.2.1.4.2.2. *Interferometric Waveguide Biosensors*. The optical navigation property of waveguides is utilized in these interferometric waveguide biosensors, making them a type of cutting-edge biosensor. As explained in the earlier section, the analyte adsorption at the interface results in a phase shift in the guided mode due to a change in the refractive index. When the reference signal is combined with the phase-shifted signal, an interference pattern is produced that provides a quantitative reading of the bioanalyte.[301] The experimental interferometric sensing setup is depicted in Figure 21 with mechanical and electrical noise generators. Figure 22 provides a broad category for interferometric waveguide biosensors, which is briefly explored below.

2.2.1.4.2.2.1. *Mach−Zehnder Interferometer (MZI) Biosensor*. The Mach−Zehnder interferometer (MZI) is a type of interferometer that uses two arms, one of which serves as a reference and the other as a sensor. To create the two beams, a single source of monochromatic light is split in half and sent down each of the arms.[301] Light entering the sensor arm reacts with the analyte, causing a phase shift, while light entering the reference arm remains unaffected. These are put back together, and the result is transformed into fluctuations in field intensity, from which analyte concentrations can be calculated.[341] Short, schematic explanation of MZI categorization is provided in Figure 23.

Misiakos et al. fabricated a broad-band MZI sensor having a detection limit of 10^{-6}−10^{-7} RIU.[341] In the 90s alone, several hybrid MZI interferometer sensors were developed, and Heideman and co-workers were successful in getting a sensitivity of 4×10^{-6} RIU.[342] The integration of broadband MZI (silicon nitride waveguide) on a lab-on-chip arrangement enhanced the multibiomolecular analyte detection to a sensitive pM level.[343,344]

2.2.1.4.2.2.2. *Hartman Interferometric Biosensor*. Hartman interferometric biosensors came as a solution to reduce the sensor surface complexity of a fully integrated MZI, which led to heavy costs and complicated fabrication techniques.[345] The components of the Hartman interferometer include an input grating, waveguiding films, and an optical element. These interferometers were used to detect pathogens, nucleic acid, proteins, etc.[346] This category of biosensor is not appreciated and promoted much, as its design was not successful in reducing the complexity needed.[301]

2.2.1.4.2.2.3. *Young Interferometric Biosensor*. The sensitivity decline issue of biosensors, related to field variations addressed in the Young interferometer sensor, through the well-known configuration known as dual polarization interferometry (DPI);

https://doi.org/10.1021/acsomega.4c07991
ACS Omega 2024, 9, 48918−48987

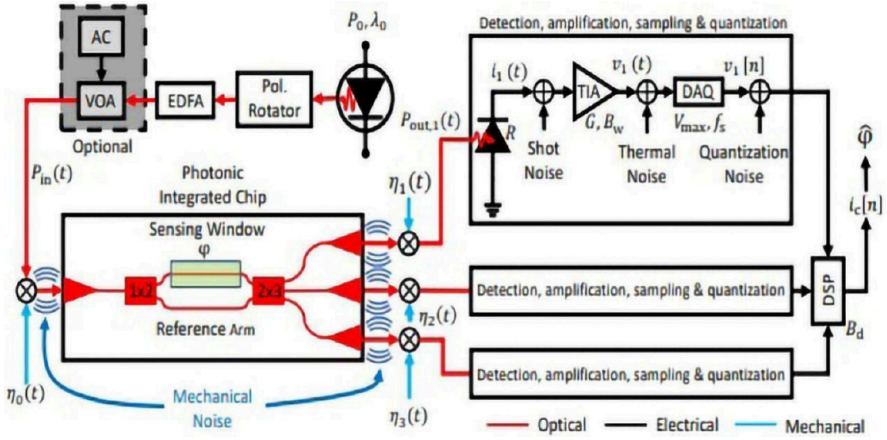

Figure 21. Experimental setup of the interferometric sensing system, with mechanical and electrical noise sources[340] [Reprinted with permission from Leuermann, J.; Fernández-Gavela, A.; Torres-Cubillo, A.; Postigo, S.; Sánchez-Postigo, A.; Lechuga, L. M.; Halir, R.; Molina-Fernández, Í. Optimizing the Limit of Detection of Waveguide-Based Interferometric Biosensor Devices. Sensors 2019, 19 (17). 10.3390/s19173671]. Copyright [2019] [Leuermann et al, Licensee MDPI, Basel, Switzerland].

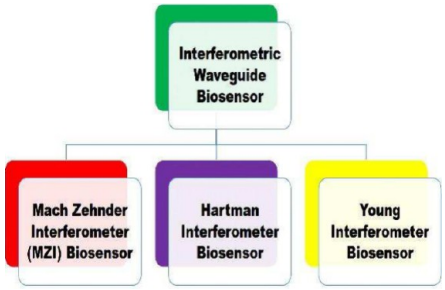

Figure 22. Schematic representation of interferometric waveguide biosensor classification.

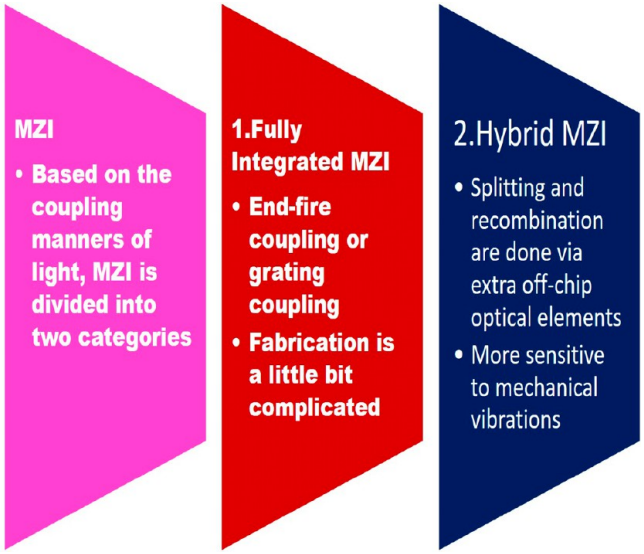

Figure 23. Classification of MZIs based on coupling manners of light.

which uses a slab waveguide system where only one transverse direction confines the guided modes (lateral modes-infinite).[347] This configuration allows the instantaneous switching of polarization which is the key to immediate analyte detection.[301] Figure 24 represents the working principle of DPI.[348] In DPI, the sensor waveguide is in contact with the sample and it is vertically above the reference waveguide. The output from both the waveguide interferes to produce the pattern in the far field. The fringe positions get shifted instantaneously with the modifications or variations in the sample layer.[301]

Many researchers have developed an interesting taste in the field of Integration of DPI with other detecting techniques recently, due to the enhancement in the sensing capability. DPI + quartz crystal microbalance (QCM) with dissipation was implemented by Ouberai et al., which studied the effect of different parameters at the interface.[349] DPI+ellipsometric studies done by Liang and coresearchers revealed that lower NaCl concentration leads to the uniform distribution of ssDNA (single-stranded DNA) initiators whereas, accumulation on the surface was the outcome of higher concentration values.[350] When a sensor chip is Integrated with a Young interferometer, then the interference patterns obtained are recorded by the CCD camera, and fast Fourier transform (FFT) is the technique used for measurements.[351] Schmitt et al. succeeded in enhancing the detection limit to 9×10^{-9} RIU for chip-assisted interferometric sensing.[352] Even DPI provides real-time quantitative data with high sensitivity; the trouble in the compilation of all the interference fringes and the relatively high cost of the equipment set its limitation.[347]

2.2.1.4.3. *Optical Fiber*. Optical fiber is a common type of dielectric waveguide with a circular cross-section, consisting of a core and cladding with different refractive indices. Total internal reflection occurs when light rays traveling from a dense to a less dense medium encounter an angle of incidence larger than the critical angle, resulting in an evanescent field at the interface and a net flow of energy across the reflecting surface as the light rays interact with molecules within the penetration depth.[353] Attenuated total reflection (ATR) sensors take advantage of the fact that reflectance decreases at the contact.[353]

The fluorescence emitted by the fluorophore is focused on detectors in TIRF (Total Internal Reflection of Fluorescence) sensors. Optical fiber biosensors can operate based on spectroscopic techniques such as Raman, SPR, fluorescence, phosphorescence, absorption, etc., or a combination of these.[353] The optical properties of silica-based optic fiber were improved through the doping of GeO_2, Al_2O_3, B_2O_3, and F, and the fiber optic biosensor may be divided into intrinsic and extrinsic types.[354] Researchers Ferreira and co. were able to successfully use an optical fiber biosensor to detect *E. coli* 0157:H7 in the

https://doi.org/10.1021/acsomega.4c07991
ACS Omega 2024, 9, 48918−48987

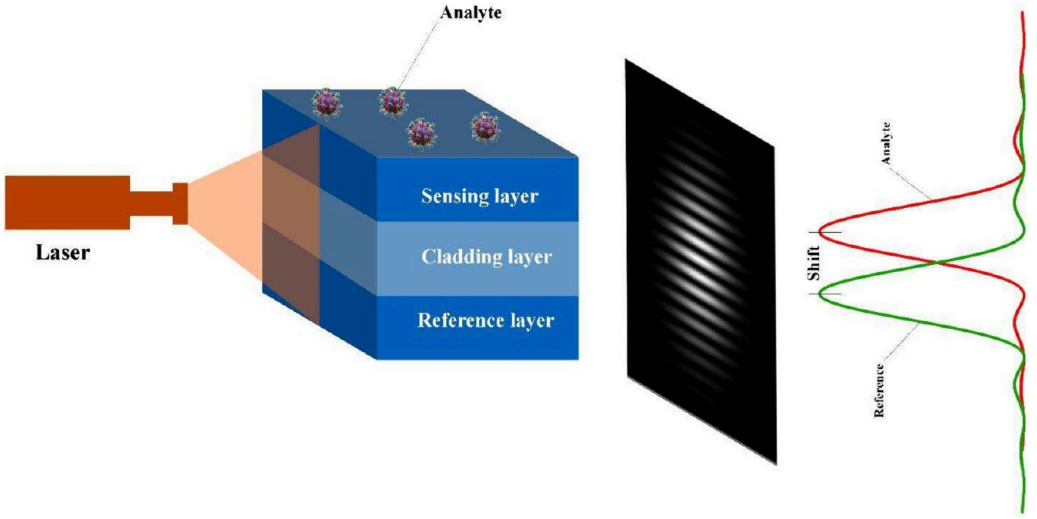

Figure 24. Pictorial representation of DPI.

early 2000s.[355] The results showed that the detection limit of E.Coli varied from 6.0×10^3 CFU/mL ± 1 log for polystyrene to 6.0×10^3 CFU/ mL ± 1 log for silica.[356] Geng and co-workers designed an optic fiber immunosensor that could detect *Listeria monocytogenes* in food with a sensitivity of 4.3×10^3 CFU/ mL.[357] The biotinylated selective antibodies were immobilized on polystyrene fibers and used to detect *Bacillus anthracis* spores in less than 60 min with a limit of detection of 3.2×10^5 spores/ mL, as demonstrated by the work of Tims and Lim et al.[358] Polystyrene fibers sped up the reaction time for *Salmonella typhimurium* detection from 40 to 20 min, and the limit of detection was increased to about 5×10^5 CFU/mL.[359]

M. Yunianto and colleagues created a fiber optic sensor for measuring serum cholesterol levels by transmitting light via an optical fiber that had been damaged.[360] Serum concentrations between 140 and 250 mg per deciliter (mg/dL) were shown to be optimal. A UV−vis spectrometer test and a light spectrometer test were conducted. The UV−vis spectrometer showed excellent linearity (0.96), while the light spectrometer test showed 0.94 linearity in white light LED. When imaging fiber optic microarrays, Epstein and coworkers employed a modified epi-fluorescence microscope with a xenon arc lamp for excitation.[361] Fibers were placed into a big piece and positioned using an X-Y stage; imaging was performed using a charge-coupled device (CCD) camera with a resolution of up to 3 m diameter sensor.[361]

Literature from 2016 discusses several techniques for fabricating polymer optical fiber sensors,[362] various optical fiber designs,[363] and the imbuing of molecular imprinting technology (MIT) with surface plasmon resonance (SPR) and long-range surface plasmon resonance (LSPR).[364] The work of Anuj K. Sharma and colleagues describes the several types of optic fibers and LPSR methods that have been developed over the past decade to improve the area of fiber optic sensors. Fiber optic SPR sensor developments in terms of detecting capabilities are discussed in this review.[365] Single-mode fibers (SMFs) are optical fibers that have a core diameter between 1 and 10 m and support only the fundamental mode (Gaussian-shaped field distribution across core and cladding) in two orthogonal polarizations.[365] The light interaction of SMF sensors occurs in the fiber itself, allowing for minor phase shifts in the modulated light, which contributes to their renown for great sensitivity. Multimode fiber (MMF), in which light can propagate along many channels, was developed because of the limitations imposed on SMF sensor performance by Polarization instability as a result of temperature fluctuations and mechanical deformations. In this case, the diameter of the core is between 75 and 200 m.[365]

Graphene, as discovered by Fu et al., increased the sensitivity of a biosensor based on fiber optic surface plasmon resonance.[366] Zhang et al.'s unique, promising design provides the answer to many real-world problems in the field of optical fiber biosensors. Two tandem SPR sections are integrated into a single optical fiber in this design, which eliminates the impact of temperature fluctuations and noise-related issues.[367] Kanso et al. used analyte modeling in their simulation research to look at how the roughness of metal layers affected the performance of SPR sensors.[368] The performance of an optic fiber sensor is critically dependent on the interaction of surface plasmons with the analyte at resonance, which is related to the dip in the SPR curve.[365]

DNA−protein interaction can be detected with the use of Pollet et al.'s fiber optic SPR sensor, which is made possible by a self-assembled monolayer (SAM) of polyethylene glycol (PEG) functionalized with Streptavidin that coats the gold-layer-sputtered optic fiber.[369] The SPR characteristics of Siver nanolayers were used by Sharma et al. for the accurate detection of A, B, and O blood types.[370] According to theoretical studies, ITO-coated optic fiber sensors are more sensitive than gold-coated ones, and the SPR wavelength of conducting metal oxides like Indium tin oxide (ITO) is in the Infrared range.[365] Although optical fiber sensors can be integrated into several ways for many different analyte detection purposes, their availability in a user-friendly approach is slightly limited by difficulties for miniaturization and its relatively higher cost, both of which can be eliminated through future research works.[371]

2.2.1.4.4. *Optical Resonator*. When light is restricted to move within a cavity, self-interference occurs, resulting in an electrical oscillation with specific resonant frequencies.[371] Here, any modification in the resonant parameters will be unveiled as a change in the light intensity, making the microcavity an optical signal transducer.[301] The optical cavities are divided into the following categories whose Q factor is the parameter that defines its efficiency:[372]

https://doi.org/10.1021/acsomega.4c07991
ACS Omega 2024, 9, 48918−48987

- Fabry−Perot microcavity
- Whispering Gallery Mode (WGM) resonator
- Asymmetric Cavity
- Photonic Crystal Cavity

2.2.1.4.4.1. *Biosensors Based on WGM Resonator*. In the WGM, the resonant modes got confined in the cavity obeying Snell's Law and undergoing the total internal reflection.[373] The mathematical representations of the relation between resonant frequencies and cavity radius are given in Equation 9[373] and that between transmitted and input power is given in Equation 10:[374]

$$2\pi \mathbf{R}_{\mathbf{WGM}} = (\mathbf{m}\lambda)/\mathbf{n}_{\mathbf{eff}} \tag{9}$$

where the resonance wavelength is represented by λ, RWGM is the radius of the cavity, n_{eff} is the effective mode index of the WGM mode, and m is the polar order of the WGM modes;

$$\mathbf{P}_{\mathbf{out}}(\omega) = \mathbf{P}_0[1 - \{\mathbf{K}(\mathbf{FWHM}/2)^2\}^* (\{\omega - \omega_0\}^2 + \{\mathbf{FWHM}/2\}^2)^{-1}\}] \tag{10}$$

where the symbols represent the following parameters. $P_{out}(\omega)$ − transmitted power; P_0 − input power; K − coupling coefficient (determines how much energy is coupled into the cavity); ω_0 − resonance frequency; fwhm − full-width at the half-maximum of the resonance spectrum profile.

Jiangang Zhu et al. developed a novel group of nano couplers based on nano scatterer's Rayleigh Scattering and plasmonic effects and successfully demonstrated the whispering gallery microlaser optical effects.[375] The coupling of free space light into whispering gallery modes is represented in Figure 25.

WGM resonators are available in different configurations, such as microspheres, microring, microdisk, etc.[301] In the spherical cavity, only certain modes are allowed due to self-interference of the recirculating rays; which is very different from the "open-loop" evanescent field sensor principle of optical fibers or waveguides.[376] Both the resonance condition and the dielectric properties within the evanescent field will get changed due to the size increase, which happened because of the adsorption, and it will be perceived as a redshift, obeying the relation as shown in equation 11:[376]

$$(\Delta\lambda/\lambda) \propto (\Delta R/\mathbf{R}) \tag{11}$$

This relation becomes crucial in the biomolecular detection scenario, as the biomolecular layer thickness becomes significant compared to sphere size at regime[376]

Research shows high Q factor values for the microsphere resonators in the near IR-VIS regions, making it suitable even for single molecule detection.[301] Liquid-core optical ring resonator (LCORR) where the light is confined along the perimeter can be combined with microfluidics, which will promote the sensing ability and such a design put forward by Andres et al. for glucose detection exhibited a limit of detection value less than 10^{-6}.[377,378] Silicon-on-insulator (SOI) wafers where silicon substrate and waveguides are separated by a silica buffer can be combined with MEMS (Micro Electro Mechanical Systems or with recent NEMS (Nano Electro Mechanical Systems) for multianalyte detection.[349] Nadgaran and coresearchers' design using triangular nanoprisms of gold coupled with hybrid WGM microtoroids delivered a Q factor value of 3.6×10^4 and a red shift of 26.45 fm while detecting a single BSA protein.[379]

2.2.1.4.5. *Others*. 2.2.1.4.5.1. *Photonic Crystal-Based Biosensors*. Photonic crystals (PCs) are characterized by a photonic band gap (PBG), which is the frequency range over which propagation of light inside the crystal is not possible. The presence of defects whose shape, size, etc., can be tuned, will introduce localized photonic energy states in the gap, resulting in higher field confinement, small mode volume, and low extinction loss and thereby making the PC a better candidate in the detection field.[380] A sensor for virus detection having a limit of detection of 1.4 nM was designed by Miller and coresearchers, in which they made a channel for the propagation of modes within the band gap of a 2D PC silicon slab with a triangular lattice of air holes, by removing the central array of air holes.[381] Figure 26 schematically represents the working of an IgG detector using a photonic crystal developed by Park et al.[382] A color change from green to orange (observed using an optical microscope with a CCD camera) occurred on adding 10 mg/mL of IgG solution, which was the result of a large band gap shift of the order of 50 nm (measured using spectrum analyzer)

An avidin detection of the order of 15nM was executed through an integrated system of PC sensors and a PDMS microfluidic system designed by Scullion et al.,.[383] A portable, fast, user-friendly biosensor for detecting the influenza virus (H1N1) with a detection limit of 138 pg/mL was designed by Park and coresearchers, in which optical signals from quantum dot aptamer beacons were amplified by the three-dimensional PC and were captured using an ordinary smartphone camera.[384] The working principle is shown in Figure 27.

Figure 28 is the photo and SEM image of a sensor made with a flexible PC structure designed by Xu et al.[385] Zhao and coresearchers gave out the successful integration of microneedle arrays with PC barcodes.[386] These multianalyte detecting bar code patches which can be put on just like a sticker, in the body, open up a way toward the painless, noninvasive, fast, multifunctional futuristic sensor platforms (Figure 29).

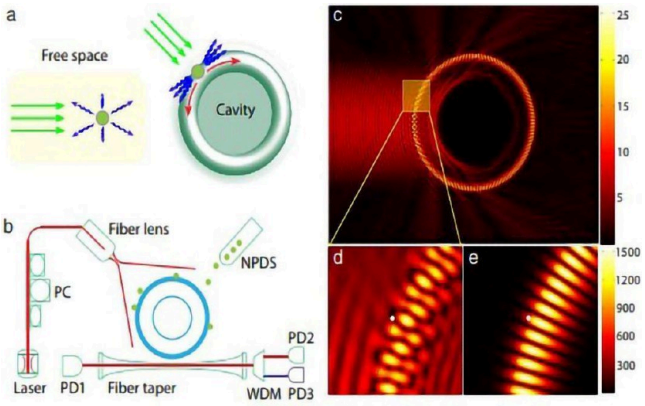

Figure 25. (a) Due to Purcell enhancement, almost all the light is collected into the cavity mode when the nanoscatterer is near the cavity. (b) Schematic representation of the experimental setup for characterization of nano coupler. PC-polarization controller, WDM-wavelength division multiplexer, NPDS nanoparticle delivery system. (c) Finite element simulation showing that free space light cannot couple into a WGM resonator by direct illumination. (d) Magnified view of the WGM area shown in c. (e) Shows how effectively the nanoparticle on the surface of resonator helps for the excitation from free space. (White dots are nanoparticles)[375] [Reprinted with permission from Zhu, J.; Özdemir, S. K.; Yilmaz, H.; Peng, B.; Dong, M.; Tomes, M.; Carmon, T.; Yang, L. Interfacing Whispering-Gallery Microresonators and Free Space Light with Cavity Enhanced Rayleigh Scattering. Sci Rep 2014, 4 (1), 6396. 10.1038/srep06396]. Copyright [2014] [Zhu et al. Nature/scientific reports].

https://doi.org/10.1021/acsomega.4c07991
ACS Omega 2024, 9, 48918−48987

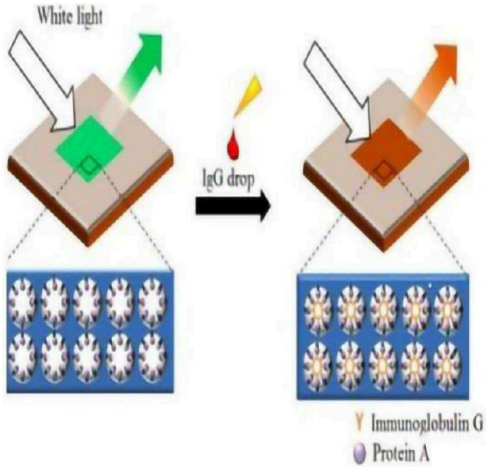

Figure 26. Schematic representation of IgG detector using photonic crystal[382] [Reprinted with permission from Choi, E.; Choi, Y.; Nejad, Y. H. P.; Shin, K.; Park, J. Label-Free Specific Detection of Immunoglobulin G Antibody Using Nanoporous Hydrogel Photonic Crystals. Sens Actuators B Chem 2013, 180, 107−113. 10.1016/j.snb.2012.03.053]. Copyright [2012] [Elsevier B.V.].

2.2.1.4.5.2. *Optical Biosensors with Nanomaterials*. The properties like large surface-to-volume ratio, quantum confinement, etc. of nanomaterials make them a good candidate in the biosensor field.[387] The major advantage of using nanomaterials in the detection field is that physio-chemical reaction outputs are tunable in the case of NPs.[387] A brief description of the classification of Nanomaterial optic biosensors is explained in the following sections.

2.2.1.4.5.2.1. *Quantum Dots*. Band gap tunability to the desired energy value is the major advantage of semiconductor nanoparticles or Quantum Dots (QD). The smaller the size, the larger the band gap, and vice-versa. In addition to this, properties like photostability, high quantum yield, broad absorption, narrow emission, etc. further help the QD to be the first choice

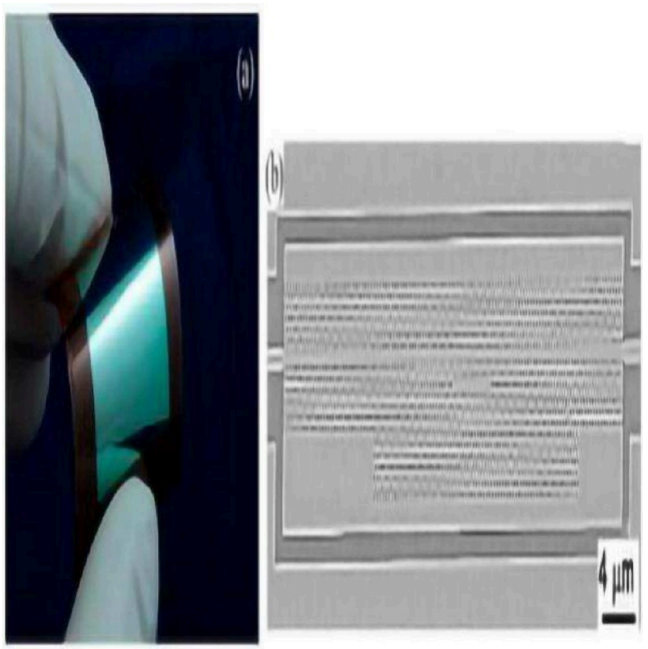

Figure 28. (a) Photo of the proposed microcavity sensor which was made up of a flexible monocrystalline PC structure. (b) SEM image of the PC microcavity[385] [Reprinted with permission from Xu, X.; Subbaraman, H.; Chakravarty, S.; Hosseini, A.; Covey, J.; Yu, Y.; Kwong, D.; Zhang, Y.; Lai, W.-C.; Zou, Y.; Lu, N.; Chen, R. T. Flexible Single-Crystal Silicon Nanomembrane Photonic Crystal Cavity. ACS Nano 2014, 8 (12), 12265−12271. 10.1021/nn504393j]. Copyright [2014] [American Chemical Society].

for making a sensitive fluorescent bioanalyte detector.[388,389] QD does not need multiple excitation sources as its excitation wavelength will be distant from emission wavelengths, enabling it to be used in multiplex arrays. QDs are excellent fluorescent energy transfer (FRET) sensor candidates as there is no significant overlapping between the excitation and emission

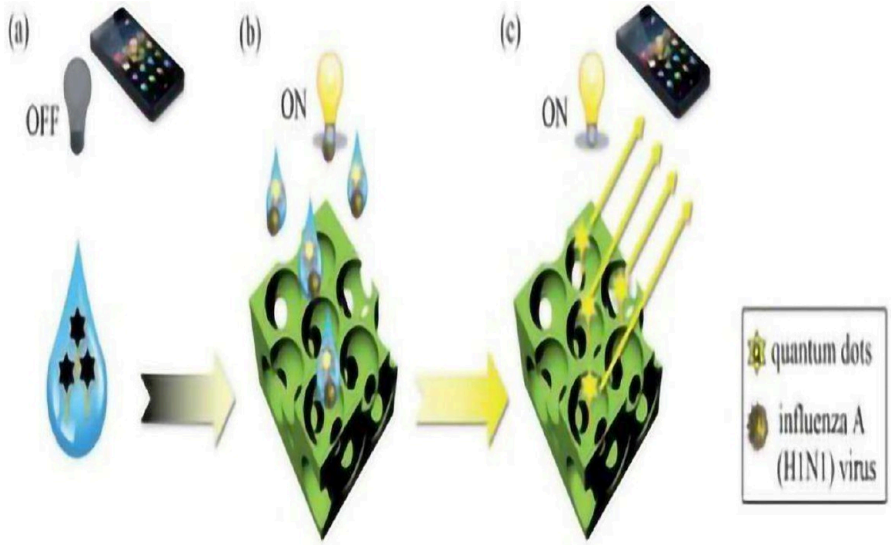

Figure 27. Principle of the "OFF−ON" detection utilizing quantum dots conjugates and nanoporous PC. (a) "OFF" state, i.e., loading the prepared quenched quantum dots conjugates. (b) "ON" state, i.e., capturing the H1N1 virus and recovering quantum dots signal. (c) Quantum dots signal was enhanced by the emission light propagating in the PC structure to make the virus detection visualized[384] [Reprinted with permission from Lee, N.; Wang, C.; Park, J. User-Friendly Point-of-Care Detection of Influenza A (H1N1) Virus Using Light Guide in Three-Dimensional Photonic Crystal. RSC Adv 2018, 8 (41), 22991−22997. 10.1039/C8RA02596G]. Copyright [2018] [The Royal Society of Chemistry].

https://doi.org/10.1021/acsomega.4c07991
ACS Omega 2024, 9, 48918−48987

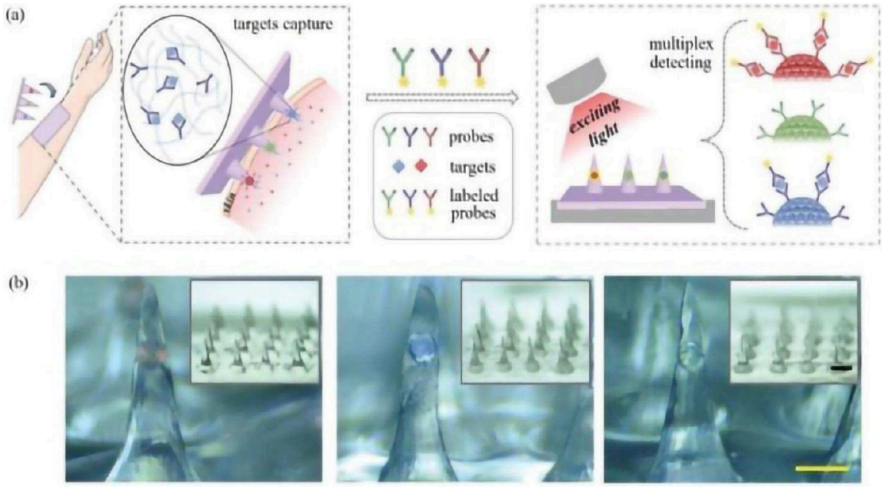

Figure 29. (a) Sketch of application of the proposed microneedle arrays which were integrated with PC barcodes in the detection of biomarkers in skin interstitial fluid. (b) Optical images of the microneedle arrays with one barcode loaded in a single tip.[386] [Reprinted with permission from Zhang, X.; Chen, G.; Bian, F.; Cai, L.; Zhao, Y. Encoded Microneedle Arrays for Detection of Skin Interstitial Fluid Biomarkers. Advanced Materials 2019, 31 (37), 1902825. 10.1002/adma.201902825]. Copyright [2019] [John Wiley and Sons].

spectra.[388,389] Figure 30 represents the schematic diagram of the size dependency of QDs.[390]

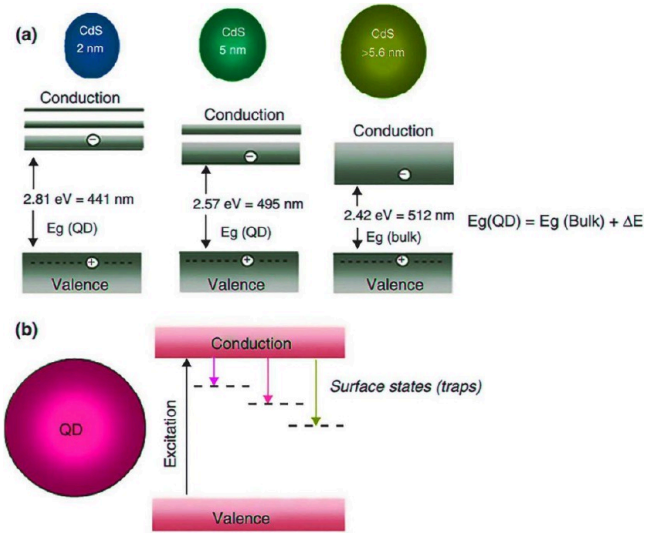

Figure 30. A schematic representation of the band structure in solids: (a) quantum confinement effect on changing quantum dot size; (b) surface trap sites with their electronic energy states localized within the QDs bandgap[390] [Reprinted with permission from Mansur, H. S. Quantum Dots and Nanocomposites. WIREs Nanomedicine and Nanobiotechnology 2010, 2 (2), 113−129. 10.1002/wnan.78]. Copyright [2010] [John Wiley and Sons].

Several QD fluorescent pathogen detectors are available such as detectors for *E. coli* O157:H7,[391] Bacillus thurinigensis,[392] respiratory syncytial virus, etc.; which exploit the QD-FRET principle.[393] Several issues need to be addressed while considering the QD−antibody conjugation. They are

1). The number of antibodies per QD control is very difficult.
2). The proper functionalization needs proper orientation of the antibody or aptamer, control which is also difficult.
3). Room temperature denaturing may happen to antibodies, hence they need to be cryopreserved. But at the same time, QD cryopreservation is not advisable.[387]

Long and the research group developed carrier-protein haptens and conjugated with the QDs to overcome the practical difficulties while dealing with QD/antibody group.[394] Carboxyl QDs were conjugated with fluorescently labeled antibodies in the experiment to detect 2,4-dichlorophenoxyacetic acid (2,4-D) (pesticide). 2,4-D/BSA conjugates were allowed to interact with the optical immunosensor probe. Increasing concentrations of the analyte lessened the fluorescence, and the detection limit was 0.5 nM.[393] Figure 31 represents the Schematic QD-based FRET genosensor.[395] Here the dye-sensitized complementary DNA conjugates with the QD-DNA hybrid and that results in the QD-sensitized dye FRET signals indicating the presence of labeled DNA.[396]

CdTe QD functionalized with Citrus tristeza virus (CTV) coat protein derived antibody performs as a specific analyte detecting helper in CTV detecting sensors.[397,398] Shojaei et al. developed a sensor using the antibody derived from CTV coat protein attached to Au NP and CdTe.[399] Coat protein on QD and recombinant coat protein on rhodamine 123 were designed as the donor−acceptor pair in a sensor that used FRET detection,[397] and they are schematically represented in Figure 32.

Table 4 illustrates different QD configurations used for various biomolecular detection.

2.2.1.4.5.2.2. *Gold Nanoparticles*. In the earlier sections, details of several gold nanoparticle-based SPR biosensors -were discussed. Generally, size-dependent color change or FRET is the method of detection used in gold-based biosensors.[387] Several Gold NP-based sensors are available for the detection of heavy metal ion presence. 5ng/ml detection limit was obtained for the Hg2+ ion detection through the sensor developed by Darbha and co-workers.[408] Cysteine conjugated Gold NP sensor made Cu2+ ion detection rapid (sensitivity 10^{-5} M) and gave for visual approval with a color change.[409] Long et al in their review on optical biosensors mentioned the detector developed by Cheng et al. using a rhodamine 6G conjugated Au NP fluorescent sensor for Hg^{2+} detection with a 0.012 ppb detection limit.[387] In 2012, Fang Luo and coresearchers developed a novel fluorescent assay detection method using gold nanoparticle.[410] Only the presence of the target molecule revealed the fluorescence, as there were enhancements of fluorescent dyes

https://doi.org/10.1021/acsomega.4c07991
ACS Omega 2024, 9, 48918−48987

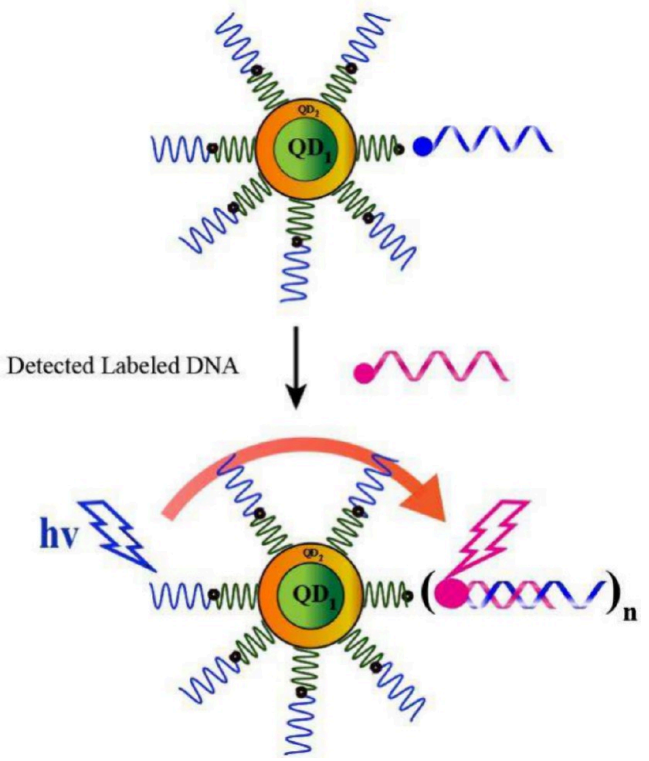

Figure 31. Schematic QD-based FRET genosensor[395] [Adapted with permission from [Zhang, H.; Feng, G.; Guo, Y.; Zhou, D. Electronic Supporting Information (ESI) Robust, Specific Ratiometric Biosensing Using a Copper-Free Clicked Quantum Dot-DNA Aptamer Sensor Experimental Section; 2013]. Copyright [2013] [The Royal Society of Chemistry].

and size changes to the ssDNA-attached gold NP. The model was able to conduct in vitro-specific detection of adenosine, thrombin, and cocaine. Figure 33 illustrates the schematic representation of aptamer-based fluorescence biosensors using unmodified AuNPs.[411]

Zeng et al. coupled horse radish peroxide (HRP) with gold NP to find out the glucose level.[412] Han et al. developed a colorimetric ELISA with gold NP for the detection of ractopamine.[413] The H_2O_2 will oxidize gold (III) ions and will result in a red color. In the absence of ractopamine, NPs will aggregate and will result in a purple color. The limit of detection was 0.35 ng mL^{-1} in urine. The design for H_2O_2 detection using gold nanoparticles is schematically represented in Figure 34.[414]

The various steps involved in a sandwich-type gold nanoparticle-based biosensor for *E. granulosus* are described below and is schematically represented in Figure 35.[415]

- Step I: Colloid gold nanoparticles were synthesized using chitosan.
- Step II: Chi−GNPs surface was activated by GA and conjugated with protein A.
- Step III: Hydatid cyst antigen (Ag B) was immobilized on the NC membrane, membranes were blocked with BSA, and then, treated with serum sample, and finally, each sample was dipped into Chi−GNPs−GA−P.A conjugate

2.2.1.4.5.2.3. *Graphene and Carbon Nanotubes.* Optical biosensors based on QDs are excellent in terms of their sensitivity and specificity in the case of in vitro detection of biomolecules. What makes biosensors with Graphene a little upper hand, is its biocompatibility in addition to other properties such as excellent mechanical strength, electrical and thermal conductivity, fast electron transportation, and large active surface area available. Electrochemical biosensors with graphene are known for their excellent sensitivity, but graphene's optical properties are not that much exploited in the sensor fabrication field.[387] Wen and coresearchers fabricated a DNA detector working based on surface-enhanced Raman spectroscopy with a graphene-Au NP substrate, which showed a detection limit of 10 pM.[416]

CRET (chemiluminescence resonance energy transfer) in which nonradiative energy is transferred from donor to acceptor without any external excitation.[387] A 1.6 ng mL^{-1} limit of detection was found in a graphene CRET platform sensor developed by He et al., for C-reactive protein (CRP).[417] The advantage of using Graphene Oxide (GO) is that it can undergo easy conjugation with the biomolecules through its functional end groups. Rotavirus detection was executed by using a GO immunosensor in which the virus was attached to the ant-rotavirus functionalized GO substrate when it was introduced; which resulted in the fluorescent quenching of GO.[418] A detailed review of graphene-based biosensors is done by Phitsini

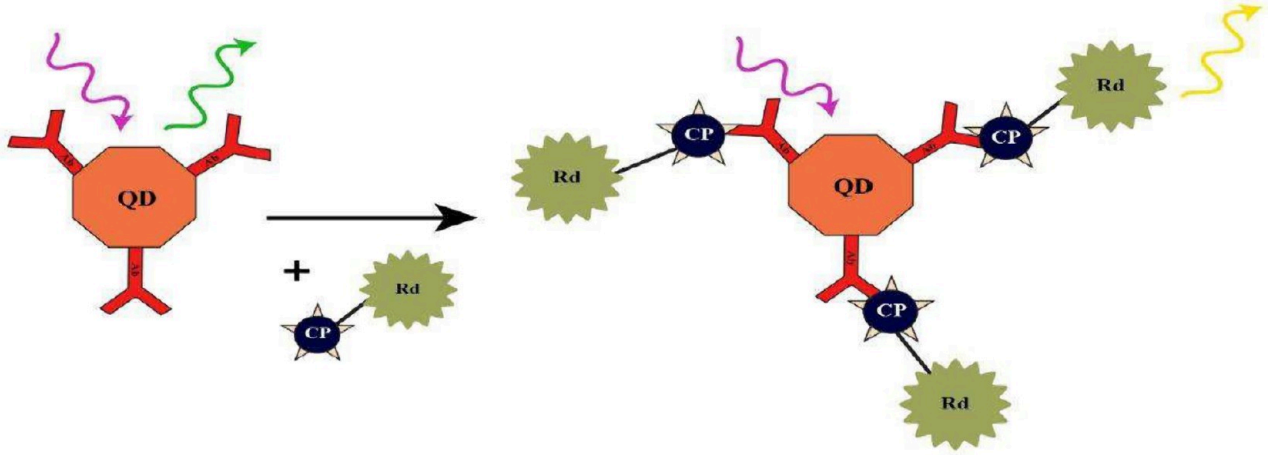

Figure 32. Schematic presentation of specific CVT nano biosensor[397] [Reprinted (Adapted with permission from Reza, M.; Samiee, F.; Tabatabie, M.; Mohsenifar, A. Sensors and Transducers Development of Quantum Dot-Based Nanobiosensors against Citrus Tristeza Virus (CTV); 2017; Vol. 213. http://www.sensorsportal.com].Copyright [2017] [IFSA Publishing, S. L, http://www.sensorsportal.com/HTML/DIGEST/P_RP_0227.htm].

https://doi.org/10.1021/acsomega.4c07991
ACS Omega 2024, 9, 48918−48987

Table 4. Tabular Representation of Different QD Configurations for Biomolecular Detection

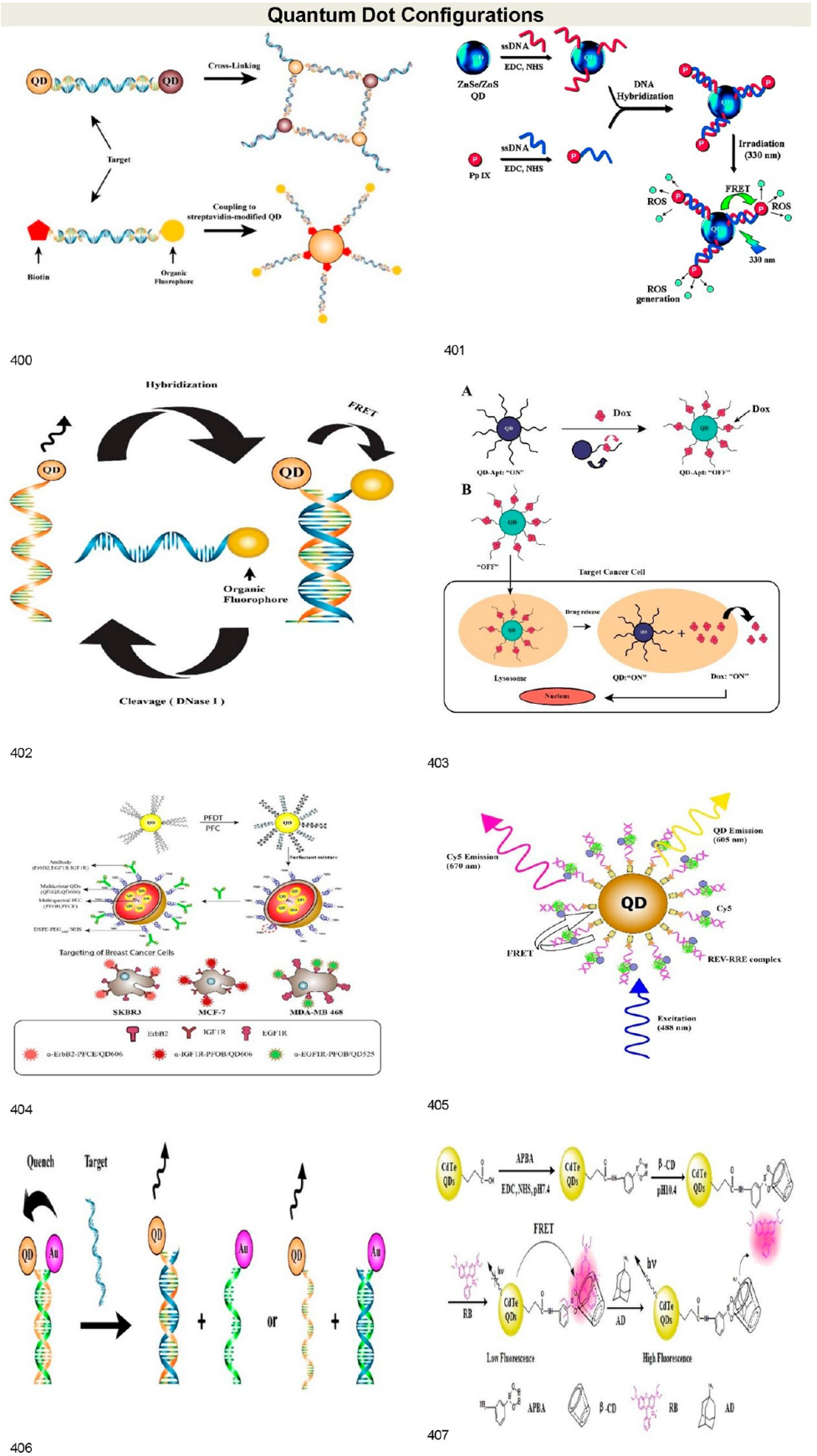

[a](Adapted with permissions - References 400−406) (400) Yeh, H.-C.; Ho, Y.-P.; Wang, T.-H. Quantum Dot−Mediated Biosensing Assays for Specific Nucleic Acid Detection. Nanomedicine 2005, 1 (2), 115−121. 10.1016/j.nano.2005.03.004. Copyright [2005] [Elsevier Inc.]. (401) Singh,

https://doi.org/10.1021/acsomega.4c07991
ACS Omega 2024, 9, 48918−48987

Table 4. continued

S.; Chakraborty, A.; Singh, V.; Molla, A.; Hussain, S.; Singh, M. K.; Das, P. DNA Mediated Assembly of Quantum Dot−Protoporphyrin IX FRET Probes and the Effect of FRET Efficiency on ROS Generation. Phys. Chem. Chem. Phys. 2015, 17 (8), 5973− 5981. 10.1039/C4CP05306K. Copyright [2015] [The Royal Society of Chemistry]. (402) Gill, R.; Willner, I.; Shweky, I.; Banin, U. Fluorescence Resonance Energy Transfer in CdSe/ZnS-DNA Conjugates: Probing Hybridization and DNA Cleavage. J Phys Chem B 2005, 109 (49), 23715−23719. 10.1021/jp054874p. Copyright [2005] [American Chemical Society]. (403) Abu-Salah, K. M.; Zourob, M. M.; Mouffouk, F.; Alrokayan, S. A.; Alaamery, M. A.; Ansari, A. A. DNA-Based Nanobiosensors as an Emerging Platform for Detection of Disease. Sensors 2015, 15 (6), 14539−14568. 10.3390/s150614539 [www.mdpi.com/journal/sensors]. (404) Bae, P. K.; Chung, B. H. Multiplexed Detection of Various Breast Cancer Cells by Perfluorocarbon/Quantum Dot Nanoemulsions Conjugated with Antibodies. Nano Converg 2014, 1 (1), 23. 10.1186/s40580-014-0023-5. Copyright [2014] [Bae and Chung; licensee Springer]. (405) Zhang, C.; Johnson, L. W. Quantum-Dot-Based Nanosensor for RRE IIB RNA-Rev Peptide Interaction Assay. J Am Chem Soc 2006, 128 (16), 5324−5325. 10.1021/ja060537y. Copyright [2006] [American Chemical Society]. (406) DAI, Z.; ZHANG, J.; DONG, Q.; GUO, N.; XU, S.; SUN, B.; BU, Y. Adaption of Au Nanoparticles and CdTe Quantum Dots in DNA Detection* *Supported by the Natural Science Foundation of Tianjin (Nos. 06TXTJJC14400, 07JCYBJC15900) and Young Teacher Foundation of Tianjin Polytechnic University (No. 029624). Chin J Chem Eng 2007, 15 (6), 791−794. 10.1016/S1004-9541(08)60004-X. Copyright [2007] [Chinese Journal of Chemical Engineering]. (Reprinted with permissions - Reference 407) (407) Ai, X.; Niu, L.; Li, Y.; Yang, F.; Su, X. A Novel ß-Cyclodextrin-QDs Optical Biosensor for the Determination of Amantadine and Its Application in Cell Imaging. Talanta 2012, 99, 409−414. 10.1016/J.TALANTA.2012.05.072. Copyright [2012] [Elsevier B.V.].

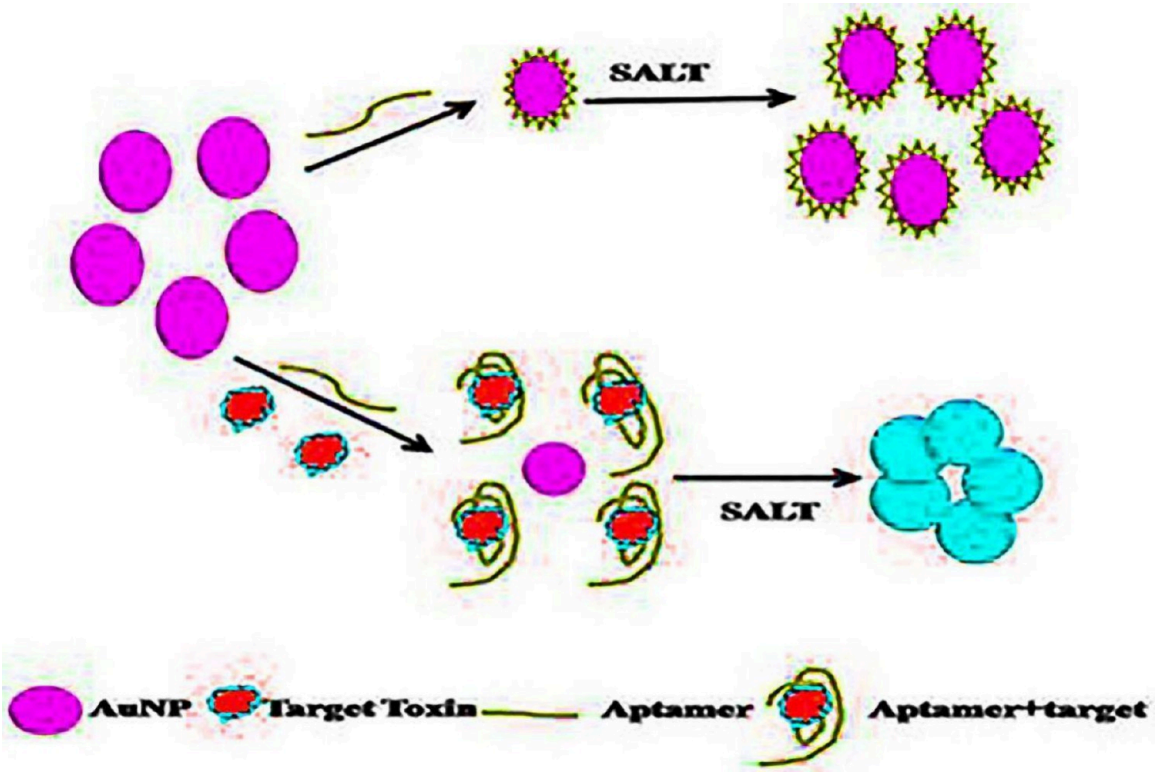

Figure 33. Schematic representation of gold nanoparticle-based colorimetric detection assay format.[411] [Reprinted with permission from Mondal, B.; Ramlal, S.; Lavu, P. S.; N, B.; Kingston, J. Highly Sensitive Colorimetric Biosensor for Staphylococcal Enterotoxin B by a Label-Free Aptamer and Gold Nanoparticles. Front Microbiol 2018, 9. 10.3389/fmicb.2018.00179]. Copyright [2018] [Mondal, Ramlal, Lavu, N and Kingston, Frontiers in Microbiology]

Suvarnaphaet and Suejit Pechprasarn in which the biosensor works related to pristine and modified (graphene oxide, graphene quantum dot, reduced graphene oxide) are discussed. Various configurations for optical sensing are schematically categorized in the review.[419] Figure 36 schematically represents the graphene, GO, and rGO.[420]

2.2.1.4.5.2.4. *Magnetic Nanoparticles*. Superparamagnetic nanomaterials can be used for specific attachment of the desired analyte molecule and the analyte separation can be easily done. Biosensors for use in a wide variety of applications, including medical diagnosis, food safety, environmental monitoring, etc., have made extensive use of magnetic nanobeads (MNB). There have been numerous reports of the use of magnetic beads ranging in size from nanometers to micrometers for the separation and detection of a wide range of biological and chemical targets, such as *Escherichia coli* O157:H7,[421,422] *Salmonella typhimurium*,[423] *Listeria monocytogenes*,[424] Avian Influenza A Virus,[425] cancer cells,[426,427] and so on. Because of their many advantages over larger magnetic microbeads (>500 nm in diameter), such as greater specific area, faster reaction kinetics, less steric hindrance, and more homogeneous distribution, 20- to 200-nanometer-diameter magnetic nanobeads (MNBs) have attracted a lot of attention in recent years. In many of their uses, MNBs must do double duty:[428]

https://doi.org/10.1021/acsomega.4c07991
ACS Omega 2024, 9, 48918−48987

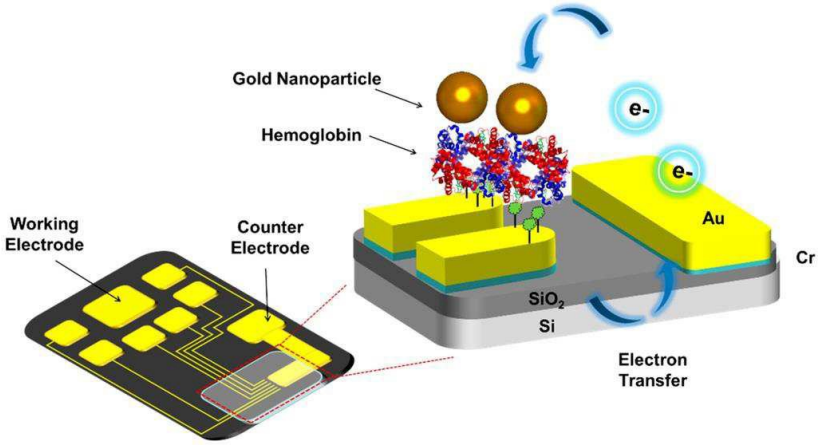

Figure 34. Schematic representation of fabricated hemoglobin/gold nanoparticle heterolayer immobilized on the microgap for H_2O_2 detection[414] [Reproduced with permission from Lee, T.; Kim, T.-H.; Yoon, J.; Chung, Y.-H.; Lee, J. Y.; Choi, J.-W. Investigation of Hemoglobin/Gold Nanoparticle Heterolayer on Micro-Gap for Electrochemical Biosensor Application. Sensors 2016, 16 (5). 10.3390/s16050660]. Copyright [2016] [Lee et al. Licensee MDPI, Basel, Switzerland].

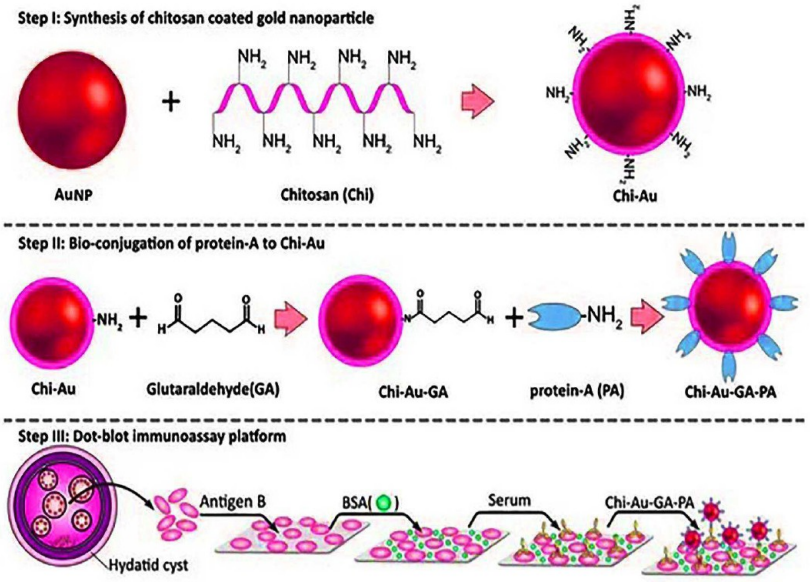

Figure 35. Schematic illustration of sandwich type E. *granulosus* biosensor[415] [Reprinted from Safarpour, H.; Majdi, H.; Masjedi, A.; Pagheh, A. S.; Pereira, M. de L.; Rodrigues Oliveira, S. M.; Ahmadpour, E. Development of Optical Biosensor Using Protein A-Conjugated Chitosan−Gold Nanoparticles for Diagnosis of Cystic Echinococcosis. Biosensors (Basel) 2021, 11 (5). 10.3390/bios11050134]. Copyright [2021] [Safarpur et al. Licensee MDPI, Basel, Switzerland].

- as a magnetic carrier, allowing for the separation of targets from complicated samples to reduce background interferences; and
- as a magnetic label, amplifying signals to improve detection sensitivity.

When produced, magnetic nanobeads (MNBs) typically have two parts: a magnetic core that provides MNBs with their superparamagnetic capabilities and a polymer shell that confers additional functional groups on MNBs.[428] In the presence of an external magnetic field, MNBs are driven along the field lines by their superparamagnetic capabilities, before dispersing once the field is no longer present. By virtue of their functional groups, MNBs can be further modified with a wide range of biochemical components to facilitate selective binding to biological and chemical targets. The magnetic force on the MNBs is proportional to

1). the magnetization and
2). physical size of the MNBs; as well as
3). the magnetic intensity and
4). gradient of the magnetic field

making the core material and physical size of the MNBs two important characteristics that play a key role in the behavior of the MNBs under a magnetic field. Out of the many magnetic core materials, many commercial items and scientific studies rely on iron oxides because of their high magnetization, low cost, and outstanding biocompatibility.[428]

For magnetic nanobeads to couple with specific biological recognition elements for selective binding with targets to accomplish separation, detection, or both, the polymer shell is critical. Coating the cores with polymeric stabilizers/surfactants, depositing really thin layers of inorganic metals onto the cores, or enveloping the cores into liposomes are all common ways to

https://doi.org/10.1021/acsomega.4c07991
ACS Omega 2024, 9, 48918−48987

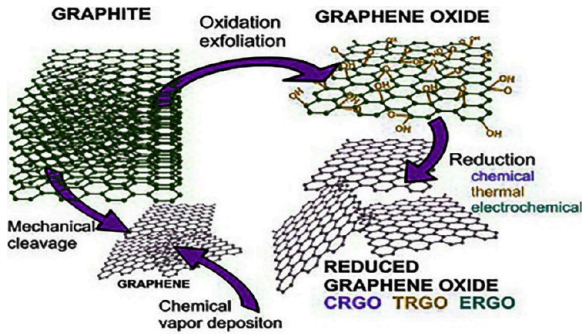

Figure 36. Schematic diagram of the formation of graphene, GO, and rGO from graphite[420] [Reprinted with permission from Filip, J.; Tkac, J. Is Graphene Worth Using in Biofuel Cells? Electrochim Acta 2014, 136, 340−354. 10.1016/j.electacta.2014.05.119]. Copyright [2014] [Elsevier Ltd. All rights reserved].

generate polymer shells, which can increase the stability of MNBs by preventing irreversible agglomeration and allowing for more even distribution.[429] After proper functionalization with hydroxyl groups and amino groups, further activation with 1-(3-dimethylaminopropyl)-3-ethyl carbodiimide hydrochloride (EDC) and n-hydroxy-succinimide sodium salt (NHSS) allows the functionalized groups especially the carboxyl or amino groups on the MNBs to bind with proteins such streptavidin, antibodies, protein A, etc.[428] Different separation techniques are discussed in Table 5 and illustrated in Figure 37.

Magnetic nanobeads' electromagnetic responses at a single or dual mixing frequency are used in electromagnetic biosensors because they are proportional to the concentration of magnetic targets. Nonlinear magnetization properties of magnetic nanobeads form the basis for the electromagnetic responses.[430] Since MNBs are frequently employed to isolate targets from mixed samples, they provide for a great detection signal in and of themselves. The electromagnetic detector or reader is at the heart of this biosensor and consists primarily of three coils:

(1) an outer driving coil (onto which a sinusoidal magnetic driving field at low frequency is applied to drive the MNBs into saturation);
(2) a middle excitation coil, (onto which a magnetic exciting field with high frequency is generated to magnetize the MNBs); and
(3) an inner detection coil, (onto which the induced signal is picked up to calculate the concentration of MNBs).

This method, known as magnetic frequency mixing, determines the nature of the induced signal. Because the exciting field magnetizes the MNBs, the induced signal is robust when the driving field is shut off and as the MNBs are magnetically saturated when the driving field is turned on to its maximum, the induced signal is faint. The aggregate frequency at which the amplitude of these two signals is greatest is used to measure the concentration of MNBs. At concentrations as low as 2.5 ng/mL,[431] *Yersinia pestis* may be detected by this electromagnetic biosensor. Also, by coupling this magnetic nanobead detector with a nitrocellulose membrane, a comparable electromagnetic biosensor was described for the rapid detection of two influenza A viruses with a low detection limit of pictograms of virus per well.[432]

Electromagnetic biosensors are rapid, easy, and cheap. However, the inherent background noise from heterogeneous MNBs and the poor detection signal from trace amounts of magnetic nanobeads impair electromagnetic biosensor sensitivity and make practical applications difficult. Superparamagnetic MNBs and repeated magnetic induction-based MNB measurements may solve this.

DNA/microRNA,[433] bacteria/viruses,[434−436] and protein biomarkers[437,438] have all been detected using magnetic relaxation switching (MRS) biosensors, a novel form of magnetic nanobead-based biosensor. Depending on whether they assess longitudinal (T1) or transverse (T2) relaxation, MRS biosensors can be classified into one of two categories.[429] When MNBs are in a scattered or aggregated condition due to the presence of targets, the T2 of the biosensor might shift, and this shift is typically measured by T2-mediated MRS biosensors. As a result of their interaction with the targets, MNBs in solution can undergo a transition from a dispersed to an aggregated form, which can lead to a drop in T2.[429] T2 is larger when no target is present in the sample because MNBs stay scattered; however, T2 is lower when targets are present because MNBs aggregate after being conjugated with them. *Salmonella enterica* was detected in milk samples down to 103 CFU/mL using this MRS biosensor.[439] Poly vinyl alcohol (PVA) functionalized magnetic nanobeads were used to create a T2-mediated MRS biosensor for the detection of boric acid or borate ester (BA/BE) relying on the covalent interaction of the hydroxyl groups of PVA and BA/BE, which leads to their aggregation.[440]

Developed magnetic immunoassay techniques directly detect the magnetic field generated by the magnetically labeled targets using a sensitive magnetometer.[441] Weitschies et al. propose a novel magnetic relaxation/remanence immunoassay (MARIA) employing a superconducting quantum interference device (SQUID) as a magnetic field sensor.[442] This technique involves immersing an immobilized target in a suspension of superparamagnetic nanoparticles bound to antibodies specific to the target. To align the dipole moments of the particles, a periodic external magnetic field is used. The SQUID detects the magnetic field generated by the target-bound particles. Magnetic marker monitoring (MMM) can provide insight into the digestive tract transit of a solid oral dose form. Only the bandwidth of the data-collecting technology restricts the passage's temporal resolution. The resulting spatial resolution was on the order of a few millimeters. This is significantly further than what is possible with standard techniques like γ -scintigraphy. MMM's key benefits are:

1). It may be used in any setting without worrying about radiation exposure.

2). It provides an opportunity to learn even more about the behavior and fate of solid pharmaceutical formulations as they travel through the digestive tract.

3). Furthermore, MMM provides data on how the digestive tract reacts as it passes the magnetically tagged object. This quality may prove especially helpful in identifying digestive system problems.

4). The utilization of a minimal quantity of magnetic material to label the pellet, as well as the compact size of the pellet contained within the capsule, indicate that the implementation of MMM is not limited solely to items of considerable dimensions, such as a capsule.

5). Moreover, the method of multiple unit pellet system (MMPS) can be readily employed for the encapsulation of any orally delivered, monolithic, pharmacological dosage form.

https://doi.org/10.1021/acsomega.4c07991
ACS Omega 2024, 9, 48918−48987

Table 5. Comparison of Different Magnetic Separation Techniques

Conventional magnetic separation	High-gradient magnetic separation	Magnetophoretic separation	Magnetic continuous flow separation	Magnetic grid separation
First, in a tiny centrifuge tube, the MNBs with antibodies are combined with the sample containing targets to generate the MNB−analyte complexes.	After being magnetized by an externally applied magnetic field, the soft magnetic materials in the form of balls or wires in a separation column are then employed to trap the immune MNBs as they stream through the column.	First, enough MNBs are coupled with the sample targets to create the magnetic targets that will serve as the sample flow	Before being evenly dispersed in a fluidic channel, the immune MNBs are caught by an external magnetic field.	The antibody-modified MNCs were initially utilized to create an MNC virtual net in a tiny rectangle glass tube that was wrapped in copper tape.
The sample solution background can then be pipetted away, and the magnetic targets can be caught against the tube wall using an external magnetic field.	The column is constantly fed with a large sampling volume containing the targets, and the targets are separated from the background as the antibodies on the MNBs catch only the targets	A gradient magnetic field is given to a magnetophoretic channel into which the sample and carrier flows are injected.	The sample holding the targets is then injected into the channel, where it is bound specifically to the MNBs.	Then, the tube was injected with the *E. coli* O157:H7 specimen, which the immune MNCs then captured to create the magnetic bacterium.
The magnetic targets are then resuspended using a reduced volume of buffer solution.	Once the magnetic field has been removed, the magnetic targets can be collected from the column and sent on to the detection step further down the line.	As the magnetic field pulls the magnetic targets in the direction of a greater gradient, the targets are continuously separated from the rest of the sample while the nonmagnetic background stays put in the flow.	Finally, after the magnetic field has been removed, the channel is purged, and the magnetic target complexes are concentrated in a tiny volume of buffer solution.	After the external magnetic field was removed, the magnetic pathogens were finally gathered.
		At last, the magnetic targets are gathered at the allotted exit, where they can be enriched by yet another magnetic field.		With this magnetic grid separation, 85% of the *E. coli* O157:H7 bacteria could be removed from a 10 mL sample in just 10 min.[428]
				The creation of the MNC net based on Lenz's Law was the key achievement because it made it possible for high MNC chains to develop in the separation channel at a high flow rate.
ADVANTAGES (over centrifugation and filtration)	**ADVANTAGES**	**ADVANTAGES (over traditional methods)**	**ADVANTAGES (over magnetophoretic separation)**	**ADVANTAGES**
(1) High concentration since significantly less buffer solution is needed to resuspend the magnetic targets, and (2) High specificity because of the antibodies' ability to preferentially react with the targets.	(1) A sizable volume of sample may be separated	(1) Automatic and continuous flow helps to separate the analyte from a large volume of material.	(1). A smaller quantity of the MNBs is needed to achieve a high separation efficiency	With dot-array high gradient magnetic fields, the dispersed MNBs can create MNB chains in the fluid separation channel
(2) Just a minimal quantity of the MNBs is required.		**DISADVANTAGES**	**DISADVANTAGES**	The improved control of the MNBs to form chains and distribute uniformly in the channel can be done by using an iron hoop to change the direction of magnetic field lines resulting in a 70%, fast, 1-h separation efficiency of pathogen (Salmonella) from a 50 mL food sample
		(1). A large number of conjugated MNBs are required to raise the cost-effective	(1) The MNBs often clumped together when they were ensnared against the canal wall, with only the top layer of MNBs being able to successfully catch their prey.	
		(2). Complete elimination of contaminants is not always possible	(3). In addition, the efficiency of the interaction seen between targets and the MNBs was typically poor because it was based largely on the diffusion of the targets from the liquid phase to the solid phase, where the MNBs were located	

https://doi.org/10.1021/acsomega.4c07991
ACS Omega 2024, 9, 48918−48987

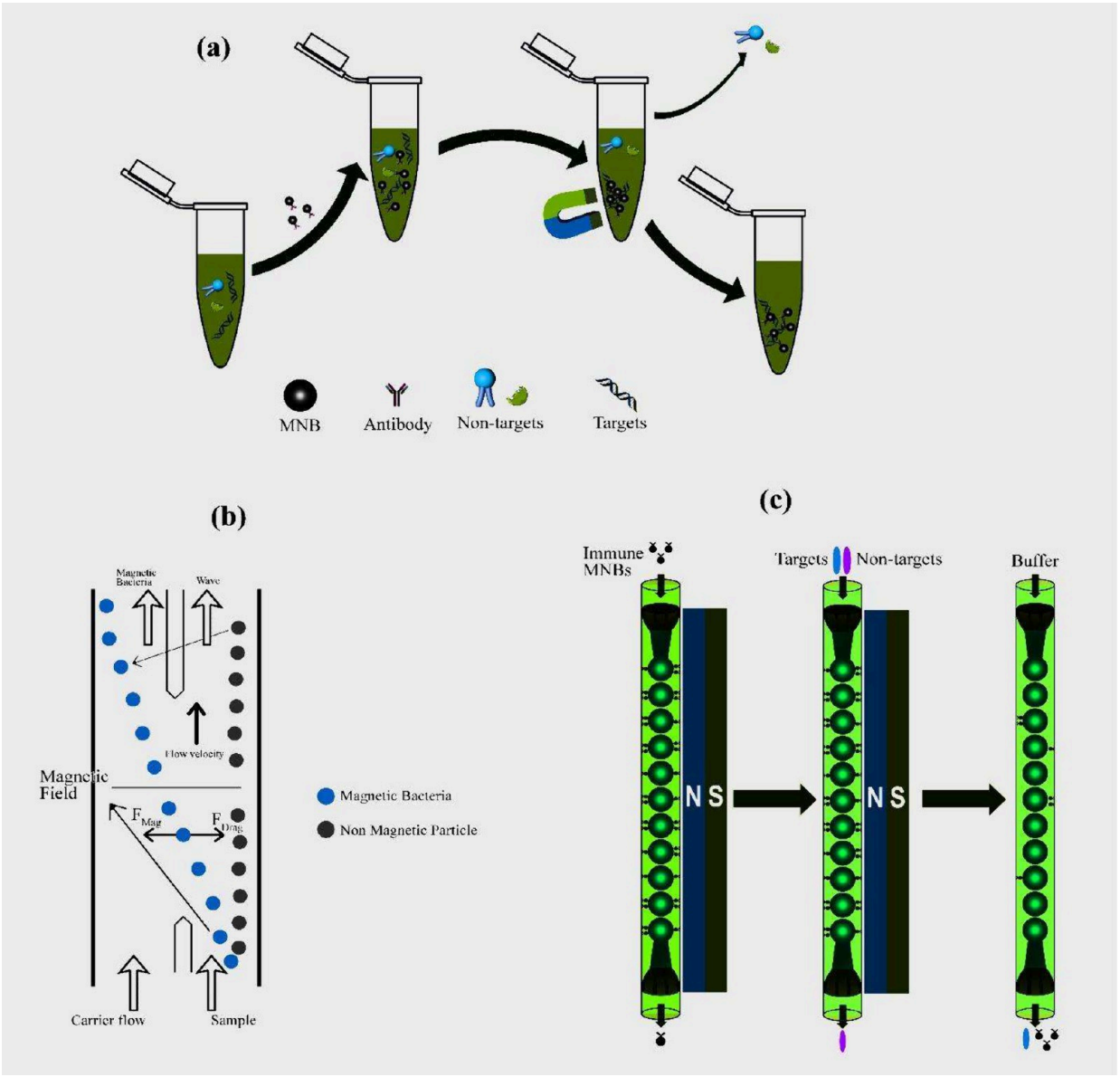

Figure 37. Schematic diagrams of various magnetic separations: (a) Conventional magnetic separation, (b) magnetophoretic separation, (c) magnetic continuous flow separation[428] [Adapted with permission from Wang, L.; Lin, J. Recent Advances on Magnetic Nanobead Based Biosensors: From Separation to Detection. TrAC Trends in Analytical Chemistry 2020, 128, 115915. 10.1016/j.trac.2020.115915]. Copyright [2020] [Elsevier B.V. All rights reserved].

However, magnetic marker monitoring (MMM) has a restriction of the localization to only one magnetically marked object.[441]

Xiao et al. describe in detail the optomagnetic biosensors which employ alternating magnetic fields to generate periodic movements of magnetic labels.[443] The strategies discussed are consolidated in the flowchart in Figure 38. As stated earlier in this section optomagnetic sensing strategy requires that the magnetic particles (or aggregates) exhibit some type of optical anisotropy, caused either by (magnetically or binding-induced) clustering/alignment or by the intrinsic shape anisotropy of the particles.[444] The magnetic field-enhanced agglutination assays (MFEAs) employ an external alternating magnetic field to induce the magnetic particles' dipole−dipole attraction to enhance interparticle binding kinetics. Both homogeneous and gradient magnetic fields can be used for MFEAs, inducing the formation of magnetic particle chains and clusters in the suspension, respectively. The colliding frequency is significantly increased in MFEAs due to the magnetic force-controlled particle encounter, stirring, and increased local particle concentration (due to the magnetic field gradient), all of which help to overcome the limitations governed by Brownian translational diffusion.

In addition, because of the magnetic interaction between their dipoles, MNPs can self-organize into various shapes when subjected to a magnetic field.[443] Magnetic objects, like MNP dimers/multimers or shape anisotropic magnetic structures (like magnetic nanorods), can experience rotational motion in relation to the field when subjected to a rotating magnetic field. Using an oscillating magnetic field for magnetic actuation resulted in less phase lag in magnetic nanoparticles (MNP) than a rotating magnetic field, according to the reports. As a result, bioassays are more sensitive:

https://doi.org/10.1021/acsomega.4c07991
ACS Omega 2024, 9, 48918−48987

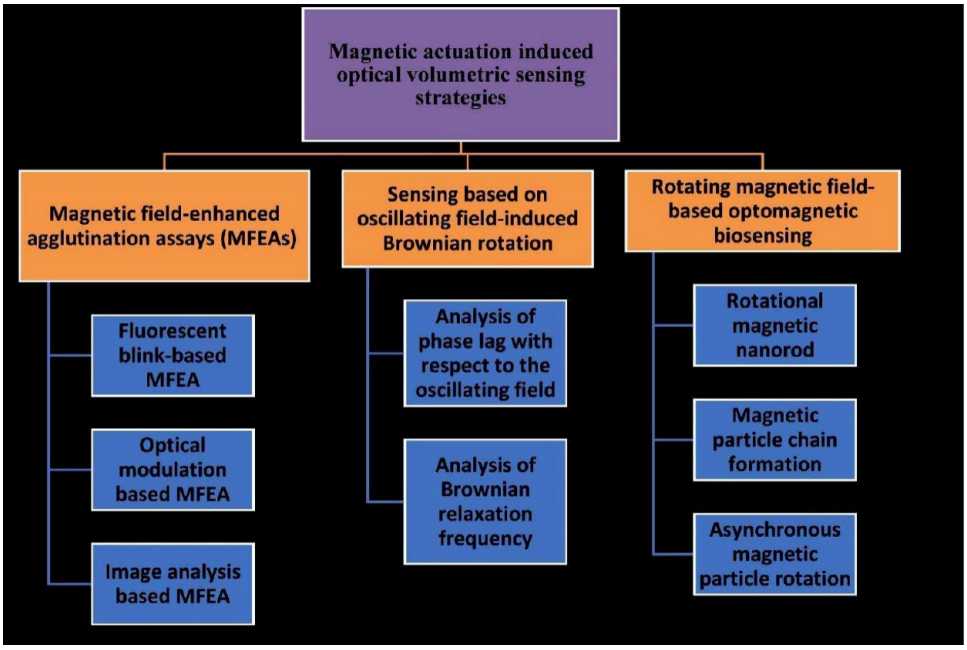

Figure 38. Volumetric sensing strategies of optomagnetic sensors.

- When subjected to a magnetic field, magnetic nanoparticles (MNPs) aggregate due to dipole attraction.
- Distance between MNPs considerably impacts the strength of this attraction.
- Individual magnetic nanoparticles (MNP) can undergo Brownian relaxation without clustering by adjusting their concentration and oscillating field strength/ frequency.
- MNPs are randomly oriented near zero magnetic fields but partially align their magnetic moments under nonzero magnetic fields.
- If MNPs have optical anisotropy, particle rotation changes light intensity. To measure the increase in the hydrodynamic size of magnetic nanoparticles, measure the change in transmitted light's second harmonic to an oscillating magnetic field.
- This method gave optomagnetic biosensor's performance comparable to pricey magnetic susceptometers.[445]

Advantages

- Low cost
- Ease of use

Disadvantages

- The imprecise and low limit of detection (LOD) is caused by the increased
- interparticle binding kinetics, which in turn amplify the nonspecific reactions and result in a noisy background.
- The technique of integrating multistep assays onto a chip is intricate.
- Multiplex sensing requires labels or analytes to exhibit distinct signals, whereas
- volumetric optomagnetic sensing lacks the ability to differentiate signals.

A brief consolidation of optical biosensor performance is given in Table 6.

2.2.2. Biorecognition Elements Based. The overall well-being of the population relies heavily on the prompt identification of diseases and the subsequent administration of suitable therapy. The successful design of a biosensor depends on a comprehensive understanding of the properties of the biorecognition element and its effects on the bioanalytes. The sensor's performance requires a specific affinity toward the analyte.[456] The sensor field employs a wide range of biorecognition elements, which can be classified into many categories as shown in the graphic chart (Figure 39).

Table 6. A Brief Tabulation of Optical Biosensor Performance

Transducer	Analyte	Limit of Detection	Ref
SPR	As(III)	1 nM	323
LSPR multiarray	Immunoglobulins, C-reactive proteins, fibrinogen	100 ng/L	446
LSPR nanochip	Ovarian cancer marker HE4	4 pM	447
LSPR (gold nanorods)	Ochratoxin (Mycotoxin)	<1 nM	448
MachZehnder Interferometer (MZI) with double-slot hybrid plasmonic (DSHP) waveguide	2-propanol	Sensitivity 1061 nm/RIU	449
Broad-band MZI	-	10^{-6}–10^{-7} RIU	450
Hybrid MZI interferometer	-	Sensitivity 4 × 10^{-6} RIU	451
ZnO films	GVA	1 pg/mL–10 ng/mL	452
CdSe/ZnS	Methylated DNA	1 aM	453
CdSe/ZnS	PSA	0.05 nM	453
Fe3O4/CdSe	Cancer cell	98 cells/mL	454
Magnetic NP	atrazine	3 pg/L	455

Noticeable elements from each category are discussed further.

2.2.2.1. Antibody-Related Biosensor/Immunosensor. Antibodies are natural protein structures having a three-dimensionality. The structure of antibodies is shown in Figure 40.

Only the specific antigen corresponding to the respective antibody site will come and bind, forming an antigen–antibody

https://doi.org/10.1021/acsomega.4c07991
ACS Omega 2024, 9, 48918–48987

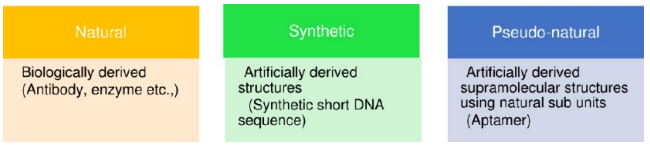

Figure 39. Graphic classification chart showing the different categories of biorecognition elements.

immunocomplex whose interaction profiles can be measured through various transducing methods.[456] Immunosensors are one of the fastest growing sensing technologies because of their fast and specific detection.[458] Antibody technology used generally is monoclonal antibody (mAb) technology or hybridoma technology[459] immobilization of Abs on sensor substrates also depends on the sensitivity and limit of detection of the sensor. If the antibody binds through the constant region Fc, then the antigen binding sites will be available to the maximum extent and the sensitivity will be higher. If the binding occurs through the antigen binding sites surrounding the VH and CH regions, the antigen binding possibility will decrease reducing the sensitivity.[460] In addition to the orientation of attachment of Abs, the extent of linkage to the substrate is also an important factor considering the binding of cognate antigen to the specific antigen binding sites of antibodies.[456] Getting a specific substrate surface with proper antibody immobilization can be done with functionalization using specific groups such as glutaraldehyde, cabodiimide, succinimide ester, etc.[461] Figure 41 and Table 7 represent and compare the different antibody immobilization techniques.

Graphene-based biosensors are well-known for their excellent sensitivity. Figure 42 schematically represents the immobilization of different biorecognition elements on the surface.[462] As previously mentioned, the many functional groups on Graphene Oxide (GO) allow for the attachment of numerous types of antibodies. The most versatile strategy for GO Ab functionalization among the three options, namely EDC/NHS chemical conjugation, electrostatic bonding, and bonding through PASE linker, is the first one. This is because it involves a direct attachment between the carboxyl and amine groups. In this method, EDC refers to 1-ethyl-3-(3-dimethylamino propyl) carbodiimide, NHS stands for N-hydroxy succinimide, and PASE represents 1-pyrene butanoic acid succinimidyl ester.[463]

Various virus and bacteria detectors were developed for using Graphene − Ab platform for clinical diagnostics; for instance, detectors for Zika virus Afsahi,[464] dengue,[465] rotavirus,[418] avian flu virus H7(Au NP modified Graphene),[466] Hepatitis C Virus, HCV (surface modification by AgNP[467]), and E.Coli,[468] *Salmonella typhimurium*,[469] etc. Lee et al.,[470] in 2010 developed a carcinoembryonic antigen (CEA) detector using Aluminum Nitride FBAR (Film Bulk Acoustic Resonator). AIN film deposition was done using the RF Sputtering method. On the substrate, 0.2−10 mg/mL of anti-CEA protein was functionalized and the measuring mode worked at the resonant frequency of 2.477 GHz. After the specific adhesion of CEA on the corresponding Ab, the resonant frequency was shifted drastically, which ensured the CEA presence.

2.2.2.2. DNA Sensor. The pursuit of comprehending the human genome has sparked a revolution in genome analysis, resulting in the creation of DNA-based biosensors capable of detecting a wide range of bioanalytes.[471] The synthesis and reproduction of nucleic acid recognition layers offer a distinct advantage over antibody or enzyme-modified layers.[471] The

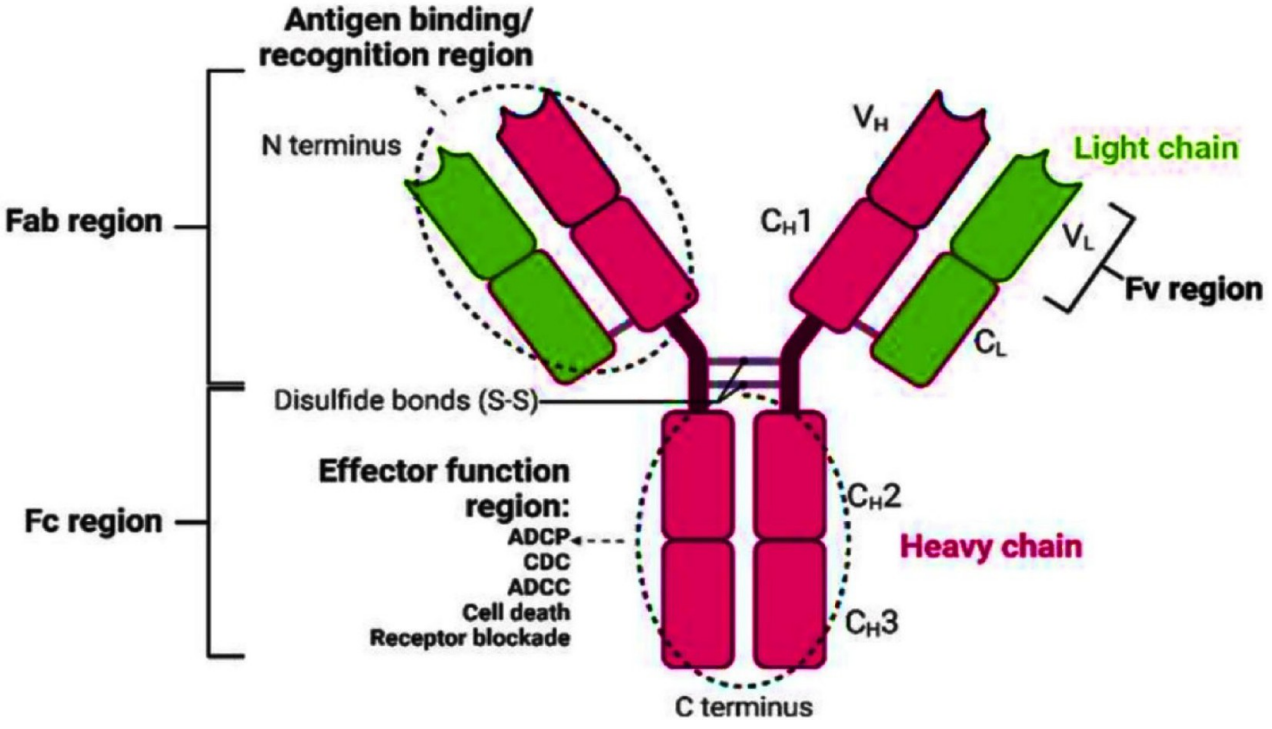

Figure 40. Monoclonal antibody (mAb) structure[457] [ADCP: antibody-dependent cell phagocytosis; CDC: complement-dependent cytotoxicity; ADCC: antibody-dependent cell cytotoxicity; C: constant; V: variable; L: light chain; H: heavy chain][Reprinted with permission from Liguori, L.; Polcaro, G.; Nigro, A.; Conti, V.; Sellitto, C.; Perri, F.; Ottaiano, A.; Cascella, M.; Zeppa, P.; Caputo, A.; Pepe, S.; Sabbatino, F. Bispecific Antibodies: A Novel Approach for the Treatment of Solid Tumors. Pharmaceutics 2022, 14 (11). 10.3390/pharmaceutics14112442]. Copyright [2022] [Liguori et al. Licensee MDPI, Basel, Switzerland].

https://doi.org/10.1021/acsomega.4c07991
ACS Omega 2024, 9, 48918−48987

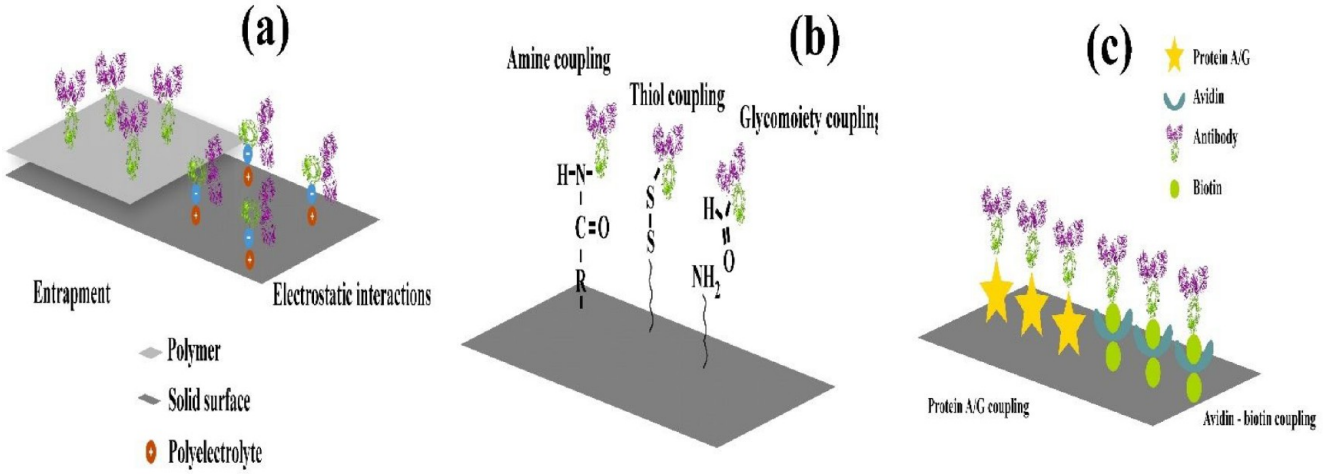

Figure 41. Antibody immobilizations: (a) noncovalent, (b) covalent, (c) affinity.

Table 7. Comparison of Different Antibody Immobilization Techniques

Immobilization Approaches [459]		
Non-Covalent	Covalent	Affinity
Forces − electrostatic or ionic bonds, hydrophobic interactions, and van der Waals forces	Involves surface modification through the groups such as hydroxy, thiol, carboxy, or amino groups	Covalent immobilization's disadvantages− partial denaturation and the lack of definite orientation
Adsorption−physisorption or chemisorption	Surface modification techniques−chemical modification, photochemical grafting, plasma gas discharge, ionizing radiation graft copolymerization, etc.	Affinity immobilization involves
Ab entrapment into conducting polymer films is another Ab immobilization		The use of biotin−avidin or immobilizing intermediate binding proteins, such as Protein A or G, first onto the sensor surface onto which Abs are attached.

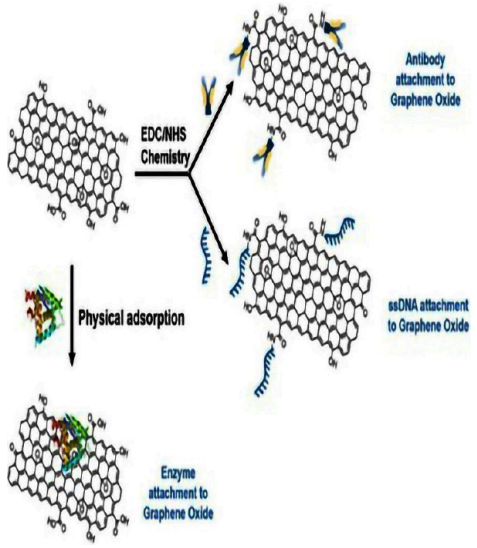

Figure 42. Immobilization schemes of different biorecognition elements on graphene surface[462] [Reprinted with permission from [Peña-Bahamonde, J.; Nguyen, H. N.; Fanourakis, S. K.; Rodrigues, D. F. Recent Advances in Graphene-Based Biosensor Technology with Applications in Life Sciences. J Nanobiotechnology 2018, 16 (1), 75. 10.1186/s12951-018-0400-z]. Copyright [2018] [Janire Peña-Bahamonde et al, Springer Nature].

immobilization of DNA should ensure both accessibility to the target analyte and secure attachment to the substrate.[472,473] DNA molecules can be affixed to the substrate using many methods, similar to the ones mentioned for antibody attachment. For example, thiolated DNA can be connected to a gold nanoparticle substrate, biotinylated DNA can be linked to an avidin-streptavidin complex, or DNA can be simply adsorbed onto electrodes.[471] The sensor's sensitivity can be enhanced through two methods: utilizing dendrimers, which possess several branch-like functional groups suitable for DNA hybridization,[474] or employing Peptide Nucleic Acid (PNA) that features a pseudo peptide bond instead of a sugar−phosphate backbone.[475]

Graphene-based DNA sensors utilize $\pi-\pi$ interactions for immobilizing DNA and primarily employ electrochemical and fluorescence transducers. These sensors assess fluctuations in physical quantities resulting from DNA hybridization or nucleobase oxidation.[462] The EDC/NHS immobilization technique is the most versatile method, as previously discussed. Akhavan et al. utilized the presence of sharp and active edges of reduced graphene nanowalls (RGNW) to promote the uniform electron transport between the DNA and the electrode in the DPV mode.[476] The detection sensitivity for dsDNA ranged from 0.1 fM to 10 mM. The fluorescent DNA biosensor utilizes a fluorescently labeled single-stranded DNA (ssDNA) that is functionalized to the substrate. This ssDNA is designed to be complementary to the target DNA. The operating principle of this biosensor is based on the quenching effect of graphene.[462] Qaddare et al. created a very sensitive DNA sensor for detecting the HIV-1 gene. The sensor utilizes luminous carbon dots combined with AuNPs/GO as a sensing platform. The sensor is capable of detecting the gene at a femtomolar level of sensitivity.[477] The chosen measurement technology was FRET (fluorescence resonance energy transfer). The fluorescence was emitted upon hybridization with the target DNA sequence, and the minimum detectable concentration was 15 femtomolar (fM). Systemic lupus erythematosus is an autoimmune illness.

https://doi.org/10.1021/acsomega.4c07991
ACS Omega 2024, 9, 48918−48987

Buhl et al. have created a DNA sensor that utilizes SPR technology to identify the presence of disease-causing dsDNA autoantibodies.[478] In the detection system, human transferrin was modified with biotin, and a synthetic oligonucleotide was linked to its corresponding sequence that matches the specific antigenic structure to be identified.

To functionalize ssDNA tagged with 6-mercapto-1-hexane and Au NPs, Xu et al. created a CuS-Graphene composite platform.[479] To characterize the material, impedance spectroscopy and cyclic voltammetry were employed. The target DNA was detected as low as 0.1 pM. Schematic illustration of the electrochemical DNA biosensor fabrication process is shown in Figure 43.

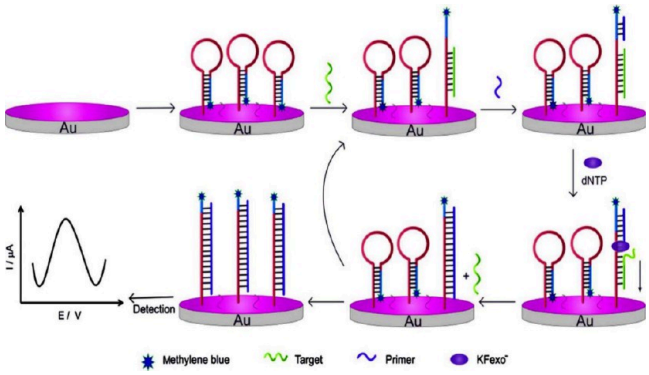

Figure 43. Schematic illustration of the electrochemical DNA biosensor fabrication process[480] [Reprinted with permission from Wang, T.; Zhang, Z.; Li, Y.; Xie, G. Amplified Electrochemical Detection of MecA Gene in Methicillin-Resistant *Staphylococcus aureus* Based on Target Recycling Amplification and Isothermal Strand-Displacement Polymerization Reaction. Sens Actuators B Chem 2015, 221, 148−154. 10.1016/j.snb.2015.06.057]. Copyright [2015] [Elsevier B.V. All rights reserved].

Riyadh Abdulmalek Hassan et al. have recently created an innovative electrochemical biosensor to identify carrageenan. They achieved this by immobilizing calf thymus dsDNA on a carbon-based solid-phase extraction (SPE) and employing the redox indicator methylene blue.[481] The measurement technique employed was differential pulse voltammetry (DPV), and the determined limit of detection was 0.08 mg/L. Figure 44 depicts the competitive electrostatic interaction between dsDNA and carrageenan in their conjugation with methylene blue. It also shows the electrical setup of the DNA device utilized in this research study.[481] Despite the high specificity, quick analysis, and multianalyte detection ability of DNA sensors, their significant drawback is in the deteriorating nature of DNA, which necessitates particle analysis and specialized storage settings.

2.2.2.3. Enzymes-Based Biosensor. Enzyme-based biosensors are readily available and more stable than DNA biosensors.[462] Developing an enzyme-based biosensor offers advantages such as the production of biocompatible and reusable byproducts, as well as the ability to catalyze specific reactions.[482] However, high temperatures can negatively impact stability by causing enzyme denaturation, resulting in poor performance.[462] Various physical factors, including pH, presence of chemical inhibitors, solvent polarity, ionic strength, and temperature, can affect the performance of an enzyme sensor.[462] Technological advancements such as site-directed mutagenesis, chemical modifications, and recombinant DNA technology can enhance enzyme stability.[482] Figure 45 illustrates the timeline classification of enzyme-based biosensors,[101] while Figure 46 depicts the enzyme-labeled indirect detection of antigen and antibody.[483]

The preceding segments of the classification within the transducer category encompassed various biosensors that are dependent on enzymes. Hence, the subsequent article offers a succinct summary of enzyme biosensors that rely on graphene. Using graphene as a substrate for enzyme-based biosensors has numerous advantages, including

- higher stability,
- improved enzymatic activity,
- superior immobilization of enzymes, and direct electron transmission between electrodes and enzymes.[484]

Out of the immobilization methods stated before, direct physical adsorption without the use of chemicals is considered the best option for attaching enzymes to the surface of graphene.[462]

Mechanisms of electrochemical enzyme biosensor[485]

1) Based on the catalytic properties of enzymes, i.e., undetectable form to detectable form of analyte.
2) Based on enzyme activity, i.e., inhibition or moderation.

The laccase and horse radish peroxidase (HRP) enzymes are widely utilized in the biosensor business because of their versatility and cost-effectiveness.[462] Enzymes can be immobilized using a combination of reduced graphene oxide (rGO) and a magnetic Fe_3O_4 substrate, resulting in improved sensitivity.[486] In a study by Filip et al., they immobilized bilirubin oxidase on a graphene oxide (GO) substrate to identify aberrations in liver function.[487] Glucose sensors utilizing glucose oxidase (GOx) are widely prevalent in the industry. Feng and his colleagues developed a detector using a composite substrate of graphene and polyaniline. This detector achieved a detection range of 10 μM−1.48 Mm.[488]

2.2.2.4. Phage Sensor. A "bacteriophage" is a type of virus that specifically infects harmful bacteria cells and inhibits their reproduction, ultimately causing their destruction through lysis. Figure 47 depicts the mechanism of action of a bacteriophage.

Bacteriophage-based biosensors are rapidly emerging as a promising sensor option for the particular detection of pathogens.[490,491] According to Lu et al., the combination of phage cocktails or collections of phage-derived recognition proteins can be utilized to precisely target pathogenic bacteria.[492] Richter confirmed the effectiveness of targeting a specific strain of pathogen using a specific bacteriophage.[493] Bioprobes can range from whole phage probes to phage display peptide (PDP) probes to the more recently developed receptor binding proteins (RBP) from phage probes.[494] Srivastava and colleagues created a sensor capable of detecting bacteria. The sensor has a limit of detection (LOD) of 100 CFU/mL. This was achieved by immobilizing the T4 phage on a modified Si/Ag film/glutaraldehyde/4-aminothiophenol substrate.[495] The transduction approach they employed was SERS technology. Horikawa et al. conducted research using the E2 phage to detect strains of *Salmonella enterica* ser and *Salmonella typhimurium*. They employed magnetoelastic transduction techniques for this purpose.[491]

Ullah et al. found that the presence of functional groups like carboxyl, hydroxyl, and aldehyde on the surface of bacteriophages allows them to interact with various protein groups on the surface of the analyte cell. These functional groups also assist in immobilizing the bacteriophages on the substrate surface.[496]

https://doi.org/10.1021/acsomega.4c07991
ACS Omega 2024, 9, 48918−48987

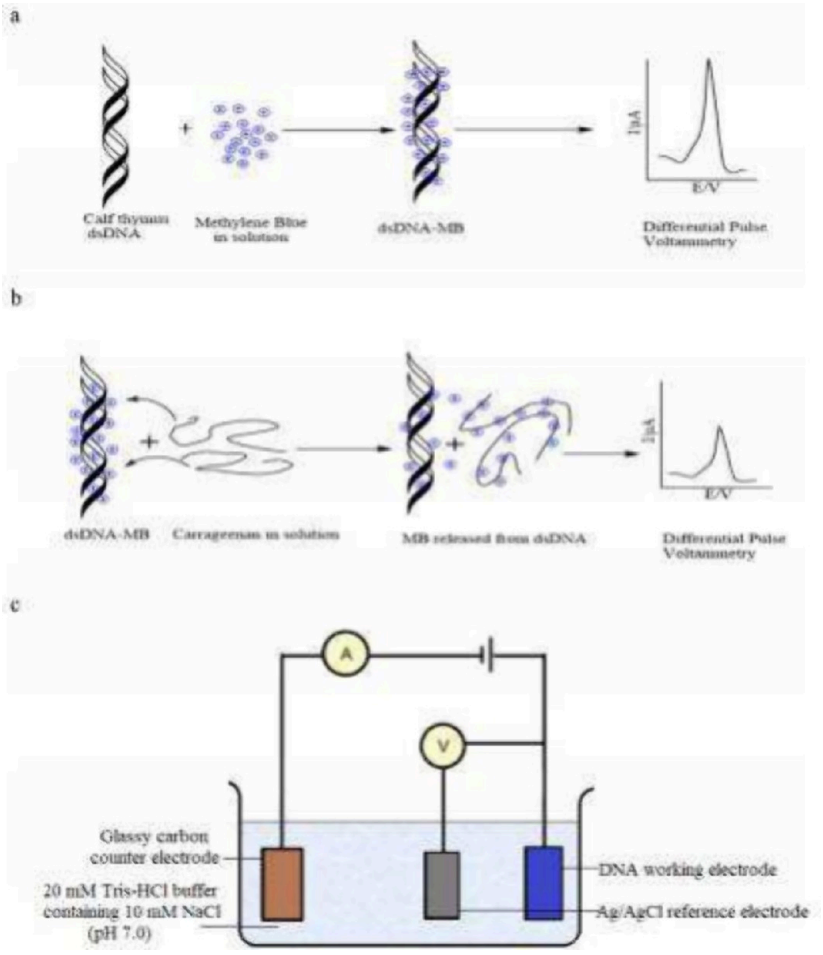

Figure 44. Schematic illustration of competitive electrostatic interaction of dsDNA and carrageenan toward binding with methylene blue. (a) High DPV signal obtained after accumulation of MB in the dsDNA. (b) Lower DPV signal generated after immersion of the dsDNA electrode in the carrageenan solution. (c) The experimental setup of the three-electrode system consists of a carbon SPE working electrode, an Ag/AgCl reference electrode, and a glassy carbon counter electrode[481] [Reprinted with permission from [Hassan, R. A.; Heng, L. Y.; Tan, L. L. Novel DNA Biosensor for Direct Determination of Carrageenan. Sci Rep 2019, 9 (1), 6379. 10.1038/s41598-019-42757-y]. Copyright [2019] [www.nature.com/scientificreports/].

Anany et al. stated that to immobilize the phage systemically, the substrate surface should be functionalized with positively charged groups. This is because the head of the phage carries a net negative charge, allowing the positively charged tail portion to bind to the receptors on the target bacteria.[497] Different methods, including laser printing, adsorption, and inkjet, for the immobilization of phages on paper strips are also available. Fernandes and his colleagues devised a magneto-resistive phage sensor by fixing phage onto gold nanoparticles.[498] Figure 48 illustrates a schematic representation of how an impedimetric phage sensor operates.[499]

Rajnovic et al. have recently created a detection system that has a limit of detection (LOD) of 108 pfu/mL. This technique relies on the significant reduction in optical density resulting from cell lysis. The researchers tested over 90 distinct combinations of bacteria and phage concentrations.[500] Merwe et al. provide a comprehensive overview of bacterial detection methods utilizing phages in their brief review.[501] Gizem Ertürk et al. have created a new type of biosensor called a molecularly imprinted capacitive biosensor for detecting phages. This biosensor is capable of quickly and accurately detecting phages in river water, allowing for real-time monitoring of contamination levels.[502]

2.2.2.5. Cell-Based Biosensors. Biosensors utilizing antibodies, DNA, and similar components are indeed costly, as previously mentioned. An economical approach to biosensor development involves utilizing the cell itself as the biorecognition element. The reasons for this are as follows:[503]

1) Cells can reproduce themselves and produce elements like antibodies without the need for additional processes to purify the antibodies.
2) They can provide insights into the feasibility of the analyte.
3) Optimal cell biorecognition elements, such as E.Coli, possess the ability to be modified through genetic engineering and can be cultivated with ease.

Cell detectors have been developed to identify the presence of metabolites[504] and hazardous compounds in urine,[505] as well as nitrogen oxides in serum and urine.[506] Cell-based biosensors are limited by their reliance on intracellular interaction with analytes.[507] The utilization of both surface display technology and antibody engineering will facilitate the identification of extracellular analytes.[503] The study conducted by Kylilis et al. involved the creation of a biological alternative to the Latex Agglutination Test (LAT). They achieved this by utilizing *E. coli* with a surface display of single domain antibodies (nanobodies)

https://doi.org/10.1021/acsomega.4c07991
ACS Omega 2024, 9, 48918−48987

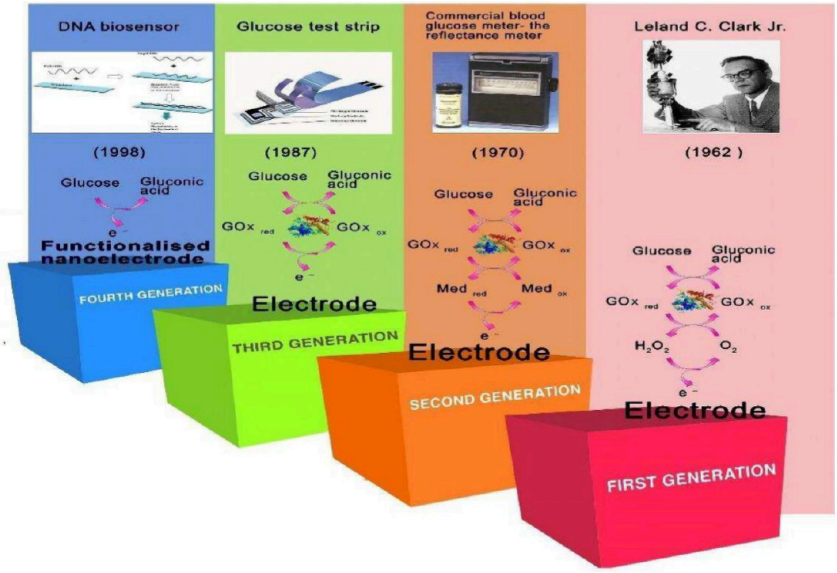

Figure 45. Chronological classification of enzyme-based biosensors[101] [Reprinted with permission from Sumitha, M. S.; Xavier, T. S. Recent Advances in Electrochemical Biosensors − A Brief Review. Hybrid Advances 2023, 2, 100023. 10.1016/j.hybadv.2023.100023]. Copyright [2023] [Sumitha M S, Xavier T S. Elsevier B.V.].

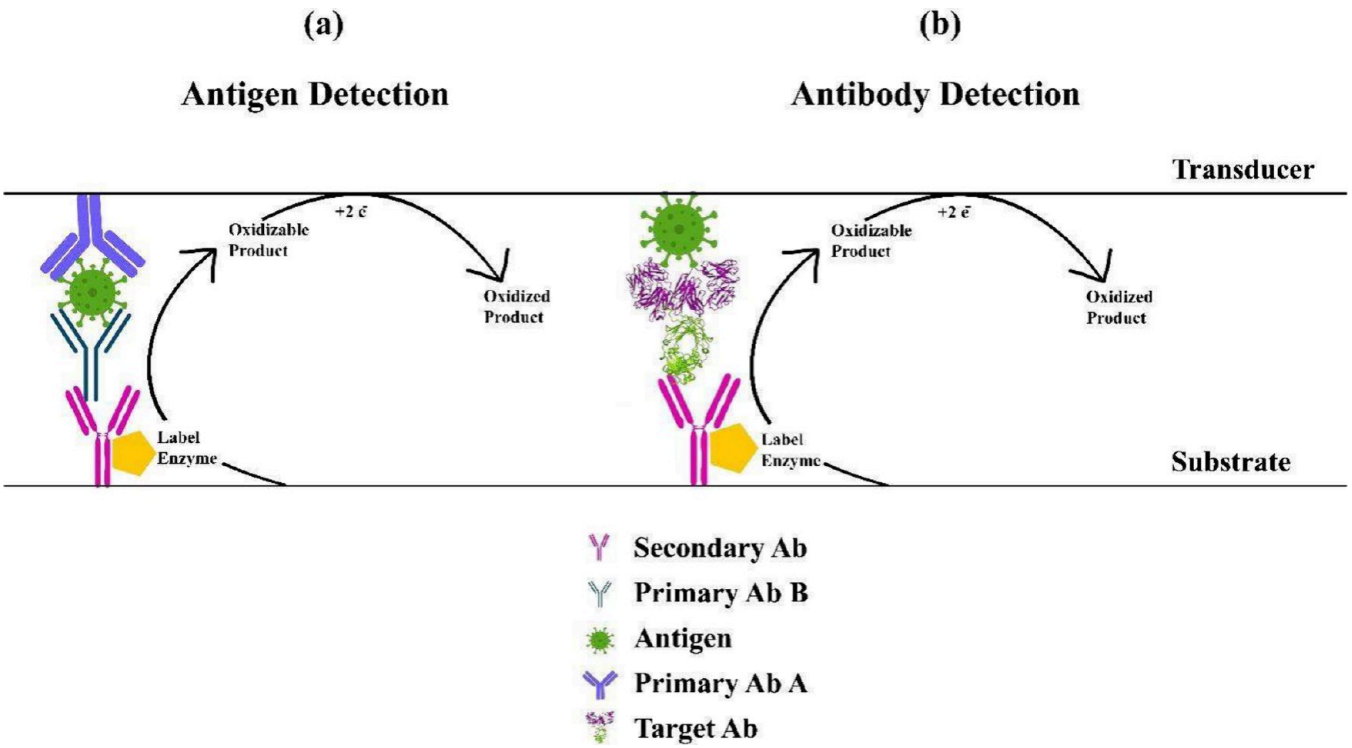

Figure 46. Schematic representation of the configuration of enzyme-labeled biosensors for the detection of (a) antigen and (b) antibody.

as the component that performs biorecognition.[503] The nanobodies were chemically bonded to a paired dimeric GFP analyte, and the limit of detection (LOD) was mainly influenced by the overall quantity of nanobodies available. The device was created as a comprehensive cell biosensor designed to detect the human fibrinogen (hFIb) factor, a well-established biomarker for cardiovascular disease. This sensor device, which detects extracellular proteins, is cost-effective and does not necessitate the transcription or translation of the reporter protein.[503] Wong et al. have created a cell-based biosensor using Anabaena torulosa to detect heavy metals.[508] The bacteria adhered to cellulose by the process of filtering. The measurement was conducted using optical fiber technology. The lower limit of detection (LLD) for heavy metals and pesticides ranged from 0.025 to 1.195 μg/L.

Electrical cell-substrate impedance sensing (ECIS) and light addressable potentiometric sensors, along with fluorescent imaging, are commonly used methods for transduction and detection in the fabrication of mammalian cell biosensors.[559] Electrochemical impedance sensing (EIS) platforms are highly regarded in the advancement of whole-cell biosensors. This is because they

https://doi.org/10.1021/acsomega.4c07991
ACS Omega 2024, 9, 48918−48987

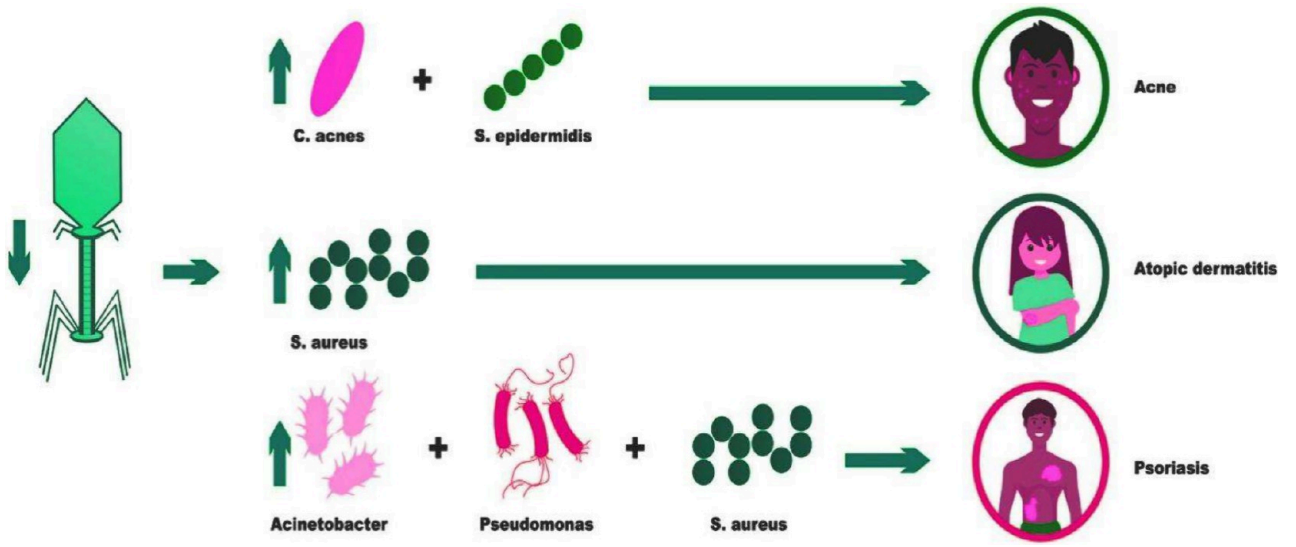

Figure 47. Influence of phage deficiency in acne, atopic dermatitis, and psoriasis[489] [Reprinted with permission from Natarelli, N.; Gahoonia, N.; Sivamani, R. K. Bacteriophages and the Microbiome in Dermatology: The Role of the Phageome and a Potential Therapeutic Strategy. Int J Mol Sci 2023, 24 (3). 10.3390/ijms24032695]. Copyright [2023] [Natarelli et al. Licensee MDPI, Basel, Switzerland].

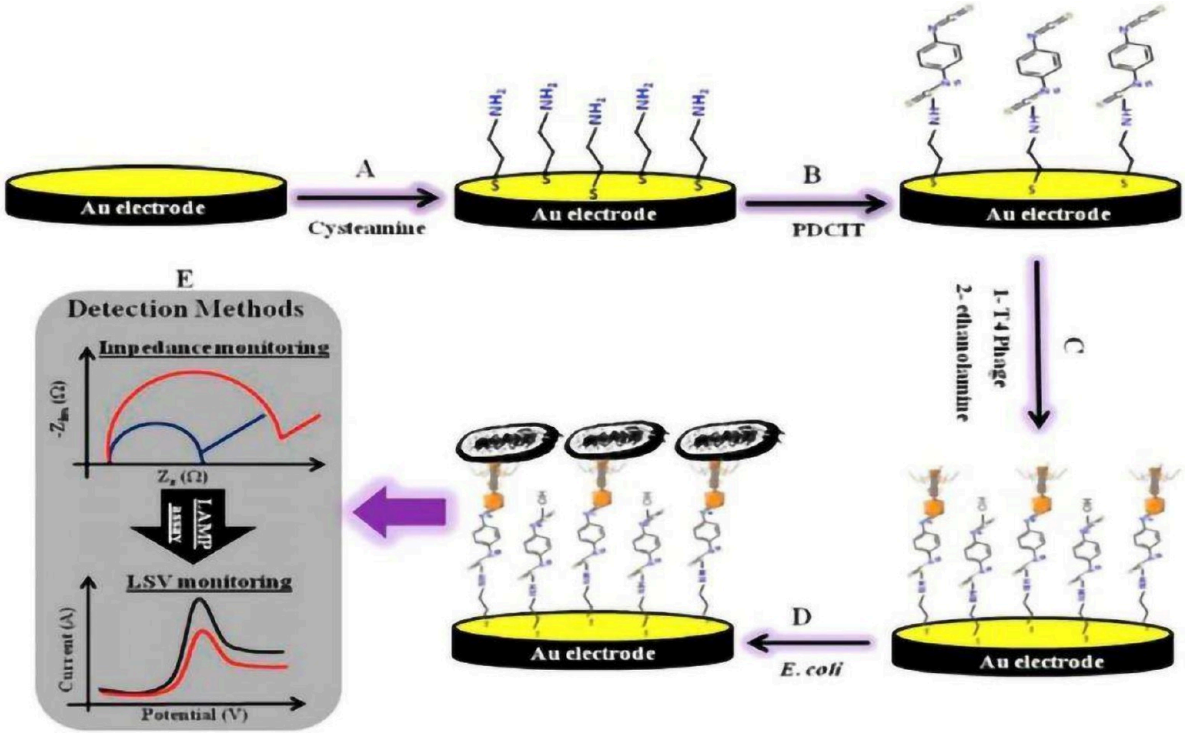

Figure 48. Schematic illustration of impedimetric biosensor based on T4-phage. (A) Cysteamine is assembled on a gold electrode. (B) Stimulation by cross-linker, i.e., 1,4-dithiocyanate (PDICT). (C) T4 phage immobilization and blocking with the addition of ethanolamine. (D) *E. coli* cells capturing. (E) *E. coli* cell detection, based on impedimetric /LAMP dual-response[499] [Reprinted with permission from [Tlili, C.; Sokullu, E.; Safavieh, M.; Tolba, M.; Ahmed, M. U.; Zourob, M. Bacteria Screening, Viability, And Confirmation Assays Using Bacteriophage-Impedimetric/Loop-Mediated Isothermal Amplification Dual-Response Biosensors. Anal. Chem 2013, 85 (10), 4893−4901. 10.1021/ac302699x]. Copyright [2013] [American Chemical Society].

- can monitor cell-substrate interaction without the need for labels;
- can assess various aspects [attachment, spreading, motility, growth, proliferation, cell-to-cell interactions, the metabolic and electrophysiological status].

In addition, various techniques for measuring impedance at specific locations have been created and utilized to study specific properties of samples in complex heterogeneous structures or mixtures, as well as in cell and particle research. These techniques include electrical impedance tomography, scanning electrochemical microscopy, and microelectrode arrays.[509] The development of mammalian-cell-based devices for monitoring and modulating physiological processes in humans is a promising and rising area in therapeutic synthetic biology.

https://doi.org/10.1021/acsomega.4c07991
ACS Omega 2024, 9, 48918−48987

2.2.2.6. Biomimetic Biosensor. Aptamers are short chains of nucleotides or peptides, typically consisting of around 40 bases, that have a high degree of specificity for particular target molecules. They are chosen from a sizable pool of randomly generated sequences. Riboswitches contain endogenous aptamers. An electrochemical biosensor that generates an electrochemical signal in response to the interaction between an analyte and an aptamer is referred to as an E-AB (electrochemical aptamer based) biosensor. These biosensors offer advantages over other aptamer-based biosensors, such as fluorescence aptamer biosensors, as they enable real-time in vivo measurements. The efficiency is contingent upon the aforementioned criteria

1) Density packing of DNA/RNA
2) Nature of Self-Assembled Monolayer
3) Potentiostat frequency

Figure 49 schematically illustrates two types of aptamer biosensor.[510]

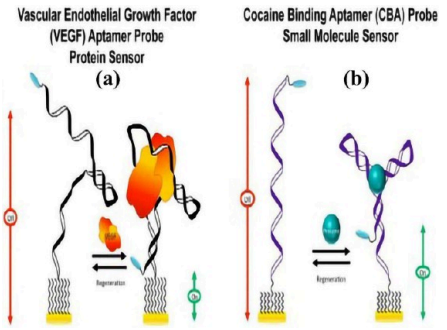

Figure 49. (a) VEGF detecting aptamer E-AB biosensor. On target attachment, the partially unfolded aptamer probe folds completely resulting in a closed structure and the variation in the electron transfer kinetics leads to an elevated MB current (b) An aptamer cocaine detector. Here before the target binding, the aptamer probe is fully or partially extended and once the target binds with the aptamer it kind of forms a "three-way junction", which will alter the electron transfer kinetics and the output current[510] [Reprinted with permission from [Rebecca Lai, Research Area 1: Biosensor Design | The Lai Lab. http://chemweb.unl.edu/lai/research-area-one-biosensor-design/ (accessed 2024−10−18)] [Department of Chemistry | Hamilton Hall 651| University of Nebraska-Lincoln | Lincoln, NE 68588 | 402−472−5340].

A molecularly imprinted substrate is a synthetic polymer material with chemically active and particular recognition sites that mimic the natural biorecognition elements. It is utilized for the detection of different bioanalytes.[511,512] Molecular imprinting is a process where a monomer is polymerized along with an analyte within a template.[513] The elimination of the template results in the presence of distinct binding sites in the product, leading to the formation of molecularly imprinted polymers (MIPs).[513] The adaptability of MIPs allows for their development with nearly all biomolecules, making them an ideal choice in the field of sensors. Vera L. V. Granado et al. provided a comprehensive analysis of the fabrication techniques for potentiometric and amperometric MIP-based biosensors. Electropolymerization was used to deposit a conducting polymer on the electrode, which included spherical MIP particles with a diameter of 1 μm.[513] Table 8 gives a brief consolidated comparison of various transduction techniques used for various bioanalytes.

Table 8. Transduction Techniques Used for Various Biological Elements

Electrode/biorecognition element	Analyte	Transduction technique	Ref
Antibody	HIV-1 virion infectivity factor	Piezoelectric	514
Antibody	*Listeria monocytogenes*	Electrochemical	515
Antibody	Entamoeba histolytica antigens	Amperometric	516
Antiadenovirus, Group II (HEV) polyclonal antibody	Adenovirus	Optoelectronic	517
Anti-CT	Cholera toxin	SPR	518
Anti-HIV-1 gp120 antibody	HIV	Fluorescence	519
Cy3 Ab	Alzheimer disease	SERS	520
Horse polyclonal anti-SARS-CoV [C]	SARS-associated coronavirus (SARS-CoV)	piezoelectric	521
GO probe functionalized with DNA	ssDNA	FRET	522
GO-DNA	*Staphylococcus aureus* DNA	Fluorescence	523
GO/pencil graphite electrode (GO/PGE)+DNA (HBV)	Hepatitis B virus	Electrochemical	524
Graphene/Au+DNA	BRCA1 DNA	Electrochemical	525
Graphene−Nafon composite film+DNA	ssDNA of HIV-1 gene	Impedimetric	526
Laccase	Caffeic acid	electrochemical	527
HRP	H_2O_2	Electrochemical	528
S. aureus phage St.au9IVS5 (displaying peptide RVRSAPSSS)	*S. aureus*	Fluorescent Microscopy	529
Phage for *P. aeruginosa*	*P. aeruginosa*	Raman	530
S. arlettae specific phages	*S. arlettae*	EIS	531
B1−7064 Phage	*Bacillus cereus*	Amperometric	532
AT20	*E. coli* G2−2	Bioluminescence	533

2.2.3. MEMS Based. Li et al. investigated the development of advanced electrical connections for two-dimensional semiconductors, focusing on monolayer molybdenum disulfide (MoS_2). The authors achieve a notable improvement by hybridizing MoS_2 with semimetallic antimony, reducing contact resistance to 42 ohm-micrometers while preserving stability at 125 °C. This approach provides significant improvements in transistor performance, surpassing current silicon-based technologies, and has possibilities for scalable next-generation electronics.[534]

A category of devices called microelectromechanical systems (MEMS) has emerged as a result of the remarkable progress made in the miniaturization of electronics.[535] MEMS devices are extensively employed for many purposes and are succinctly classified in Figure 50. Transducers, specifically sensors or actuators, are the most prevalent form of MEMS. They are capable of converting one signal type into another signal type. Alternatively, they can be fabricated as cantilever or string configurations, which correspond to structures resembling single- or double-clamped beams, respectively. The operation of MEMS devices relies on energy transduction, which facilitates the passage of information from the sensing unit to the controller. The controller then uses a control algorithm to make decisions and then sends commands to the actuation unit. The advantages and challenges faced by MEMS devices are listed below in Table 9.

In the field of medicine and healthcare, MEMS devices also referred to as bio micro electromechanical systems (BioMEMS), micro total analysis systems (μTAS). Lab-on-chips (LoCs), or

https://doi.org/10.1021/acsomega.4c07991
ACS Omega 2024, 9, 48918−48987

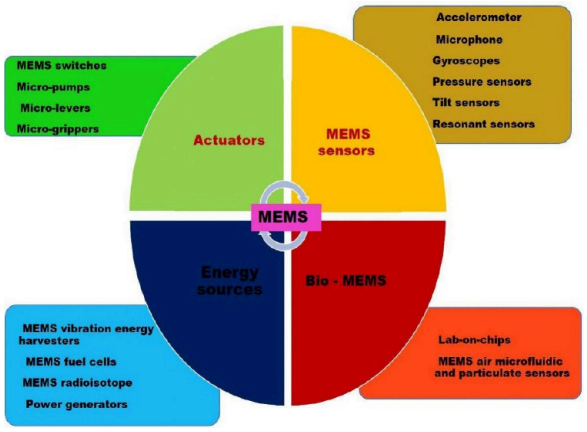

Figure 50. MEMS classifications and uses.

Table 9. Advantages and Disadvantages or Challenges of MEMS Devices

Advantages	Disadvantages/challenges
Low power consumption	Due to the small size significant power transfer is not possible
Lightweight	The base material cannot be loaded with a large load
Ease of integration	Design standards are not well-developed
High performance in wearable electronics	Complex thermo mechanical behaviors
High resonant frequency	Complex motion controls
Low cost (due to bulk production)	Expensive materials
High sensitivity	Some reliability issues
High accuracy	Temperature-dependent effects
New career opportunities	Low operational speed, contamination, break/crack possibility, and poor fatigue properties

biochips, have the potential to be used in various applications such as drug synthesis, drug delivery, microsurgery, micro therapy, diagnostics and prevention, artificial organs, genome synthesis and sequencing, and cell manipulation and characterization too.[535] This is schematically represented in Figure 51.

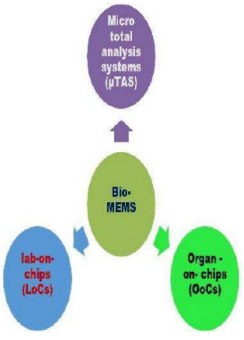

Figure 51. Schematic diagram of MEMS in biology.

MEMS devices are made mostly of silicon and silicon compounds, like integrated circuits.[536] The field considers doped single crystalline silicon and polycrystalline silicon (polysilicon) as representative materials due to their unique properties, such as strength, conductivity, resilience, robustness, reliability, easy processing, process reproducibility, and low unit costs.[537] Silicon dioxide can be utilized for insulation, passivation, and sacrificial purposes, while silicon nitride can be used for insulation.[538] Even though silicon is abundant in nature, its expanding functionality and complexity have made it insufficient for MEMS and demand the incorporation of new materials such as single-crystal silicon carbide, germanium-based materials, metals, metal nanocomposites, and polymers. Photolithography, oxidation, sputtering, thin layer deposition, and other well-known micromachining processes utilized in the integrated circuit domain have been employed to produce MEMS/Bio-MEMS devices. Both surface micromachining and bulk micromachining are extensively utilized in microfabrication.

2.2.3.1. Bulk Micromachining. Bulk micromachining is a process that includes selectively etching or removing material from the bulk substrate to create MEMS devices. By selectively removing excess material, it is possible to create microelectromechanical systems (MEMS) components such as beams, cantilevers, and membranes. The elimination of the majority of the material can be accomplished by wet/dry chemical techniques or physical techniques. A frequently employed technique is chemical wet/dry etching, in which a reactive chemical, either in a wet or dry state, selectively removes the exposed areas of the bulk material. Chemical wet etching is advantageous when a rapid etch rate is necessary. Dry etching is advantageous for creating structures with high aspect ratios and complex geometries that cannot be achieved with wet etching procedures.[539] The drawbacks of bulk micromachining include difficulties in controlling the etch depth over time throughout the substrate due to variations in the diffusion of etchant species, etchant aging, loading effects, and variations in substrate thickness. Furthermore, devices that do not require electronics to be connected with MEMS devices will find bulk micromachining to be economically inefficient.[539]

2.2.3.2. Surface Micromachining. The technique of surface micromachining entails depositing and creating a mechanically supportive layer, known as the "sacrificial layer", on the substrate. This is followed by depositing and creating thin films, referred to as the "structural layers", on top of the sacrificial layer. Upon finishing the fabrication process, the sacrificial layer is specifically removed, resulting in the liberation of the movable micromechanical devices from the substrate.[539] Figure 52 depicts the fabrication processes in surface micromachining.

The primary benefit of surface micromachining is that it allows for the creation of structures with much lower dimensions compared to bulk micromachining. Additionally, surface micromachined devices can be easily integrated with electronic components. Polymeric devices offer distinct advantages over silicon devices considering bio-MEMS. These advantages include their biocompatibility, the ability to tune the surface groups for different applications, the feasibility of creating complex 3-D structures, and cost-effective fabrication processes. Figure 53 schematically shows the various classifications of polymeric device fabrication techniques.

Biosensing and biomolecule immobilization on nanogold substrates were covered earlier. Silicon oxide and nitride, CMOS-compatible materials, are commonly employed in MEMS/Bio-MEMS structures. In cantilever structures and BIOFETs, silicon nitride/oxide serves as structural layers or dielectrics. Immobilization techniques for binding biomolecules on these layers are highly relevant. Silicon nitride sheets are nonporous and uncharged, preventing biomolecule attachment via electrostatic or physical adsorption. Silanization with head groups such as NH_2, COOH, and CHO is a common approach for modifying silicon oxide and nitride surfaces Plasma and

https://doi.org/10.1021/acsomega.4c07991
ACS Omega 2024, 9, 48918−48987

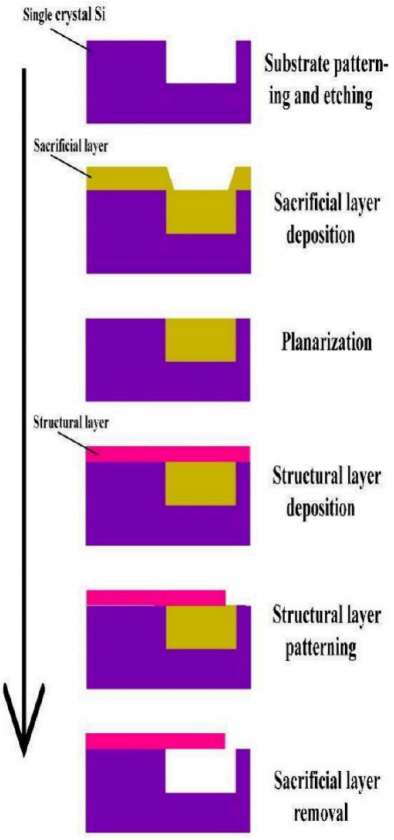

Figure 52. Surface micromachining processes.

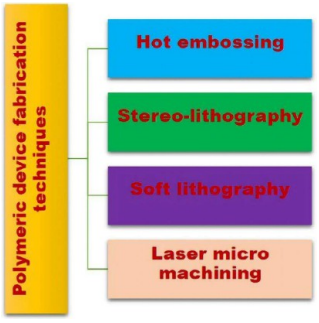

Figure 53. Schematic representation of various polymeric device fabrication techniques.

oxygen create oxynitride, followed by anhydrous silanization. Nonplasma processes are preferred to avoid damage to suspended objects and substrate surfaces from high-energy particles. Acrylic acid vapor treatment at radio frequency plasma leads to the formation of carboxylic groups on silicon nitride surfaces. Silicon oxide surface absorbs water, forming hydroxylated surfaces that can be changed by silane molecules, analogous to silicon nitride. Surface modification is important for biomolecule covalent attachment.[539] A wide range of noninvasive Bio-MEMS technologies and devices have been documented and created. Capacitive or impedimetric sensors are a type of sensor that can be easily integrated into microchannels in a miniaturized configuration. They are also sensitive enough to detect molecules in a sample volume of nano- or microliters.

The creation of microphysiological systems has advanced through the combined progress in microsystems engineering, tissue engineering, and stem cell biology. Consequently, numerous designs for microscale culture systems have been created to recreate tissue and organ functioning at unprecedented levels. There are two main approaches to developing micro physiological systems to better mimic biological processes: (1) creating 3D culture systems with more complex structures, and (2) engineering microfluidic 3D culture devices that include dynamic fluid flow, known as organ chips (organ-on-a-chip).[540]

Through micropump perfusion, microfluidics allows for the dynamic growth of cells and the timely discharge of waste and nutrition. The cellular milieu in which cells reside is more akin to in vivo settings than static culture. Furthermore, the application of fluid shear stress results in the development of organ polarity.[541] Crucially, the chip applies essential physical force to the regular biological processes of endothelial cells by triggering cell surface chemicals and related signaling cascades. Furthermore, the inclusion of fluid in the organs on a chip device enables biological evaluations to be conducted at the individual organ level.[542] The chip system may summarize fluid flow using either a simple "rocker" motion on a chip or a more complex programmable "pulsatile" format.[543] The fluid predominantly functions as a laminar flow at the microscale level, creating a steady gradient of biological molecules that are controlled in both space and time. Biological events, such as angiogenesis, invasion, and migration, involve different biochemical signals that are influenced by concentration gradients.[543] By adjusting flow velocity and channel shape with the use of microvalves and micropumps, microfluidics mimics intricate physiological processes seen in the human body and creates stable, 3D gradients of biochemical concentration. Typical physiological pressures experienced in daily life include arterial pressure, pulmonary pressure, and skeletal pressure. The pressures mentioned are crucial for the maintenance of mechanically strained tissues, including skeletal muscle, bone, cartilage, and blood vessels.[544] Microfluidics utilize elastic porous membranes to generate periodic mechanical stresses. Mechanical stimulation is recognized as a crucial factor in determining differentiation throughout physiological processes.[545] A complex and well-organized arrangement of several cells is necessary for the human body's organization to generate functional whole-body connections. Cell patterning is controlled using microfluidics to create intricately geometrized in vitro physiological models. Surface alterations, templates, and 3D printing aid in the process of arranging cells on the chip. The utilization of the 3D printing technique allows for the creation of hydrogel scaffolds that possess intricate pathways, hence facilitating the patterning of cells at several scales. 3D printing offers the benefit of enabling user-defined digital masks, which allows for versatility in cell patterns. This versatility is crucial for reconstructing the cellular milieu in vitro.[543] Li et al. devised techniques to achieve the fast arrangement of different types of cells on glass chips through controlled manipulation of their spatial arrangement.[546] This process involves continuously seeding cells on a glass chip while also covering it with polyvinyl acetate and ablation with a carbon dioxide laser. This technique facilitates regulated interactions between epithelial and mesenchymal cells. Furthermore, it is possible to arrange mesenchymal cells with comparable characteristics on glass chips. This technique is beneficial for doing extensive research and pharmaceutical experiments on the interaction between skin epithelial and mesenchymal cells. It can also be used to create patterns in other types of cells. Thus, the critical elements influencing in vitro organ culture are cell

https://doi.org/10.1021/acsomega.4c07991
ACS Omega 2024, 9, 48918−48987

patterning, gradient concentration, fluid shear force, dynamic mechanical stress, etc.

A continual circulation of media and interactions between tissues is necessary for an assortment of physiological pathways. Organ chips, when used individually, do not accurately capture the intricate nature, functional alterations, and overall integrity of organ function. The "multiorgan-on-a-chip", also known as the "human-on-a-chip",[547] is a device that may create many organs at the same time, which has garnered significant research interest. From two-dimensional cell cultures to animal models and three-dimensional organoids to OOC, technology has evolved to allow more options for applications such as disease models and drug screening. Figure 54 gives the schematic representation of the evolution of the models and the application of OOC.

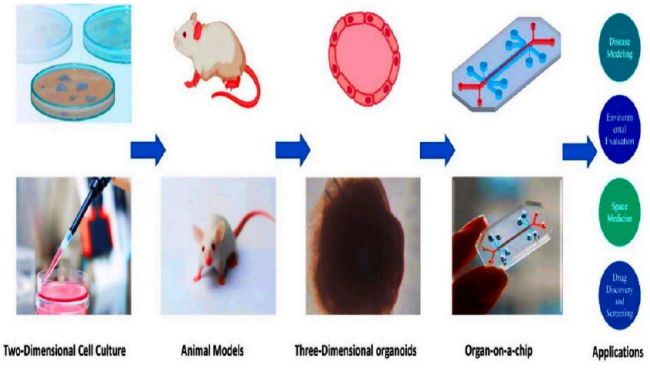

Figure 54. Schematic representation of the evolution of the models and applications of OOC[548] [Reprinted the image with permission fromJiang, L.; Li, Q.; Liang, W.; Du, X.; Yang, Y.; Zhang, Z.; Xu, L.; Zhang, J.; Li, J.; Chen, Z.; Gu, Z. Organ-On-A-Chip Database Revealed—Achieving the Human Avatar in Silicon. Bioengineering 2022, 9 (11). 10.3390/bioengineering9110685]. Copyright [2022] [Jiang etal, Licensee MDPI, Basel, Switzerland].

2.2.4. Based on the Nature of the Substrate Platform. The preceding sections discussed the categorization of biosensors according to the methods of transduction, the components responsible for biorecognition, and the use of microfluidics in the sensor platform. A thorough grasp of the biosensor, including its types, principles, recent research outcomes, etc., can be obtained by performing an additional categorization based on the substrate's nature. Biosensors can be classified into two categories based on the type of substrate: electrospun and paper-based biosensors. These two will discussed briefly in the following sections.

2.2.4.1. Electrospun Biosensors. Electrospinning is a method for manufacturing polymeric nanofibers, which was first developed and patented in the 1930s specifically for textile fiber production.[549] Electrospinning enables the production of nanofibers with diameters ranging from nanometers to micrometers. These nanofibers can be created by using either an electrostatically driven polymer solution or a molten form.[550] Figure 55 illustrates the experimental configuration of the electrospinning device and displays a scanning electron microscope (SEM) image of a nanofiber produced through electrospinning.

The following parameters affect the nature and dimensions of polymeric nanofibers:[552]

1. Polymer and solution parameters (Molecular weight, conductivity, surface tension, viscosity)
2. Process variables (applied voltage, flow rate, collector distance)
3. Environmental conditions (temperature, humidity, auxiliary gas)

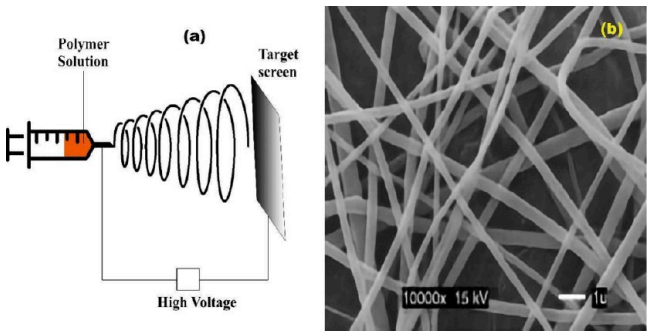

Figure 55. (a) Schematic representation of electrospinning experimental setup (b) electrospun Nylon 6 nanofibers in the form of nonwoven fabric[551] [Reprinted with permission from Fong, H. Electrospun Nylon 6 Nanofiber Reinforced BIS-GMA/TEGDMA Dental Restorative Composite Resins. Polymer (Guildf) 2004, 45 (7), 2427−2432. 10.1016/j.polymer.2004.01.067]. Copyright [2004] [Elsevier Ltd.].

Numerous fields, including tissue engineering, biosensing, energy storage, catalysis, and others, benefit from the use of electrospun fibers due to their well-known large active surface area, porosity, easy functionalizations, and tunability of fiber and pore dimensions.[553,554] Electrospun biosensors outperform other types of sensors in terms of sensitivity, selectivity, and response time due to their distinctive quantum features. The utilization of electrospun nanofibers as biosensors can be categorized into two methods.

1. Direct Use of Electrospun Fibers[555]

- Here functional polymers like PAN, PANI, etc. are electrospun and are directly used as the inducing agents of the respective biosensors
- Simple, fast, multianalyte detection possibility, better biocompatibility, etc.

Indirect Use of Electrospun Fibers [556]

- Here, electrospun nanofibers are template-like, on which further functionalizations are done and are then used as biosensing electrodes.

In 2019, Jeong et al. created a detector for cortisol utilizing N-doped carbon nanofibers, which is based on a field-effect transistor (FET).[557] The substrate transducer layer of the Field-Effect Transistor (FET) consisted of electrospun Polyvinyl Alcohol (PVA) nanofibers embedded with polypyrrole. Carbon nanofibers are renowned for their exceptional electrical conductivity and expansive active surface area.[553] Wang and his team utilized this characteristic and created a detector for levodopa and uric acid. The detector consisted of MoS_2 NSA/CNFs nanofibers as the electrode, which were produced using electrospinning and hydrothermal synthesis.[558] Demiroglu and his colleagues have confirmed that the conductivity of an electrode is increased when it is treated with carbon nanofibers in an acetaminophen-DPV sensor.[559] Wang et al. developed a biosensor using a *Burkholderia cepacia* lipase (BCL)@MOF nanofibrous material (MOF-Metal Organic Nanofiber) to detect the presence of methyl parathion in vegetables. The BCL@MOF nanofibers were attached to the glassy carbon electrode using a chitosan cross-linker. The limit of detection

https://doi.org/10.1021/acsomega.4c07991
ACS Omega 2024, 9, 48918−48987

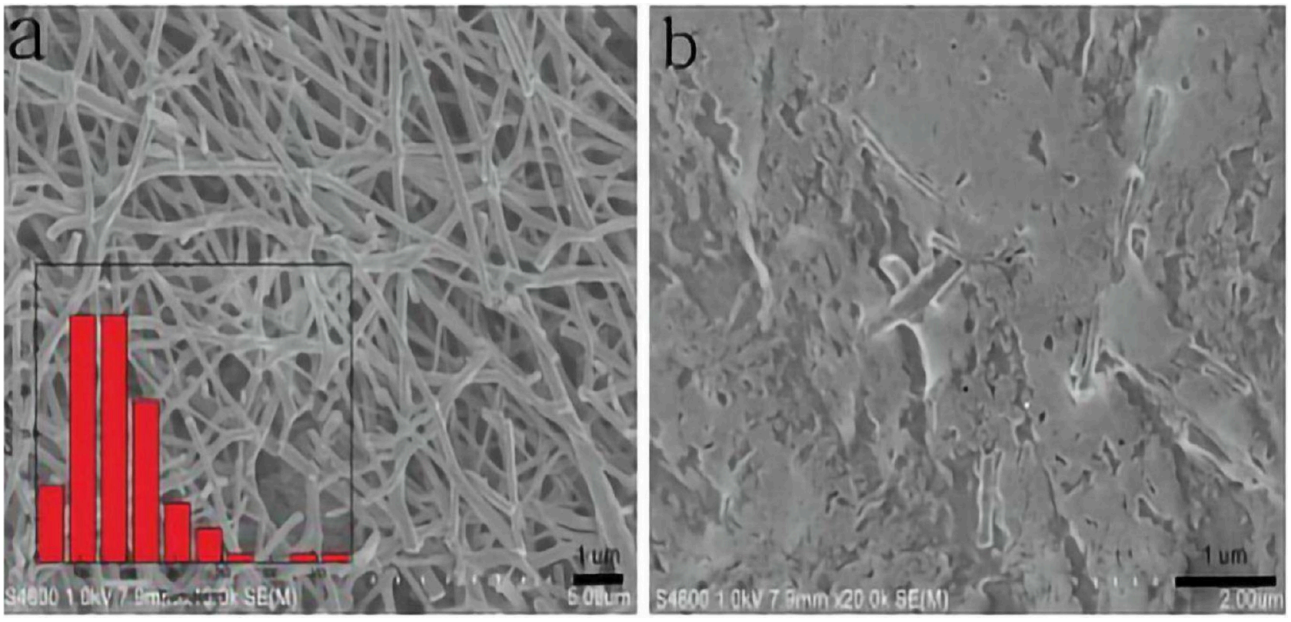

Figure 56. SEM images of the (a) ECNFs and (b) the surface of laccase−Nafion−ECNFs/GCE[563] (Inset: the diameter distribution diagram of the ECNFs) [Reprinted with permission from Li, D.; Pang, Z.; Chen, X.; Luo, L.; Cai, Y.; Wei, Q. A Catechol Biosensor Based on Electrospun Carbon Nanofibers. Beilstein Journal of Nanotechnology 2014, 5, 346−354. 10.3762/bjnano.5.39.]. Copyright [2014] [Li et al; licensee Beilstein-Institut.].

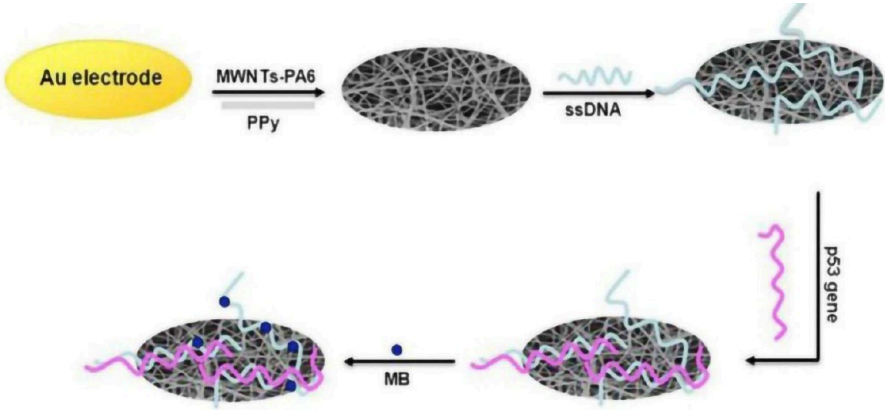

Figure 57. Schematic representation of the preparation of the electrochemical biosensor (MB − methylene blue)[565] [Reprinted with permission from [Wang, X.; Wang, X.; Wang, X.; Chen, F.; Zhu, K.; Xu, Q.; Tang, M. Novel Electrochemical Biosensor Based on Functional Composite Nanofibers for Sensitive Detection of P53 Tumor Suppressor Gene. Anal. Chim Acta 2013, 765, 63−69. 10.1016/j.aca.2012.12.037]. Copyright [2012] [Elsevier B.V.].

(LOD) for this conjugation was 0.067 μM.[560] Salahandish et al. discovered that by enhancing the original electrode with multiple layers of PANI nanofibers, the detection limit and response time for the SK-BR3 breast cancer biomarker were significantly enhanced.[561] Moreover, the QCM biosensor exhibited a significant increase in binding efficiency, reaching a 10-fold improvement, when the gold electrode surface was altered using electrospun bovine serum albumin nanofiber.[562]

Dawei et al. devised an innovative polyphenol biosensor by integrating CNFs, laccase, and Nafion to detect catechol. This biosensor exhibits a detection limit of 0.63 μM with a response time of 2 s.[563] Figure 56 displays the SEM pictures of electrospun carbon nano fiber (ECNFs) and the surface of laccase-Nafion-electrospun carbon nano fibers/glassy carbon electrode. The first photo includes an inset showing the distribution of fiber diameters.

The benefits of electrospun nanofibers for cancer diagnosis and detection are covered by Sahar et al. in their review.[564] Figure 57 depicts a schematic depiction of an electrochemical nanofiber-based biosensor designed for the detection of the p53 gene.[565]

The detection of cancer antigen-CA125 was performed using a unique electrospun nanofiber platform composed of PAN/MWCNT/ZnAc.[566] The antiCa125 antibody was attached to the nanofiber surface utilizing EDC/NHS conjugation. LOD was 1.13 $\times 10^{-3}$ units per milliliter (U/mL). The process is depicted in Figure 58.

Juliana and her colleagues created an immunosensor to detect the pancreatic cancer antigen CA19−9.[567] The immobilization of anti-CA19−9 antibodies occurs within a 3D structure, which is achieved by applying a coating of either multiwalled carbon nanotubes (MWCNTs) or gold nanoparticles (AuNPs) onto electrospun nanofibrous mats composed of polyamide 6 and poly (allylamine hydrochloride). The experiment was conducted utilizing impedance spectroscopy. The limit of detection achieved for MWCNT coating was 1.84 U mL^{-1}, while for Au

https://doi.org/10.1021/acsomega.4c07991
ACS Omega 2024, 9, 48918−48987

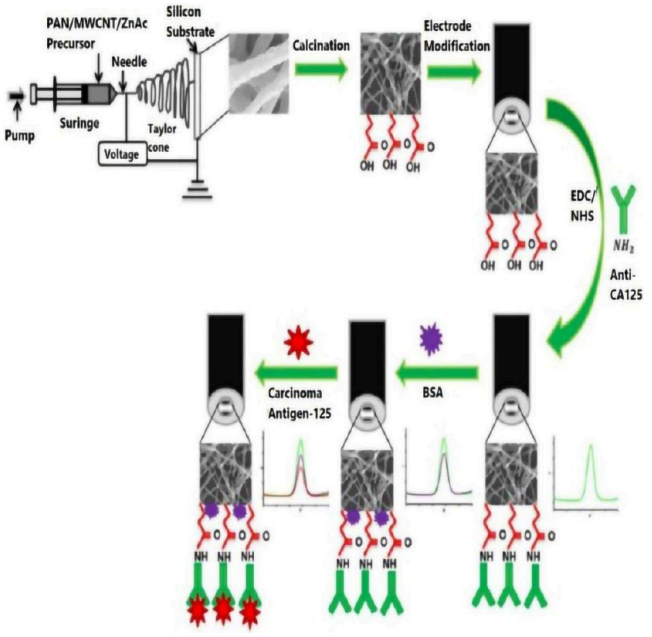

Figure 58. Schematic representation of the fabrication of carcinoma antigen-125 immunosensor[566] [Reprinted with permission from [Paul, K. B.; Singh, V.; Vanjari, S. R. K.; Singh, S. G. One Step Biofunctionalized Electrospun Multiwalled Carbon Nanotubes Embedded Zinc Oxide Nanowire Interface for Highly Sensitive Detection of Carcinoma Antigen-125. Biosens Bioelectron 2017, 88, 144−152. 10.1016/j.bios.2016.07.114]. Copyright [2016] [Elsevier B.V.].

NP it was 1.57 U mL^{-1}.[567] Table 10 presents the LODs of four distinct glucose detectors that are based on electrospun fibers.

Table 10. Electrospun Fiber Sensors for Glucose Detection

Analyte	Transduction technique	Nanofibers/electrode specifications/transducer	LOD (in μM)	Ref
Glucose	Amperometric	L-Cys-GOx/PVA/ZnO NFs/Au electrode	1	568
Glucose	Amperometric	GOx/Mesoporous ECNFs/SPE	-	569
Glucose	Amperometric	MWCNTs/Au NPs/PAN NFs/Au electrode	4	570
Glucose	EIS	Au NPs/GOx-PVA-PEI NFs/Au electrode	0.9	571

2.2.4.2. Paper Based. Point-of-care (POC) devices are what spurred the biosensor industry's extraordinary expansion. These devices are renowned for their user-friendly interface, simplicity in sample manipulation, portability, requirement of minimal sample volume, and cost-effective manufacturing.[572] A paper-based analytical device (PAD) is a POC (point-of-care) device that utilizes cellulose fibers as its primary substrate. It has become increasingly popular in diverse industries.[573] The choice of appropriate paper material is crucial for the optimal functioning of the paper sensor. Table 8 displays the transduction specifics of different paper-based sensors. Whatman brand chromatography paper exhibits favorable flow speed, retention time, and other characteristics, rendering it the highest-rated paper substrate for biosensors.[574] Nitrocellulose possesses functional groups that enable it to covalently bond with the analyte molecule, allowing for its entrapment. These molecules' membranes are extensively utilized in ELISA and AuNP-based sensing platforms.[575] Another often employed type of paper is a biomimetic substrate platform known as bioactive paper. In this case, the biomolecules are attached to the cellulose fiber scaffold either by aldehyde or amide bonding, inkjet printing,[576] or graft copolymerization.[577] Alternative cost-effective solutions for paper-based sensor substrates include glossy paper[578] and paper towel.[579] The new review work by Amrita et al. provides a thorough comparison and discussion of the merits and disadvantages of several paper sensor fabrication processes, including photolithography, inkjet printing, laser cutting, hydrophobic silanization, and origami-kirigami approaches.[574]

Ratajczak and Magdalena Stobiecka provide comprehensive descriptions of diverse paper-based biosensors utilized for the early detection of cancer in their recently accepted review article.[580] The addition of graphene sheets and carbon nanotubes will improve the biosensor's electrical conductivity and catalytic capabilities. In 2018, Ji et al. developed a paper-based immunosensor with a LOD of 1−18 ng/mL for the detection of prostate cancer.[581] On the micropore filter paper, multiwalled carbon nanotubes were applied, followed by functionalization of the paper with PSA antibodies using EDC/NHS conjugation. Subsequently, measurements of relative electrical resistance were conducted. Figure 59 illustrates the operational mechanism of the PSA paper sensor in a diagrammatic manner.

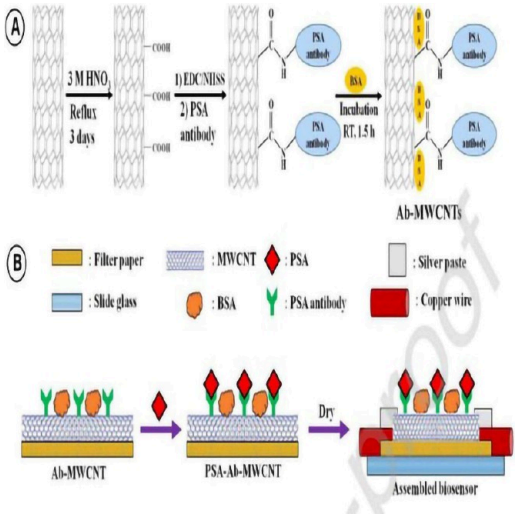

Figure 59. (a) Functionalization of PSA antibody on MWCNT. (b) Steps leading to an assembled biosensor substrate[581] [Reprinted with permission from [Ji, S.; Lee, M.; Kim, D. Detection of Early Stage Prostate Cancer by Using a Simple Carbon Nanotube@paper Biosensor. Biosens Bioelectron 2018, 102, 345−350. 10.1016/j.bios.2017.11.035]. Copyright [2017] [Elsevier B.V.].

Given that cell-labeled sensors have a short shelf life, paper-based sensors without any cell functionalization are becoming more and more popular. Gräwe A and colleagues have created a Fluorescent cell-free paper sensor capable of detecting mercury ions and gamma hydroxybutyrate, a substance commonly used as a date-rape medication. The detection methods employed are straightforward, allowing anyone with a smartphone to access and analyze the results.[582] Figure 60 illustrates the optical detection of a paper sensor using cell-free protein synthesis (CFPS) technology. The sensor is enclosed in a 3D container and measurements are taken using a smartphone.[582]

https://doi.org/10.1021/acsomega.4c07991
ACS Omega 2024, 9, 48918−48987

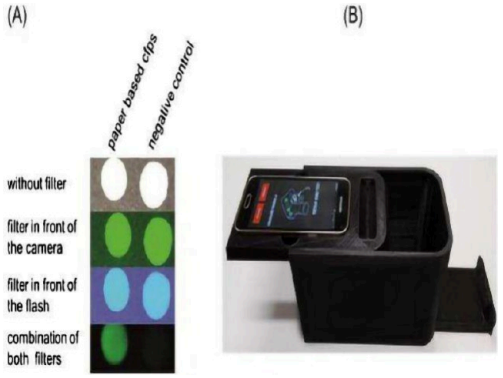

Figure 60. (a) Optical readout with different filter combinations and (b) 3D case and smartphone for bioanalysis[582] [Reprinted with permission from Gräwe, A.; Dreyer, A.; Vornholt, T.; Barteczko, U.; Buchholz, L.; Drews, G.; Ho, U. L.; Jackowski, M. E.; Kracht, M.; Lüders, J.; Bleckwehl, T.; Rositzka, L.; Ruwe, M.; Wittchen, M.; Lutter, P.; Müller, K.; Kalinowski, J. A Paper-Based, Cell-Free Biosensor System for the Detection of Heavy Metals and Date Rape Drugs. PLoS One 2019, 14 (3), e0210940, 10.1371/journal.pone.0210940]. Copyright [2019] [Gräwe et al PLoS One].

Scala-Benuzzi et al. developed a paper-based fluorescent immunosensor to detect ethinylestradiol.[583] The sensor has a limit of detection (LOD) of 0.05 ng L^{-1}.Figure 61 illustrates the

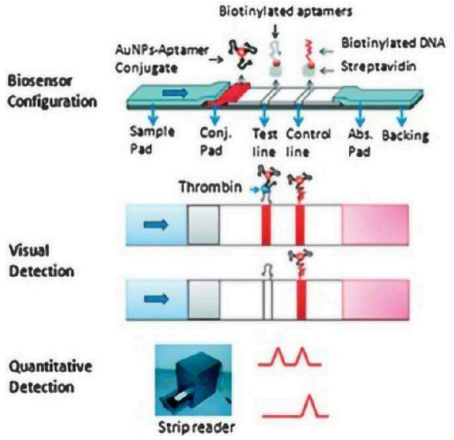

Figure 61. Working configuration of aptamer-based paper strip sensor[584] [Reprinted with permission from [Xu, H.; Mao, X.; Zeng, Q.; Wang, S.; Kawde, A.-N.; Liu, G. Aptamer-Functionalized Gold Nanoparticles as Probes in a Dry-Reagent Strip Biosensor for Protein Analysis. Anal. Chem 2009, 81 (2), 669−675. 10.1021/ac8020592]. Copyright [2008] [American Chemical Society].

configuration and operation of a strip sensor.[584] Mahato and Chandra developed a naked-eye detector for detecting adulterations in milk samples.[585] The detector utilizes the catalytic activity of alkaline phosphatase (ALP) and integrates digital image colorimetry (DIC) with a smartphone for optical readout. ALP antibodies were immobilized on a paper substrate, and the binding of ALP molecules from the sample caused a change in ALP-BCIP (5-bromo-4-chloro 3-indolyl phosphate) activity. The LOD was determined to be 0.87 ± 0.07 U/mL.[585]

Fan and colleagues have created a cellulose paper sensor that is made of pure cellulose and has a screen-printed electrode. This sensor has been modified to include reduced graphene oxide (rGO) to detect the cancer antigen CA125. Figure 62 illustrates the operational setups of a lateral flow nucleic acid biosensor (LFNAB) in a diagrammatic manner.[586] Table 11 presents a summary of various types of paper used in the biosensor field.

3. RECENT RESEARCH WORKS IN BIOSENSORS

The growing field of biosensor technologies for disease detection has garnered significant academic interest, particularly in response to the COVID-19 pandemic. Xi et al. discuss a G-quadruplex-based biosensor, which utilizes the unique G-quadruplex structure identified in the SARS-CoV-2 genome, offering a novel approach for detecting disease-causing viruses.[596] Similarly, Cui et al. analyze various COVID-19 detection methods, emphasizing the use of AI-related, SPR, and SERS-based sensors.[597] Another important development is described in Graphene field-effect transistor biosensor for detection of biotin with ultrahigh sensitivity and specificity by Wang et al., where a graphene-based FET with a detection limit of 90 fg/mL is engineered, exploiting biotin−avidin conjugation chemistry with Cr/Au electrodes.[598] Furthermore, a new probe for DNA sensing and drug delivery is introduced for employing p-nitrophenyl carbonate (NPC), which is highly reactive to amines and offers enhanced optical stability.[599] Neurotransmitter detection is also advanced by Banerjee et al. where various neurotransmitter sensors using CV/FSCV and DPV measurement techniques are reviewed.[600] Additionally, Heredia et al., report a novel method for gold nanoparticle adhesion using starch hydrogels, achieving a detection limit of 25 ng/mL.[601] Ozbeck et al. present a potentiometric PVC membrane-based biosensor that measures concentrations of valproic acid and other ions in blood samples, with a detection limit of 9.75×10^{-7} mol/L for valproic acid.[602] A mathematical modeling of a pH-based potentiometric biosensor for detecting organophosphorus pesticides is explored by Shanti et al., using the Akbari-Ganji approach. They derived analytical expressions for substrate concentrations, with MATLAB employed for simulations.[603] These studies collectively contribute to the expanding research on biosensors for diagnostic and therapeutic applications.

Öndes et al. developed a novel and exceptionally stable urea biosensor utilizing poly(2-hydroxyethyl methacrylate-glycidyl methacrylate) nanoparticles as a nanocarrier for the urease enzyme. An ammonium-selective electrode was used to create the potentiometric urea biosensor, which incorporated urease-immobilized nanoparticles. LOD was 0.77 μM and the response time was 30 s.[604] The study done by Ribeiro et al., introduces a potentiometric biosensor designed for point-of-care analysis that can detect amyloid β-42; which relies on the molecular imprint polymer (MIP) process, where covalently immobilized Aβ-42 is utilized to generate distinct detecting cavities on the surface of SWCNTs. The target peptide was extracted from the polymer matrix through the enzymatic degradation catalyzed by proteinase K. The capacity of the sensing material to reattach to Aβ-42 was exhibited by integrating the MIP material as an electroactive compound in a PVC/plasticizer combination, which was then applied to a solid conductive substrate made of graphite. LOD was found to be 0.72 μg/mL.[605] In the research work done by Bouri et al., a filter paper is coated with Pt and then covered with a Nafion membrane to create a working electrode. The Pt electrode's versatile capability enables the identification of H_2O_2 produced through the oxidation of galactose in the presence of the galactose oxidase enzyme.[606] A bioselective membrane has been developed by Lyudmyla et al., as a potentiometric sensor. The membrane is built on butyryl-cholinesterase and pH-sensitive field-effect transistors (FETs),

https://doi.org/10.1021/acsomega.4c07991
ACS Omega 2024, 9, 48918−48987

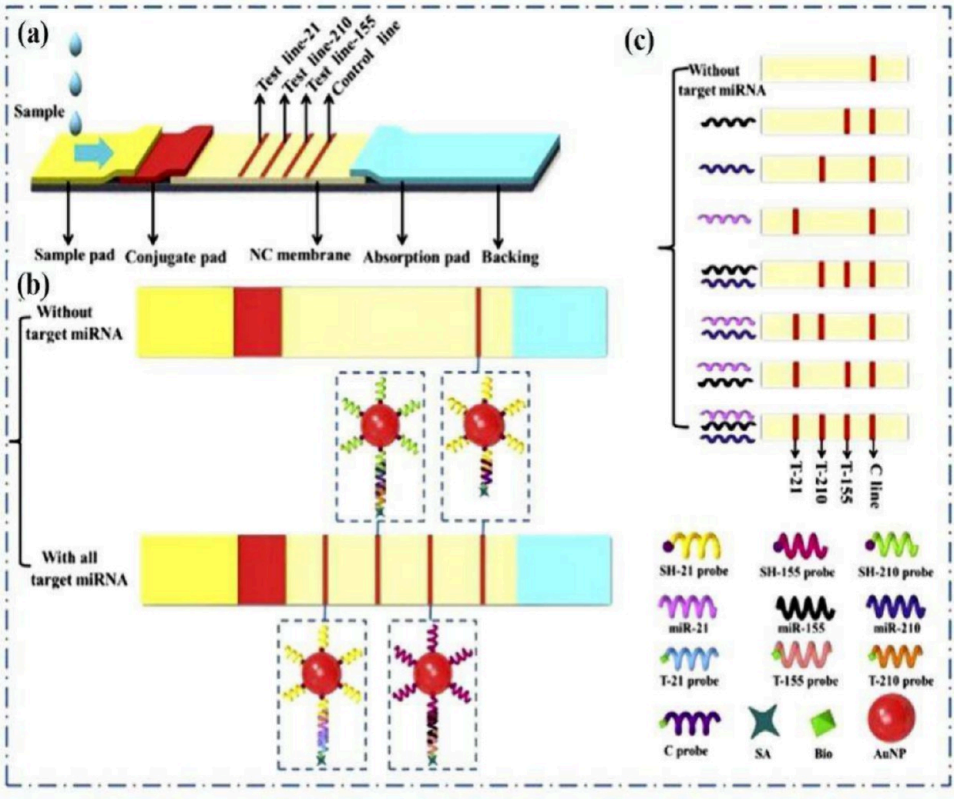

Figure 62. (A) working configuration of lateral flow nucleic acid biosensors (LFNAB); (B) LFNAB action with and without the presence of target microRNA; (C) multiple analyte detection[586] [Reprinted with permission from [Zheng, W.; Yao, L.; Teng, J.; Yan, C.; Qin, P.; Liu, G.; Chen, W. Lateral Flow Test for Visual Detection of Multiple MicroRNAs. Sens Actuators B Chem 2018, 264, 320−326. 10.1016/j.snb.2018.02.159]. Copyright [2018] [Elsevier B.V.].

Table 11. Summary of Various Types of Paper Used in the Biosensor Field

Type of Paper	Analyte	Transduction Techniques	Ref
Whatman RC60 regenerated membrane filter	Bromide, chloride, iodide	CV	587
Whatman No. 1 filter paper	CEA and CA125	DPV	588
Whatman Chromatographic Paper 3 mm	*Staphylococcus aureus*	DPV	589
180 gsm office paper	Hemoglobin	EIS	590
PVDF filter membrane	WBC	CV and DPV	591
Filter paper (102 mm, 15 mm)	Glucose	CV and chrono-amperometric	592
Cellulose acetate filter paper	Small molecules	CV and amperometric	593
Whatman grade 1 chromatic filter paper	Protein	Colorimetric	594
Whatman grade 1 chromatic filter paper	K-562 cell	Electrochemical	595

which have been enhanced with gold nanoparticles (GNPs). The laboratory prototype of the biosensor has a linear range of 0.025−0.2 mM, the lowest limit of detection of 0.018 mM, and a response time of 1.4 min.[607] It is crucial to promptly recognize and monitor topiramate (TOP) medication, which is among the most frequently used anticonvulsant and antiepileptic medications in humans. In this work, Khalifa et al., new molecularly imprinted polymer (MIP) based potentiometric (MIP/PVC/GCE) and voltammetric (MIP/GO/GCE) sensors were created for the sensitive and selective measurement of TOP.[608] An experimental paradigm was utilized, by Soldatkin and colleagues, employing the bioselective components of acetylcholinesterase (AChE), butyrylcholinesterase (BuChE), and glucose oxidase (GOD) in biosensors. The immobilization of enzymes on conductometric transducers' surfaces was achieved through the cross-linking of the respective enzymes using glutaraldehyde.[609]

The biosensor fabricated by Berketa et al. is based on a recombinant arginine deiminase (ADI) enzyme from Mycoplasma hominis, which was synthesized in *Escherichia coli* to detect the presence of L-arginine. The biosensor was created by immobilizing ADI on the sensitive surface of the conductometric transducer's interdigitated electrodes through cross-linking with glutaraldehyde.[610] Zouaoui et al., present the development of a mathematical model to accurately describe and optimize the configuration of the urea biosensor. The biosensor utilizes interdigitated gold microelectrodes that have been modified with a urease enzyme membrane. The presented model specifically emphasizes the enzymatic reaction and diffusion phenomena that take place within the enzyme membrane and the diffusion layer.[611] The conductometric biosensor can specifically identify and measure the levels of two model proteins and samples of the SARS-CoV-2 RBD spike protein variant in real time. It is highly sensitive and capable of detecting concentrations as low as 7 pg/ml within 10 min of sample incubation. The biosensor is equipped with a battery-free, wireless near-field communication (NFC) interface to enable rapid and contactless detection of different strains of SARS-CoV-2. The smartphone's capability to promptly detect and display real-time results for different strains of SARS-CoV-2 can effectively mitigate the spread of the outbreak by promptly

https://doi.org/10.1021/acsomega.4c07991
ACS Omega 2024, 9, 48918−48987

notifying users of their infection status.[612] In the work done by Razmshoar et al., the suggested limit for the discharge of Methanol vapor of the sensor is 200 ppm (ppm); which utilizes alcohol oxidase (AOX) attached to electrospun nanofibers made from a blend of polystyrene and poly(amidoamine) dendritic polymer (PS-PAMAM-ESNFs) on interdigitated electrodes (IDEs). The conductometric sensor exhibits a sensitivity of 150.53 μS.cm^{-1}.[613]

Using glucose as a common analyte, Lui et al., present an amperometric biosensor on a toothbrush. The toothbrush is coated with carbon graphite ink and Ag/AgCl ink, which serve as the sensing electrodes. Subsequently, the enzyme is immobilized. The sensor exhibits exceptional detection capabilities for glucose within a concentration range of 0.18 mM to 5.22 mM and achieves a rapid detection time of under 5 min.[614] L-Lactic acid (LA) is a noteworthy biomarker for the detection of several illnesses, including cancer. Tvorynska et al., fabricated a readily replaceable lactate oxidase (LOx)-based minireactor, positioned in front of a screen printed electrode with silver amalgam and it serves as a transducer with covalently immobilized LOx and filled with mesoporous silica powder (SBA-15). Amperometric detection has excellent operational (93.8% of the initial signal after 350 measurements) and storage (96.9% of the initial biosensor response after 7 months) stability.[615] L-Dopa, a naturally occurring bioactive molecule found in many Leguminosae plants, is the most efficacious pharmacological treatment for alleviating symptoms of Parkinson's disease. Motor difficulties arise due to variations in plasma levels of L-DOPA with the development of the disease. Cembalo et al., present a new amperometric biosensor for detecting L-Dopa. The biosensor utilizes tyrosinase that is cocrosslinked onto a graphene oxide layer created by electrodeposition and the LOD is found to be 0.84 μM.[616]

Jalalvand et al. created an innovative biosensor that utilizes multivariate calibration techniques to accurately measure the levels of triglycerides (TGs) in lyophilized serum samples.[617] (Electrode used: modified glassy carbon electrode). The investigation by Pedersen et al., revealed that the suggested approach for functionalization was appropriate for both the thin films and the majority of the solid-phase extractions (SPEs). The thin-film electrodes provided a precise surface chemistry that was suitable for thiol-based self-assembled monolayer (SAM) formations. Additionally, high-quality SAMs were effectively produced on most of the solid-phase electrodes, allowing for the effective immobilization of antibodies. LOD was determined to be 1.0 ng/mL.[618] Wang et al. present the development of a highly effective, enzyme-free, and uncomplicated biosensor that prevents fouling. The biosensor is based on a self-screened peptide aptamer. The surface of a glassy carbon electrode (GCE) was modified using a polyaniline (PANI) polymer to provide antifouling interfaces. The peptide aptamer, consisting of the amino acid sequence Cys-Pro-Pro-Pro-Pro-Arg-Glu-Asn-Ile-Gln-Arg-Leu-Thr, was attached to the electrode using a cysteine linker that can conduct electricity. The electrode was then used to measure the presence of L-Lys.[619] Paziewska-nowak et al., present a novel impedimetric biosensor that employs a distinctive H2N-(CH2)6−5′[TAGAGGATCAAA-AAA]4TAGAGGATCAAA3′ dsDNA oligonucleotide as a biorecognition element to specifically detect lactoferrin in human saliva. LOD was found to be 1.25 nM.[620] Procalcitonin (PCT) shows great promise as a highly sensitive biomarker for severe inflammation and infection in the early diagnosis of sepsis. The study done by Selimoglu et al. present a biosensor for PCT (procalcitonin) detection that utilizes graphene doped with silver nanoparticles (Ag Np). The LOD (limit of detection) value of the PCT/Ab/AgNp/SLG@ITO impedimetric biosensor that was created was found to be 0.55 ng mL^{-1}.[621] An impedance biosensor was created to identify miRNA-10b by utilizing Cu^{2+} modified NH2-metal organic frameworks (NMOF@Cu^{2+}) in combination with a three-dimensional (3D) DNA walker signal amplification technique by Tang et al., The plentiful Cu^{2+} can attach to the MOF via a coordination reaction with NH2, acting as a scaffold to rapidly form CuFe Prussian blue analogue@NMOF (CuFe PBA@NMOF). The carboxyl group in the organic ligands of the NMOF can construct DNA strands (complementary strand, CS) for biorecognition reactions. The target activated a 3D DNA walker, leading to the removal of substantial amounts of assistant strands (AS) which were then connected to the surface of GCE. CS-NMOF@Cu^{2+} can be formed on the GCE by combining it with AS. LOD of 0.5 pM under optimal conditions was achieved.[622]

Calabrese and researchers created an electrochemical biosensor that performs impedimetric readings on both liquid and air samples to detect VOC compounds in food. The biosensor utilizes the pig odorant-binding protein (pOBP) as the molecular recognition component. We assessed the binding strength of pOBP to three distinct volatile organic molecules (1-octen-3-ol, trans-2-hexen-1-ol, and hexanal) associated with food rotting. LOD was found to be 0.1 μM.[623] Swiftly detecting and quantifying fentanyl in bodily fluids is essential for law enforcement to combat fentanyl abuse and for medical professionals to promptly care for victims. An innovative freestanding surface-enhanced Raman spectroscopy (SERS) biosensor named FrEnSERS biosensor is presented by Su et al., for accurate label-free identification of trace quantities of fentanyl in biological fluids, demonstrating outstanding enrichment capabilities. The biosensor comprises a reduced graphene oxide membrane coated with many hydrophobic gold nanostars. The FrEnSERS biosensor has good sensitivity and accuracy in detecting fentanyl in serum and urine over a wide range, with a detection limit of 0.47 ng/mL for serum and 0.73 ng/mL for urine.[624] Fiore et al., describe an initial paper-based microfluidic system that uses filter paper to regulate flow and introduce reagents for a reagent-free competitive magnetic-bead-based immunosensor. This device is specifically built for measuring cortisol in sweat. The paper-based microfluidic design was fabricated using wax printing and laser-cutting techniques to enable capillary-driven microfluidics. Monoclonal antibodies bound to magnetic beads aid in identifying cortisol in the reaction zone, allowing for accurate detection of the target substance. The interaction between the target cortisol and labeled cortisol with the acetylcholinesterase enzyme results in a response that is inversely proportional to the concentration of the target cortisol between 10 to 140 ng/mL by folding the pad holding the enzymatic substrate. A paper-based microfluidic device was connected to a Near-Field Communication wireless module to create a versatile integrated wearable gadget for detecting cortisol in sweat.[625] Verma et al., describe the development of an affordable real-time sensing module designed to detect uric acid on a simple, disposable paper surface. The detecting method uses a capacitive measurement apparatus with ZnO hexagonal rods on Cu interdigitated electrodes (IDEs) on hydrophobic A4 paper. The Arduino IDE software is used to code the Arduino Mega board to detect variations in capacitance and display the corresponding uric acid levels on an LCD screen.

https://doi.org/10.1021/acsomega.4c07991
ACS Omega 2024, 9, 48918−48987

The experiment showed a direct correlation between uric acid levels ranging from 0.1 mM to 1 mM, with a sensitivity of 9.00 μF mM^{-1} cm^{-2} at 0.1 mM.[626] Cheng et al. developed a cost-effective, compact optical biosensor for detecting blood urea nitrogen (BUN) levels in blood obtained from the fingertip. The biosensor features a simple, stackable, and layered paper-based strip design. It offers a linear optical reaction to BUN concentration and reduces the complexity of the optical scanner. The approach demonstrated a wide detection range of 2.46 to 38.14 mM and a low detection limit of 0.03 mM. The device may connect to a cloud-enabled smartphone via Bluetooth to transmit test data (IoMT).[627]

Pornprom et al., introduce a cost-effective paper-based electrochemical biosensor that uses a gold particle-decorated carboxyl graphene (AuPs/GCOOH)-modified electrode to detect heat shock protein (Hsp16.3), a biomarker indicating the onset of TB infection. The device pattern was created to assist in detecting operations and printed on low-cost filter paper to form hydrophobic and hydrophilic regions using a wax printing technique. Immunoassays were performed in a half-sandwich format as it is a reagent-free technique that avoids the necessity for a labeling step. The immunosensor was developed by drop casting GCOOH, electrochemically coating AuPs, and creating a biorecognition layer against Hsp16.3 utilizing EDC/NHS-sulfo standard chemistry. Hsp16.3 led to a notable decrease in the electrochemical signal of the redox probe [Fe(CN)6]3−/4− due to the insulating properties of the immunocomplexes produced. GCOOH aids in the direct immobilization of antibodies, whereas AuPs enhance the electrochemical properties of the sensor. The suggested immunosensor, requiring only a small sample amount of 5 μL, showed outstanding performance with a detection limit of 0.01 ng/mL. This method is highly specialized for Hsp16.3 and can rapidly identify TB-infected sera in just 20 min without the need for pre-enrichment. This makes it a feasible choice for early tuberculosis detection in regions with restricted resources.[628] Feng et al. created an advanced electrochemiluminescence (ECL) biosensor by merging a flexible paper-based sensing tool with a disposable three-electrode detecting setup. An aptamer was utilized as the recognition element in creating a cellulose paper that detects *Staphylococcus aureus* (S. aureus). The paper also contained probe DNA-GOD, which was linked to glucose oxidase (GOD) to amplify signaling. The aptamer-S. aureus pair enabled the precise liberation of probe DNA-GOD in a quantifiable manner. The remaining probe DNA-GOD on the paper-based aptasensor was activated by glucose, causing a significant decrease in the ECL signal. Ru(bpy)32+ molecules were added to porous zinc-based metal−organic frameworks (MOFs) to improve the electrochemiluminescence capabilities of the biosensor, leading to the creation of Ru(bpy)32+ functionalized MOF nanoflowers (Ru-MOF-5 NFs).[629] The work of Khorshed et al. introduces a portable biosensor that uses lectin array technology to identify glycans in IgG based on impedance. It utilized biotinylated *Griffonia simplicifolia* (GSL II) and *Ricinus communis* agglutinin I (RCA I) lectins in our biosensor setup to measure the N-acetyl glucosamine (GlcNAc) to galactose (Gal) ratio, known as the agalactosylation factor (AF). Streptavidin gold nanoparticles were linked to biotinylated lectin attached to the carbohydrate in the glycoprotein to amplify the variation in impedance signal and improve detection sensitivity. Furthermore, it demonstrates the feasibility of using the biosensor to distinguish between COVID-19-positive patient samples and negative patients.[630]

4. ARTIFICIAL INTELLIGENCE, MACHINE LEARNING, INTERNET OF THINGS (IOT), AND BIOSENSORS

The advancement of artificial intelligence (AI) has significantly impacted biosensors and changed the approach to bioanalytical applications. Biosensors, which integrate biological elements with transducers, usually provide exceptional sensitivity and accuracy in detection. However, the incorporation of AI technology has greatly improved their performance to unmatched levels. Machine learning algorithms, particularly those used in deep learning, have demonstrated remarkable capability in extracting important patterns and insights from complex biological data generated by biosensors. This combination allows biosensors to precisely detect analytes and enhance their responses gradually. Artificial intelligence (AI) and biosensors have been extensively used in various fields, including medical diagnostics, environmental monitoring, and food quality management. AI-powered biosensors in medical contexts have accelerated illness detection by studying intricate biomolecular interactions, hence enhancing customized and proactive healthcare. AI-driven environmental biosensors offer instant identification and tracking of contaminants, facilitating efficient resource management and environmental conservation. Artificial intelligence (AI) plays a vital role in improving the speed and accuracy of biosensor data analysis, facilitating quick decision-making in critical scenarios. Despite significant advancements, there are still issues with ethical considerations, data security, and standards. The integration of artificial intelligence (AI) with biosensors has significant promise as it progresses, influencing the advancement of analytical technologies and fostering chances for scientific exploration and creativity. Data science and machine learning have proven effective in several computer vision applications such as autonomous vehicles, motion detection, image categorization, and smart robots. The job descriptions are properly defined, making the problem transparent and allowing for easy verification of the answer. Healthcare responsibilities have inherent safety and security hazards, leading to privacy concerns. The absence of precise definitions for these challenges hinders the ability to conclusively identify their solutions. Assessing the likelihood of severe and even deadly illness in individuals infected with pathogens like the SARS-CoV-2 virus is an urgent and essential concern. Data science has been used to suggest prediction measures using a variety of genetic and physiological markers, as well as symptoms.[631]

Integrating machine learning into conventional biosensors has the potential to enhance measurement accuracy and data interpretation reliability.[632] Measurements are affected by variability, uncertainty, drifts, and noise, which impede precision and might pose challenges and incur costs. Advanced physics simulations that could help create detailed and comprehensive data sets have not been produced or widely adopted yet. Moreover, numerous biosensing systems suffer from a lack of substantial parallelism, which hampers the collection of comprehensive information for multiple analytes. Machine learning can be categorized in multiple ways depending on different criteria. Machine learning can be categorized into four divisions according to the learning system: unsupervised learning, supervised learning, semisupervised learning, and reinforcement learning. Unsupervised learning involves working with training samples when the labeled information is not provided. The goal is to uncover the intrinsic characteristics and patterns of the data by using unlabeled training samples.

https://doi.org/10.1021/acsomega.4c07991
ACS Omega 2024, 9, 48918−48987

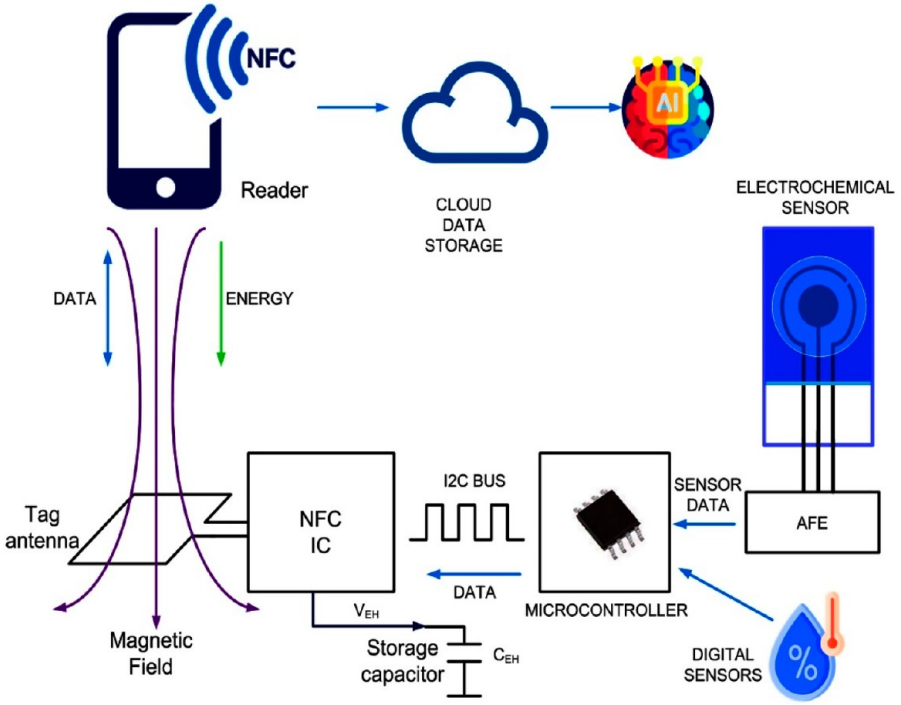

Figure 63. Schematic illustration of a typical block diagram of a batteryless NFC sensor[637] [Reprinted with permission from Lazaro, A.; Villarino, R.; Lazaro, M.; Canellas, N.; Prieto-Simon, B.; Girbau, D. Recent Advances in Batteryless NFC Sensors for Chemical Sensing and Biosensing. Biosensors (Basel) 2023, 13 (8). 10.3390/bios13080775]. Copyright [2023] [Lazaro et al. Licensee MDPI, Basel, Switzerland].

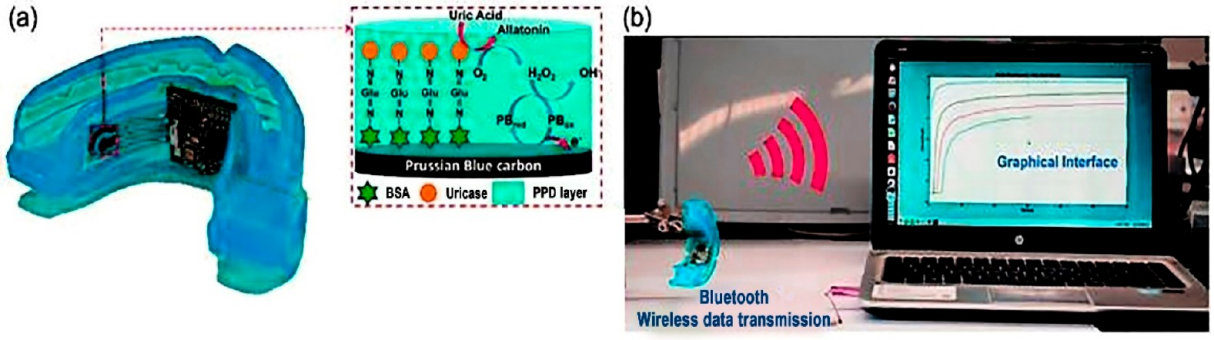

Figure 64. Applications of BLE in wireless devices. (a) The wearable mouthguard salivary uric acid biosensor design integrated a wireless amperometric circuit board.[638] (b) Real-time monitoring of salivary uric acid level using the integrated mouthguard biosensor with BLE 4.0 graphic interface on a laptop[638] [Reprinted with permission from [Kim, J.; Imani, S.; de Araujo, W. R.; Warchall, J.; Valdés-Ramírez, G.; Paixão, T. R. L. C.; Mercier, P. P.; Wang, J. Wearable Salivary Uric Acid Mouthguard Biosensor with Integrated Wireless Electronics. Biosens Bioelectron 2015, 74, 1061−1068. 10.1016/j.bios.2015.07.039]. Copyright [2015] [Elsevier B.V.].

Unsupervised learning has been widely applied in the organization of computing clusters, social network analysis, market segmentation, and astronomical data analysis.[633] The study done by Taha et al., evaluate the most efficient strategies for managing the pandemic, considering developments in optical sensor technology for detecting COVID-19.[634] The review also involves examining alternative medical service delivery methods utilized during the pandemic, including telehealth/telemonitoring, tele-management, tele-screening, and teleconsultation. The optical detection system presented uses teleservices and artificial intelligence to identify and categorize COVID-19 patients in healthcare settings. Examining the categorization of nanophotonic biosensors with tele-modules might help understand the methods and technology utilized for detecting SARS-CoV-2 biomarkers.[634]

The Internet of Medical Things is an expanding network of interconnected medical devices and systems that create an ideal setting for the advancement of biosensors. The study done by Bhupinder Singh delineates the structure of the Internet of Medical Things (IoMT), encompassing intelligent medical equipment, encrypted data transfer, and sophisticated data analysis.[635] Biosensors are described as crucial components in the IoMT system, transitioning from passive devices to active participants in patient care. An e study examines ethical issues with patient data privacy, security vulnerabilities in IoMT ecosystems, and the importance of robust regulatory frameworks to avoid misuse. It delves into the challenges faced by healthcare firms in adopting technologies, including issues like interoperability, scalability, and integration problems. The study explores emerging topics such as implanted biosensors, applications of nanotechnology, and the utilization of artificial intelligence for

https://doi.org/10.1021/acsomega.4c07991
ACS Omega 2024, 9, 48918−48987

data processing despite encountering obstacles. The study commences by elucidating the fundamental principles of biosensors and their diverse applications in healthcare. The article delves into various biosensors, including glucose monitoring for diabetics and wearable electrocardiogram (ECG) devices, showcasing their significance in early disease detection, ongoing monitoring, and personalized medication.[635]

Alam et al. collected COVID-19 data over a year by utilizing various data sets obtained from advanced biosensor technologies.[636] These data sets comprise patient symptoms, bodily condition, COVID-19 sorts (Alpha, Beta, Gamma, And Delta), and recovered cases. The data preparation function aims to eliminate unwanted noise and data. Optimal selection and feature extraction are performed using the principle component of African buffalo optimization (PCABO). A shuffle shepherd optimization-based generalized deep convolutional fuzzy network (SSO-GDCFN) is proposed for diagnosing COVID-19 illness states, types, and recovery categories. The proposed generalized deep convolutional fuzzy network integrates the deep convolutional approach with generalized approximation reasoning-based intelligent control. The SSO algorithm is utilized to enhance the parameters of the approach. The research's implementation is conducted using the MATLAB program. The efficacy of the recommended strategy has been validated through a comparison of the simulation outcomes generated by the proposed technique with those of several conventional methods. Figure 63 represents the typical block diagram of a NFC sensor and Figure 64 represents the applications of Bluetooth low energy (BLE) devices.

5. CHALLENGES AND FUTURE TRENDS

Substantial progress has been made; yet, many obstacles persist concerning the extensive adoption of biosensors in healthcare. In clinical settings, the dependability and longevity of biosensors are essential due to their extended application. The regulatory framework is a significant challenge, as biosensors are required to adhere to strict testing and approval procedures to confirm their safety and efficacy in clinical settings. This process can be laborious and expensive, presenting challenges for smaller businesses or startups. Furthermore, biosensors that can identify biomarkers and deliver quantitative data are crucial for efficient clinical decision-making. Achieving improved sensitivity and selectivity for specific biomarkers or analytes remains a technical challenge. Inaccurate or ambiguous readings may lead to misdiagnoses or erroneous data, which is particularly critical in medical diagnostics.

Many biosensors, particularly enzymatic and biological varieties, face limitations concerning shelf life and stability. Maintaining operational efficiency over extended periods, especially in varying climatic circumstances, is difficult. The incorporation of biosensors into wearable technology for continuous, real-time monitoring, such as glucose or heart rate sensors, has challenges concerning power consumption, miniaturization, and data accuracy. Mass-producing biosensors while maintaining uniformity, quality, and cost-effectiveness is a substantial challenge. Augmenting output may also result in fluctuations in sensor performance. Biosensors generate significant volumes of data, raising issues related to data storage, management, and security. In healthcare, the confidentiality of patient information is a critical issue, and compliance with regulations such as GDPR (The General Data Protection Regulation, or GDPR, 2018) and HIPAA (The Health Insurance Portability and Accountability Act of 1996 (HIPAA)) is imperative. Alternative diagnostic techniques, such as laboratory assays and imaging modalities, contend with biosensors. Biosensors must offer a clear benefit in terms of speed, cost, or convenience to distinguish themselves. For biosensors to succeed in the consumer market, there must be assurance in the accuracy and reliability of the devices. Issues with prior biosensor devices, like imprecise measurements, could negatively impact the reputation of promising technologies in the marketplace.

Biologists, chemists, physicists, electronics engineers, and data analytics specialists are all needed for biosensor development. Logistical challenges and a lack of inspiration could result from coordinating interdisciplinary teams. Integrating biosensors with digital health platforms, such as cloud-based data systems and mobile health applications, is the main emphasis of the research. Healthcare providers can get vital information through these technologies' real-time data analysis and remote patient monitoring. Traditional healthcare is likely to include biosensor technology more and more in the coming years. This technology has the potential to revolutionize diagnosis, patient management, and tailored medication. Recent developments show that these technologies have a lot of potential in the future, even though there are still problems with stability, repeatability, and regulatory hurdles. As biosensors continue to advance in capability, they will play an increasingly important role in healthcare delivery, patient monitoring, and illness identification.

The future of medical biosensors is set for substantial transformation through the incorporation of artificial intelligence (AI), providing considerable advancements in healthcare diagnosis and monitoring. AI-driven biosensors provide the capability to transform health data detection and analysis through real-time, continuous monitoring and offering predictive analytics for early illness identification. Through the integration of machine learning algorithms, these biosensors can evaluate extensive volumes of intricate biological data, identify trends, and discern small anomalies associated with the early onset of diseases such as cancer, diabetes, and cardiovascular disorders. This improves diagnostic precision and facilitates individualized treatment strategies. Moreover, AI can enhance biosensor efficacy by optimizing calibration procedures, reducing noise, and augmenting the specificity and sensitivity of the devices. AI-powered biosensors, when integrated with wearable or implantable technology, can provide remote patient monitoring, notifying healthcare personnel of significant alterations in a patient's state and allowing for prompt actions. As AI advances, it will facilitate the development of self-learning biosensors that adjust to unique physiological patterns, paving the way for a future characterized by highly personalized, proactive, and predictive healthcare. The collaboration of AI and biosensor technology will improve patient care quality and expand global access to healthcare solutions, especially via telemedicine and remote diagnostics.

6. CONCLUSION

The significance of biosensors has increased throughout the global pandemic due to their critical role in the rapid and precise detection of infectious illnesses. Biosensors are crucial instruments that provide the swift identification of specific biological markers, such as antigens or antibodies, associated with infections like viruses. In light of the persistent health challenges, biosensors are essential for facilitating accurate and comprehensive testing. They enable the rapid detection of illnesses and

https://doi.org/10.1021/acsomega.4c07991
ACS Omega 2024, 9, 48918−48987

the execution of prompt public health measures. Their ability to provide timely results, often with remarkable accuracy and precision, is essential in controlling and preventing the spread of infectious illnesses. Biosensors alleviate pressure on healthcare systems by improving testing protocols and enabling swift responses. This enhances our ability to efficiently manage and mitigate the impacts of pandemics. The integration of biosensors into diagnostic techniques is becoming increasingly essential for an effective and resilient public health system, as technological improvements continue. The review offers a thorough catalog of nearly all biosensor categories, clarifying fundamental concepts, subclassifications, new developments, benefits of different approaches, output efficiencies, and supplementary details. This comprehensive review publication categorizes biosensors according to substrate characteristics, thereby offering a unique contribution to the field. The selection of an appropriate transduction mechanism has a substantial influence on the performance and applications of biosensors. Biosensors utilize several approaches to transform biological processes into detectable signals. Optical transduction techniques, including surface plasmon resonance, fluorescence, and absorbance, allow for highly sensitive and real-time monitoring. They excel in the realm of biomolecular interactions and the alteration of biological material. In contrast, electrochemical transduction is characterized by its ease of miniaturization and high sensitivity to electrical signals produced during metabolic processes. This method is extensively employed by glucose and DNA biosensors. The piezoelectric transduction method utilizes the frequency shift in quartz crystal microbalances to accurately detect even the slightest changes in mass, without the requirement of using labels. The advantages and disadvantages of each transduction method impact aspects like as cost, sensitivity, and specificity. The effectiveness of a method relies on the particular needs of the biosensing application.

The incorporation of AI has markedly enhanced biosensors' capacity to analyze data, identify patterns, and render conclusions. Artificial intelligence algorithms improve the sensitivity and specificity of biosensors by facilitating rapid and accurate processing of complex biological data. Machine learning is an artificial intelligence approach that allows biosensors to integrate new data and adapt to their environment, hence improving their effectiveness. The integration of artificial intelligence (AI) into biosensors enables concurrent real-time monitoring and predictive analysis. This advancement facilitates the rapid detection of illnesses and the delivery of customized healthcare.

The Internet of Things (IoT) has markedly accelerated the progress of biosensor technology by enabling seamless network access, hence promoting efficient data transmission and remote monitoring. The integration of IoT-enabled biosensors enables rapid data collection, storage, and analysis, hence improving the efficiency of healthcare systems. This linkage facilitates continuous monitoring of health indicators, swift identification of anomalies, and timely intervention. The use of IoT-enabled biosensors in healthcare promotes the development of novel systems that prioritize patient-centered methodologies and improve healthcare results.

Wearable biosensors in healthcare technology are transformative as they provide continuous patient monitoring without intrusive procedures. Wearable real-time biosensors offer multiple benefits, including the continuous assessment of diverse physiological indicators, thereby improving our understanding of an individual's health status. Furthermore, these biosensors can continuously monitor essential physiological parameters, enabling the early detection of health problems and the implementation of preventive measures. Users and healthcare professionals may easily access and assess the comprehensive health data offered by wearable biosensors, hence improving decision-making. Moreover, it enables consumers to engage actively in their healthcare by providing essential information about their health metrics. This fosters a sense of personal responsibility for their well-being and enhances patient engagement. Wearable biosensors, connected to the Internet of Things (IoT), provide remote patient monitoring by healthcare practitioners, enhancing the efficiency of healthcare delivery and reducing the necessity for frequent hospital visits. This is especially beneficial for persons with chronic diseases.

In summary, biosensors play a crucial role in healthcare and medical diagnostics. Nanobiosensors, engineered to identify perilous infections like COVID-19 and Zika, exemplify only a few applications of these versatile devices. Biosensors have become indispensable tools owing to their capacity to swiftly, sensitively, and precisely identify biological markers linked to various illnesses. The domain of cancer nano biosensors possesses the capacity to markedly improve patient outcomes through its remarkable accuracy and early detection abilities, facilitating timely intervention. The advancement of biosensors for infectious diseases has greatly enhanced global initiatives in monitoring, controlling, and avoiding the spread of infectious agents. This was especially apparent in their vital function during the COVID-19 pandemic. These advanced approaches improve diagnostic accuracy and allow for continuous monitoring, enabling swift responses and interventions in public health. The ongoing technology breakthroughs have increased the importance of biosensors in the pursuit of enhanced, more efficient, and widely accessible healthcare solutions for various medical conditions. The continuous advancement and incorporation of these technologies into global healthcare systems underscore their vital importance in transforming disease identification and treatment. The biomedical research community is pivotal to the future of human health and survival within this global epidemic, particularly concerning the early diagnosis and screening of diverse infectious diseases. The paper outlines the tactics implemented for detecting diverse bioanalytes and highlights areas where the scientific community may unite as one entity.

AUTHOR INFORMATION

Corresponding Authors

Sumitha Manoharan Nair Sudha Kumari − *Centre for Advanced Materials Research, Department of Physics, Government College for Women, Thiruvananthapuram, University of Kerala, Kerala 695014, India*; Email: sumithamnair@gmail.com

Xavier Thankappan Suryabai − *Centre for Advanced Materials Research, Department of Physics, Government College for Women, Thiruvananthapuram, University of Kerala, Kerala 695014, India*; orcid.org/0000-0001-8955-0743; Email: xavierkattukulam@gmail.com

Complete contact information is available at: https://pubs.acs.org/10.1021/acsomega.4c07991

Notes

The authors declare no competing financial interest.

https://doi.org/10.1021/acsomega.4c07991
ACS Omega 2024, 9, 48918−48987

■ ACKNOWLEDGMENTS

We thankfully acknowledge the Centralized Common Instrumentation Centre (CCIF), Kerala Government Project Performance Linked Encouragement for Academic Studies (PLEASE), and Government College for Women, Thiruvananthapuram, University of Kerala and DST-FIST for the execution of this work.

■ FULL FORM ABBREVIATION

AChE	acetylcholinesterase
AF	agalactosylation factor
AOX	alcohol oxidase
AOX	alcohol oxidase
ACE-2	angiotensin-converting enzyme 2
Ab	antibody
ADI	arginine deiminase
AI	artificial intelligence
ALD	atomic layer deposition
BioMEMS	bio micro electromechanical systems
BUN	blood urea nitrogen
BLE	Bluetooth low energy
BSA	bovine serum albumin
BAW	bulk acoustic wave
BCL	*Burkholderia cepacia* lipase
BuChE	butyrylcholinesterase
CD	carbon dots
CNTs	carbon nanotubes
CMCS	carboxymethyl chitosan
CEA	carcinoembryonic antigen
CFPS	cell-free protein synthesis
CCD	charge-coupled device
R_{ct}	charge-transfer resistance
CRET	chemiluminescence resonance energy transfer
CTV	citrus tristeza virus
CMOS	complementary metal-oxide-semiconductor
*Cc*PDH	*Coprinopsis cinerea* pyranose dehydrogenase
CRP	C-reactive protein
CV	cyclic voltammetry
DEP	dielectrophoretic
DPV	differential pulse voltammetry
C_{dl}	double-layer capacitance
DSHP	double-slot hybrid plasmonic
DPI	dual polarization interferometry
ECIS	electrical cell-substrate impedance sensing
ECG	electrocardiogram
E-AB	electrochemical aptamer based
EIS	Electrochemical impedance spectroscopy
ECL	Electrochemiluminescence
R_s	electrolyte resistance
ECNFs	electrospun carbon nano fibers
ELISA	enzyme-based immunosorbent assay
EGFR	epidermal growth factor receptor
E.coli	*Escherichia coli*
FFT	fast Fourier transform
FET	field-effect transistor
FBAR	film bulk acoustic resonator
FPW	flexural plate wave
FRET	fluorescent energy transfer
FTIR	Fourier transform infrared
GOx	glucose oxidase
GO	graphene oxide
Hsp	heat shock protein
HCV	Hepatitis C virus
HOMO	highest occupied molecular orbit
LUMO	lowest utilized molecular orbit
HRP	horse radish peroxide
HER-3	human epidermal growth factor receptor-3
hFIb	human fibrinogen
IgG	immunoglobulin G
ITO	Indium tin oxide
IDEs	interdigitated electrodes
IGRAs	interferon-gamma release assays
IoMT	Internet of Medical Things
LoCs	lab-on-chips
LFNAB	lateral flow nucleic acid biosensor
LAT	latex agglutination test
LMG	leucomalachite green
LOD	limit of detection
LDA	linear discriminant analysis
LCORR	liquid-core optical ring resonator
LSPR	localized surface plasmon resonance
LLD	lower limit of detection
MZI	MachZehnder interferometer
MFEAs	magnetic field-enhanced agglutination assays
MMM	magnetic marker monitoring
MNB	magnetic nanobeads
MRS	magnetic relaxation switching
MARIA	magnetic relaxation/remanence immunoassay
MG	malachite green
R_{mt}	mass transfer resistance
MB	methylene blue
μTAS	micro total analysis systems
MEMS	microelectromechanical systems
MIT	molecular imprinting technology
MIPs	molecularly imprinted polymers
mAb	monoclonal antibody
MMF	multimode fiber
MMPS	multiple unit pellet system
MSC	multiplicative scattering correction
MWCNT	multiwalled carbon nanotube
MAP	*Mycobacterium avium* subsp. paratuberculosis
NEMS	nano electro mechanical systems
NRs	nanorods
NWs	nanowires
NFC	near-field communications
NHS	N-hydroxy succinimide
NHSS	N-hydroxy-succinimide sodium salt
NT-proBNP	N-terminal pro-brain natriuretic peptide
OPLS-DA	orthogonal projection to latent structures discriminant analysis
PAD	paper-based analytical device
PLS-DA	partial least squares discriminant analysis
PNA	peptide nucleic acid
PDP	phage display peptide
PBG	photonic band gap
PC	photonic crystals
pOBP	pig odorant-binding protein

https://doi.org/10.1021/acsomega.4c07991
ACS Omega 2024, 9, 48918−48987

PAMONO	plasmon assisted microscopy of nano-objects
NPC	p-nitrophenyl carbonate
POC	point-of-care
PVA	poly vinyl alcohol
PEG	polyethylene glycol
PPO	polyphenol oxidase
PPyNT	polypyrrole nanotubes
Pt-PPy/UOx/Grap	polypyrrole/uricase/graphene composite
PS-PAMAM-ESNFs	polystyrene and poly(amidoamine) dendritic polymer
PVDF	polyvinylidene fluoride
PCA	principal component analysis
PCABO	principle component of African buffalo optimization
PSPP	propagating surface plasmon polariton
QDs	quantum dots
QCM	quartz crystal microbalance
REMI	Raman encoded molecular imaging
ROS	reactive oxygen species
RBP	receptor binding proteins
RGNW	reduced graphene nanowalls
rGO	reduced graphene oxide
RCA I	*Ricinus communis* agglutinin I
RMGE	round-type microgap electrode
SARS-CoV	SARS-associated coronavirus
SEM	scanning electron microscope
SPM	scanning probe microscope
SPE	screen printed electrode
SAM	self-assembled monolayers
SSO-GDCFN	shuffle shepherd optimization-based generalized deep convolutional fuzzy network
SOI	silicon-on-insulator
SMFs	single-mode fibers
ssDNA	single-stranded DNA
SWCNTs	single-walled carbon nanotubes
SPN	small plasmonic nanostars
SPE	solid-phase extraction
SWV	square wave voltammetry
SpA	staphylococcal protein A
S. aureus	*Staphylococcus aureus*
SMLR	stepwise multiple linear regression
SrCuO2	strontium copper oxide
SQUID	superconducting quantum interference device
SOD	superoxide dismutase
SPR	surface plasmon resonance
SERS	surface-enhanced Raman spectroscopy
SENSORS	surface-enhanced spatially offset Raman spectroscopy
TBA	thrombin-binding aptamers
TERS	tip-enhanced Raman spectroscopy
TMV	tobacco mosaic virus
TOP	Topiramate
TST	tuberculin skin test
TB	tuberculosis
VEGF	vascular endothelial-derived growth factor
W	Warburg impedance
WNV	West Nile Virus
WGM	whispering gallery mode
EDC	1-(3-dimethylaminopropyl)-3-ethyl carbodiimide hydrochloride
PASE	1-pyrene butanoic acid succinimidyl ester
MBTH	3-methyl-2-benzothiazolinone hydrazine

REFERENCES

(1) Hemdan, M.; Ali, M. A.; Doghish, A. S.; Mageed, S. S. A.; Elazab, I. M.; Khalil, M. M.; Mabrouk, M.; Das, D. B.; Amin, A. S. Innovations in Biosensor Technologies for Healthcare Diagnostics and Therapeutic Drug Monitoring: Applications, Recent Progress, and Future Research Challenges. *Sensors* **2024**, *24* (16), 5143.

(2) Kandimalla, V. B.; Tripathi, V. S.; Ju, H. Biosensors Based on Immobilization of Biomolecules in Sol-Gel Matrices. *Electrochemical Sensors, Biosensors and their Biomedical Applications* **2008**, 503−529.

(3) Abuzeid, H. R.; Abdelaal, A. F.; Elsharkawy, S.; Ali, G. A. M. Basic Principles and Applications of Biological Sensors Technology. In *Handbook of Nanosensors: Materials and Technological Applications*; Ali, G. A. M., Chong, K. F., Makhlouf, A. S. H., Eds.; Springer Nature Switzerland: Cham, 2024; pp 1-45. DOI: 10.1007/978-3-031-16338-8_28-1.

(4) Mobed, A.; Razavi, S.; Ahmadalipour, A.; Shakouri, S. K.; Koohkan, G. Biosensors in Parkinson's Disease. *Clin. Chim. Acta* **2021**, *518*, 51−58.

(5) Maddocks, G. M.; Eisenstein, M.; Soh, H. T. Biosensors for Parkinson's Disease: Where Are We Now, and Where Do We Need to Go? *ACS Sens* **2024**, *9* (9), 4307−4327.

(6) Iqbal, M. J.; Javed, Z.; Herrera-Bravo, J.; Sadia, H.; Anum, F.; Raza, S.; Tahir, A.; Shahwani, M. N.; Sharifi-Rad, J.; Calina, D.; Cho, W. C. Biosensing Chips for Cancer Diagnosis and Treatment: A New Wave towards Clinical Innovation. *Cancer Cell Int* **2022**, *22* (1), 354.

(7) Mustafa, S. K.; Khan, M. F.; Sagheer, M.; Kumar, D.; Pandey, S. Advancements in Biosensors for Cancer Detection: Revolutionizing Diagnostics. *Medical Oncology* **2024**, *41* (3), 73.

(8) Ma, R.; Shao, R.; An, X.; Zhang, Q.; Sun, S. Recent Advancements in Noninvasive Glucose Monitoring and Closed-Loop Management Systems for Diabetes. *J. Mater. Chem. B* **2022**, *10* (29), 5537−5555.

(9) Reddy, V. S.; Agarwal, B.; Ye, Z.; Zhang, C.; Roy, K.; Chinnappan, A.; Narayan, R. J.; Ramakrishna, S.; Ghosh, R. Recent Advancement in Biofluid-Based Glucose Sensors Using Invasive, Minimally Invasive, and Non-Invasive Technologies: A Review. *Nanomaterials* **2022**, *12* (7), 1082.

(10) Perumal, V.; Hashim, U. Advances in Biosensors: Principle, Architecture and Applications. *J Appl Biomed* **2014**, *12* (1), 1−15.

(11) Khodaparast, M.; Sharley, D.; Marshall, S.; Beddoe, T. Advances in Point-of-Care and Molecular Techniques to Detect Waterborne Pathogens. *NPJ Clean Water* **2024**, *7* (1), 74.

(12) Tripathi, A.; Bonilla-Cruz, J. Review on Healthcare Biosensing Nanomaterials. *ACS Appl Nano Mater* **2023**, *6* (7), 5042−5074.

(13) Mekuye, B.; Abera, B. Nanomaterials: An Overview of Synthesis, Classification, Characterization, and Applications. *Nano Select* **2023**, *4* (8), 486−501.

(14) Sarhadi, V. K.; Armengol, G. Molecular Biomarkers in Cancer. *Biomolecules* **2022**, *12* (8), 1021.

(15) Malik, S.; Singh, J.; Goyat, R.; Saharan, Y.; Chaudhry, V.; Umar, A.; Ibrahim, A. A.; Akbar, S.; Ameen, S.; Baskoutas, S. Nanomaterials-Based Biosensor and Their Applications: A Review. *Heliyon* **2023**, *9* (9), No. e19929.

(16) Chadha, U.; Bhardwaj, P.; Agarwal, R.; Rawat, P.; Agarwal, R.; Gupta, I.; Panjwani, M.; Singh, S.; Ahuja, C.; Selvaraj, S. K.; Banavoth, M.; Sonar, P.; Badoni, B.; Chakravorty, A. Recent Progress and Growth in Biosensors Technology: A Critical Review. *Journal of Industrial and Engineering Chemistry* **2022**, *109*, 21−51.

(17) Arlett, J. L.; Myers, E. B.; Roukes, M. L. Comparative Advantages of Mechanical Biosensors. *Nat Nanotechnol* **2011**, *6* (4), 203−215.

(18) Kaushal, V.; Gupta, R. Role of Artificial Intelligence in Diagnosis of Infectious Diseases. In *Biomedical Translational Research: Technologies for Improving Healthcare*; Sobti, R. C., Sobti, A., Eds.; Springer

https://doi.org/10.1021/acsomega.4c07991
ACS Omega 2024, 9, 48918−48987

Nature Singapore: Singapore, 2022; pp 115−133. DOI: 10.1007/978-981-16-4345-3_8.
(19) Yoo, E.-H.; Lee, S.-Y. Glucose Biosensors: An Overview of Use in Clinical Practice. *Sensors (Basel)* **2010**, *10*, 4558−4576.
(20) Guo, L.; Zhao, Y.; Huang, Q.; Huang, J.; Tao, Y.; Chen, J.; Li, H.-Y.; Liu, H. Electrochemical Protein Biosensors for Disease Marker Detection: Progress and Opportunities. *Microsyst Nanoeng* **2024**, *10* (1), 65.
(21) Zeng, Y.; Huang, Z.; Liu, Y.; Xu, T. Printed Biosensors for the Detection of Alzheimer's Disease Based on Blood Biomarkers. *J Anal Test* **2024**, *8* (2), 133−142.
(22) Kujawska, M.; Bhardwaj, S. K.; Mishra, Y. K.; Kaushik, A. Using Graphene-Based Biosensors to Detect Dopamine for Efficient Parkinson's Disease Diagnostics. *Biosensors (Basel)* **2021**, *11* (11), 433.
(23) Farzin, L.; Shamsipur, M.; Samandari, L.; Sheibani, S. HIV Biosensors for Early Diagnosis of Infection: The Intertwine of Nanotechnology with Sensing Strategies. *Talanta* **2020**, *206*, 120201.
(24) Teniou, A.; Rhouati, A.; Marty, J.-L. Recent Advances in Biosensors for Diagnosis of Autoimmune Diseases. *Sensors* **2024**, *24* (5), 1510.
(25) Abdel-Karim, R. Nanotechnology-Enabled Biosensors: A Review of Fundamentals, Materials, Applications, Challenges, and Future Scope. *Biomedical Materials & Devices* **2024**, *2* (2), 759−777.
(26) Korotcenkov, G.; Ahmad, R. G.; Guleria, P.; Kumar, V. Introduction to Biosensing. In *Handbook of II-VI Semiconductor-Based Sensors and Radiation Detectors: Vol. 3: Sensors, Biosensors and Radiation Detectors*; Korotcenkov, G., Ed.; Springer International Publishing: Cham, 2023; pp 441−474. DOI: 10.1007/978-3-031-24000-3_17.
(27) Karunakaran, R.; Keskin, M. Chapter 11 - Biosensors: Components, Mechanisms, and Applications. In *Analytical Techniques in Biosciences*; Egbuna, C., Patrick-Iwuanyanwu, K. C., Shah, M. A., Ifemeje, J. C., Rasul, A., Eds.; Academic Press, 2022; pp 179−190. DOI: 10.1016/B978-0-12-822654-4.00011-7.
(28) Khattab, A. M. Basics of Biological Sensors. In *Handbook of Nanosensors: Materials and Technological Applications*; Ali, G. A. M., Chong, K. F., Makhlouf, A. S. H., Eds.; Springer Nature Switzerland: Cham, 2024; pp 1−43. DOI: 10.1007/978-3-031-16338-8_26-1.
(29) Polat, E. O.; Cetin, M. M.; Tabak, A. F.; Bilget Güven, E.; Uysal, B. Ö.; Arsan, T.; Kabbani, A.; Hamed, H.; Gül, S. B. Transducer Technologies for Biosensors and Their Wearable Applications. *Biosensors (Basel)* **2022**, *12* (6), 385.
(30) Malhotra, S.; Verma, A.; Tyagi, N.; Kumar, V. BIOSENSORS: PRINCIPLE, TYPES AND APPLICATIONS. *Int. J. Adv. Res. Innov. Ideas Educ.* **2017**, *3* (2), 3639.
(31) Pumera, M.; Ambrosi, A.; Bonanni, A.; Chng, E. L. K.; Poh, H. L. Graphene for Electrochemical Sensing and Biosensing. *Trends in Analytical Chemistry* **2010**, *29* (9), 954−965.
(32) Yu, X.; Cheng, H.; Zhang, M.; Zhao, Y.; Qu, L.; Shi, G. Graphene-Based Smart Materials. *Nat Rev Mater* **2017**, *2* (9), 17046.
(33) Anadkat, D.; Pandya, A.; Jaiswal, A.; Dungani, S.; Sanchela, A. V. Experimental Comparison between Graphene and Reduced Graphene Oxide along with Significant Conversion of RGO from N-to p-Type. *Journal of Materials Science: Materials in Electronics* **2024**, *35* (12), 821.
(34) Bellier, N.; Baipaywad, P.; Ryu, N.; Lee, J. Y.; Park, H. Recent Biomedical Advancements in Graphene Oxide- and Reduced Graphene Oxide-Based Nanocomposite Nanocarriers. *Biomater Res* **2022**, *26* (1), 65.
(35) Abid; Sehrawat, P.; Islam, S. S.; Mishra, P.; Ahmad, S. Reduced Graphene Oxide (RGO) Based Wideband Optical Sensor and the Role of Temperature, Defect States and Quantum Efficiency. *Sci Rep* **2018**, *8* (1), 3537.
(36) Al Qaraghuli, M. M.; Kubiak-Ossowska, K.; Ferro, V. A.; Mulheran, P. A. Antibody-Protein Binding and Conformational Changes: Identifying Allosteric Signalling Pathways to Engineer a Better Effector Response. *Sci Rep* **2020**, *10* (1), 13696.
(37) Jokerst, J. V.; Raamanathan, A.; Christodoulides, N.; Floriano, P. N.; Pollard, A. A.; Simmons, G. W.; Wong, J.; Gage, C.; Furmaga, W. B.; Redding, S. W.; McDevitt, J. T. Nano-Bio-Chips for High Performance Multiplexed Protein Detection: Determinations of Cancer Biomarkers in Serum and Saliva Using Quantum Dot Bioconjugate Labels. *Biosens Bioelectron* **2009**, *24* (12), 3622.
(38) Sánchez-Tirado, E.; González-Cortés, A.; Yáñez-Sedeño, P.; Pingarrón, J. M. Carbon Nanotubes Functionalized by Click Chemistry as Scaffolds for the Preparation of Electrochemical Immunosensors. Application to the Determination of TGF-Beta 1 Cytokine. *Analyst* **2016**, *141* (20), 5730−5737.
(39) Shamsazar, A.; Soheili-Moghaddam, M.; Asadi, A. A Novel Electrochemical Immunosensor Based on MWCNT/CuO Nanocomposite for Effectively Detection of Carcinoembryonic Antigen (CEA). *Microchemical Journal* **2024**, *196*, 109643.
(40) Kim, S.; Malik, J.; Seo, J. M.; Cho, Y. M.; Bien, F. Subcutaneously Implantable Electromagnetic Biosensor System for Continuous Glucose Monitoring. *Sci Rep* **2022**, *12* (1), 17395.
(41) Demir, E.; Kırboga, K. K.; Isık, M. Chapter 8 - An Overview of Stability and Lifetime of Electrochemical Biosensors. In *Novel Nanostructured Materials for Electrochemical Bio-Sensing Applications*; Manjunatha, J. G., Ed.; Elsevier, 2024; pp 129−158. DOI: 10.1016/B978-0-443-15334-1.00022-5.
(42) Touhami, A. *Biosensors and Nanobiosensors: Design and Applications*; One Central Press, 2014.
(43) Bouropoulos, N.; Kouzoudis, D.; Grimes, C. The Real-Time, in Situ Monitoring of Calcium Oxalate and Brushite Precipitation Using Magnetoelastic Sensors. *Sensors and Actuators B-chemical* **2005**, *109* (2), 227−232.
(44) Cai, Q. Y.; Jain, M. K.; Grimes, C. A. A Wireless, Remote Query Ammonia Sensor. *Sens Actuators B Chem* **2001**, *77* (3), 614−619.
(45) Cai, Q. Y.; Grimes, C. A. A Salt-Independent PH Sensor. *Sens Actuators B Chem* **2001**, *79* (2−3), 144−149.
(46) Cai, Q. Y.; Cammers-Goodwin, A.; Grimes, C. A. A Wireless, Remote Query Magnetoelastic CO2 Sensor. *J Environ Monit* **2000**, *2* (6), 556−560.
(47) Wu, S.; Zhu, Y.; Cai, Q.; Zeng, K.; Grimes, C. A. A Wireless Magnetoelastic α-Amylase Sensor. *Sensors and Actuators B-chemical* **2007**, *121* (2), 476−481.
(48) Shankar, K.; Zeng, K.; Ruan, C.; Grimes, C. A. Quantification of Ricin Concentrations in Aqueous Media. *Sensors and Actuators B-chemical* **2005**, *107* (2), 640−648.
(49) Ruan, C.; Zeng, K.; Varghese, O. K.; Grimes, C. A. A Magnetoelastic Bioaffinity-Based Sensor for Avidin. *Biosens Bioelectron* **2004**, *19* (12), 1695−1701.
(50) Guntupalli, R.; Hu, J.; Lakshmanan, R. S.; Huang, T. S.; Barbaree, J. M.; Chin, B. A. A Magnetoelastic Resonance Biosensor Immobilized with Polyclonal Antibody for the Detection of Salmonella Typhimurium. *Biosens Bioelectron* **2007**, *22* (7), 1474−1479.
(51) Ruan, C.; Zeng, K.; Varghese, O. K.; Grimes, C. A. Magnetoelastic Immunosensors: Amplified Mass Immunosorbent Assay for Detection of Escherichia Coli O157:H7. *Anal. Chem.* **2003**, *75* (23), 6494−6498.
(52) Wan, J.; Johnson, M. L.; Guntupalli, R.; Petrenko, V. A.; Chin, B. A. Detection of Bacillus Anthracis Spores in Liquid Using Phage-Based Magnetoelastic Micro-Resonators. *Sensors and Actuators B-chemical* **2007**, *127* (2), 559−566.
(53) Le Bras, Y.; Greneche, J.-M. Magneto-Elastic Resonance: Principles, Modeling and Applications Provisional Chapter Magneto-Elastic Resonance: Principles, Modeling and Applications. *Resonance*, 2017. DOI: 10.5772/intechopen.70523.
(54) Grimes, C. A.; Roy, S. C.; Rani, S.; Cai, Q. Theory, Instrumentation and Applications of Magnetoelastic Resonance Sensors: A Review. *Sensors* **2011**, *11* (3), 2809−2844.
(55) Shen, W.; Lakshmanan, R. S.; Mathison, L. C.; Petrenko, V. A.; Chin, B. A. Phage Coated Magnetoelastic Micro-Biosensors for Real-Time Detection of Bacillus Anthracis Spores. *Sensors and Actuators B-chemical* **2009**, *137* (2), 501−506.
(56) Zeng, K.; Ong, K. G.; Yang, X.; Grimes, C. A. Board Level Integrated Microsystem Design and Associated Technique for Impedance Analysis of Resonator Sensors. *Sens Lett* **2006**, *4* (4), 388−397.

https://doi.org/10.1021/acsomega.4c07991
ACS Omega 2024, 9, 48918−48987

(57) Shen, W.; Mathison, L. C.; Petrenko, V. A.; Chin, B. A. Design and Characterization of a Magnetoelastic Sensor for the Detection of Biological Agents. *J Phys D Appl Phys* **2010**, *43* (1), 015004.
(58) Zeng, K.; Ong, K. G.; Mungle, C.; Grimes, C. A. Time Domain Characterization of Oscillating Sensors: Application of Frequency Counting to Resonance Frequency Determination. *Rev. Sci. Instrum.* **2002**, *73*, 4375−4380.
(59) Zeng, K.; Grimes, C. A. Threshold-Crossing Counting Technique for Damping Factor Determination of Resonator Sensors. *Rev. Sci. Instrum.* **2004**, *75* (12), 5257−5261.
(60) Shen, W.; Mathison, L. C.; Petrenko, V. A.; Chin, B. A. A Pulse System for Spectrum Analysis of Magnetoelastic Biosensors. *Appl. Phys. Lett.* **2010**, *96* (16), 163502 DOI: 10.1063/1.3386528.
(61) Grimes, C. A.; Roy, S. C.; Rani, S.; Cai, Q. Theory, Instrumentation and Applications of Magnetoelastic Resonance Sensors: A Review. *Sensors* **2011**, *11* (3), 2809−2844.
(62) Zhang, K.; Chai, Y. Numerical Study on Mass Sensitivity of Magnetoelastic Biosensors with Concentrated Mass Load under Different Resonance Modes. *J Sens* **2016**, *2016*, 1.
(63) Johnson, M. L.; Wan, J.; Huang, S.; Cheng, Z.; Petrenko, V. A.; Kim, D. J.; Chen, I. H.; Barbaree, J. M.; Hong, J. W.; Chin, B. A. A Wireless Biosensor Using Microfabricated Phage-Interfaced Magnetoelastic Particles. *Sens Actuators A Phys* **2008**, *144* (1), 38−47.
(64) Zu, H.; Wu, H.; Wang, Q. M. High-Temperature Piezoelectric Crystals for Acoustic Wave Sensor Applications. *IEEE Trans Ultrason Ferroelectr Freq Control* **2016**, *63* (3), 486−505.
(65) Hees, J.; Heidrich, N.; Pletschen, W.; Sah, R. E.; Wolfer, M.; Williams, O. A.; Lebedev, V.; Nebel, C. E.; Ambacher, O. Piezoelectric Actuated Micro-Resonators Based on the Growth of Diamond on Aluminum Nitride Thin Films. *Nanotechnology* **2013**, *24* (2), 025601.
(66) Meyers, F. N.; Loh, K. J.; Dodds, J. S.; Baltazar, A. Active Sensing and Damage Detection Using Piezoelectric Zinc Oxide-Based Nanocomposites. *Nanotechnology* **2013**, *24* (18), 185501.
(67) Ferreira, P.; Hou, R. Z.; Wu, A.; Willinger, M. G.; Vilarinho, P. M.; Mosa, J.; Laberty-Robert, C.; Boissière, C.; Grosso, D.; Sanchez, C. Nanoporous Piezo- and Ferroelectric Thin Films. *Langmuir* **2012**, *28* (5), 2944−2949.
(68) Wang, H.; Wereszczak, A. A. Effects of Electric Field and Biaxial Flexure on the Failure of Poled Lead Zirconate Titanate. *IEEE Trans Ultrason Ferroelectr Freq Control* **2008**, *55* (12), 2559−2570.
(69) Struth, B.; Decher, G.; Schmitt, J.; Hofmeister, W.; Neiβendorfer, F.; Pietsch, U.; Brezesinski, G.; Mohwald, H.; et al. Chemical Modification of Topaz Surfaces. *Materials Science & Engineering C-Biomimetic and Supramolecular Systems* **1999**, *10*, 97−101.
(70) Levitskii, R. R.; Zachek, I. R.; Verkholyak, T. M.; Moina, A. P. Dielectric, Piezoelectric, and Elastic Properties of the Rochelle SaltNaKC4H4O6·4H2O: A Theory. *Phys Rev B* **2003**, *67* (17), 174112 DOI: 10.1103/PhysRevB.67.174112.
(71) Sinha, T. K.; Ghosh, S. K.; Maiti, R.; Jana, S.; Adhikari, B.; Mandal, D.; Ray, S. K. Graphene-Silver-Induced Self-Polarized PVDF-Based Flexible Plasmonic Nanogenerator Toward the Realization for New Class of Self Powered Optical Sensor. *ACS Appl Mater Interfaces* **2016**, *8* (24), 14986−14993.
(72) Pohanka, M. The Piezoelectric Biosensors: Principles and Applications, a Review. *Int. J. Electrochem. Sci*, 2017; Vol. *12*, pp 496−506.
(73) Keiji Kanazawa, K.; Gordon, J. G. The Oscillation Frequency of a Quartz Resonator in Contact with Liquid. *Anal. Chim. Acta* **1985**, *175* (C), 99−105.
(74) Devkota, J.; Ohodnicki, P. R.; Greve, D. W. SAW Sensors for Chemical Vapors and Gases. *Sensors (Basel)* **2017**, *17* (4), 801.
(75) Shana, Z. A.; Radtke, D. E.; Kelkar, U. R.; Josse, F.; Haworth, D. T. Theory and Application of a Quartz Resonator as a Sensor for Viscous Liquids. *Anal. Chim. Acta* **1990**, *231* (C), 317−320.
(76) Ogi, H.; Nagai, H.; Fukunishi, Y.; Hirao, M.; Nishiyama, M. 170-MHz Electrodeless Quartz Crystal Microbalance Biosensor: Capability and Limitation of Higher Frequency Measurement. *Anal. Chem.* **2010**, *82* (4), 1568.
(77) Michalzik, M.; Wilke, R.; Büttgenbach, S. Miniaturized QCM-Based Flow System for Immunosensor Application in Liquid. *Sens Actuators B Chem* **2005**, *111*−*112* (SUPPL), 410−415.
(78) Kim, N.; Son, S. H.; Kim, C. T.; Cho, Y. J.; Kim, C. J.; Kim, W. Y. Direct-Binding Quartz Crystal Microbalance Immunosensor to Detect Carp Metallothionein. *Sens Actuators B Chem* **2011**, *157* (2), 627−634.
(79) Li, D.; Wang, J.; Wang, R.; Li, Y.; Abi-Ghanem, D.; Berghman, L.; Hargis, B.; Lu, H. A Nanobeads Amplified QCM Immunosensor for the Detection of Avian Influenza Virus H5N1. *Biosens Bioelectron* **2011**, *26* (10), 4146−4154.
(80) Mustafa, M. K.; Nabok, A.; Parkinson, D.; Tothill, I. E.; Salam, F.; Tsargorodskaya, A. Detection of β-Amyloid Peptide (1−16) and Amyloid Precursor Protein (APP770) Using Spectroscopic Ellipsometry and QCM Techniques: A Step Forward towards Alzheimers Disease Diagnostics. *Biosens Bioelectron* **2010**, *26* (4), 1332−1336.
(81) Mannelli, I.; Minunni, M.; Tombelli, S.; Wang, R.; Spiriti, M. M.; Mascini, M. Direct Immobilisation of DNA Probes for the Development of Affinity Biosensors. *Bioelectrochemistry* **2005**, *66* (1−2), 129−138.
(82) Sakti, S. P.; Chabibah, N.; Ayu, S. P.; Padaga, M. C.; Aulanni'am, A. Development of QCM Biosensor with Specific Cow Milk Protein Antibody for Candidate Milk Adulteration Detection. *J Sens* **2016**, *2016*, 1807647.
(83) Durmus, N. G.; Lin, R. L.; Kozberg, M.; Dermici, D.; Khademhosseini, A.; Demirci, U. Acoustic-Based Biosensors. *Encyclopedia of Microfluidics and Nanofluidics* **2014**, 1.
(84) Devkota, J.; Ohodnicki, P. R.; Greve, D. W.; Luo, J.; Xuan, W.; Fu, R. Y. Q. SAW Sensors for Chemical Vapors and Gases. *Sensors* **2017**, *17* (4), 801.
(85) Shiokawa, S.; Kondoh, J. Surface Acoustic Wave Sensors. *Jpn J Appl Phys* **2004**, *43* (5S), 2799.
(86) Liu, J.; Lu, Y. Response Mechanism for Surface Acoustic Wave Gas Sensors Based on Surface-Adsorption. *Sensors* **2014**, *14* (4), 6844−6853.
(87) Kirimli, C. E.; Shih, W. H.; Shih, W. Y. DNA Hybridization Detection with 100 ZM Sensitivity Using Piezoelectric Plate Sensors with an Improved Noise-Reduction Algorithm. *Analyst* **2014**, *139* (11), 2754−2763.
(88) Yao, H.; Fernández, C. S.; Xu, X.; Wynendaele, E.; De Spiegeleer, B. A Surface Acoustic Wave (SAW) Biosensor Method for Functional Quantification of E. Coli l-Asparaginase. *Talanta* **2019**, *203*, 9−15.
(89) Gray, E. R.; Turbé, V.; Lawson, V. E.; Page, R. H.; Cook, Z. C.; Ferns, R. B.; Nastouli, E.; Pillay, D.; Yatsuda, H.; Athey, D.; McKendry, R. A. Ultra-Rapid, Sensitive and Specific Digital Diagnosis of HIV with a Dual-Channel SAW Biosensor in a Pilot Clinical Study. *NPJ Digit Med* **2018**, *1* (1). DOI: 10.1038/s41746-018-0041-5.
(90) Zheng, D.; Guo, P.; Xiong, J.; Wang, S. Streptavidin Modified ZnO Film Bulk Acoustic Resonator for Detection of Tumor Marker Mucin 1. *Nanoscale Res Lett* **2016**, *11* (1), 1−8.
(91) Kuznetsova, L. A.; Coakley, W. T. Applications of Ultrasound Streaming and Radiation Force in Biosensors. *Biosens Bioelectron* **2007**, *22* (8), 1567−1577.
(92) Krishnamoorthy, S.; Iliadis, A. A.; Bei, T.; Chrousos, G. P. An Interleukin-6 ZnO/SiO2/Si Surface Acoustic Wave Biosensor. *Biosens Bioelectron* **2008**, *24* (2), 313−318.
(93) Capobianco, J. A.; Shih, W. Y.; Adams, G. P.; Shih, W.-H. Label-Free Her2 Detection and Dissociation Constant Assessment in Diluted Human Serum Using a Longitudinal Extension Mode of a Piezoelectric Microcantilever Sensor. *Sens Actuators B Chem* **2011**, *160* (1), 349−356.
(94) Kumar Singh, A.; Singh, M. QCM Sensing of Melphalan via Electropolymerized Molecularly Imprinted Polythiophene Films. *Biosens Bioelectron* **2015**, *74*, 711−717.
(95) Singh, A. K.; Singh, M. Electrochemical and Piezoelectric Monitoring of Taurine via Electropolymerized Molecularly Imprinted Films. *Journal of Molecular Recognition* **2017**, *30* (12), No. e2652.
(96) He, J.-H.; He, C.-H.; Qian, M.-Y.; Alsolami, A. A. Piezoelectric Biosensor Based on Ultrasensitive MEMS System. *Sens Actuators A Phys* **2024**, *376*, 115664.

(97) Li, H.; Long, M.; Su, H.; Tan, L.; Shi, X.; Du, Y.; Luo, Y.; Deng, H. Carboxymethyl Chitosan Assembled Piezoelectric Biosensor for Rapid and Label-Free Quantification of Immunoglobulin Y. *Carbohydr. Polym.* **2022**, *290*, 119482.
(98) D'Ambrogio, G.; Zahhaf, O.; Le, M.-Q.; Bordet, M.; Lermusiaux, P.; Della Schiava, N.; Liang, R.; Cottinet, P.-J.; Capsal, J.-F. Piezoelectric Biosensor for Smart Cardiovascular Grafts Based on NaNbO3 Fibers/PDMS Structured Composite. *Mater Des* **2022**, *223*, 111195.
(99) Clark, L. C.; Lyons, C. ELECTRODE SYSTEMS FOR CONTINUOUS MONITORING IN CARDIOVASCULAR SURGERY. *Ann. N.Y. Acad. Sci.* **1962**, *102* (1), 29−45.
(100) Sanati, A.; Jalali, M.; Raeissi, K.; Karimzadeh, F.; Kharaziha, M.; Mahshid, S. S.; Mahshid, S. A Review on Recent Advancements in Electrochemical Biosensing Using Carbonaceous Nanomaterials. *Microchimica Acta* **2019**, *186* (12), 1−22.
(101) Sumitha, M. S.; Xavier, T. S. Recent Advances in Electrochemical Biosensors - A Brief Review. *Hybrid Advances* **2023**, *2*, 100023.
(102) Mohanapriya, D.; Satija, J.; Senthilkumar, S.; Kumar Ponnusamy, V.; Thenmozhi, K. Design and Engineering of 2D MXenes for Point-of-Care Electrochemical Detection of Bioactive Analytes and Environmental Pollutants. *Coord. Chem. Rev.* **2024**, *507*, 215746.
(103) Wang, L.; Li, H.; Su, W.; Zhang, W.; Xu, Z.; Wang, J.; Chen, J. Fabrication of a Free-Standing MWCNT Electrode by Electric Field Force for an Ultra-Sensitive MicroRNA-21 Nano-Genosensor. *Small* **2022**, *18* (25), 2201791.
(104) Li, K.; Li, M.; Sun, L.; Fang, J.; Wang, C.; Wang, X.; Qiao, Z.; Ruan, D. Ultrasensitive Composite Electrochemical Sensor with Printed Wrinkled CNTs Nanostructure for Simultaneous Detection. *Mater Today Chem* **2024**, *39*, 102156.
(105) Thévenot, D. R.; Toth, K.; Durst, R. A.; Wilson, G. S. ELECTROCHEMICAL BIOSENSORS: RECOMMENDED DEFINITIONS AND CLASSIFICATION*. *Anal. Lett.* **2001**, *34* (5), 635−659.
(106) Cho, I.-H.; Kim, D. H.; Park, S. Electrochemical Biosensors: Perspective on Functional Nanomaterials for on-Site Analysis. *Biomater Res* **2020**, *24* (1), 6.
(107) Bode, B.; Gross, K.; Rikalo, N.; Schwartz, S.; Wahl, T.; Page, C.; Gross, T.; Mastrototaro, J. Alarms Based on Real-Time Sensor Glucose Values Alert Patients to Hypo- and Hyperglycemia: The Guardian Continuous Monitoring System. *https://home.liebertpub.com/dia* **2004**, *6* (2), 105−113.
(108) Yoo, E. H.; Lee, S. Y. Glucose Biosensors: An Overview of Use in Clinical Practice. *Sensors* **2010**, *10* (5), 4558−4576.
(109) Kumar, V.; Khan, A. A.; Tripathi, A.; Dixit, P. K.; Bajaj, U. K. Role of Oxidative Stress in Various Diseases: Relevance of Dietary Antioxidants. *The Journal of Phytopharmacology* **2015**, *4* (2), 126−132.
(110) Tomassetti, M.; Serone, M.; Angeloni, R.; Campanella, L.; Mazzone, E. Amperometric Enzyme Sensor to Check the Total Antioxidant Capacity of Several Mixed Berries. Comparison with Two Other Spectrophotometric and Fluorimetric Methods. *Sensors* **2015**, *15* (2), 3435−3452.
(111) Fu, J.; Qiao, H.; Li, D.; Luo, L.; Chen, K.; Wei, Q. Laccase Biosensor Based on Electrospun Copper/Carbon Composite Nanofibers for Catechol Detection. *Sensors* **2014**, *14* (2), 3543−3556.
(112) Pilo, M.; Farre, R.; Lachowicz, J. I.; Masolo, E.; Panzanelli, A.; Sanna, G.; Senes, N.; Sobral, A.; Spano, N. Design of Amperometric Biosensors for the Detection of Glucose Prepared by Immobilization of Glucose Oxidase on Conducting (Poly)Thiophene Films. *J Anal Methods Chem* **2018**, *2018*, 1849439.
(113) Pupim Ferreira, A. A.; Venturini, C.; Souza Castilho, M. de; Canaverolo, N.; Vinicius, M.; dos Santos, G. P.; Sadao, C.; Vicente, A.; Yamanak, H. Amperometric Biosensor for Diagnosis of Disease. *State of the Art in Biosensors - Environmental and Medical Applications* **2013**, DOI: 10.5772/53656.
(114) Gao, Z.; Tansil, N. A DNA Biosensor Based on the Electrocatalytic Oxidation of Amine by a Threading Intercalator. *Anal. Chim. Acta* **2009**, *636* (1), 77−82.
(115) Wang, K.; Sun, Z.; Feng, M.; Liu, A.; Yang, S.; Chen, Y.; Lin, X. Design of a Sandwich-Mode Amperometric Biosensor for Detection of PML/RARα Fusion Gene Using Locked Nucleic Acids on Gold Electrode. *Biosens Bioelectron* **2011**, *26* (6), 2870−2876.
(116) Ionescu, R. E.; Herrmann, S.; Cosnier, S.; Marks, R. S. A Polypyrrole CDNA Electrode for the Amperometric Detection of the West Nile Virus. *Electrochem commun* **2006**, *8* (11), 1741−1748.
(117) de Fátima Giarola, J.; Mano, V.; Pereira, A. C. Development and Application of a Voltammetric Biosensor Based on Polypyrrole/Uricase/Graphene for Uric Acid Determination. *Electroanalysis* **2018**, *30* (1), 119−127.
(118) Pisoschi, A. M. Potentiometric Biosensors: Concept and Analytical Applications-An Editorial. *Biochem Anal Biochem* **2016**, *5*, 3 DOI: 10.4172/2161-1009.1000e164.
(119) Pisoschi, A.; Andrei, D.; Negulescu, G. GLUCOSE DETERMINATION BY CELLOPHANE-BASED AND NYLON- BASED ENZYMIC ELECTRODES; APPLICATION ON JUICES AND WINE ANALYSIS.
(120) Pisoschi, A. M.; Danet, A. F.; Negulescu, G. P. INFLUENCE OF THE BUFFER CAPACITY ON GLUCOSE POTENTIOMETRIC DETERMINATION IN SYNTHETIC SOLUTIONS AND IN REAL SAMPLES WITH DIFFERENT ACIDITIES. *Proc. Rom. Acad. Series B* **2007**, *2*, 75.
(121) Pisoschi, A. M.; Danet, A. COMPARISON BETWEEN NYLON-BASED AND NITROCELLULOSE-BASED POTENTIOMETRIC BIOSENSORS IN GLUCOSE ASSESSMENT. *Analele Universitatii Bucuresti : Chimie* **2006**, *I*, 39−44.
(122) Pisoschi, A.; Danet, A. The Construction and the Determination of the Analytical Characteristics of a Potentiometrical Biosensor for Glucose. *Revista de Chimie* **2004**, *55*, 843−850.
(123) Adeloju, S. B.; Moline, A. N. Fabrication of Ultra-Thin Polypyrrole-Glucose Oxidase Film from Supporting Electrolyte-Free Monomer Solution for Potentiometric Biosensing of Glucose. *Biosens Bioelectron* **2001**, *16* (3), 133−139.
(124) Larramendy, M.; Soloneski, S. *Genotoxicity - A Predictable Risk to Our Actual World* **2018**, DOI: 10.5772/intechopen.69556.
(125) Kolli, R.; Peltola, E.; Levon, K. Choice of Reference Electrode Is Critical for Potentiometric Whole Cell-Based Sensor. *Electroanalysis* **2015**, *27*, 1636.
(126) Rösner, L. S.; Walter, F.; Ude, C.; John, G. T.; Beutel, S. Sensors and Techniques for On-Line Determination of Cell Viability in Bioprocess Monitoring. *Bioengineering* **2022**, *9* (12), 762.
(127) Peng, Y.; Lu, B.; Deng, Y.; Yang, N.; Li, G. A Dual-Recognition-Controlled Electrochemical Biosensor for Accurate and Sensitive Detection of Specific Circulating Tumor Cells. *Biosens Bioelectron* **2022**, *201*, 113973.
(128) Koncki, R. Recent Developments in Potentiometric Biosensors for Biomedical Analysis. *Anal. Chim. Acta* **2007**, *599* (1), 7−15.
(129) Yotter, R. A.; Wilson, D. M. Sensor Technologies for Monitoring Metabolic Activity in Single Cells - Part II: Nonoptical Methods and Applications. *IEEE Sensors Journal.* **2004**, *4*, 412−429.
(130) Simsek, H.; Alpar, S.; Uçar, N.; Aksu, F.; Ceyhan, I.; Gözalan, A.; Cesur, S.; Ertek, M. Comparison of Tuberculin Skin Testing and T-SPOT.TB for Diagnosis of Latent and Active Tuberculosis. *Jpn J Infect Dis* **2010**, *63* (2), 99−102.
(131) Metcalfe, J. Z.; Cattamanchi, A.; McCulloch, C. E.; Lew, J. D.; Ha, N. P.; Graviss, E. A. Test Variability of the QuantiFERON-TB Gold in-Tube Assay in Clinical Practice. *Am J Respir Crit Care Med* **2013**, *187* (2), 206−211.
(132) Ramos, A.; Carvalho, T.; Ribeiro, M.; Guimaraes, J. T. Capilia™ TB-Neo Assay: A New Tool for Rapid Distinction between Tuberculous and Non-Tuberculous Mycobacteria. *Int J Tuberc Lung Dis* **2016**, *20* (6), 753−756.
(133) Bjerrum, S.; Schiller, I.; Dendukuri, N.; Kohli, M.; Nathavitharana, R. R.; Zwerling, A. A.; Denkinger, C. M.; Steingart, K. R.; Shah, M. Lateral Flow Urine Lipoarabinomannan Assay for Detecting Active Tuberculosis in People Living with HIV. *Cochrane Database Syst Rev* **2019**, *10* (10), CD011420 DOI: 10.1002/14651858.CD011420.pub3.

(134) Gupta, S.; Kakkar, V. Recent Technological Advancements in Tuberculosis Diagnostics - A Review. *Biosens Bioelectron* **2018**, *115*, 14−29.
(135) Nour-Neamatollahi, A.; Siadat, S. D.; Yari, S.; Tasbiti, A. H.; Ebrahimzadeh, N.; Vaziri, F.; Fateh, A.; Ghazanfari, M.; Abdolrahimi, F.; Pourazar, S.; Bahrmand, A. A New Diagnostic Tool for Rapid and Accurate Detection of Mycobacterium Tuberculosis. *Saudi J Biol Sci* **2016**, *25* (3), 418−425.
(136) Golichenari, B.; Nosrati, R.; Farokhi-Fard, A.; Faal Maleki, M.; Gheibi Hayat, S. M.; Ghazvini, K.; Vaziri, F.; Behravan, J. Electrochemical-Based Biosensors for Detection of Mycobacterium Tuberculosis and Tuberculosis Biomarkers. *Crit Rev Biotechnol* **2019**, *39* (8), 1056−1077.
(137) Hung Tzang, C.; Yuan, R.; Yang, M. Voltammetric Biosensors for the Determination of Formate and Glucose-6-Phosphate Based on the Measurement of Dehydrogenase-Generated NADH and NADPH. *Biosens Bioelectron* **2001**, *16* (3), 211−219.
(138) Yashas, S. R.; Sandeep, S.; Shivakumar, B. P.; Swamy, N. K. Potentiometric Polyphenol Oxidase Biosensor for Sensitive Determination of Phenolic Micropollutant in Environmental Samples. *Environmental Science and Pollution Research* **2020**, *27* (22), 27234−27243.
(139) Korpan, Y. I.; Gonchar, M. V; Sibirny, A. A.; Martelet, C.; El'skaya, A. V; Gibson, T. D.; Soldatkin, A. P. Development of Highly Selective and Stable Potentiometric Sensors for Formaldehyde Determination. *Biosens Bioelectron* **2000**, *15* (1), 77−83.
(140) Marchenko, S. V.; Kucherenko, I. S.; Hereshko, A. N.; Panasiuk, I. V.; Soldatkin, O. O.; El'skaya, A. V.; Soldatkin, A. P. Application of Potentiometric Biosensor Based on Recombinant Urease for Urea Determination in Blood Serum and Hemodialyzate. *Sensors and Actuators B-chemical* **2015**, *207* (PB), 981−986.
(141) Dzyadevych, S.; Jaffrezic-Renault, N. Conductometric Biosensors. *Biological Identification* **2014**, 153.
(142) Shul'ga, A. A.; Soldatkin, A. P.; El'skaya, A. V.; Dzyadevich, S. V.; Patskovsky, S. V.; Strikha, V. I. Thin-Film Conductometric Biosensors for Glucose and Urea Determination. *Biosens Bioelectron* **1994**, *9* (3), 217−223.
(143) Shul'ga, A. A.; Sandrovsky, A. C.; Strikha, V. I.; Soldatkin, A. P.; Starodub, N. F.; El'skaya, A. V. Overall Characterization of ISFET-Based Glucose Biosensor. *Sens Actuators B Chem* **1992**, *10* (1), 41−46.
(144) Gounden, V.; Bhatt, H.; Jialal, I. Renal Function Tests. *StatPearls* **2023**.
(145) Saiapina, O. Y.; Dzyadevych, S. V.; Jaffrezic-Renault, N.; Soldatkin, O. P. Development and Optimization of a Novel Conductometric Bi-Enzyme Biosensor for L-Arginine Determination. *Talanta* **2012**, *92*, 58−64.
(146) Hnaiein, M.; Hassen, W. M.; Abdelghani, A.; Fournier-Wirth, C.; Coste, J.; Bessueille, F.; Leonard, D.; Jaffrezic-Renault, N. A Conductometric Immunosensor Based on Functionalized Magnetite Nanoparticles for E. Coli Detection. *Electrochem commun* **2008**, *10* (8), 1152−1154.
(147) Hnaien, M.; Hassen, W. M.; Abdelghani, A.; Cotte, S.; Leonard, D.; Bessueille, F.; Jaffrezic-Renault, N. A Conductometric Biosensor for the Estimation of the Number of Cleaving Sites in Peptides and Proteins. *Electrochem commun* **2009**, *11* (1), 165−168.
(148) Hnaien, M.; Ruffin, E.; Bordes, C.; Marcillat, O.; Lagarde, F.; Jaffrezic-Renault, N.; Briançon, S. Integrity Characterization of Myoglobin Released from Poly(ε-Caprolactone) Microspheres Using Two Analytical Methods: UV/Vis Spectrometry and Conductometric Bi-Enzymatic Biosensor. *Eur J Pharm Biopharm* **2011**, *78* (2), 298−305.
(149) Pyeshkova, V.; Soldatkin, O. O.; Kukla, A. L.; Saiapina, O. Y. ENZYME CONDUCTOMETRIC BIOSENSOR FOR LACTOSE CONTENT DETERMINATION (In Ukrainian). *Biotechnologia Acta* **2008**, 1.
(150) Pyeshkova, V. M.; Saiapina, O. Y.; Soldatkin, O. O.; Dzyadevych, S. V. Enzyme Conductometric Biosensor for Maltose Determination. *Biopolym Cell* **2009**, *25* (4), 272−278.
(151) *tailieunhanh - DNA covalent attachment on conductometric biosensor for modified genetic soybean detection*. https://tailieunhanh.com/vn/tlID1314464_dna-covalent-attachment-on-conductometric-biosensor-for-modified-genetic-soybean-detection.html (accessed 2024−03−01).
(152) Okafor, C.; Grooms, D.; Alocilja, E.; Bolin, S. Fabrication of a Novel Conductometric Biosensor for Detecting Mycobacterium Avium Subsp. Paratuberculosis Antibodies. *Sensors (Basel)* **2008**, *8* (9), 6015−6025.
(153) Trebbe, U.; Niggemann, M.; Cammann, K. P. D.; Fiaccabrino, G. C.; Koudelka-Hep, M.; Dzyadevich, S. V; Shulga, O. V. A New Calcium-Sensor Based on Ion-Selective Conductometric Microsensors - Membranes and Features. *Fresenius J Anal Chem* **2001**, *371*, 734−739.
(154) Majeed, S.; Naqvi, S. T. R.; ul Haq, M. N.; Ashiq, M. N. Chapter 10 - Electroanalytical Techniques in Biosciences: Conductometry, Coulometry, Voltammetry, and Electrochemical Sensors. In *Analytical Techniques in Biosciences*; Egbuna, C., Patrick-Iwuanyanwu, K. C., Shah, M. A., Ifemeje, J. C., Rasul, A., Eds.; Academic Press, 2022; pp 157−178. DOI: 10.1016/B978-0-12-822654-4.00004-X.
(155) Canali, C.; Larsen, L. B.; Martinsen, Ø. G.; Heiskanen, A. Conductometric Analysis in Bio-Applications: A Universal Impedance Spectroscopy-Based Approach Using Modified Electrodes. *Sens Actuators B Chem* **2015**, *212*, 544−550.
(156) Nizameev, I. R.; Gainullin, R. R.; Nizameeva, G. R.; Lebedeva, E. M.; Kuznetsova, V. V.; Spiridonov, S. V. Interdigital Gold Electrodes for a Conductometric Gas Sensor on the Glass Surface. *St. Petersburg Polytechnic University Journal. Physics and Mathematics* **2023**, *68* (3.1), 384−389.
(157) Turlybekuly, A.; Sarsembina, M.; Mentbayeva, A.; Bakenov, Z.; Soltabayev, B. CuO/TiO2 Heterostructure-Based Sensors for Conductometric NO2 and N2O Gas Detection at Room Temperature. *Sens Actuators B Chem* **2023**, *397*, 134635.
(158) Pan, T.; Xu, Y.; Li, Q.; Pang, H. Designed Nickel-Cobalt-Based Bimetallic Oxide Slender Nanosheets for Efficient Urea Electrocatalytic Oxidation. *Int. J. Hydrogen Energy* **2024**, *57*, 388−393.
(159) Yang, Y.; Lin, S.; Hu, J. An Ultrasonically Catalyzed Conductometric Metal Oxide Gas Sensor System with Machine Learning-Based Ambient Temperature Compensation. *Sens Actuators B Chem* **2023**, *385*, 133721.
(160) Zhu, H.; Guo, Y.; Zheng, F.; Li, C.; Wu, J.; Wang, T.; Fu, Y.; Zhang, X. Introducing Oxygen Vacancies on Sodium Titanate via NaBH4 Treatment for Conductometric Hydrogen Gas Sensors. *Sens Actuators B Chem* **2023**, *375*, 132916.
(161) Din, M. I.; Ahmed, M.; Ahmad, M.; Iqbal, M.; Ahmad, Z.; Hussain, Z.; Khalid, R.; Samad, A. Investigating the Activity of Carbon Fiber Electrode for Electricity Generation from Waste Potatoes in a Single-Chambered Microbial Fuel Cell. *J Chem* **2023**, *2023*, 8520657.
(162) Nur Afnan Uda, M.; Kamal Yousif Dafhalla, A.; Dhahi, T. S.; Adam, T.; Chandra Bose Gopinath, S.; Bahari ambek, A.; Nur Aiman Uda, M.; Mohammed, M.; Azizah Parmin, N.; Hulwani Ibrahim, N.; Hashim, U. Conductometric Immunosensor for Specific Escherichia Coli O157:H7 Detection on Chemically Funcationalizaed Interdigitated Aptasensor. *Heliyon* **2024**, *10*, e26988.
(163) Dudchenko, O. Y.; Pyeshkova, V. M.; Soldatkin, O. O.; Akata, B.; Kasap, B. O.; Soldatkin, A. P.; Dzyadevych, S. V. Development of Silicalite/Glucose Oxidase-Based Biosensor and Its Application for Glucose Determination in Juices and Nectars. *Nanoscale Res Lett* **2016**, *11* (1), 1−7.
(164) Bahadır, E. B.; Sezgintürk, M. K. A Review on Impedimetric Biosensors. *Artif Cells Nanomed Biotechnol* **2016**, *44*, 248−262.
(165) Yuan, X.-Z.; Song, C.; wang, H.; Zhang, J. *Electrochemical Impedance Spectroscopy in PEM Fuel Cells* **2010**, DOI: 10.1007/978-1-84882-846-9.
(166) Hou, L.; Cui, Y.; Xu, M.; Gao, Z.; Huang, J.; Tang, D. Graphene Oxide-Labeled Sandwich-Type Impedimetric Immunoassay with Sensitive Enhancement Based on Enzymatic 4-Chloro-1-Naphthol Oxidation. *Biosens Bioelectron* **2013**, *47*, 149−156.
(167) Elshafey, R.; Tavares, A. C.; Siaj, M.; Zourob, M. Electrochemical Impedance Immunosensor Based on Gold Nanoparticles-Protein G for the Detection of Cancer Marker Epidermal Growth Factor Receptor in Human Plasma and Brain Tissue. *Biosens Bioelectron* **2013**, *50*, 143−149.

https://doi.org/10.1021/acsomega.4c07991
ACS Omega 2024, 9, 48918−48987

(168) Canbaz, M. Ç.; Simsek, Ç. S.; Sezgintürk, M. K. Electrochemical Biosensor Based on Self-Assembled Monolayers Modified with Gold Nanoparticles for Detection of HER-3. *Anal. Chim. Acta* **2014**, *814*, 31−38.
(169) Asav, E.; Sezgintürk, M. K. A Novel Impedimetric Disposable Immunosensor for Rapid Detection of a Potential Cancer Biomarker. *Int J Biol Macromol* **2014**, *66*, 273−280.
(170) Sonuç, M. N.; Sezgintürk, M. K. Ultrasensitive Electrochemical Detection of Cancer Associated Biomarker HER3 Based on Anti-HER3 Biosensor. *Talanta* **2014**, *120*, 355−361.
(171) Hou, L.; Gao, Z.; Xu, M.; Cao, X.; Wu, X.; Chen, G.; Tang, D. DNAzyme-Functionalized Gold-Palladium Hybrid Nanostructures for Triple Signal Amplification of Impedimetric Immunosensor. *Biosens Bioelectron* **2014**, *54*, 365−371.
(172) Regan, E. M.; Hallett, A. J.; Wong, L. C. C.; Saeed, I. Q.; Langdon-Jones, E. E.; Buurma, N. J.; Pope, S. J. A.; Estrela, P. A Novel Cobalt Complex for Enhancing Amperometric and Impedimetric DNA Detection. *Electrochim. Acta* **2014**, *128*, 10−15.
(173) Yumak, T.; Kuralay, F.; Muti, M.; Sinag, A.; Erdem, A.; Abaci, S. Preparation and Characterization of Zinc Oxide Nanoparticles and Their Sensor Applications for Electrochemical Monitoring of Nucleic Acid Hybridization. *Colloids Surf B Biointerfaces* **2011**, *86* (2), 397−403.
(174) Chang, H.; Wu, S. H. Hybridization of FePt/ZnS Nanocore-Shell Structure with DNAs of Different Sequences. *Mater Trans* **2010**, *51* (11), 2094−2098.
(175) Zhang, X. Y.; Zhou, L. Y.; Luo, H. Q.; Li, N. B. A Sensitive and Label-Free Impedimetric Biosensor Based on an Adjunct Probe. *Anal. Chim. Acta* **2013**, *776*, 11−16.
(176) Bonanni, A.; Esplandiu, M. J.; del Valle, M. Impedimetric Genosensors Employing COOH-Modified Carbon Nanotube Screen-Printed Electrodes. *Biosens Bioelectron* **2009**, *24* (9), 2885−2891.
(177) Gupta, V. K.; Yola, M. L.; Qureshi, M. S.; Solak, A. O.; Atar, N.; Üstündag, Z. A Novel Impedimetric Biosensor Based on Graphene Oxide/Gold Nanoplatform for Detection of DNA Arrays. *Sens Actuators B Chem* **2013**, *188*, 1201−1211.
(178) Sassolas, A.; Blum, L. J.; Leca-Bouvier, B. D. Immobilization Strategies to Develop Enzymatic Biosensors. *Biotechnol Adv* **2012**, *30* (3), 489−511.
(179) Reddy, K. K.; Gobi, K. V. Artificial Molecular Recognition Material Based Biosensor for Creatinine by Electrochemical Impedance Analysis. *Sens Actuators B Chem* **2013**, *183*, 356−363.
(180) Shervedani, R. K.; Mehrjardi, A. H.; Zamiri, N. A Novel Method for Glucose Determination Based on Electrochemical Impedance Spectroscopy Using Glucose Oxidase Self-Assembled Biosensor. *Bioelectrochemistry* **2006**, *69* (2), 201−208.
(181) Maalouf, R.; Hassen, W.; Fournier-Wirth, C.; Coste, J.; Jaffrezic-Renault, N. Comparison of Two Innovatives Approaches for Bacterial Detection: Paramagnetic Nanoparticles and Self-Assembled Multilayer Processes. *Microchimica Acta* **2008**, *163*, 157−161.
(182) Furst, A. L.; Francis, M. B. Impedance-Based Detection of Bacteria. *Chem Rev* **2019**, *119* (1), 700−726.
(183) Kulbacka, J.; Choromańska, A.; Rossowska, J.; Wezgowiec, J.; Saczko, J.; Rols, M. P. Cell Membrane Transport Mechanisms: Ion Channels and Electrical Properties of Cell Membranes. *Adv Anat Embryol Cell Biol* **2017**, *227*, 39−58.
(184) Willis, M. R. Dielectric and Electronic Properties of Biological Materials by R Pethig. Pp 376. John Wiley & Sons, Chichester and New York. 1979. £15. *Biochem Educ* **1980**, *8* (1), 31−31.
(185) Borkholder, D. *Cell Based Biosensors Using Microelectrodes*, 1998.
(186) Lin, L.; Liu, Y.; Tang, L.; Li, J. Electrochemical DNA Sensor by the Assembly of Graphene and DNA-Conjugated Gold Nanoparticles with Silver Enhancement Strategy. *Analyst* **2011**, *136* (22), 4732−4737.
(187) Ebrahimi, A.; Alam, M. A. Evaporation-Induced Stimulation of Bacterial Osmoregulation for Electrical Assessment of Cell Viability. *Proc Natl Acad Sci U S A* **2016**, *113* (26), 7059−7064.
(188) Wegener, J.; Keese, C. R.; Giaever, I. Electric Cell-Substrate Impedance Sensing (ECIS) as a Noninvasive Means to Monitor the Kinetics of Cell Spreading to Artificial Surfaces. *Exp. Cell Res.* **2000**, *259* (1), 158−166.
(189) Guan, J.-G.; Miao, Y.-Q.; Zhang, Q.-J. Impedimetric Biosensors. *J Biosci Bioeng* **2004**, *97* (4), 219−226.
(190) Gómez, R.; Bashir, R.; Sarikaya, A.; Ladisch, M. R.; Sturgis, J.; Robinson, J. P.; Geng, T.; Bhunia, A. K.; Apple, H. L.; Wereley, S. Microfluidic Biochip for Impedance Spectroscopy of Biological Species. *Biomed Microdevices* **2001**, *3* (3), 201−209.
(191) Manaresi, N.; Romani, A.; Medoro, G.; Altomare, L.; Leonardi, A.; Tartagni, M.; Guerrieri, R. A CMOS Chip for Individual Cell Manipulation and Detection. *Solid-State Circuits, IEEE Journal of* **2003**, *38*, 2297−2305.
(192) Ferreira, J.; Seoane, F.; Ansede, A.; Bragos, R. AD5933-Based Spectrometer for Electrical Bioimpedance Applications. *J Phys Conf Ser* **2010**, *224*, 012011.
(193) Sharma, N. K.; Nain, A.; Singh, K.; Rani, N.; Singal, A. Impedimetric Sensors: Principles, Applications and Recent Trends. *IJITEE* **2019**, 1 DOI: 10.35940/ijitee.J9806.0881019.
(194) Veal, B. W.; Baldo, P. M.; Paulikas, A. P.; Pliquett, U.; Barthel, A. Interfacing the AD5933 for Bio-Impedance Measurements with Front Ends Providing Galvanostatic or Potentiostatic Excitation. *J Phys Conf Ser* **2012**, *407* (1), 012019.
(195) Kim, M.; Iezzi, R.; Shim, B. S.; Martin, D. C. Impedimetric Biosensors for Detecting Vascular Endothelial Growth Factor (VEGF) Based on Poly(3,4-Ethylene Dioxythiophene) (PEDOT)/Gold Nanoparticle (Au NP) Composites. *Front Chem* **2019**, *7*. DOI: 10.3389/fchem.2019.00234.
(196) Lu, Z.; Wu, L.; Dai, X.; Wang, Y.; Sun, M.; Zhou, C.; Du, H.; Rao, H. Novel Flexible Bifunctional Amperometric Biosensor Based on Laser Engraved Porous Graphene Array Electrodes: Highly Sensitive Electrochemical Determination of Hydrogen Peroxide and Glucose. *J Hazard Mater* **2021**, *402*, 123774.
(197) Hroncekova, S.; Bertok, T.; Hires, M.; Jane, E.; Lorencova, L.; Vikartovska, A.; Tanvir, A.; Kasak, P.; Tkac, J. Ultrasensitive Ti3C2TX MXene/Chitosan Nanocomposite-Based Amperometric Biosensor for Detection of Potential Prostate Cancer Marker in Urine Samples. *Processes* **2020**, *8* (5), 580.
(198) Othman, A. M.; Wollenberger, U. Amperometric Biosensor Based on Coupling Aminated Laccase to Functionalized Carbon Nanotubes for Phenolics Detection. *Int J Biol Macromol* **2020**, *153*, 855−864.
(199) Öndes, B.; Sunna, Ç.; Kilimci, U.; Uygun, M.; Uygun, D. A. Boron Nitride Nanosheet Modified Amperometric Biosensor for Uric Acid Determination. *Microchemical Journal* **2023**, *194*, 109240.
(200) Wang, H.; Wang, X.; Cheng, J. Bionic Enzyme-Assisted Ion-Selective Amperometric Biosensor Based on 3D Porous Conductive Matrix for Point-of-Care Nitrite Testing. *ACS Nano* **2022**, *16* (9), 14849−14859.
(201) Povedano, E.; Ruiz-Valdepeñas Montiel, V.; Gamella, M.; Serafín, V.; Pedrero, M.; Moranova, L.; Bartosik, M.; Montoya, J. J.; Yáñez-Sedeño, P.; Campuzano, S.; Pingarrón, J. M. A Novel Zinc Finger Protein-Based Amperometric Biosensor for MiRNA Determination. *Anal Bioanal Chem* **2020**, *412* (21), 5031−5041.
(202) Gigli, V.; Tortolini, C.; Capecchi, E.; Angeloni, A.; Lenzi, A.; Antiochia, R. Novel Amperometric Biosensor Based on Tyrosinase/Chitosan Nanoparticles for Sensitive and Interference-Free Detection of Total Catecholamine. *Biosensors (Basel)* **2022**, *12* (7), 519.
(203) Öndes, B.; Evli, S.; Sahin, Y.; Uygun, M.; Uygun, D. A. Uricase Based Amperometric Biosensor Improved by AuNPs-TiS2 Nanocomposites for Uric Acid Determination. *Microchemical Journal* **2022**, *181*, 107725.
(204) Nugba, B. E.; Mousa, N. O.; Osman, A.; El-Moneim, A. A. Non-Enzymatic Amperometric Biosensor with Anchored Ni Nanoparticles for Urinary Glucose Quantification. *Diam Relat Mater* **2023**, *137*, 110171.
(205) Flauzino, J. M. R.; Peres, R. C. S.; Alves, L. M.; Vieira, J. G.; dos Santos, J. G.; Brito-Madurro, A. G.; Madurro, J. M. DNA Electrochemical Biosensor for Detection of Alicyclobacillus Acidoterrestris Utilizing Hoechst 33258 as Indicator. *Bioelectrochemistry* **2021**, *140*, 107801.

https://doi.org/10.1021/acsomega.4c07991
ACS Omega 2024, 9, 48918−48987

(206) Park, J. A.; Kwon, N.; Park, E.; Kim, Y.; Jang, H.; Min, J.; Lee, T. Electrochemical Biosensor with Aptamer/Porous Platinum Nanoparticle on Round-Type Micro-Gap Electrode for Saxitoxin Detection in Fresh Water. *Biosens Bioelectron* **2022**, *210*, 114300.
(207) Ibáñez-Redín, G.; Rosso Cagnani, G. O.; Gomes, N.; Raymundo-Pereira, P. A. S.; Machado, S. A.; Gutierrez, M. A.; Krieger, J. E.; Oliveira, O. N. Wearable Potentiometric Biosensor for Analysis of Urea in Sweat. *Biosens Bioelectron* **2023**, *223*, 114994.
(208) Torres-Chavolla, E.; Alocilja, E. C. Nanoparticle Based DNA Biosensor for Tuberculosis Detection Using Thermophilic Helicase-Dependent Isothermal Amplification. *Biosens Bioelectron* **2011**, *26* (11), 4614−4618.
(209) Yuan, Y.; Li, L.; Zhao, M.; Zhou, J.; Chen, Z.; Bai, L. An Aptamer Based Voltammetric Biosensor for Endotoxins Using a Functionalized Graphene and Molybdenum Disulfide Composite as a New Nanocarrier. *Analyst* **2019**, *144* (4), 1253−1259.
(210) Mutlaq, S.; Albiss, B.; Al-Nabulsi, A. A.; Osaili, T.; Al-Jaberi, T.; Olaimat, A. N.; Liu, S. Q.; Ayyash, M. M. Detection of Salmonella Enteritidis in Milk Using Conductometric Immunosensor Coated on Polyaniline/Zinc Oxide Nanocomposite. *https://home.liebertpub.com/fpd* **2023**, *20* (5), 177−185.
(211) Zeng, J.; Duarte, P. A.; Ma, Y.; Savchenko, O.; Shoute, L.; Khaniani, Y.; Babiuk, S.; Zhuo, R.; Abdelrasoul, G. N.; Charlton, C.; Kanji, J. N.; Babiuk, L.; Edward, C.; Chen, J. An Impedimetric Biosensor for COVID-19 Serology Test and Modification of Sensor Performance via Dielectrophoresis Force. *Biosens Bioelectron* **2022**, *213*, 114476.
(212) Jesadabundit, W.; Jampasa, S.; Patarakul, K.; Siangproh, W.; Chailapakul, O. Enzyme-Free Impedimetric Biosensor-Based Molecularly Imprinted Polymer for Selective Determination of L-Hydroxyproline. *Biosens Bioelectron* **2021**, *191*, 113387.
(213) Abdelhamied, N.; Abdelrahman, F.; El-Shibiny, A.; Hassan, R. Y. A. Bacteriophage-Based Nano-Biosensors for the Fast Impedimetric Determination of Pathogens in Food Samples. *Sci Rep* **2023**, *13* (1), 3498 DOI: 10.1038/s41598-023-30520-3.
(214) Cancino-Bernardi, J.; Comparetti, E. J.; Ferreira, N. N.; Miranda, R. R.; Tuesta, M. M.; Sampaio, I.; Inácio da Costa, P.; Zucolotto, V. A SARS-CoV-2 Impedimetric Biosensor Based on the Immobilization of ACE-2 Receptor-Containing Entire Cell Membranes as the Biorecognition Element. *Talanta* **2023**, *253*, 124008.
(215) *Label-free impedimetric thrombin sensor based on poly(pyrrole-nitrilotriacetic acid)-aptamer film*; Millipore Sigma, 2012. https://www.sigmaaldrich.com/IN/en/tech-docs/paper/293174 (accessed 2024−03−02).
(216) Chen, B.; Kiely, J.; Williams, I.; Luxton, R. A Non-Faradaic Impedimetric Biosensor for Monitoring of Caspase 9 in Mammalian Cell Culture. *Bioelectrochemistry* **2023**, *153*, 108456.
(217) Rohman, A.; Windarsih, A.; Lukitaningsih, E.; Rafi, M.; Betania, K.; Fadzillah, N. A. The Use of FTIR and Raman Spectroscopy in Combination with Chemometrics for Analysis of Biomolecules in Biomedical Fluids: A Review. *Biomed Spectrosc Imaging* **2020**, *8* (3−4), 55−71.
(218) Baker, M. J.; Hussain, S. R.; Lovergne, L.; Untereiner, V.; Hughes, C.; Lukaszewski, R. A.; Thiéfin, G.; Sockalingum, G. D. Developing and Understanding Biofluid Vibrational Spectroscopy: A Critical Review. *Chem Soc Rev* **2016**, *45* (7), 1803−1818.
(219) Mitchell, A. L.; Gajjar, K.; Theophilou, G.; Martin, F. L.; Martin-Hirsch, P. P. L. Vibrational Spectroscopy of Biofluids for Disease Screening or Diagnosis: Translation from the Laboratory to a Clinical Setting. *J Biophotonics* **2014**, *7*, 153.
(220) Moros, J.; Garrigues, S.; de la Guardia, M. Vibrational Spectroscopy Provides a Green Tool for Multi-Component Analysis. *TrAC Trends in Analytical Chemistry* **2010**, *29* (7), 578−591.
(221) Leal, L. B.; Nogueira, M. S.; Canevari, R. A.; Carvalho, L. F. C. S. Vibration Spectroscopy and Body Biofluids: Literature Review for Clinical Applications. *Photodiagnosis Photodyn Ther* **2018**, *24*, 237−244.
(222) Tiemeier, H.; Van Tuijl, H. R.; Hofman, A.; Kiliaan, A. J.; Breteler, M. M. B. Plasma Fatty Acid Composition and Depression Are Associated in the Elderly: The Rotterdam Study. *Am. J. Clin. Nutr.* **2003**, *78* (1), 40−46.
(223) Deidda, R.; Sacre, P.-Y.; Clavaud, M.; Coïc, L.; Avohou, H.; Hubert, P.; Ziemons, E. Vibrational Spectroscopy in Analysis of Pharmaceuticals: Critical Review of Innovative Portable and Handheld NIR and Raman Spectrophotometers. *TrAC Trends in Analytical Chemistry* **2019**, *114*, 251−259.
(224) Glassford, S. E.; Byrne, B.; Kazarian, S. G. Recent Applications of ATR FTIR Spectroscopy and Imaging to Proteins. *Biochim. Biophys. Acta* **2013**, *1834* (12), 2849−2858.
(225) Xavier, T. S.; Joe, I. H. FT-IR, Raman and DFT Study of 2-Amino-5-Fluorobenzoic Acid and Its Biological Activity with Other Halogen (Cl, Br) Substitution. *Spectrochim Acta A Mol Biomol Spectrosc* **2011**, *79* (2), 332−337.
(226) Maes, M.; Christophe, A.; Delanghe, J.; Altamura, C.; Neels, H.; Meltzer, H. Y. Lowered Omega3 Polyunsaturated Fatty Acids in Serum Phospholipids and Cholesteryl Esters of Depressed Patients. *Psychiatry Res* **1999**, *85* (3), 275−291.
(227) Baghai, T. C.; Varallo-Bedarida, G.; Born, C.; Häfner, S.; Schüle, C.; Eser, D.; Rupprecht, R.; Bondy, B.; Von Schacky, C. Major Depressive Disorder Is Associated with Cardiovascular Risk Factors and Low Omega-3 Index. *Journal of Clinical Psychiatry* **2011**, *72* (9), 1242−1247.
(228) Pichardo-Molina, J. L.; Frausto-Reyes, C.; Barbosa-García, O.; Huerta-Franco, R.; González-Trujillo, J. L.; Ramírez-Alvarado, C. A.; Gutiérrez-Juárez, G.; Medina-Gutiérrez, C. Raman Spectroscopy and Multivariate Analysis of Serum Samples from Breast Cancer Patients. *Lasers Med Sci* **2007**, *22* (4), 229−236.
(229) Baker, M. J.; Hughes, C. S.; Hollywood, K. A. Biophotonics: Vibrational Spectroscopic Diagnostics. *Biophotonics: Vibrational Spectroscopic Diagnostics* **2016**, 1−94.
(230) Rohman, A.; Windarsih, A.; Riyanto, S.; Sudjadi; Ahmad, S. A. S.; Rosman, A. S.; Yusoff, F. M. Fourier Transform Infrared Spectroscopy Combined with Multivariate Calibrations for the Authentication of Avocado Oil. *Int J Food Prop* **2016**, *19*, 680−687.
(231) Lai, Y.; Ni, Y.; Kokot, S. Discrimination of Rhizoma Corydalis from Two Sources by Near-Infrared Spectroscopy Supported by the Wavelet Transform and Least-Squares Support Vector Machine Methods. *Vib Spectrosc* **2011**, *56* (2), 154−160.
(232) Sultana, R.; Zafarullah, S.; Kirubamani, H. Utility of FTIR Spectroscopic Analysis of Saliva of Diabetic Pregnant Women in Each Trimester. *Indian J Sci Technol* **2011**, *4*, 967.
(233) Xie, J.; Zhang, H.; Li, J.; Cai, F. Window Subtracted Wave Band Selection Method for the FTIR/ATR Spectrum Analysis. *Progress in Electromagnetics Research M* **2018**, *68*, 53−59.
(234) Perez-Guaita, D.; Ventura-Gayete, J.; Pérez-Rambla, C.; Sancho-Andreu, M.; Garrigues, S.; de la Guardia, M. Evaluation of Infrared Spectroscopy as a Screening Tool for Serum Analysis: Impact of the Nature of Samples Included in the Calibration Set. *Microchemical Journal* **2013**, *106*, 202−211.
(235) Spalding, K.; Bonnier, F.; Bruno, C.; Blasco, H.; Board, R.; Benz-de Bretagne, I.; Byrne, H. J.; Butler, H. J.; Chourpa, I.; Radhakrishnan, P.; Baker, M. J. Enabling Quantification of Protein Concentration in Human Serum Biopsies Using Attenuated Total Reflectance - Fourier Transform Infrared (ATR-FTIR) Spectroscopy. *Vib Spectrosc* **2018**, *99*, 50−58.
(236) Gok, S.; Aydin, O. Z.; Sural, Y. S.; Zorlu, F.; Bayol, U.; Severcan, F. Bladder Cancer Diagnosis from Bladder Wash by Fourier Transform Infrared Spectroscopy as a Novel Test for Tumor Recurrence. *J Biophotonics* **2016**, *9* (9), 967−975.
(237) Lima, K. M. G.; Gajjar, K. B.; Martin-Hirsch, P. L.; Martin, F. L. Segregation of Ovarian Cancer Stage Exploiting Spectral Biomarkers Derived from Blood Plasma or Serum Analysis: ATR-FTIR Spectroscopy Coupled with Variable Selection Methods. *Biotechnol. Prog.* **2015**, *31* (3), 832−839.
(238) Wang, R.; Wang, Y. Fourier Transform Infrared Spectroscopy in Oral Cancer Diagnosis. *Int J Mol Sci* **2021**, *22* (3), 1206.
(239) Zhao, Y.; Ji, N.; Li, X.; Hou, J.; Li, M.; Yang, Y.; Tian, P.; Sun, X.; Xiao, X.; Yin, L. Study on a Non-Invasive Method for Rapid Screening

Human Serum Albumin Injectables by Raman Spectroscopy. *J Innov Opt Health Sci* **2017**, *10*, 1650030.
(240) Kengne-Momo, R. P.; Daniel, Ph.; Lagarde, F.; Jeyachandran, Y. L.; Pilard, J. F.; Durand-Thouand, M.-J.; Thouand, G. Protein Interactions Investigated by the Raman Spectroscopy for Biosensor Applications. *Int J Spectrosc* **2012**, *2012*, 1−7.
(241) Lemma, T.; De Barros Souza, F.; Tellez Soto, C. A.; Martin, A. A. An FT-Raman, FT-IR, and Quantum Chemical Investigation of Stanozolol and Oxandrolone. *Biosensors (Basel)* **2018**, *8* (1), 2.
(242) Notingher, I.; Verrier, S.; Haque, S. A.; Polak, J. M.; Hench, L. L. Spectroscopic Study of Human Lung Epithelial Cells (A549) in Culture: Living Cells versus Dead Cells. *Biopolymers* **2003**, *72*, 230−240.
(243) Owen, C. A.; Selvakumaran, J.; Notingher, I.; Jell, G.; Hench, L. L.; Stevens, M. M. In Vitro Toxicology Evaluation of Pharmaceuticals Using Raman Micro-spectroscopy. *J Cell Biochem* **2006**, *99*, 178.
(244) Moore, T. J.; Moody, A. S.; Payne, T. D.; Sarabia, G. M.; Daniel, A. R.; Sharma, B. In Vitro and In Vivo SERS Biosensing for Disease Diagnosis. *Biosensors (Basel)* **2018**, *8*, 46.
(245) Sharma, B.; Frontiera, R. R.; Henry, A.-I.; Ringe, E.; Van Duyne, R. P. SERS: Materials, Applications, and the Future. *Materials Today* **2012**, *15* (1), 16−25.
(246) Fleischmann, M.; Hendra, P. J.; McQuillan, A. J. Raman Spectra of Pyridine Adsorbed at a Silver Electrode. *Chem. Phys. Lett.* **1974**, *26* (2), 163−166.
(247) Abalde-Cela, S.; Aldeanueva-Potel, P.; Mateo-Mateo, C.; Rodríguez-Lorenzo, L.; Álvarez-Puebla, R. A.; Liz-Marzán, L. M. Surface-Enhanced Raman Scattering Biomedical Applications of Plasmonic Colloidal Particles. *J R Soc Interface* **2010**, *7*, S435−S450.
(248) Qian, X.-M.; Nie, S. M. Single-Molecule and Single-Nanoparticle SERS: From Fundamental Mechanisms to Biomedical Applications. *Chem. Soc. Rev.* **2008**, *37* (5), 912−920.
(249) Oh, Y. J.; Park, S. G.; Kang, M. H.; Choi, J. H.; Nam, Y.; Jeong, K. H. Beyond the SERS: Raman Enhancement of Small Molecules Using Nanofluidic Channels with Localized Surface Plasmon Resonance. *Small* **2011**, *7* (2), 184−188.
(250) Choi, C. J.; Xu, Z.; Wu, H. Y.; Liu, G. L.; Cunningham, B. T. Surface-Enhanced Raman Nanodomes. *Nanotechnology* **2010**, *21* (41), 415301.
(251) Momenpour, A. *RAMAN BIOSENSORS*, Ph.D. Thesis, University of Ottawa, 2017.
(252) Morton, S. M.; Jensen, L. Understanding the Molecule-Surface Chemical Coupling in SERS. *J. Am. Chem. Soc.* **2009**, *131* (11), 4090−4098.
(253) Jensen, L.; Aikens, C. M.; Schatz, G. C. Electronic Structure Methods for Studying Surface-Enhanced Raman Scattering. *Chem. Soc. Rev.* **2008**, *37* (5), 1061−1073.
(254) Stewart, M. E.; Anderton, C. R.; Thompson, L. B.; Maria, J.; Gray, S. K.; Rogers, J. A.; Nuzzo, R. G. Nanostructured Plasmonic Sensors. *Chem Rev* **2008**, *108* (2), 494−521.
(255) Orendorff, C. J.; Gearheart, L.; Jana, N. R.; Murphy, C. J. Aspect Ratio Dependence on Surface Enhanced Raman Scattering Using Silver and Gold Nanorod Substrates. *Phys. Chem. Chem. Phys.* **2006**, *8* (1), 165−170.
(256) Orendorff, C. J.; Gole, A.; Sau, T. K.; Murphy, C. J. Surface-Enhanced Raman Spectroscopy of Self-Assembled Monolayers: Sandwich Architecture and Nanoparticle Shape Dependence. *Anal. Chem.* **2005**, *77* (10), 3261−3266.
(257) McNay, G.; Eustace, D.; Smith, W. E.; Faulds, K.; Graham, D. Surface-Enhanced Raman Scattering (SERS) and Surface-Enhanced Resonance Raman Scattering (SERRS): A Review of Applications. *Appl. Spectrosc.* **2011**, *65* (8), 825−837.
(258) Long, D. A. Handbook of Vibrational Spectroscopy, Volumes 1−5. Edited by J. M. Chalmers and P. R. Griffiths. John Wiley & Sons, Chichester, 2002, Pp. 3862. *J. Raman Spectrosc.* **2005**, *36* (3), 271−271.
(259) Gangadharan, D. T.; Xu, Z.; Liu, Y.; Izquierdo, R.; Ma, D. Recent Advancements in Plasmon-Enhanced Promising Third-Generation Solar Cells. *Nanophotonics*; Walter de Gruyter GmbH, 2017; pp 153−175. DOI: 10.1515/nanoph-2016-0111.
(260) Huang, X.; El-Sayed, I. H.; Qian, W.; El-Sayed, M. A. Cancer Cell Imaging and Photothermal Therapy in the Near-Infrared Region by Using Gold Nanorods. *J. Am. Chem. Soc.* **2006**, *128* (6), 2115−2120.
(261) Vo-Dinh, T. SERS Chemical Sensors and Biosensors: New Tools for Environmental and Biological Analysis☆. *Sensors and Actuators B-chemical* **1995**, *29*, 183−189.
(262) Tiwari, V. S.; Khetani, A.; Monfared, A. M. T.; Smith, B.; Anis, H.; Trudeau, V. L. Detection of Amino Acid Neurotransmitters by Surface Enhanced Raman Scattering and Hollow Core Photonic Crystal Fiber. *Proceedings of the SPIE* **2012**, *8233*, 104−109.
(263) Siek, M.; Kaminska, A.; Kelm, A.; Rolinski, T.; Holyst, R.; Opallo, M.; Niedziolka-Jonsson, J. Electrodeposition for Preparation of Efficient Surface-Enhanced Raman Scattering-Active Silver Nanoparticle Substrates for Neurotransmitter Detection. *Electrochim. Acta* **2013**, *89*, 284−291.
(264) Chen, Y.; Chen, M.; Lin, J.; Lai, W.; Huang, W.; Chen, H.; Weng, G. Label-Free Optical Detection of Acute Myocardial Infarction Based on Blood Plasma Surface-Enhanced Raman Spectroscopy. *J. Appl. Spectrosc.* **2016**, *83*, 798.
(265) Matousek, P.; Clark, I. P.; Draper, E. R. C.; Morris, M. D.; Goodship, A. E.; Everall, N.; Towrie, M.; Finney, W. F.; Parker, A. W. Subsurface Probing in Diffusely Scattering Media Using Spatially Offset Raman Spectroscopy. *Appl. Spectrosc.* **2005**, *59* (4), 393−400.
(266) Moody, A. S.; Baghernejad, P. C.; Webb, K. R.; Sharma, B. Surface Enhanced Spatially Offset Raman Spectroscopy Detection of Neurochemicals Through the Skull. *Anal. Chem.* **2017**, *89* (11), 5688−5692.
(267) Tian, F.; Conde, J.; Bao, C. Gold Nanostars for Efficient In Vitro and In Vivo Real-Time SERS Gold Nanostars for Efficient In Vitro and In Vivo Real-Time SERS Detection and Drug Delivery via Plasmonic-Tunable Raman/FTIR Detection and Drug Delivery via Plasmonic-Tunable Raman/FTIR Imaging Imaging. *Biomaterials* **2016**, *106*, 87−97.
(268) Pucetaite, M.; Velicka, M.; Pilipavičius, J.; Beganskiene, A.; Ceponkus, J.; Sablinskas, V. Uric Acid Detection by Means of SERS Spectroscopy on Dried Ag Colloidal Drops. *J. Raman Spectrosc.* **2016**, *47*, 681−686.
(269) Pettinger, B.; Domke, K. F.; Zhang, D.; Picardi, G.; Schuster, R. Tip-Enhanced Raman Scattering: Influence of the Tip-Surface Geometry on Optical Resonance and Enhancement. *Surf. Sci.* **2009**, *603*, 1335−1341.
(270) He, Y.; Wang, Y.; Yang, X.; Xie, S.; Yuan, R.; Chai, Y. Metal Organic Frameworks Combining CoFe2O4 Magnetic Nanoparticles as Highly Efficient SERS Sensing Platform for Ultrasensitive Detection of N-Terminal Pro-Brain Natriuretic Peptide. *ACS Appl Mater Interfaces* **2016**, *8* (12), 7683−7690.
(271) Dab, C.; Thomas, R.; Ruediger, A. Design of a Plasmonic Platform to Improve the SERS Sensitivity for Molecular Detection. *Photonic Sensors* **2020**, *10* (3), 204−214.
(272) Pettinger, B. Single-Molecule Surface- and Tip-Enhanced Raman Spectroscopy. *Molecular Physics* **2010**, *108*, 2039−2059.
(273) Bantz, K. C.; Meyer, A. F.; Wittenberg, N. J.; Im, H.; Kurtulus, Ö.; Lee, S. H.; Lindquist, N. C.; Oh, S.-H.; Haynes, C. L. Recent Progress in SERS Biosensing. *Phys. Chem. Chem. Phys.* **2011**, *13* (24), 11551−11567.
(274) Lal, S.; Link, S.; Halas, N. J. Nano-Optics from Sensing to Waveguiding. *Nat Photonics* **2007**, *1* (11), 641−648.
(275) Barhoumi, A.; Zhang, D.; Tam, F.; Halas, N. J. Surface-Enhanced Raman Spectroscopy of DNA. *J. Am. Chem. Soc.* **2008**, *130* (16), 5523−5529.
(276) Zhang, X.; Zhao, J.; Whitney, A. V; Elam, J. W.; Van Duyne, R. P. Ultrastable Substrates for Surface-Enhanced Raman Spectroscopy: Al2O3 Overlayers Fabricated by Atomic Layer Deposition Yield Improved Anthrax Biomarker Detection. *J. Am. Chem. Soc.* **2006**, *128* (31), 10304−10309.
(277) Green, M.; Liu, F.-M.; Cohen, L.; Köllensperger, P.; Cass, T. SERS Platforms for High Density DNA Arrays. *Faraday Discuss.* **2006**, *132* (0), 269−280.

(278) He, L.; Langlet, M.; Stambouli, V. Surface-Enhanced Raman Spectroscopy Label-Free Detection of DNA Complementary PolyA and PolyT Polybases on Ag/TiO2 Platform. *ChemistrySelect* **2016**, *1* (17), 5501−5509.
(279) Muhammad, M.; Huang, Q. A Review of Aptamer-Based SERS Biosensors: Design Strategies and Applications. *Talanta* **2021**, *227*, 122188.
(280) Guerrini, L.; Alvarez-Puebla, R. A. Surface-Enhanced Raman Spectroscopy in Cancer Diagnosis, Prognosis and Monitoring. *Cancers (Basel)* **2019**, *11* (6), 748.
(281) Tripathy, S.; Singh, S. G. Label-Free Electrochemical Detection of DNA Hybridization: A Method for COVID-19 Diagnosis. *Transactions of the Indian National Academy of Engineering 2020 5:2* **2020**, *5* (2), 205−209.
(282) Cialla, D.; Deckert-Gaudig, T.; Budich, C.; Laue, M.; Möller, R.; Naumann, D.; Deckert, V.; Popp, J. Raman to the Limit: Tip-enhanced Raman Spectroscopic Investigations of a Single Tobacco Mosaic Virus. *J. Raman Spectrosc.* **2009**, *40*, 240−243.
(283) Qian, X.; Peng, X. H.; Ansari, D. O.; Yin-Goen, Q.; Chen, G. Z.; Shin, D. M.; Yang, L.; Young, A. N.; Wang, M. D.; Nie, S. In Vivo Tumor Targeting and Spectroscopic Detection with Surface-Enhanced Raman Nanoparticle Tags. *Nat. Biotechnol.* **2008**, *26* (1), 83−90.
(284) Zhang, Y.; Yang, P.; Habeeb Muhammed, M. A.; Alsaiari, S. K.; Moosa, B.; Almalik, A.; Kumar, A.; Ringe, E.; Khashab, N. M. Tunable and Linker Free Nanogaps in Core-Shell Plasmonic Nanorods for Selective and Quantitative Detection of Circulating Tumor Cells by SERS. *ACS Appl Mater Interfaces* **2017**, *9* (43), 37597−37605.
(285) Webb, J. A.; Ou, Y. C.; Faley, S.; Paul, E. P.; Hittinger, J. P.; Cutright, C. C.; Lin, E. C.; Bellan, L. M.; Bardhan, R. Theranostic Gold Nanoantennas for Simultaneous Multiplexed Raman Imaging of Immunomarkers and Photothermal Therapy. *ACS Omega* **2017**, *2* (7), 3583−3594.
(286) Park, J.; Hwang, M.; Choi, B.; Jeong, H.; Jung, J. H.; Kim, H. K.; Hong, S.; Park, J. H.; Choi, Y. Exosome Classification by Pattern Analysis of Surface-Enhanced Raman Spectroscopy Data for Lung Cancer Diagnosis. *Anal. Chem.* **2017**, *89* (12), 6695−6701.
(287) Qiao, X.; Su, B.; Liu, C.; Song, Q.; Luo, D.; Mo, G.; Wang, T. Selective Surface Enhanced Raman Scattering for Quantitative Detection of Lung Cancer Biomarkers in Superparticle@MOF Structure. *Adv. Mater.* **2018**, *30* (5), 1702275 DOI: 10.1002/adma.201702275.
(288) Yang, K.; Hu, Y.; Dong, N.; Zhu, G.; Zhu, T.; Jiang, N. A Novel SERS-Based Magnetic Aptasensor for Prostate Specific Antigen Assay with High Sensitivity. *Biosens Bioelectron* **2017**, *94*, 286−291.
(289) Maneeprakorn, W.; Bamrungsap, S.; Apiwat, C.; Wiriyachaiporn, N. Surface-Enhanced Raman Scattering Based Lateral Flow Immunochromatographic Assay for Sensitive Influenza Detection. *RSC Adv.* **2016**, *6* (113), 112079−112085.
(290) Jia, X.; Wang, C.; Rong, Z.; Li, J.; Wang, K.; Qie, Z.; Xiao, R.; Wang, S. Dual Dye-Loaded Au@Ag Coupled to a Lateral Flow Immunoassay for the Accurate and Sensitive Detection of Mycoplasma Pneumoniae Infection. *RSC Adv* **2018**, *8*, 21243−21251.
(291) Kim, W. H.; Lee, J. U.; Song, S.; Kim, S.; Choi, Y. J.; Sim, S. J. A Label-Free, Ultra-Highly Sensitive and Multiplexed SERS Nanoplasmonic Biosensor for MiRNA Detection Using a Head-Flocked Gold Nanopillar. *Analyst* **2019**, *144* (5), 1768−1776.
(292) Mosier-Boss, P. A. Review on SERS of Bacteria. *Biosensors (Basel)* **2017**, *7* (4), 51.
(293) Goulart, A. C. C.; Silveira, L.; Carvalho, H. C.; Dorta, C. B.; Pacheco, M. T. T.; Zângaro, R. A. Diagnosing COVID-19 in Human Serum Using Raman Spectroscopy. *Lasers Med Sci* **2022**, *37* (4), 2217−2226.
(294) Cao, J.; Hu, S.; Tang, W.; Wang, Y.; Yang, Y.; Wang, F.; Guo, X.; Ying, Y.; Liu, X.; Wen, Y.; Yang, H. Reactive Hydrogel Patch for SERS Detection of Environmental Formaldehyde. *ACS Sens* **2023**, *8* (5), 1929−1938.
(295) Yang, H.; Zhao, C.; Li, R.; Shen, C.; Cai, X.; Sun, L.; Luo, C.; Yin, Y. Noninvasive and Prospective Diagnosis of Coronary Heart Disease with Urine Using Surface-Enhanced Raman Spectroscopy. *Analyst* **2018**, *143* (10), 2235−2242.
(296) Eom, G.; Kim, H.; Hwang, A.; Son, H.-Y.; Choi, Y.; Moon, J.; Kim, D.; Lee, M.; Lim, E.-K.; Jeong, J.; Huh, Y.-M.; Seo, M.-K.; Kang, T.; Kim, B. Nanogap-Rich Au Nanowire SERS Sensor for Ultrasensitive Telomerase Activity Detection: Application to Gastric and Breast Cancer Tissues Diagnosis. *Adv Funct Mater* **2017**, *27*, 1701832.
(297) Esmati, M.; Hajari, N.; Eskandari, V. Flexible Plasmonic Paper Substrates as Surface-Enhanced Raman Scattering (SERS) Biosensors Enable Sensitive Detection of Sunitinib Malate Drug. *Plasmonics* **2024**, *19* (1), 21−31.
(298) Wei, X.; Song, W.; Fan, Y.; Sun, Y.; Li, Z.; Chen, S.; Shi, J.; Zhang, D.; Zou, X.; Xu, X. A SERS Aptasensor Based on a Flexible Substrate for Interference-Free Detection of Carbendazim in Apple. *Food Chem.* **2024**, *431*, 137120.
(299) Lu, Y.; Liu, Q.; Fu, B.; Li, P.; Xu, W. Label-Free MIP-SERS Biosensor for Sensitive Detection of Colorectal Cancer Biomarker. *Talanta* **2023**, *258*, 124461.
(300) Tripathi, M. N.; Jangir, P.; Aakriti; Rai, S.; Gangwar, M.; Nath, G.; Saxena, P. S.; Srivastava, A. A Novel Approach for Rapid and Sensitive Detection of Zika Virus Utilizing Silver Nanoislands as SERS Platform. *Spectrochim Acta A Mol Biomol Spectrosc* **2023**, *302*, 123045.
(301) Chen, C.; Wang, J. Optical Biosensors: An Exhaustive and Comprehensive Review. *Analyst* **2020**, *145* (5), 1605−1628.
(302) Zanchetta, G.; Lanfranco, R.; Giavazzi, F.; Bellini, T.; Buscaglia, M. Emerging Applications of Label-Free Optical Biosensors. *Nanophotonics*; Walter de Gruyter GmbH, 2017; pp 627−645. DOI: 10.1515/nanoph-2016-0158.
(303) Singh, P. Surface Plasmon Resonance: A Boon for Viral Diagnostics. *Reference Module in Life Sciences* **2017**, DOI: 10.1016/B978-0-12-809633-8.12245-9.
(304) Chen, H.; Liu, F.; Koh, K.; Lee, J.; Ye, Z.; Yin, T.; Sun, L. Sensitive Detection of Tuberculosis Using Nanoparticle-Enhanced Surface Plasmon Resonance. *Microchimica Acta* **2013**, *180* (5−6), 431−436.
(305) Sau, T. K.; Rogach, A. L.; Jäckel, F.; Klar, T. A.; Feldmann, J. Properties and Applications of Colloidal Nonspherical Noble Metal Nanoparticles. *Adv. Mater.* **2010**, *22* (16), 1805−1825.
(306) Ho, H. P.; Lam, W. W. Application of Differential Phase Measurement Technique to Surface Plasmon Resonance Sensors. *Sens Actuators B Chem* **2003**, *96* (3), 554−559.
(307) Ho, H. P.; Law, W. C.; Wu, S. Y.; Liu, X. H.; Wong, S. P.; Lin, C.; Kong, S. K. Phase-Sensitive Surface Plasmon Resonance Biosensor Using the Photoelastic Modulation Technique. *Sens Actuators B Chem* **2006**, *114* (1), 80−84.
(308) Wang, J.; Lin, W.; Cao, E.; Xu, X.; Liang, W.; Zhang, X. Surface Plasmon Resonance Sensors on Raman and Fluorescence Spectroscopy. *Sensors (Basel)* **2017**, *17* (12), 2719.
(309) Murali, S.; Rustandi, R.; Zheng, X.; Payne, A.; Shang, L. Applications of Surface Plasmon Resonance and Biolayer Interferometry for Virus-Ligand Binding. *Viruses* **2022**, *14*, 717.
(310) *XanTec bioanalytics GmbH | Tech notes | Principles of SPR*; XanTec bioanalytics GmbH, 2024. https://www.xantec.com/technotes/spr_principle.php (accessed 2024−03−03).
(311) Homola, J. Surface Plasmon Resonance Sensors for Detection of Chemical and Biological Species. *Chem Rev* **2008**, *108* (2), 462−493.
(312) Homola, J. Surface Plasmon Resonance Biosensors: Advances and Applications. In *International Conference on Optical Fibre Sensors*; OFS, 2009.
(313) Unser, S.; Bruzas, I.; He, J.; Sagle, L. Localized Surface Plasmon Resonance Biosensing: Current Challenges and Approaches. *Sensors* **2015**, *15* (7), 15684−15716.
(314) Zhang, Z.; Xu, P.; Yang, X.; Liang, W.; Sun, M. Surface Plasmon-Driven Photocatalysis in Ambient, Aqueous and High-Vacuum Monitored by SERS and TERS. *Journal of Photochemistry and Photobiology C-photochemistry Reviews* **2016**, *27*, 100−112.
(315) Zeng, S.; Yu, X.; Law, W.-C.; Zhang, Y.; Hu, R.; Dinh, X.-Q.; Ho, H.-P.; Yong, K.-T. Size Dependence of Au NP-Enhanced Surface

Plasmon Resonance Based on Differential Phase Measurement. *Sens Actuators B Chem* **2013**, *176*, 1128−1133.
(316) Mayer, K. M.; Hafner, J. H. Localized Surface Plasmon Resonance Sensors. *Chem Rev* **2011**, *111* (6), 3828−3857.
(317) Nehl, C. L.; Liao, H.; Hafner, J. H. Optical Properties of Star-Shaped Gold Nanoparticles. *Nano Lett* **2006**, *6* (4), 683−688.
(318) Hao, F.; Nehl, C. L.; Hafner, J. H.; Nordlander, P. Plasmon Resonances of a Gold Nanostar. *Nano Lett* **2007**, *7* (3), 729−732.
(319) Damborský, P.; Švitel, J.; Katrlík, J. Optical Biosensors. *Essays Biochem* **2016**, *60*, 91−100.
(320) Riedel, T.; Rodriguez-Emmenegger, C.; de los Santos Pereira, A.; Bedajánková, A.; Jinoch, P.; Boltovets, P. M.; Brynda, E. Diagnosis of Epstein-Barr Virus Infection in Clinical Serum Samples by an SPR Biosensor Assay. *Biosens Bioelectron* **2014**, *55*, 278−284.
(321) Pimková, K.; Bocková, M.; Hegnerová, K.; Suttnar, J.; Cermak, J.; Homola, J.; Dyr, J. Surface Plasmon Resonance Biosensor for the Detection of VEGFR-1—a Protein Marker of Myelodysplastic Syndromes. *Anal Bioanal Chem* **2012**, *402*, 381−387.
(322) Pennacchio, A. E.; Ruggiero, G. D.; Staiano, M. F.; Piccialli, G.; Oliviero, G.; Lewkowicz, A.; Synak, A.; Bojarski, P.; d'Auria, S. A Surface Plasmon Resonance Based Biochip for the Detection of Patulin Toxin. *Opt Mater (Amst)* **2014**, *36*, 1670−1675.
(323) Choi, Y.; Kwak, H.; Hong, S. Quantification of Arsenic(Iii) in Aqueous Media Using a Novel Hybrid Platform Comprised of Radially Porous Silica Particles and a Gold Thin Film. *Anal. Methods* **2014**, *6* (17), 7054−7061.
(324) Altintas, Z.; Uludag, Y.; Gurbuz, Y.; Tothill, I. E. Surface Plasmon Resonance Based Immunosensor for the Detection of the Cancer Biomarker Carcinoembryonic Antigen. *Talanta* **2011**, *86*, 377−383.
(325) Malhotra, B. D.; Ali, Md. A. Plasmonic Nanostructures: Fiber-Optic Biosensors. *Nanomaterials for Biosensors* **2018**, 161.
(326) Schnurr, B.; Ahrens, T.; Regenass, U. Optical Assays in Drug Discovery. *Comprehensive Medicinal Chemistry II* **2007**, 577.
(327) Hämäläinen, M. D.; Markgren, P. O.; Schaal, W.; Karlén, A.; Classon, B.; Vrang, L.; Samuelsson, B.; Hallberg, A.; Danielson, U. H. Characterization of a Set of HIV-1 Protease Inhibitors Using Binding Kinetics Data from a Biosensor-Based Screen. *J Biomol Screen* **2000**, *5*, 353−359.
(328) Turner, A. P. F. Biosensors. *Curr Opin Biotechnol* **1994**, *5* (1), 49−53.
(329) Kim, W.-G.; Song, H.; Kim, C.; Moon, J.-S.; Kim, K.; Lee, S.-W.; Oh, J.-W. Biomimetic Self-Templating Optical Structures Fabricated by Genetically Engineered M13 Bacteriophage. *Biosens Bioelectron* **2016**, *85*, 853−859.
(330) Shpacovitch, V.; Sidorenko, I.; Lenssen, J. E.; Temchura, V.; Weichert, F.; Müller, H.; Überla, K.; Zybin, A.; Schramm, A.; Hergenröder, R. Application of the PAMONO-Sensor for Quantification of Microvesicles and Determination of Nano-Particle Size Distribution. *Sensors (Basel)* **2017**, *17* (2), 244.
(331) Gopinath, S. C. B.; Kumar, P. K. R. Aptamers That Bind to the Hemagglutinin of the Recent Pandemic Influenza Virus H1N1 and Efficiently Inhibit Agglutination. *Acta Biomater* **2013**, *9* (11), 8932−8941.
(332) Wang, R.; Zhao, J.; Jiang, T.; Kwon, Y. M.; Lu, H.; Jiao, P.; Liao, M.; Li, Y. Selection and Characterization of DNA Aptamers for Use in Detection of Avian Influenza Virus H5N1. *J Virol Methods* **2013**, *189* (2), 362−369.
(333) Hearty, S.; Conroy, P. J.; Ayyar, B. V.; Byrne, B.; O'Kennedy, R. Surface Plasmon Resonance for Vaccine Design and Efficacy Studies: Recent Applications and Future Trends. *Expert Rev Vaccines* **2010**, *9* (6), 645−664.
(334) Lee, B. Review of the Present Status of Optical Fiber Sensors. *Optical Fiber Technology* **2003**, *9* (2), 57−79.
(335) Westerveld, W. J.; Leinders, S. M.; Van Dongen, K. W. A.; Urbach, H. P.; Yousefi, M. Extension of Marcatili's Analytical Approach for Rectangular Silicon Optical Waveguides. *Journal of Lightwave Technology* **2012**, *30* (14), 2388−2401.
(336) Kozma, P.; Kehl, F.; Ehrentreich-Förster, E.; Stamm, C.; Bier, F. F. Integrated Planar Optical Waveguide Interferometer Biosensors: A Comparative Review. *Biosens Bioelectron* **2014**, *58*, 287−307.
(337) Dell'Olio, F.; Passaro, V. M. N. Optical Sensing by Optimized Silicon Slot Waveguides. *Opt Express* **2007**, *15*, 4977−4993.
(338) Oulton, R. F.; Sorger, V. J.; Genov, D. A.; Pile, D. F. P.; Zhang, X. A Hybrid Plasmonic Waveguide for Subwavelength Confinement and Long-Range Propagation. *Nat Photonics* **2008**, *2* (8), 496−500.
(339) Barrios, C. A.; Gylfason, K. B.; Sánchez, B.; Griol, A.; Sohlström, H.; Holgado, M.; Casquel, R. Slot-Waveguide Biochemical Sensor. *Opt. Lett.* **2007**, *32* (21), 3080−3082.
(340) Leuermann, J.; Fernández-Gavela, A.; Torres-Cubillo, A.; Postigo, S.; Sánchez-Postigo, A.; Lechuga, L. M.; Halir, R.; Molina-Fernández, C. D. Optimizing the Limit of Detection of Waveguide-Based Interferometric Biosensor Devices. *Sensors* **2019**, *19* (17), 3671.
(341) Misiakos, K.; Raptis, I.; Makarona, E.; Botsialas, A.; Salapatas, A.; Oikonomou, P.; Psarouli, A.; Petrou, P. S.; Kakabakos, S. E.; Tukkiniemi, K.; Sopanen, M.; Jobst, G. All-Silicon Monolithic Mach-Zehnder Interferometer as a Refractive Index and Bio-Chemical Sensor. *Opt Express* **2014**, *22* (22), 26803.
(342) Heideman, R. G.; Kooyman, R. P. H.; Greve, J. Performance of a Highly Sensitive Optical Waveguide Mach-Zehnder Interferometer Immunosensor. *Sensors and Actuators B-chemical* **1993**, *10*, 209−217.
(343) Prieto, F.; Sep lveda, B.; Calle, A.; Llobera, A.; Dom nguez, C.; Abad, A.; Montoya, A.; Lechuga, L. M. An Integrated Optical Interferometric Nanodevice Based on Silicon Technology for Biosensor Applications. *Nanotechnology* **2003**, *14* (8), 907−912.
(344) Psarouli, A.; Salapatas, A.; Botsialas, A.; Petrou, P. S.; Raptis, I.; Makarona, E.; Jobst, G.; Tukkiniemi, K.; Sopanen, M.; Stoffer, R.; Kakabakos, S. E.; Misiakos, K. Monolithically Integrated Broad-Band Mach-Zehnder Interferometers for Highly Sensitive Label-Free Detection of Biomolecules through Dual Polarization Optics. *Sci Rep* **2015**, *5*, 17600 DOI: 10.1038/srep17600.
(345) Hartman, N.; Wyvill, J. C.; Campbell, D. P.; Edmonds, P. Rapid Response Biosensor for Detection and Identification of Common Foodborne Pathogens. In *Other Conferences*; SPIE, 1995.
(346) Gajos, K.; Budkowski, A.; Petrou, P.; Pagkali, V.; Awsiuk, K.; Rysz, J.; Bernasik, A.; Misiakos, K.; Raptis, I.; Kakabakos, S. Protein Adsorption/Desorption and Antibody Binding Stoichiometry on Silicon Interferometric Biosensors Examined with TOF-SIMS. *Appl. Surf. Sci.* **2018**, *444*, 187−196.
(347) Escorihuela, J.; González-Martínez, M. Á.; López-Paz, J. L.; Puchades, R.; Maquieira, Á.; Gimenez-Romero, D. Dual-Polarization Interferometry: A Novel Technique To Light up the Nanomolecular World. *Chem Rev* **2015**, *115* (1), 265−294.
(348) Escorihuela, J.; González-Martínez, M.; López-Paz, J.; Puchades, R.; Maquieira, A.; Gimenez-Romero, D. DUAL POLARIZATION INTERFEROMETRY. A TECHNIQUE TO LIGHT UP THE NANOMOLECULAR WORLD. *Chem. Rev.* **2015**, *115*, 265.
(349) Ouberai, M.; Xu, K.; Welland, M. Effect of the Interplay between Protein and Surface on the Properties of Adsorbed Protein Layers. *Biomaterials* **2014**, *35*, 6157.
(350) Huang, F.; Xu, P.; Liang, H. Using Dual-Polarization Interferometry to Study Surface-Initiated DNA Hybridization Chain Reactions in Real Time. *Biosens Bioelectron* **2014**, *51*, 317−323.
(351) Schmitt, K.; Schirmer, B.; Brandenburg, A. Label-Free Detection of Biomolecules by Waveguide Interferometry. *Proc. SPIE* **2005**, *5855*, 459−462.
(352) Schmitt, K.; Schirmer, B.; Hoffmann, C.; Brandenburg, A.; Meyrueis, P. Interferometric Biosensor Based on Planar Optical Waveguide Sensor Chips for Label-Free Detection of Surface Bound Bioreactions. *Biosens Bioelectron* **2007**, *22* (11), 2591−2597.
(353) Marazuela, M.; Moreno-Bondi, M. Fiber-Optic Biosensors - an Overview. *Anal Bioanal Chem* **2002**, *372* (5), 664−682.
(354) Taitt, C. R.; Anderson, G. P.; Ligler, F. S. Evanescent Wave Fluorescence Biosensors. *Biosens Bioelectron* **2005**, *20* (12), 2470−2487.

https://doi.org/10.1021/acsomega.4c07991
ACS Omega 2024, 9, 48918−48987

(355) Ferreira, A. P.; Werneck, M. M.; Ribeiro, R. M. Development of an Evanescent-Field Fibre Optic Sensor for Escherichia Coli O157:H7. *Biosens Bioelectron* **2001**, *16* (6), 399−408.
(356) DeMARCO, D. R.; LIM, D. V. DIRECT DETECTION OF ESCHERICHIA COLI 0157:H7 IN UNPASTEURIZED APPLE JUICE WITH AN EVANESCENT WAVE BIOSENSOR. *J Rapid Methods Autom Microbiol* **2001**, *9* (4), 241−257.
(357) Geng, T.; Morgan, M. T.; Bhunia, A. K. Detection of Low Levels of Listeria Monocytogenes Cells by Using a Fiber-Optic Immunosensor. *Appl. Environ. Microbiol.* **2004**, *70* (10), 6138−6146.
(358) Tims, T. B.; Lim, D. V. Rapid Detection of Bacillus Anthracis Spores Directly from Powders with an Evanescent Wave Fiber-Optic Biosensor. *J Microbiol Methods* **2004**, *59* (1), 127−130.
(359) Kramer, M. F.; Lim, D. V. A Rapid and Automated Fiber Optic-Based Biosensor Assay for the Detection OfSalmonella in Spent Irrigation Water Used in the Sprouting of Sprout Seeds. *J Food Prot* **2004**, *67* (1), 46−52.
(360) Yunianto, M.; Permata, A. N.; Eka, D.; Ariningrum, D.; Wahyuningsih, S.; Marzuki, A. Design of a Fiber Optic Biosensor for Cholesterol Detection in Human Blood. *IOP Conf Ser Mater Sci Eng* **2017**, *176*, 012014.
(361) Epstein, J. R.; Leung, A. P. K.; Lee, K.-H.; Walt, D. R. High-Density, Microsphere-Based Fiber Optic DNA Microarrays. *Biosens Bioelectron* **2003**, *18* (5), 541−546.
(362) Jin, Y.; Granville, A. M. Polymer Fiber Optic Sensors-A Mini Review of Their Synthesis and Applications. *J Biosens Bioelectron* **2016**, *7*, 194.
(363) Klantsataya, E.; Jia, P.; Ebendorff-Heidepriem, H.; Monro, T. M.; François, A. Plasmonic Fiber Optic Refractometric Sensors: From Conventional Architectures to Recent Design Trends. *Sensors* **2017**, *17* (1), 12.
(364) Gupta, B. D.; Shrivastav, A. M.; Usha, S. P. Surface Plasmon Resonance-Based Fiber Optic Sensors Utilizing Molecular Imprinting. *Sensors* **2016**, *16* (9), 1381.
(365) Sharma, A. K.; Pandey, A. K.; Kaur, B. A Review of Advancements (2007−2017) in Plasmonics-Based Optical Fiber Sensors. *Optical Fiber Technology* **2018**, *43*, 20−34.
(366) Fu, H.; Zhang, S.; Chen, H.; Weng, J. Graphene Enhances the Sensitivity of Fiber-Optic Surface Plasmon Resonance Biosensor. *IEEE Sens J* **2015**, *15* (10), 5478−5482.
(367) Zhang, Z.; Zhao, P.; Sun, F.; Xiao, G.; Wu, Y. Self-Referencing in Optical-Fiber Surface Plasmon Resonance Sensors. *IEEE Photonics Technology Letters* **2007**, *19* (24), 1958−1960.
(368) Kanso, M.; Cuenot, S.; Louarn, G. Sensitivity of Optical Fiber Sensor Based on Surface Plasmon Resonance: Modeling and Experiments. *Plasmonics* **2008**, *3* (2−3), 49−57.
(369) Pollet, J.; Delport, F.; Janssen, K. P. F.; Jans, K.; Maes, G.; Pfeiffer, H.; Wevers, M.; Lammertyn, J. Fiber Optic SPR Biosensing of DNA Hybridization and DNA-Protein Interactions. *Biosens Bioelectron* **2009**, *25* (4), 864−869.
(370) Sharma, A. K.; Jha, R.; Pattanaik, H. S. Design Considerations for Surface Plasmon Resonance Based Detection of Human Blood Group in near Infrared. *J. Appl. Phys.* **2010**, *107* (3), 034701.
(371) Bosch, M. E.; Sánchez, A. J. R.; Rojas, F. S.; Ojeda, C. B. Recent Development in Optical Fiber Biosensors. *Sensors* **2007**, *7* (6), 797−859.
(372) Vahala, K. J. Optical Microcavities. *Nature* **2003**, *424* (6950), 839−846.
(373) Bozzola, A.; Perotto, S.; De Angelis, F. Hybrid Plasmonic-Photonic Whispering Gallery Mode Resonators for Sensing: A Critical Review. *Analyst*; Royal Society of Chemistry, 2017; pp 883−898. DOI: 10.1039/c6an02693a.
(374) Foreman, M. R.; Swaim, J. D.; Vollmer, F. Whispering Gallery Mode Sensors. *Adv Opt Photonics* **2015**, *7* (2), 168−240.
(375) Zhu, J.; Özdemir, S. K.; Yilmaz, H.; Peng, B.; Dong, M.; Tomes, M.; Carmon, T.; Yang, L. Interfacing Whispering-Gallery Microresonators and Free Space Light with Cavity Enhanced Rayleigh Scattering. *Sci Rep* **2014**, *4* (1), 6396.
(376) Himmelhaus, M.; Krishnamoorthy, S.; Francois, A. Optical Sensors Based on Whispering Gallery Modes in Fluorescent Microbeads: Response to Specific Interactions. *Sensors* **2010**, *10* (6), 6257−6274.
(377) Ward, J. M.; Dhasmana, N.; Nic Chormaic, S. Hollow Core, Whispering Gallery Resonator Sensors. *Eur Phys J Spec Top* **2014**, *223* (10), 1917−1935.
(378) Zamora, V.; Díez, A.; Andrés, M. V; Gimeno, B. Cylindrical Optical Microcavities: Basic Properties and Sensor Applications. *Photonics Nanostruct* **2011**, *9* (2), 149−158.
(379) Nadgaran, H.; Afkhami Garaei, M. Enhancement of a Whispering Gallery Mode Microtoroid Resonator by Plasmonic Triangular Gold Nanoprism for Label-Free Biosensor Applications. *J. Appl. Phys.* **2015**, *118* (4), 043101 DOI: 10.1063/1.4927266.
(380) Johnson, S. G.; Mekis, A.; Fan, S.; Joannopoulos, J. D. Molding the Flow of Light. *Comput Sci Eng* **2001**, *3* (6), 38−47.
(381) Pal, S.; Yadav, A. R.; Lifson, M. A.; Baker, J. E.; Fauchet, P. M.; Miller, B. L. Selective Virus Detection in Complex Sample Matrices with Photonic Crystal Optical Cavities. *Biosens Bioelectron* **2013**, *44*, 229−234.
(382) Choi, E.; Choi, Y.; Nejad, Y. H. P.; Shin, K.; Park, J. Label-Free Specific Detection of Immunoglobulin G Antibody Using Nanoporous Hydrogel Photonic Crystals. *Sens Actuators B Chem* **2013**, *180*, 107−113.
(383) Scullion, M. G.; Krauss, T. F.; Di Falco, A. Slotted Photonic Crystal Sensors. *Sensors* **2013**, *13* (3), 3675−3710.
(384) Lee, N.; Wang, C.; Park, J. User-Friendly Point-of-Care Detection of Influenza A (H1N1) Virus Using Light Guide in Three-Dimensional Photonic Crystal. *RSC Adv* **2018**, *8* (41), 22991−22997.
(385) Xu, X.; Subbaraman, H.; Chakravarty, S.; Hosseini, A.; Covey, J.; Yu, Y.; Kwong, D.; Zhang, Y.; Lai, W.-C.; Zou, Y.; Lu, N.; Chen, R. T. Flexible Single-Crystal Silicon Nanomembrane Photonic Crystal Cavity. *ACS Nano* **2014**, *8* (12), 12265−12271.
(386) Zhang, X.; Chen, G.; Bian, F.; Cai, L.; Zhao, Y. Encoded Microneedle Arrays for Detection of Skin Interstitial Fluid Biomarkers. *Adv. Mater.* **2019**, *31* (37), 1902825.
(387) Long, F.; Zhu, A.; Gu, C.; Shi, H. Recent Progress in Optical Biosensors for Environmental Applications. *State of the Art in Biosensors - Environmental and Medical Applications* **2013**, DOI: 10.5772/52252.
(388) Medintz, I. L.; Clapp, A. R.; Mattoussi, H.; Goldman, E. R.; Fisher, B.; Mauro, J. M. Self-Assembled Nanoscale Biosensors Based on Quantum Dot FRET Donors. *Nat. Mater.* **2003**, *2* (9), 630−638.
(389) Algar, W. R.; Tavares, A. J.; Krull, U. J. Beyond Labels: A Review of the Application of Quantum Dots as Integrated Components of Assays, Bioprobes, and Biosensors Utilizing Optical Transduction. *Anal. Chim. Acta* **2010**, *673* (1), 1−25.
(390) Mansur, H. S. Quantum Dots and Nanocomposites. *WIREs Nanomedicine and Nanobiotechnology* **2010**, *2* (2), 113−129.
(391) Hahn, M. A.; Keng, P. C.; Krauss, T. D. Flow Cytometric Analysis To Detect Pathogens in Bacterial Cell Mixtures Using Semiconductor Quantum Dots. *Anal. Chem.* **2008**, *80* (3), 864−872.
(392) Ikanovic, M.; Rudzinski, W. E.; Bruno, J. G.; Allman, A.; Carrillo, M. P.; Dwarakanath, S.; Bhahdigadi, S.; Rao, P.; Kiel, J. L.; Andrews, C. J. Fluorescence Assay Based on Aptamer-Quantum Dot Binding to Bacillus Thuringiensis Spores. *J Fluoresc* **2007**, *17* (2), 193−199.
(393) Bentzen, E. L.; House, F.; Utley, T. J.; Crowe, J. E.; Wright, D. W. Progression of Respiratory Syncytial Virus Infection Monitored by Fluorescent Quantum Dot Probes. *Nano Lett* **2005**, *5* (4), 591−595.
(394) Long, F.; Gu, C.; Gu, A. Z.; Shi, H. Quantum Dot/Carrier-Protein/Haptens Conjugate as a Detection Nanobioprobe for FRET-Based Immunoassay of Small Analytes with All-Fiber Microfluidic Biosensing Platform. *Anal. Chem.* **2012**, *84* (8), 3646−3653.
(395) Zhang, H.; Feng, G.; Guo, Y.; Zhou, D. Robust, Specific Ratiometric Biosensing Using a Copper-Free Clicked Quantum Dot-DNA Aptamer Sensor. *Nanoscale* **2013**, *5*, 10307.
(396) Hong, S.; Lee, C. The Current Status and Future Outlook of Quantum Dot-Based Biosensors for Plant Virus Detection. *Plant Pathol J* **2018**, *34* (2), 85.

https://doi.org/10.1021/acsomega.4c07991
ACS Omega 2024, 9, 48918−48987

(397) Reza, M.; Samiee, F.; Tabatabie, M.; Mohsenifar, A. *Sensors & Transducers Development of Quantum Dot-Based Nanobiosensors against Citrus Tristeza Virus (CTV)*; IFSA, 2017; Vol. *213*. http://www.sensorsportal.com.
(398) Shojaei, T. R.; Salleh, M. A. M.; Sijam, K.; Rahim, R. A.; Mohsenifar, A.; Safarnejad, R.; Tabatabaei, M. Fluorometric Immunoassay for Detecting the Plant Virus Citrus Tristeza Using Carbon Nanoparticles Acting as Quenchers and Antibodies Labeled with CdTe Quantum Dots. *Microchimica Acta* **2016**, *183* (7), 2277−2287.
(399) Shojaei, T. R.; Salleh, M. A. M.; Sijam, K.; Rahim, R. A.; Mohsenifar, A.; Safarnejad, R.; Tabatabaei, M. Detection of Citrus Tristeza Virus by Using Fluorescence Resonance Energy Transfer-Based Biosensor. *Spectrochim Acta A Mol Biomol Spectrosc* **2016**, *169*, 216−222.
(400) Yeh, H.-C.; Ho, Y.-P.; Wang, T.-H. Quantum Dot-Mediated Biosensing Assays for Specific Nucleic Acid Detection. *Nanomedicine* **2005**, *1* (2), 115−121.
(401) Singh, S.; Chakraborty, A.; Singh, V.; Molla, A.; Hussain, S.; Singh, M. K.; Das, P. DNA Mediated Assembly of Quantum Dot-Protoporphyrin IX FRET Probes and the Effect of FRET Efficiency on ROS Generation. *Phys. Chem. Chem. Phys.* **2015**, *17* (8), 5973−5981.
(402) Gill, R.; Willner, I.; Shweky, I.; Banin, U. Fluorescence Resonance Energy Transfer in CdSe/ZnS-DNA Conjugates: Probing Hybridization and DNA Cleavage. *J Phys Chem B* **2005**, *109* (49), 23715−23719.
(403) Abu-Salah, K. M.; Zourob, M. M.; Mouffouk, F.; Alrokayan, S. A.; Alaamery, M. A.; Ansari, A. A. DNA-Based Nanobiosensors as an Emerging Platform for Detection of Disease. *Sensors* **2015**, *15* (6), 14539−14568.
(404) Bae, P. K.; Chung, B. H. Multiplexed Detection of Various Breast Cancer Cells by Perfluorocarbon/Quantum Dot Nanoemulsions Conjugated with Antibodies. *Nano Converg* **2014**, *1* (1), 23.
(405) Zhang, C.; Johnson, L. W. Quantum-Dot-Based Nanosensor for RRE IIB RNA-Rev Peptide Interaction Assay. *J. Am. Chem. Soc.* **2006**, *128* (16), 5324−5325.
(406) DAI, Z.; ZHANG, J.; DONG, Q.; GUO, N.; XU, S.; SUN, B.; BU, Y. Adaption of Au Nanoparticles and CdTe Quantum Dots in DNA Detection* *Supported by the Natural Science Foundation of Tianjin(Nos.06TXTJJC14400, 07JCYBJC15900) and Young Teacher Foundation of Tianjin Polytechnic University (No.029624). *Chin J Chem Eng* **2007**, *15* (6), 791−794.
(407) Ai, X.; Niu, L.; Li, Y.; Yang, F.; Su, X. A Novel β-Cyclodextrin-QDs Optical Biosensor for the Determination of Amantadine and Its Application in Cell Imaging. *Talanta* **2012**, *99*, 409−414.
(408) Darbha, G. K.; Singh, A. K.; Rai, U. S.; Yu, E.; Yu, H.; Chandra Ray, P. Selective Detection of Mercury (II) Ion Using Nonlinear Optical Properties of Gold Nanoparticles. *J. Am. Chem. Soc.* **2008**, *130* (25), 8038−8043.
(409) Yang, W.; Gooding, J. J.; He, Z.; Li, Q.; Chen, G. Fast Colorimetric Detection of Copper Ions Using L-Cysteine Functionalized Gold Nanoparticles. *J Nanosci Nanotechnol* **2007**, *7*, 712−716.
(410) Luo, F.; Zheng, L.; Chen, S.; Cai, Q.; Lin, Z.; Qiu, B.; Chen, G. An Aptamer-Based Fluorescence Biosensor for Multiplex Detection Using Unmodified Gold Nanoparticles. *Chem. Commun.* **2012**, *48* (51), 6387−6389.
(411) Mondal, B.; Ramlal, S.; Lavu, P. S.; N, B.; Kingston, J. Highly Sensitive Colorimetric Biosensor for Staphylococcal Enterotoxin B by a Label-Free Aptamer and Gold Nanoparticles. *Front Microbiol* **2018**, *9*. DOI: 10.3389/fmicb.2018.00179.
(412) Zeng, D.; Luo, W.; Li, J.; Liu, H.; Ma, H.; Huang, Q.; Fan, C. Gold Nanoparticles-Based Nanoconjugates for Enhanced Enzyme Cascade and Glucose Sensing. *Analyst* **2012**, *137* (19), 4435−4439.
(413) Han, S.; Zhou, T.; Yin, B.; He, P. Gold Nanoparticle-Based Colorimetric ELISA for Quantification of Ractopamine. *Mikrochim. Acta* **2018**, *185* (4), 210 DOI: 10.1007/s00604-018-2736-3.
(414) Lee, T.; Kim, T.-H.; Yoon, J.; Chung, Y.-H.; Lee, J. Y.; Choi, J.-W. Investigation of Hemoglobin/Gold Nanoparticle Heterolayer on Micro-Gap for Electrochemical Biosensor Application. *Sensors* **2016**, *16* (5), 660.
(415) Safarpour, H.; Majdi, H.; Masjedi, A.; Pagheh, A. S.; Pereira, M. de L.; Rodrigues Oliveira, S. M.; Ahmadpour, E. Development of Optical Biosensor Using Protein A-Conjugated Chitosan-Gold Nanoparticles for Diagnosis of Cystic Echinococcosis. *Biosensors (Basel)* **2021**, *11* (5), 134.
(416) Wen, Y.; Xing, F.; He, S.; Song, S.; Wang, L.; Long, Y.; Li, D.; Fan, C. A Graphene-Based Fluorescent Nanoprobe for Silver(i) Ions Detection by Using Graphene Oxide and a Silver-Specific Oligonucleotide. *Chem. Commun.* **2010**, *46* (15), 2596−2598.
(417) He, S.; Song, B.; Li, D.; Zhu, C.; Qi, W.; Wen, Y.; Wang, L.; Song, S.; Fang, H.; Fan, C. A Graphene Nanoprobe for Rapid, Sensitive, and Multicolor Fluorescent DNA Analysis. *Adv Funct Mater* **2010**, *20* (3), 453−459.
(418) Jung, J. H.; Cheon, D.; Liu, F.; Lee, K.; Seo, T. A Graphene Oxide Based Immuno-Biosensor for Pathogen Detection. *Angew. Chem., Int. Ed. Engl.* **2010**, *49*, 5708−5711.
(419) Suvarnaphaet, P.; Pechprasarn, S. Graphene-Based Materials for Biosensors: A Review. *Sensors (Basel)* **2017**, *17* (10), 2161.
(420) Filip, J.; Tkac, J. Is Graphene Worth Using in Biofuel Cells? *Electrochim. Acta* **2014**, *136*, 340−354.
(421) Liu, L.; Liu, J.; Huang, H.; Li, Y.; Zhao, G.; Dou, W. A Quantitative Foam Immunoassay for Detection of Escherichia Coli O157:H7 Based on Bimetallic Nanocatalyst-gold Platinum. *Microchemical Journal* **2019**, *148*, 702−707.
(422) Bu, S.-J.; Wang, K.-Y.; Bai, H.-S.; Leng, Y.; Ju, C.-J.; Wang, C.-Y.; Liu, W.-S.; Wan, J.-Y. Immunoassay for Pathogenic Bacteria Using Platinum Nanoparticles and a Hand-Held Hydrogen Detector as Transducer. Application to the Detection of Escherichia Coli O157:H7. *Microchimica Acta* **2019**, *186* (5), 296.
(423) Li, J.; Liu, Q.; Wan, Y.; Wu, X.; Yang, Y.; Zhao, R.; Chen, E.; Cheng, X.; Du, M. Rapid Detection of Trace Salmonella in Milk and Chicken by Immunomagnetic Separation in Combination with a Chemiluminescence Microparticle Immunoassay. *Anal Bioanal Chem* **2019**, *411* (23), 6067−6080.
(424) Wei, X.; Zhou, W.; Sanjay, S. T.; Zhang, J.; Jin, Q.; Xu, F.; Dominguez, D. C.; Li, X. Multiplexed Instrument-Free Bar-Chart SpinChip Integrated with Nanoparticle-Mediated Magnetic Aptasensors for Visual Quantitative Detection of Multiple Pathogens. *Anal. Chem.* **2018**, *90* (16), 9888−9896.
(425) Wang, Y.; Ruan, Q.; Lei, Z.-C.; Lin, S.-C.; Zhu, Z.; Zhou, L.; Yang, C. Highly Sensitive and Automated Surface Enhanced Raman Scattering-Based Immunoassay for H5N1 Detection with Digital Microfluidics. *Anal. Chem.* **2018**, *90* (8), 5224−5231.
(426) Wu, S.; Gu, L.; Qin, J.; Zhang, L.; Sun, F.; Liu, Z.; Wang, Y.; Shi, D. Rapid Label-Free Isolation of Circulating Tumor Cells from Patients' Peripheral Blood Using Electrically Charged Fe3O4 Nanoparticles. *ACS Appl Mater Interfaces* **2020**, *12* (4), 4193−4203.
(427) Xue, M.; Xiang, A.; Guo, Y.; Wang, L.; Wang, R.; Wang, W.; Ji, G.; Lu, Z. Dynamic Halbach Array Magnet Integrated Microfluidic System for the Continuous-Flow Separation of Rare Tumor Cells. *RSC Adv* **2019**, *9* (66), 38496−38504.
(428) Wang, L.; Lin, J. Recent Advances on Magnetic Nanobead Based Biosensors: From Separation to Detection. *TrAC Trends in Analytical Chemistry* **2020**, *128*, 115915.
(429) Reddy, L. H.; Arias, J. L.; Nicolas, J.; Couvreur, P. Magnetic Nanoparticles: Design and Characterization, Toxicity and Biocompatibility, Pharmaceutical and Biomedical Applications. *Chem Rev* **2012**, *112* (11), 5818−5878.
(430) Achtsnicht, S.; Pourshahidi, A. M.; Offenhäusser, A.; Krause, H. J. Multiplex Detection of Different Magnetic Beads Using Frequency Scanning in Magnetic Frequency Mixing Technique. *Sensors (Basel)* **2019**, *19* (11), 2599.
(431) Meyer, M. H. F.; Stehr, M.; Bhuju, S.; Krause, H.-J.; Hartmann, M.; Miethe, P.; Singh, M.; Keusgen, M. Magnetic Biosensor for the Detection of Yersinia Pestis. *J Microbiol Methods* **2007**, *68*, 218−224.
(432) Hong, H.-B.; Krause, H.-J.; Song, K.-B.; Choi, C.-J.; Chung, M.-A.; Son, S.; Offenhäusser, A. Detection of Two Different Influenza A Viruses Using a Nitrocellulose Membrane and a Magnetic Biosensor. *J Immunol Methods* **2011**, *365* (1), 95−100.

(433) Lu, W.; Chen, Y.; Liu, Z.; Tang, W.; Feng, Q.; Sun, J.; Jiang, X. Quantitative Detection of MicroRNA in One Step via Next Generation Magnetic Relaxation Switch Sensing. *ACS Nano* **2016**, *10* (7), 6685−6692.
(434) Zou, D.; Jin, L.; Wu, B.; Hu, L.; Chen, X.; Huang, G.; Zhang, J. Rapid Detection of Salmonella in Milk by Biofunctionalised Magnetic Nanoparticle Cluster Sensor Based on Nuclear Magnetic Resonance. *Int Dairy J* **2019**, *91*, 82−88.
(435) Zhao, Y.; Li, Y.; Jiang, K.; Wang, J.; White, W. L.; Yang, S.; Lu, J. Rapid Detection of Listeria Monocytogenes in Food by Biofunctionalized Magnetic Nanoparticle Based on Nuclear Magnetic Resonance. *Food Control* **2017**, *71*, 110−116.
(436) Jia, F.; Xu, L.; Yan, W.; Wu, W.; Yu, Q.; Tian, X.; Dai, R.; Li, X. A Magnetic Relaxation Switch Aptasensor for the Rapid Detection of Pseudomonas Aeruginosa Using Superparamagnetic Nanoparticles. *Microchimica Acta* **2017**, *184* (5), 1539−1545.
(437) Chen, Y.-T.; Medhi, R.; Nekrashevich, I.; Litvinov, D.; Xu, S.; Lee, T. R. Specific Detection of Proteins Using Exceptionally Responsive Magnetic Particles. *Anal. Chem.* **2018**, *90* (11), 6749−6756.
(438) Liu, Z.; Xianyu, Y.; Zheng, W.; Zhang, J.; Luo, Y.; Chen, Y.; Dong, M.; Wu, J.; Jiang, X. T1-Mediated Nanosensor for Immunoassay Based on an Activatable MnO2 Nanoassembly. *Anal. Chem.* **2018**, *90* (4), 2765−2771.
(439) Wang, S.; Zhang, Y.; An, W.; Wei, Y.; Liu, N.; Chen, Y.; Shuang, S. Magnetic Relaxation Switch Immunosensor for the Rapid Detection of the Foodborne Pathogen Salmonella Enterica in Milk Samples. *Food Control* **2015**, *55*, 43−48.
(440) Zhang, G.; Lu, S.; Qian, J.; Zhong, K.; Yao, J.; Cai, D.; Cheng, Z.; Wu, Z. Magnetic Relaxation Switch Detecting Boric Acid or Borate Ester through One-Pot Synthesized Poly(Vinyl Alcohol) Functionalized Nanomagnetic Iron Oxide. *ACS Appl Mater Interfaces* **2015**, *7* (30), 16837−16841.
(441) Chemla, Y. R.; Grossman, H. L.; Poon, Y.; McDermott, R.; Stevens, R.; Alper, M. D.; Clarke, J. Ultrasensitive Magnetic Biosensor for Homogeneous Immunoassay. *Proceedings of the National Academy of Sciences* **2000**, *97* (26), 14268−14272.
(442) Weitschies, W.; Kötitz, R.; Cordini, D.; Trahms, L. High-Resolution Monitoring of the Gastrointestinal Transit of a Magnetically Marked Capsule. *J. Pharm. Sci.* **1997**, *86* (11), 1218−1222.
(443) Xiao, X.; Yuan, C.; Li, T.; Fock, J.; Svedlindh, P.; Tian, B. Optomagnetic Biosensors: Volumetric Sensing Based on Magnetic Actuation-Induced Optical Modulations. *Biosens Bioelectron* **2022**, *215*, 114560.
(444) Schrittwieser, S.; Pelaz, B.; Parak, W. J.; Lentijo-Mozo, S.; Soulantica, K.; Dieckhoff, J.; Ludwig, F.; Guenther, A.; Tschöpe, A.; Schotter, J. Homogeneous Biosensing Based on Magnetic Particle Labels. *Sensors* **2016**, *16* (6), 828.
(445) Fock, J.; Parmvi, M.; Strömberg, M.; Svedlindh, P.; Donolato, M.; Hansen, M. F. Comparison of Optomagnetic and AC Susceptibility Readouts in a Magnetic Nanoparticle Agglutination Assay for Detection of C-Reactive Protein. *Biosens Bioelectron* **2017**, *88*, 94−100.
(446) Endo, T.; Kerman, K.; Nagatani, N.; Hiepa, H. M.; Kim, D.-K.; Yonezawa, Y.; Nakano, K.; Tamiya, E. Multiple Label-Free Detection of Antigen-Antibody Reaction Using Localized Surface Plasmon Resonance-Based Core-Shell Structured Nanoparticle Layer Nanochip. *Anal. Chem.* **2006**, *78* (18), 6465−6475.
(447) Yuan, J.; Duan, R.; Yang, H.; Luo, X.; Xi, M. Detection of Serum Human Epididymis Secretory Protein 4 in Patients with Ovarian Cancer Using a Label-Free Biosensor Based on Localized Surface Plasmon Resonance. *Int J Nanomedicine* **2012**, *7* (null), 2921−2928.
(448) Lee, J.-H.; Kim, B.-C.; Oh, B.-K.; Choi, J.-W. Highly Sensitive Localized Surface Plasmon Resonance Immunosensor for Label-Free Detection of HIV-1. *Nanomedicine* **2013**, *9* (7), 1018−1026.
(449) Sun, X.; Thylén, L.; Wosinski, L. Hollow Hybrid Plasmonic Mach-Zehnder Sensor. *Opt. Lett.* **2017**, *42* (4), 807−810.
(450) Misiakos, K.; Raptis, I.; Salapatas, A.; Makarona, E.; Botsialas, A.; Hoekman, M.; Stoffer, R.; Jobst, G. Broad-Band Mach-Zehnder Interferometers as High Performance Refractive Index Sensors: Theory and Monolithic Implementation. *Opt. Express* **2014**, *22* (8), 8856−8870.
(451) Heideman, R. G.; Kooyman, R. P. H.; Greve, J. Development of an Optical Waveguide Interferometric Immunosensor. *Sens Actuators B Chem* **1991**, *4* (3), 297−299.
(452) Tereshchenko, A.; Fedorenko, V.; Smyntyna, V.; Konup, I.; Konup, A.; Eriksson, M.; Yakimova, R.; Ramanavicius, A.; Balme, S.; Bechelany, M. ZnO Films Formed by Atomic Layer Deposition as an Optical Biosensor Platform for the Detection of Grapevine Virus A-Type Proteins. *Biosens Bioelectron* **2017**, *92*, 763−769.
(453) Wang, Z. Y.; Wang, L. J.; Zhang, Q.; Tang, B.; Zhang, C. Y. Single Quantum Dot-Based Nanosensor for Sensitive Detection of 5-Methylcytosine at Both CpG and Non-CpG Sites. *Chem Sci* **2018**, *9* (5), 1330−1338.
(454) Jie, G.; Zhao, Y.; Niu, S. Amplified Electrochemiluminescence Detection of Cancer Cells Using a New Bifunctional Quantum Dot as Signal Probe. *Biosens Bioelectron* **2013**, *50*, 368−372.
(455) Tudorache, M.; Tencaliec, A.; Bala, C. Magnetic Beads-Based Immunoassay as a Sensitive Alternative for Atrazine Analysis. *Talanta* **2008**, *77* (2), 839−843.
(456) Morales, M. A.; Halpern, J. M. Guide to Selecting a Biorecognition Element for Biosensors. *Bioconjug Chem* **2018**, *29* (10), 3231−3239.
(457) Liguori, L.; Polcaro, G.; Nigro, A.; Conti, V.; Sellitto, C.; Perri, F.; Ottaiano, A.; Cascella, M.; Zeppa, P.; Caputo, A.; Pepe, S.; Sabbatino, F. Bispecific Antibodies: A Novel Approach for the Treatment of Solid Tumors. *Pharmaceutics* **2022**, *14* (11), 2442.
(458) Borrebaeck, C. A. K. Antibodies in Diagnostics - from Immunoassays to Protein Chips. *Immunol Today* **2000**, *21* (8), 379−382.
(459) Sharma, S.; Byrne, H.; O'Kennedy, R. J. Antibodies and Antibody-Derived Analytical Biosensors. *Essays Biochem* **2016**, *60* (1), 9−18.
(460) Conroy, P. J.; Hearty, S.; Leonard, P.; O'Kennedy, R. J. Antibody Production, Design and Use for Biosensor-Based Applications. *Semin Cell Dev Biol* **2009**, *20* (1), 10−26.
(461) Kierny, M. R.; Cunningham, T. D.; Kay, B. K. Detection of Biomarkers Using Recombinant Antibodies Coupled to Nanostructured Platforms. *Nano Rev* **2012**, *3* (1), 17240.
(462) Peña-Bahamonde, J.; Nguyen, H. N.; Fanourakis, S. K.; Rodrigues, D. F. Recent Advances in Graphene-Based Biosensor Technology with Applications in Life Sciences. *J Nanobiotechnology* **2018**, *16* (1), 75.
(463) Fischer, M. J. E. Amine Coupling Through EDC/NHS: A Practical Approach. In *Surface Plasmon Resonance: Methods and Protocols*; Mol, N. J., Fischer, M. J. E., Eds.; Humana Press: Totowa, NJ, 2010; pp 55−73. DOI: 10.1007/978-1-60761-670-2_3.
(464) Afsahi, S.; Lerner, M. B.; Goldstein, J. M.; Lee, J.; Tang, X.; Bagarozzi, D. A.; Pan, D.; Locascio, L.; Walker, A.; Barron, F.; Goldsmith, B. R. Novel Graphene-Based Biosensor for Early Detection of Zika Virus Infection. *Biosens Bioelectron* **2018**, *100*, 85−88.
(465) Navakul, K.; Warakulwit, C.; Yenchitsomanus, P.; Panya, A.; Lieberzeit, P. A.; Sangma, C. A Novel Method for Dengue Virus Detection and Antibody Screening Using a Graphene-Polymer Based Electrochemical Biosensor. *Nanomedicine* **2017**, *13* (2), 549−557.
(466) Huang, J.; Xie, Z.; Xie, Z.; Luo, S.; Xie, L.; Huang, L.; Fan, Q.; Zhang, Y.; Wang, S.; Zeng, T. Silver Nanoparticles Coated Graphene Electrochemical Sensor for the Ultrasensitive Analysis of Avian Influenza Virus H7. *Anal. Chim. Acta* **2016**, *913*, 121−127.
(467) Valipour, A.; Roushani, M. Using Silver Nanoparticle and Thiol Graphene Quantum Dots Nanocomposite as a Substratum to Load Antibody for Detection of Hepatitis C Virus Core Antigen: Electrochemical Oxidation of Riboflavin Was Used as Redox Probe. *Biosens Bioelectron* **2017**, *89*, 946−951.
(468) Pandey, A.; Gurbuz, Y.; Ozguz, V.; Niazi, J. H.; Qureshi, A. Graphene-Interfaced Electrical Biosensor for Label-Free and Sensitive Detection of Foodborne Pathogenic E. Coli O157:H7. *Biosens Bioelectron* **2017**, *91*, 225−231.

https://doi.org/10.1021/acsomega.4c07991
ACS Omega 2024, 9, 48918−48987

(469) Sign, C.; Sumana, G. Antibody Conjugated Graphene Nanocomposites for Pathogen Detection. In *Journal of Physics: Conference Series*; Institute of Physics Publishing, 2016; Vol. *704*. DOI: 10.1088/1742-6596/704/1/012014.
(470) Lee, T. Y.; Song, J. T. Detection of Carcinoembryonic Antigen Using AlN FBAR. *Thin Solid Films* **2010**, *518* (22), 6630−6633.
(471) Wang, J. SURVEY AND SUMMARY: From DNA Biosensors to Gene Chips. *Nucleic Acids Res.* **2000**, *28* (16), 3011−3016.
(472) Herne, T. M.; Tarlov, M. J. Characterization of DNA Probes Immobilized on Gold Surfaces. *J. Am. Chem. Soc.* **1997**, *119* (38), 8916−8920.
(473) Piunno, P. A. E.; Watterson, J.; Wust, C. C.; Krull, U. J. Considerations for the Quantitative Transduction of Hybridization of Immobilized DNA. *Anal. Chim. Acta* **1999**, *400* (1), 73−89.
(474) Mecking, S.; Johnson, L. K.; Wang, L.; Brookhart, M. Mechanistic Studies of the Palladium-Catalyzed Copolymerization of Ethylene and α-Olefins with Methyl Acrylate. *J. Am. Chem. Soc.* **1998**, *120* (5), 888−899.
(475) Wengel, J.; Petersen, M.; Frieden, M.; Koch, T. Chemistry of Locked Nucleic Acids (LNA). In *Peptide Nucleic Acids, Morpholinos and Related Antisense Biomolecules*; Janson, C. G., During, M. J., Eds.; Springer US: Boston, MA, 2006; pp 114−132. DOI: 10.1007/0-387-32956-0_7.
(476) Akhavan, O.; Ghaderi, E.; Rahighi, R. Toward Single-DNA Electrochemical Biosensing by Graphene Nanowalls. *ACS Nano* **2012**, *6* (4), 2904−2916.
(477) Qaddare, S. H.; Salimi, A. Amplified Fluorescent Sensing of DNA Using Luminescent Carbon Dots and AuNPs/GO as a Sensing Platform: A Novel Coupling of FRET and DNA Hybridization for Homogeneous HIV-1 Gene Detection at Femtomolar Level. *Biosens Bioelectron* **2017**, *89*, 773−780.
(478) Buhl, A.; Metzger, J. H.; Heegaard, N. H. H.; von Landenberg, P.; Fleck, M.; Luppa, P. B. Novel Biosensor-Based Analytic Device for the Detection of Anti-Double-Stranded DNA Antibodies. *Clin Chem* **2007**, *53* (2), 334−341.
(479) Xu, C.-X.; Zhai, Q.-G.; Liu, Y.-J.; Huang, K.-J.; Lu, L.; Li, K.-X. A Novel Electrochemical DNA Biosensor Construction Based on Layered CuS-Graphene Composite and Au Nanoparticles. *Anal Bioanal Chem* **2014**, *406* (27), 6943−6951.
(480) Wang, T.; Zhang, Z.; Li, Y.; Xie, G. Amplified Electrochemical Detection of MecA Gene in Methicillin-Resistant Staphylococcus Aureus Based on Target Recycling Amplification and Isothermal Strand-Displacement Polymerization Reaction. *Sens Actuators B Chem* **2015**, *221*, 148−154.
(481) Hassan, R. A.; Heng, L. Y.; Tan, L. L. Novel DNA Biosensor for Direct Determination of Carrageenan. *Sci Rep* **2019**, *9* (1), 6379.
(482) Staiano, M.; Pennacchio, A.; Varriale, A.; Capo, A.; Majoli, A.; Capacchione, C.; D'Auria, S. Chapter Four - Enzymes as Sensors. In *Methods in Enzymology*; Thompson, R. B., Fierke, C. A., Eds.; Academic Press, 2017; Vol. *589*, pp 115−131. DOI: 10.1016/bs.mie.2017.01.015.
(483) Rocchitta, G.; Spanu, A.; Babudieri, S.; Latte, G.; Madeddu, G.; Galleri, G.; Nuvoli, S.; Bagella, P.; Demartis, M. I.; Fiore, V.; Manetti, R.; Serra, P. A. Enzyme Biosensors for Biomedical Applications: Strategies for Safeguarding Analytical Performances in Biological Fluids. *Sensors (Switzerland)*; MDPI AG, 2016. DOI: 10.3390/s16060780.
(484) Skoronski, E.; Souza, D. H.; Ely, C.; Broilo, F.; Fernandes, M.; Furigo, A.; Ghislandi, M. G. Immobilization of Laccase from Aspergillus Oryzae on Graphene Nanosheets. *Int J Biol Macromol* **2017**, *99*, 121−127.
(485) Gaudin, V. Advances in Biosensor Development for the Screening of Antibiotic Residues in Food Products of Animal Origin - A Comprehensive Review. *Biosens Bioelectron* **2017**, *90*, 363−377.
(486) Patel, S. K. S.; Choi, S. H.; Kang, Y. C.; Lee, J.-K. Eco-Friendly Composite of Fe3O4-Reduced Graphene Oxide Particles for Efficient Enzyme Immobilization. *ACS Appl Mater Interfaces* **2017**, *9* (3), 2213−2222.
(487) Filip, J.; Andicsová-Eckstein, A.; Vikartovská, A.; Tkac, J. Immobilization of Bilirubin Oxidase on Graphene Oxide Flakes with Different Negative Charge Density for Oxygen Reduction. The Effect of GO Charge Density on Enzyme Coverage, Electron Transfer Rate and Current Density. *Biosens Bioelectron* **2017**, *89*, 384−389.
(488) Feng, X.; Cheng, H.; Pan, Y.; Zheng, H. Development of Glucose Biosensors Based on Nanostructured Graphene-Conducting Polyaniline Composite. *Biosens Bioelectron* **2015**, *70*, 411−417.
(489) Natarelli, N.; Gahoonia, N.; Sivamani, R. K. Bacteriophages and the Microbiome in Dermatology: The Role of the Phageome and a Potential Therapeutic Strategy. *Int J Mol Sci* **2023**, *24* (3), 2695.
(490) Mack, J. D.; Yehualaeshet, T.; Park, M. K.; Tameru, B.; Samuel, T.; Chin, B. A. Phage-Based Biosensor and Optimization of Surface Blocking Agents to Detect Salmonella Typhimurium on Romaine Lettuce. *J Food Saf* **2017**, *37* (2), No. e12299.
(491) Wang, F.; Horikawa, S.; Hu, J.; Wikle, H. C.; Chen, I.-H.; Du, S.; Liu, Y.; Chin, B. A. Detection of Salmonella Typhimurium on Spinach Using Phage-Based Magnetoelastic Biosensors. *Sensors* **2017**, *17* (2), 386.
(492) Lu, T. K.; Bowers, J. L.; Koeris, M. S. Advancing Bacteriophage-Based Microbial Diagnostics with Synthetic Biology. *Trends Biotechnol* **2013**, *31*, 325−327.
(493) Richter, Ł.; Janczuk-Richter, M.; Niedziółka-Jönsson, J.; Paczesny, J.; Hołyst, R. Recent Advances in Bacteriophage-Based Methods for Bacteria Detection. *Drug Discov Today* **2018**, *23*, 448−455.
(494) Singh, A.; Arya, S. K.; Glass, N.; Hanifi-Moghaddam, P.; Naidoo, R.; Szymanski, C. M.; Tanha, J.; Evoy, S. Bacteriophage Tailspike Proteins as Molecular Probes for Sensitive and Selective Bacterial Detection. *Biosens Bioelectron* **2010**, *26* (1), 131−138.
(495) Srivastava, S. K.; Hamo, H. B.; Kushmaro, A.; Marks, R. S.; Grüner, C.; Rauschenbach, B.; Abdulhalim, I. Highly Sensitive and Specific Detection of E. Coli by a SERS Nanobiosensor Chip Utilizing Metallic Nanosculptured Thin Films. *Analyst* **2015**, *140* (9), 3201−3209.
(496) Ullah, M. W.; Shi, Z.; Shi, X.; Zeng, D.; Li, S.; Yang, G. Microbes as Structural Templates in Biofabrication: Study of Surface Chemistry and Applications. *ACS Sustain Chem Eng* **2017**, *5* (12), 11163−11175.
(497) Anany, H.; Chen, W.; Pelton, R.; Griffiths, M. W. Biocontrol of Listeria Monocytogenes and Escherichia Coli O157:H7 in Meat by Using Phages Immobilized on Modified Cellulose Membranes. *Appl. Environ. Microbiol.* **2011**, *77* (18), 6379−6387.
(498) Fernandes, E.; Martins, V. C.; Nóbrega, C.; Carvalho, C. M.; Cardoso, F. A.; Cardoso, S.; Dias, J.; Deng, D.; Kluskens, L. D.; Freitas, P. P.; Azeredo, J. A Bacteriophage Detection Tool for Viability Assessment of Salmonella Cells. *Biosens Bioelectron* **2014**, *52*, 239−246.
(499) Tlili, C.; Sokullu, E.; Safavieh, M.; Tolba, M.; Ahmed, M. U.; Zourob, M. Bacteria Screening, Viability, And Confirmation Assays Using Bacteriophage-Impedimetric/Loop-Mediated Isothermal Amplification Dual-Response Biosensors. *Anal. Chem.* **2013**, *85* (10), 4893−4901.
(500) Rajnovic, D.; Muñoz-Berbel, X.; Mas, J. Fast Phage Detection and Quantification: An Optical Density-Based Approach. *PLoS One* **2019**, *14*, e0216292.
(501) van der Merwe, R. G.; van Helden, P. D.; Warren, R. M.; Sampson, S. L.; Gey van Pittius, N. C. Phage-Based Detection of Bacterial Pathogens. *Analyst* **2014**, *139* (11), 2617−2626.
(502) Ertürk, G.; Lood, R. Bacteriophages as Biorecognition Elements in Capacitive Biosensors: Phage and Host Bacteria Detection. *Sens Actuators B Chem* **2018**, *258*, 535−543.
(503) Kylilis, N.; Riangrungroj, P.; Lai, H.-E.; Salema, V.; Fernández, L. Á.; Stan, G.-B. V; Freemont, P. S.; Polizzi, K. M. Whole-Cell Biosensor with Tunable Limit of Detection Enables Low-Cost Agglutination Assays for Medical Diagnostic Applications. *ACS Sens* **2019**, *4*, 370−378.
(504) Goers, L.; Ainsworth, C.; Goey, C. H.; Kontoravdi, C.; Freemont, P. S.; Polizzi, K. M. Whole-Cell Escherichia Coli Lactate Biosensor for Monitoring Mammalian Cell Cultures during Biopharmaceutical Production. *Biotechnol. Bioeng.* **2017**, *114* (6), 1290−1300.

https://doi.org/10.1021/acsomega.4c07991
ACS Omega 2024, 9, 48918−48987

(505) Horswell, J.; Dickson, S. Use of Biosensors to Screen Urine Samples for Potentially Toxic Chemicals. *J Anal Toxicol* **2003**, *27*, 372−376.
(506) Courbet, A.; Endy, D.; Renard, E.; Molina, F.; Bonnet, J. Detection of Pathological Biomarkers in Human Clinical Samples via Amplifying Genetic Switches and Logic Gates. *Sci Transl Med* **2015**, *7* (289), 289ra83−289ra83.
(507) Goers, L.; Kylilis, N.; Tomazou, M.; Wen, K. Y.; Freemont, P. S.; Polizzi, K. M. Engineering Microbial Biosensors. *Methods in Microbiology* **2013**, *40*, 119−156.
(508) Wong, L. S.; Lee, Y. H.; Surif, S. Whole Cell Biosensor Using Anabaena Torulosa with Optical Transduction for Environmental Toxicity Evaluation. *J. Sensors* **2013**, *2013*, 1−8.
(509) Gheorghiu, M. A Short Review on Cell-Based Biosensing: Challenges and Breakthroughs in Biomedical Analysis. *J Biomed Res* **2021**, *35*, 1−9.
(510) *Research Area 1: Biosensor Design | The Lai Lab*; University of Nebraska-Lincoln, 2024. http://chemweb.unl.edu/lai/research-area-one-biosensor-design/ (accessed 2024−03−07).
(511) Uzun, L.; Turner, A. P. F. Molecularly-Imprinted Polymer Sensors: Realising Their Potential. *Biosens Bioelectron* **2016**, *76*, 131−144.
(512) Cervini, P.; Cavalheiro, É. Strategies for Preparation of Molecularly Imprinted Polymers Modified Electrodes and Their Application in Electroanalysis: A Review. *Anal. Lett.* **2012**, *45*, 297−313.
(513) Granado, V. L. V; Gomes, M. T. S. R.; Rudnitskaya, A. Molecularly Imprinted Polymer Thin-Film Electrochemical Sensors. *Methods in molecular biology* **2019**, *2027*, 151−161.
(514) Encarnação, J. M.; Rosa, L.; Rodrigues, R.; Pedro, L.; da Silva, F. A.; Gonçalves, J.; Ferreira, G. N. M. Piezoelectric Biosensors for Biorecognition Analysis: Application to the Kinetic Study of HIV-1 Vif Protein Binding to Recombinant Antibodies. *J. Biotechnol.* **2007**, *132* (2), 142−148.
(515) Benhar, I.; Eshkenazi, I.; Neufeld, T.; Opatowsky, J.; Shaky, S.; Rishpon, J. Recombinant Single Chain Antibodies in Bioelectrochemical Sensors. *Talanta* **2001**, *55* (5), 899−907.
(516) Grewal, Y. S.; Shiddiky, M. J. A.; Gray, S. A.; Weigel, K. M.; Cangelosi, G. A.; Trau, M. Label-Free Electrochemical Detection of an Entamoeba Histolytica Antigen Using Cell-Free Yeast-ScFv Probes. *Chem. Commun.* **2013**, *49* (15), 1551−1553.
(517) Ahmed, S. R.; Mogus, J.; Chand, R.; Nagy, E.; Neethirajan, S. Optoelectronic Fowl Adenovirus Detection Based on Local Electric Field Enhancement on Graphene Quantum Dots and Gold Nanobundle Hybrid. *Biosens Bioelectron* **2018**, *103*, 45−53.
(518) Singh, M.; Holzinger, M.; Tabrizian, M.; Winters, S.; Berner, N. C.; Cosnier, S.; Duesberg, G. S. Noncovalently Functionalized Monolayer Graphene for Sensitivity Enhancement of Surface Plasmon Resonance Immunosensors. *J. Am. Chem. Soc.* **2015**, *137* (8), 2800−2803.
(519) Wu, Y.-M.; Cen, Y.; Huang, L.-J.; Yu, R.-Q.; Chu, X. Upconversion Fluorescence Resonance Energy Transfer Biosensor for Sensitive Detection of Human Immunodeficiency Virus Antibodies in Human Serum. *Chem. Commun.* **2014**, *50* (36), 4759−4762.
(520) Demeritte, T.; Viraka Nellore, B. P.; Kanchanapally, R.; Sinha, S. S.; Pramanik, A.; Chavva, S. R.; Ray, P. C. Hybrid Graphene Oxide Based Plasmonic-Magnetic Multifunctional Nanoplatform for Selective Separation and Label-Free Identification of Alzheimer's Disease Biomarkers. *ACS Appl Mater Interfaces* **2015**, *7* (24), 13693−13700.
(521) Zuo, B.; Li, S.; Guo, Z.; Zhang, J.; Chen, C. Piezoelectric Immunosensor for SARS-Associated Coronavirus in Sputum. *Anal. Chem.* **2004**, *76* (13), 3536−3540.
(522) Liu, F.; Choi, J. Y.; Seo, T. S. Graphene Oxide Arrays for Detecting Specific DNA Hybridization by Fluorescence Resonance Energy Transfer. *Biosens Bioelectron* **2010**, *25* (10), 2361−2365.
(523) Pang, S.; Gao, Y.; Li, Y.; Liu, S.; Su, X. A Novel Sensing Strategy for the Detection of Staphylococcus Aureus DNA by Using a Graphene Oxide-Based Fluorescent Probe. *Analyst* **2013**, *138* (9), 2749−2754.
(524) Muti, M.; Sharma, S.; Erdem, A.; Papakonstantinou, P. Electrochemical Monitoring of Nucleic Acid Hybridization by Single-Use Graphene Oxide-Based Sensor. *Electroanalysis* **2011**, *23*, 272−279.
(525) Rasheed, P. A.; Sandhyarani, N. Graphene-DNA Electrochemical Sensor for the Sensitive Detection of BRCA1 Gene. *Sens Actuators B Chem* **2014**, *204*, 777−782.
(526) Gong, Q.; Wang, Y.; Yang, H. A Sensitive Impedimetric DNA Biosensor for the Determination of the HIV Gene Based on Graphene-Nafion Composite Film. *Biosens Bioelectron* **2017**, *89*, 565−569.
(527) Vasilescu, I.; Eremia, S. A. V; Kusko, M.; Radoi, A.; Vasile, E.; Radu, G.-L. Molybdenum Disulphide and Graphene Quantum Dots as Electrode Modifiers for Laccase Biosensor. *Biosens Bioelectron* **2016**, *75*, 232−237.
(528) Liu, J.; Wang, T.; Wang, J.; Wang, E. Mussel-Inspired Biopolymer Modified 3D Graphene Foam for Enzyme Immobilization and High Performance Biosensor. *Electrochim. Acta* **2015**, *161*, 17−22.
(529) De Plano, L. M.; Carnazza, S.; Messina, G. M. L.; Rizzo, M. G.; Marletta, G.; Guglielmino, S. P. P. Specific and Selective Probes for Staphylococcus Aureus from Phage-Displayed Random Peptide Libraries. *Colloids Surf B Biointerfaces* **2017**, *157*, 473−480.
(530) Lentini, G.; Franco, D.; Fazio, E.; De Plano, L. M.; Trusso, S.; Carnazza, S.; Neri, F.; Guglielmino, S. P. P. Rapid Detection of Pseudomonas Aeruginosa by Phage-Capture System Coupled with Micro-Raman Spectroscopy. *Vib Spectrosc* **2016**, *86*, 1−7.
(531) Bhardwaj, N.; Bhardwaj, S. K.; Mehta, J.; Mohanta, G. C.; Deep, A. Bacteriophage Immobilized Graphene Electrodes for Impedimetric Sensing of Bacteria (Staphylococcus Arlettae). *Anal. Biochem.* **2016**, *505*, 18−25.
(532) Kretzer, J. W.; Lehmann, R.; Schmelcher, M.; Banz, M.; Kim, K.-P.; Korn, C.; Loessner, M. J. Use of High-Affinity Cell Wall-Binding Domains of Bacteriophage Endolysins for Immobilization and Separation of Bacterial Cells. *Appl. Environ. Microbiol.* **2007**, *73* (6), 1992−2000.
(533) Wu, Y.; Brovko, L.; Griffiths, M. W. Influence of Phage Population on the Phage-mediated Bioluminescent Adenylate Kinase (AK) Assay for Detection of Bacteria. *Lett Appl Microbiol* **2001**, *33* (4), 311−315.
(534) Li, W.; Gong, X.; Yu, Z.; Ma, L.; Sun, W.; Gao, S.; Köroglu, Ç.; Wang, W.; Liu, L.; Li, T.; Ning, H.; Fan, D.; Xu, Y.; Tu, X.; Xu, T.; Sun, L.; Wang, W.; Lu, J.; Ni, Z.; Li, J.; Duan, X.; Wang, P.; Nie, Y.; Qiu, H.; Shi, Y.; Pop, E.; Wang, J.; Wang, X. Approaching the Quantum Limit in Two-Dimensional Semiconductor Contacts. *Nature* **2023**, *613* (7943), 274−279.
(535) Chircov, C.; Grumezescu, A. M. Microelectromechanical Systems (MEMS) for Biomedical Applications. *Micromachines (Basel)* **2022**, *13* (2), 164.
(536) Bergveld, P. The Challenge of Developing MTAS. In *Micro Total Analysis Systems*; Van den Berg, A., Bergveld, P., Eds.; Springer Netherlands: Dordrecht, 1995; pp 1−4.
(537) Teh, K. S. Additive Direct-Write Microfabrication for MEMS: A Review. *Frontiers of Mechanical Engineering* **2017**, *12* (4), 490−509.
(538) Shanbhag, P. P.; Patil, N. S. BioMicroelectromechanical Systems: A Novel Approach for Drug Targeting in Chronic Diseases. *New Horiz Transl Med* **2017**, *3* (6), 265−271.
(539) Maheshwari, N.; Chatterjee, G.; Ramgopal Rao, V. *A Technology Overview and Applications of Bio-MEMS*; ISSS, 2014; Vol. 3. www.isssonline.in/journal/03paper12.pdf.
(540) Ingber, D. E. Human Organs-on-Chips for Disease Modelling, Drug Development and Personalized Medicine. *Nat Rev Genet* **2022**, *23* (8), 467−491.
(541) Theobald, J.; Ghanem, A.; Wallisch, P.; Banaeiyan, A. A.; Andrade-Navarro, M. A.; Taškova, K.; Haltmeier, M.; Kurtz, A.; Becker, H.; Reuter, S.; Mrowka, R.; Cheng, X.; Wölfl, S. Liver-Kidney-on-Chip To Study Toxicity of Drug Metabolites. *ACS Biomater Sci Eng* **2018**, *4* (1), 78−89.
(542) Haddrick, M.; Simpson, P. B. Organ-on-a-Chip Technology: Turning Its Potential for Clinical Benefit into Reality. *Drug Discov Today* **2019**, *24* (5), 1217−1223.

https://doi.org/10.1021/acsomega.4c07991
ACS Omega 2024, 9, 48918−48987

(543) Wu, Q.; Liu, J.; Wang, X.; Feng, L.; Wu, J.; Zhu, X.; Wen, W.; Gong, X. Organ-on-a-Chip: Recent Breakthroughs and Future Prospects. *Biomed Eng Online* **2020**, *19* (1), 9.
(544) Sato, T.; Clevers, H. Growing Self-Organizing Mini-Guts from a Single Intestinal Stem Cell: Mechanism and Applications. *Science (1979)* **2013**, *340* (6137), 1190−1194.
(545) Jang, K.-J.; Cho, H. S.; Kang, D. H.; Bae, W. G.; Kwon, T.-H.; Suh, K.-Y. Fluid-Shear-Stress-Induced Translocation of Aquaporin-2 and Reorganization of Actin Cytoskeleton in Renal Tubular Epithelial Cells. *Integrative Biology* **2011**, *3* (2), 134−141.
(546) Li, Y.-C.; Lin, M.-W.; Yen, M.-H.; Fan, S. M.-Y.; Wu, J.-T.; Young, T.-H.; Cheng, J.-Y.; Lin, S.-J. Programmable Laser-Assisted Surface Microfabrication on a Poly(Vinyl Alcohol)-Coated Glass Chip with Self-Changing Cell Adhesivity for Heterotypic Cell Patterning. *ACS Appl Mater Interfaces* **2015**, *7* (40), 22322−22332.
(547) Marx, U.; Walles, H.; Hoffmann, S.; Lindner, G.; Horland, R.; Sonntag, F.; Klotzbach, U.; Sakharov, D.; Tonevitsky, A.; Lauster, R. 'Human-on-a-Chip' Developments: A Translational Cutting-Edge Alternative to Systemic Safety Assessment and Efficiency Evaluation of Substances in Laboratory Animals and Man? *Alternatives to Laboratory Animals* **2012**, *40* (5), 235−257.
(548) Jiang, L.; Li, Q.; Liang, W.; Du, X.; Yang, Y.; Zhang, Z.; Xu, L.; Zhang, J.; Li, J.; Chen, Z.; Gu, Z. Organ-On-A-Chip Database Revealed—Achieving the Human Avatar in Silicon. *Bioengineering* **2022**, *9* (11), 685.
(549) Forhals, A. *PROCESS AND APPARATUS FOR PREPARING ARTIFICIAL THREADS*. US Patent US1975504A, 1934.
(550) Chronakis, I. S. Novel Nanocomposites and Nanoceramics Based on Polymer Nanofibers Using Electrospinning Process—A Review. *J Mater Process Technol* **2005**, *167* (2), 283−293.
(551) Fong, H. Electrospun Nylon 6 Nanofiber Reinforced BIS-GMA/TEGDMA Dental Restorative Composite Resins. *Polymer (Guildf)* **2004**, *45* (7), 2427−2432.
(552) Feltz, K. P.; Kalaf, E. A. G.; Chen, C.; Martin, R. S.; Sell, S. A. A Review of Electrospinning Manipulation Techniques to Direct Fiber Deposition and Maximize Pore Size. *Electrospinning* **2017**, *1* (1), 46−61.
(553) Liu, Y.; Hao, M.; Chen, Z.; Liu, L.; Liu, Y.; Yang, W.; Ramakrishna, S. A Review on Recent Advances in Application of Electrospun Nanofiber Materials as Biosensors. *Curr Opin Biomed Eng* **2020**, *13*, 174−189.
(554) Sumitha, M. S.; Shalumon, K. T.; Sreeja, V. N.; Jayakumar, R.; Nair, S. V; Menon, D. Biocompatible and Antibacterial Nanofibrous Poly(ϵ-Caprolactone)-Nanosilver Composite Scaffolds for Tissue Engineering Applications. *Journal of Macromolecular Science, Part A* **2012**, *49* (2), 131−138.
(555) Tang, L.; Xie, X.; Zhou, Y.; Zeng, G.; Tang, J.; Wu, Y.; Long, B.; Peng, B.; Zhu, J. A Reusable Electrochemical Biosensor for Highly Sensitive Detection of Mercury Ions with an Anionic Intercalator Supported on Ordered Mesoporous Carbon/Self-Doped Polyaniline Nanofibers Platform. *Biochem Eng J* **2017**, *117*, 7−14.
(556) Kafi, A. K. M.; Wali, Q.; Jose, R.; Biswas, T. K.; Yusoff, M. M. A Glassy Carbon Electrode Modified with SnO2 Nanofibers, Polyaniline and Hemoglobin for Improved Amperometric Sensing of Hydrogen Peroxide. *Microchimica Acta* **2017**, *184* (11), 4443−4450.
(557) Jeong, G.; Oh, J.; Jang, J. Fabrication of N-Doped Multidimensional Carbon Nanofibers for High-Performance Cortisol Biosensors. *Biosens Bioelectron* **2019**, *131*, 30−36.
(558) Wang, W. Q.; Yue, H. Y.; Yu, Z. M.; Huang, S.; Song, S. S.; Gao, X.; Guan, E. H.; Zhang, H. J.; Wang, Z. Synthesis and Application of MoS2 Nanosheet Arrays/Carbon Nanofibers for Simultaneous Electrochemical Determination of Levodopa and Uric Acid. *IEEE Sens J* **2019**, *19* (15), 5988−5994.
(559) Demiroglu Mustafov, S.; Mohanty, A. K.; Misra, M.; Seydibeyoglu, M. Ö. Fabrication of Conductive Lignin/PAN Carbon Nanofibers with Enhanced Graphene for the Modified Electrodes. *Carbon N Y* **2019**, *147*, 262−275.
(560) Wang, Z.; Ma, B.; Shen, C.; Cheong, L.-Z. Direct, Selective and Ultrasensitive Electrochemical Biosensing of Methyl Parathion in Vegetables Using Burkholderia Cepacia Lipase@MOF Nanofibers-Based Biosensor. *Talanta* **2019**, *197*, 356−362.
(561) Salahandish, R.; Ghaffarinejad, A.; Naghib, S. M.; Majidzadeh-A, K.; Zargartalebi, H.; Sanati-Nezhad, A. Nano-Biosensor for Highly Sensitive Detection of HER2 Positive Breast Cancer. *Biosens Bioelectron* **2018**, *117*, 104−111.
(562) Kabay, G.; Kaleli Can, G.; Mutlu, M. Amyloid-like Protein Nanofibrous Membranes as a Sensing Layer Infrastructure for the Design of Mass-Sensitive Biosensors. *Biosens Bioelectron* **2017**, *97*, 285−291.
(563) Li, D.; Pang, Z.; Chen, X.; Luo, L.; Cai, Y.; Wei, Q. A Catechol Biosensor Based on Electrospun Carbon Nanofibers. *Beilstein Journal of Nanotechnology* **2014**, *5*, 346−354.
(564) Asghari, S.; Rezaei, Z.; Mahmoudifard, M. Electrospun Nanofibers: A Promising Horizon toward the Detection and Treatment of Cancer. *Analyst* **2020**, *145* (8), 2854−2872.
(565) Wang, X.; Wang, X.; Wang, X.; Chen, F.; Zhu, K.; Xu, Q.; Tang, M. Novel Electrochemical Biosensor Based on Functional Composite Nanofibers for Sensitive Detection of P53 Tumor Suppressor Gene. *Anal. Chim. Acta* **2013**, *765*, 63−69.
(566) Paul, K. B.; Singh, V.; Vanjari, S. R. K.; Singh, S. G. One Step Biofunctionalized Electrospun Multiwalled Carbon Nanotubes Embedded Zinc Oxide Nanowire Interface for Highly Sensitive Detection of Carcinoma Antigen-125. *Biosens Bioelectron* **2017**, *88*, 144−152.
(567) Soares, J. C.; Iwaki, L. E. O.; Soares, A. C.; Rodrigues, V. C.; Melendez, M. E.; Fregnani, J. H. T. G.; Reis, R. M.; Carvalho, A. L.; Corrêa, D. S.; Oliveira, O. N., Jr Immunosensor for Pancreatic Cancer Based on Electrospun Nanofibers Coated with Carbon Nanotubes or Gold Nanoparticles. *ACS Omega* **2017**, *2* (10), 6975−6983.
(568) Ahmad, M.; Pan, C.; Luo, Z.; Zhu, J. A Single ZnO Nanofiber-Based Highly Sensitive Amperometric Glucose Biosensor. *The Journal of Physical Chemistry C* **2010**, *114* (20), 9308−9313.
(569) Bae, T.-S.; Shin, E.; Im, J. S.; Kim, J. G.; Lee, Y.-S. Effects of Carbon Structure Orientation on the Performance of Glucose Sensors Fabricated from Electrospun Carbon Fibers. *J Non Cryst Solids* **2012**, *358* (3), 544−549.
(570) Jose, M. V; Marx, S.; Murata, H.; Koepsel, R. R.; Russell, A. J. Direct Electron Transfer in a Mediator-Free Glucose Oxidase-Based Carbon Nanotube-Coated Biosensor. *Carbon N Y* **2012**, *50* (11), 4010−4020.
(571) Sapountzi, E.; Braiek, M.; Vocanson, F.; Chateaux, J.-F.; Jaffrezic-Renault, N.; Lagarde, F. Gold Nanoparticles Assembly on Electrospun Poly(Vinyl Alcohol)/Poly(Ethyleneimine)/Glucose Oxidase Nanofibers for Ultrasensitive Electrochemical Glucose Biosensing. *Sens Actuators B Chem* **2017**, *238*, 392−401.
(572) Lee, V. B. C.; Mohd-Naim, N. F.; Tamiya, E.; Ahmed, M. U. Trends in Paper-Based Electrochemical Biosensors: From Design to Application. *Anal. Sci.* **2018**, *34* (1), 7−18.
(573) Hasanzadeh, M.; Shadjou, N. Electrochemical and Photoelectrochemical Nano-Immunesensing Using Origami Paper Based Method. *Materials Science and Engineering: C* **2016**, *61*, 979−1001.
(574) Singh, A. T.; Lantigua, D.; Meka, A.; Taing, S.; Pandher, M.; Camci-Unal, G. Paper-Based Sensors: Emerging Themes and Applications. *Sensors* **2018**, *18* (9), 2838.
(575) Lisa, M.; Chouhan, R. S.; Vinayaka, A. C.; Manonmani, H. K.; Thakur, M. S. Gold Nanoparticles Based Dipstick Immunoassay for the Rapid Detection of Dichlorodiphenyltrichloroethane: An Organochlorine Pesticide. *Biosens Bioelectron* **2009**, *25* (1), 224−227.
(576) Hossain, S. M. Z.; Luckham, R. E.; McFadden, M. J.; Brennan, J. D. Reagentless Bidirectional Lateral Flow Bioactive Paper Sensors for Detection of Pesticides in Beverage and Food Samples. *Anal. Chem.* **2009**, *81* (21), 9055−9064.
(577) Tyagi, C.; Tomar, L. K.; Singh, H. Surface Modification of Cellulose Filter Paper by Glycidyl Methacrylate Grafting for Biomolecule Immobilization: Influence of Grafting Parameters and Urease Immobilization. *J. Appl. Polym. Sci.* **2009**, *111* (3), 1381−1390.
(578) Arena, A.; Donato, N.; Saitta, G.; Bonavita, A.; Rizzo, G.; Neri, G. Flexible Ethanol Sensors on Glossy Paper Substrates Operating at Room Temperature. *Sens Actuators B Chem* **2010**, *145* (1), 488−494.

https://doi.org/10.1021/acsomega.4c07991
ACS Omega 2024, 9, 48918−48987

(579) Ostrov, N.; Jimenez, M.; Billerbeck, S.; Brisbois, J.; Matragrano, J.; Ager, A.; Cornish, V. W. A Modular Yeast Biosensor for Low-Cost Point-of-Care Pathogen Detection. *Sci Adv* **2024**, *3* (6), No. e1603221.
(580) Ratajczak, K.; Stobiecka, M. High-Performance Modified Cellulose Paper-Based Biosensors for Medical Diagnostics and Early Cancer Screening: A Concise Review. *Carbohydr. Polym.* **2020**, *229*, 115463.
(581) Ji, S.; Lee, M.; Kim, D. Detection of Early Stage Prostate Cancer by Using a Simple Carbon Nanotube@paper Biosensor. *Biosens Bioelectron* **2018**, *102*, 345−350.
(582) Gräwe, A.; Dreyer, A.; Vornholt, T.; Barteczko, U.; Buchholz, L.; Drews, G.; Ho, U. L.; Jackowski, M. E.; Kracht, M.; Lüders, J.; Bleckwehl, T.; Rositzka, L.; Ruwe, M.; Wittchen, M.; Lutter, P.; Müller, K.; Kalinowski, J. A Paper-Based, Cell-Free Biosensor System for the Detection of Heavy Metals and Date Rape Drugs. *PLoS One* **2019**, *14* (3), No. e0210940-.
(583) Scala-Benuzzi, M. L.; Takara, E. A.; Alderete, M.; Soler-Illia, G. J. A. A.; Schneider, R. J.; Raba, J.; Messina, G. A. Ethinylestradiol Quantification in Drinking Water Sources Using a Fluorescent Paper Based Immunosensor. *Microchemical Journal* **2018**, *141*, 287−293.
(584) Xu, H.; Mao, X.; Zeng, Q.; Wang, S.; Kawde, A.-N.; Liu, G. Aptamer-Functionalized Gold Nanoparticles as Probes in a Dry-Reagent Strip Biosensor for Protein Analysis. *Anal. Chem.* **2009**, *81* (2), 669−675.
(585) Mahato, K.; Chandra, P. Paper-Based Miniaturized Immunosensor for Naked Eye ALP Detection Based on Digital Image Colorimetry Integrated with Smartphone. *Biosens Bioelectron* **2019**, *128*, 9−16.
(586) Zheng, W.; Yao, L.; Teng, J.; Yan, C.; Qin, P.; Liu, G.; Chen, W. Lateral Flow Test for Visual Detection of Multiple MicroRNAs. *Sens Actuators B Chem* **2018**, *264*, 320−326.
(587) Cuartero, M.; Crespo, G. A.; Bakker, E. Paper-Based Thin-Layer Coulometric Sensor for Halide Determination. *Anal. Chem.* **2015**, *87* (3), 1981−1990.
(588) Ma, C.; Li, W.; Kong, Q.; Yang, H.; Bian, Z.; Song, X.; Yu, J.; Yan, M. 3D Origami Electrochemical Immunodevice for Sensitive Point-of-Care Testing Based on Dual-Signal Amplification Strategy. *Biosens Bioelectron* **2015**, *63*, 7−13.
(589) Bhardwaj, J.; Devarakonda, S.; Kumar, S.; Jang, J. Development of a Paper-Based Electrochemical Immunosensor Using an Antibody-Single Walled Carbon Nanotubes Bio-Conjugate Modified Electrode for Label-Free Detection of Foodborne Pathogens. *Sens Actuators B Chem* **2017**, *253*, 115−123.
(590) Boonyasit, Y.; Chailapakul, O.; Laiwattanapaisal, W. A Multiplexed Three-Dimensional Paper-Based Electrochemical Impedance Device for Simultaneous Label-Free Affinity Sensing of Total and Glycated Haemoglobin: The Potential of Using a Specific Single-Frequency Value for Analysis. *Anal. Chim. Acta* **2016**, *936*, 1−11.
(591) Wang, X.; Lin, G.; Cui, G.; Zhou, X.; Liu, G. L. White Blood Cell Counting on Smartphone Paper Electrochemical Sensor. *Biosens Bioelectron* **2017**, *90*, 549−557.
(592) Li, Z.; Li, F.; Xing, Y.; Liu, Z.; You, M.; Li, Y.; Wen, T.; Qu, Z.; Ling Li, X.; Xu, F. Pen-on-Paper Strategy for Point-of-Care Testing: Rapid Prototyping of Fully Written Microfluidic Biosensor. *Biosens Bioelectron* **2017**, *98*, 478−485.
(593) Cinti, S.; Minotti, C.; Moscone, D.; Palleschi, G.; Arduini, F. Fully Integrated Ready-to-Use Paper-Based Electrochemical Biosensor to Detect Nerve Agents. *Biosens Bioelectron* **2017**, *93*, 46−51.
(594) Bruzewicz, D. A.; Reches, M.; Whitesides, G. M. Low-Cost Printing of Poly(Dimethylsiloxane) Barriers To Define Microchannels in Paper. *Anal. Chem.* **2008**, *80* (9), 3387−3392.
(595) Ge, S.; Zhang, L.; Zhang, Y.; Liu, H.; Huang, J.; Yan, M.; Yu, J. Electrochemical K-562 Cells Sensor Based on Origami Paper Device for Point-of-Care Testing. *Talanta* **2015**, *145*, 12−19.
(596) Xi, H.; Juhas, M.; Zhang, Y. G-Quadruplex Based Biosensor: A Potential Tool for SARS-CoV-2 Detection. *Biosens Bioelectron* **2020**, *167*, 112494.
(597) Cui, F.; Zhou, H. S. Diagnostic Methods and Potential Portable Biosensors for Coronavirus Disease 2019. *Biosens Bioelectron* **2020**, *165*, 112349.
(598) Wang, S.; Hossain, M. Z.; Shinozuka, K.; Shimizu, N.; Kitada, S.; Suzuki, T.; Ichige, R.; Kuwana, A.; Kobayashi, H. Graphene Field-Effect Transistor Biosensor for Detection of Biotin with Ultrahigh Sensitivity and Specificity. *Biosens Bioelectron* **2020**, *165*, 112363.
(599) Janett, E.; Diep, K.-L.; Fromm, K. M.; Bochet, C. G. A Simple Reaction for DNA Sensing and Chemical Delivery. *ACS Sens* **2020**, *5* (8), 2338−2343.
(600) Banerjee, S.; McCracken, S.; Hossain, M. F.; Slaughter, G. Electrochemical Detection of Neurotransmitters. *Biosensors (Basel)* **2020**, *10* (8), 101.
(601) Heredia, F. L.; Resto, P. J.; Parés-Matos, E. I. Fast Adhesion of Gold Nanoparticles (AuNPs) to a Surface Using Starch Hydrogels for Characterization of Biomolecules in Biosensor Applications. *Biosensors (Basel)* **2020**, *10* (8), 99.
(602) Özbek, O.; Isildak, Ö.; Isildak, I. A Potentiometric Biosensor for the Determination of Valproic Acid: Human Blood-Based Study of an Anti-Epileptic Drug. *Biochem Eng J* **2021**, *176*, 108181.
(603) Shanthi, R.; Chitra Devi, M.; Abukhaled, M.; Lyons, M. E. G.; Rajendran, L. Mathematical Modeling of PH-Based Potentiometric Biosensor Using Akbari-Ganji Method. *Int J Electrochem Sci* **2022**, *17* (3), 220349.
(604) Öndes, B.; Akpınar, F.; Uygun, M.; Muti, M.; AktasUygun, D. High Stability Potentiometric Urea Biosensor Based on Enzyme Attached Nanoparticles. *Microchemical Journal* **2021**, *160*, 105667.
(605) Ribeiro, S. C.; Fernandes, R.; Moreira, F. T. C.; Sales, M. G. F. Potentiometric Biosensor Based on Artificial Antibodies for an Alzheimer Biomarker Detection. *Applied Sciences* **2022**, *12* (7), 3625.
(606) Bouri, M.; Zuaznabar-Gardona, J. C.; Novell, M.; Blondeau, P.; Andrade, F. J. Paper-Based Potentiometric Biosensor for Monitoring Galactose in Whole Blood. *Electroanalysis* **2021**, *33* (1), 81−89.
(607) Lyudmyla, S.; Olena, Z.; Valentyna, A.; Sergiy, D. Potentiometric Enzyme Biosensor Modified with Gold Nanoparticles. *Appl Nanosci* **2023**, *13* (7), 5133−5138.
(608) Khalifa, M. E.; Ali, T. A.; Abdallah, A. B. Molecularly Imprinted Polymer Based GCE for Ultra-Sensitive Voltammetric and Potentiometric Bio Sensing of Topiramate. *Anal. Sci.* **2021**, *37* (7), 955−962.
(609) Soldatkin, O. O.; Soldatkina, O. V; Piliponskiy, I. I.; Rieznichenko, L. S.; Gruzina, T. G.; Dybkova, S. M.; Dzyadevych, S. V; Soldatkin, A. P. Application of Gold Nanoparticles for Improvement of Analytical Characteristics of Conductometric Enzyme Biosensors. *Appl Nanosci* **2022**, *12* (4), 995−1003.
(610) Berketa, K.; Saiapina, O.; Fayura, L.; Sibirny, A.; Dzyadevych, S.; Soldatkin, O. Novel Highly Sensitive Conductometric Biosensor Based on Arginine Deiminase from Mycoplasma Hominis for Determination of Arginine. *Sens Actuators B Chem* **2022**, *367*, 132023.
(611) Zouaoui, F.; Zine, N.; Errachid, A.; Jaffrezic-Renault, N. Mathematical Model and Numerical Simulation of Conductometric Biosensor of Urea. *Electroanalysis* **2022**, *34* (7), 1131−1140.
(612) Perera, G. S.; Rahman, Md. A.; Blazevski, A.; Wood, A.; Walia, S.; Bhaskaran, M.; Sriram, S. Rapid Conductometric Detection of SARS-CoV-2 Proteins and Its Variants Using Molecularly Imprinted Polymer Nanoparticles. *Adv Mater Technol* **2023**, *8* (3), 2200965.
(613) Razmshoar, P.; Besbes, F.; Madaci, A.; Mlika, R.; Bahrami, S. H.; Rabiee, M.; Martin, M.; Errachid, A.; Jaffrezic-Renault, N. A Conductometric Enzymatic Methanol Sensor Based on Polystyrene - PAMAM Dendritic Polymer Electrospun Nanofibers. *Talanta* **2023**, *260*, 124630.
(614) Liu, Y.; Yue, W.; Cui, Y. Development of an Amperometric Biosensor on a Toothbrush for Glucose. *Sensors and Actuators Reports* **2023**, *5*, 100133.
(615) Tvorynska, S.; Barek, J.; Josypcuk, B. High-Performance Amperometric Biosensor for Flow Injection Analysis Consisting of a Replaceable Lactate Oxidase-Based Mini-Reactor and a Silver Amalgam Screen-Printed Electrode. *Electrochim. Acta* **2023**, *445*, 142033.
(616) Cembalo, G.; Ciriello, R.; Tesoro, C.; Guerrieri, A.; Bianco, G.; Lelario, F.; Acquavia, M. A.; Di Capua, A. An Amperometric Biosensor

Based on a Bilayer of Electrodeposited Graphene Oxide and Co-Crosslinked Tyrosinase for L-Dopa Detection in Untreated Human Plasma. *Molecules* **2023**, *28* (13), 5239.
(617) Jalalvand, A. R. A Novel Amperometric Biosensor for Multi-Enzymatic Biosensing of Triglycerides. *Sensors International* **2023**, *4*, 100206.
(618) Pedersen, T.; Fojan, P.; Pedersen, A. K. N.; Magnusson, N. E.; Gurevich, L. Amperometric Biosensor for Quantitative Measurement Using Sandwich Immunoassays. *Biosensors (Basel)* **2023**, *13* (5), 519.
(619) Wang, W.; He, Y.; Deng, L.; Wang, H.; Liu, X.; Gui, Q.; Cao, Z.; Feng, Z.; Xiong, B.; Yin, Y. Peptide Aptamer-Based Polyaniline-Modified Amperometric Biosensor for L-Lysine Detection in Real Serum Samples. *Measurement* **2023**, *221*, 113468.
(620) Paziewska-Nowak, A.; Urbanowicz, M.; Pijanowska, D. G. Label-Free Impedimetric Biosensor Based on a Novel DNA-Type Receptor for Selective Determination of Lactoferrin in Human Saliva. *Sens Actuators B Chem* **2024**, *405*, 135377.
(621) Selimoglu, F.; Gür, B.; Ayhan, M. E.; Gür, F.; Kalita, G.; Tanemura, M.; Alma, M. H. Silver Nanoparticle Doped Graphene-Based Impedimetric Biosensor towards Sensitive Detection of Procalcitonin. *Mater. Chem. Phys.* **2023**, *297*, 127339.
(622) Tang, J.; Qin, J.; Li, J.; Liu, L.; Zeng, H. Cu2+@NMOFs-to-Bimetallic CuFe PBA Transformation: An Instant Catalyst with Oxidase-Mimicking Activity for Highly Sensitive Impedimetric Biosensor. *Biosens Bioelectron* **2023**, *222*, 114961.
(623) Calabrese, A.; Battistoni, P.; Ceylan, S.; Zeni, L.; Capo, A.; Varriale, A.; D'Auria, S.; Staiano, M. An Impedimetric Biosensor for Detection of Volatile Organic Compounds in Food. *Biosensors (Basel)* **2023**, *13* (3), 341.
(624) Su, X.; Liu, X.; Xie, Y.; Chen, M.; Zhong, H.; Li, M. Quantitative Label-Free SERS Detection of Trace Fentanyl in Biofluids with a Freestanding Hydrophobic Plasmonic Paper Biosensor. *Anal. Chem.* **2023**, *95* (7), 3821−3829.
(625) Fiore, L.; Mazzaracchio, V.; Serani, A.; Fabiani, G.; Fabiani, L.; Volpe, G.; Moscone, D.; Bianco, G. M.; Occhiuzzi, C.; Marrocco, G.; Arduini, F. Microfluidic Paper-Based Wearable Electrochemical Biosensor for Reliable Cortisol Detection in Sweat. *Sens Actuators B Chem* **2023**, *379*, 133258.
(626) Verma, G.; Singhal, S.; Rai, P. K.; Gupta, A. A Simple Approach to Develop a Paper-Based Biosensor for Real-Time Uric Acid Detection. *Anal. Methods* **2023**, *15* (24), 2955−2963.
(627) Cheng, J.; Fu, Y.; Guo, J.; Guo, J. A Low-Cost Paper-Based Blood Urea Nitrogen Optical Biosensor for Renal Surveillance in Fingertip Blood. *Sens Actuators B Chem* **2023**, *387*, 133795.
(628) Pornprom, T.; Phusi, N.; Thongdee, P.; Pakamwong, B.; Sangswan, J.; Kamsri, P.; Punkvang, A.; Suttisintong, K.; Leanpolchareanchai, J.; Hongmanee, P.; Lumjiaktase, P.; Jampasa, S.; Chailapakul, O.; Pungpo, P. Toward the Early Diagnosis of Tuberculosis: A Gold Particle-Decorated Graphene-Modified Paper-Based Electrochemical Biosensor for Hsp16.3 Detection. *Talanta* **2024**, *267*, 125210.
(629) Feng, Q.; Wang, C.; Miao, X.; Wu, M. A Novel Paper-Based Electrochemiluminescence Biosensor for Non-Destructive Detection of Pathogenic Bacteria in Real Samples. *Talanta* **2024**, *267*, 125224.
(630) Khorshed, A. A.; Savchenko, O.; Liu, J.; Shoute, L.; Zeng, J.; Ren, S.; Gu, J.; Jha, N.; Yang, Z.; Wang, J.; Jin, L.; Chen, J. Development of an Impedance-Based Biosensor for Determination of IgG Galactosylation Levels. *Biosens Bioelectron* **2024**, *245*, 115793.
(631) Sadak, O.; Sadak, F.; Yildirim, O.; Iverson, N. M.; Qureshi, R.; Talo, M.; Ooi, C. P.; Acharya, U. R.; Gunasekaran, S.; Alam, T. Electrochemical Biosensing and Deep Learning-Based Approaches in the Diagnosis of COVID-19: A Review. *IEEE Access* **2022**, *10*, 98633−98648.
(632) Lombardo, F.; Pittino, F.; Goldoni, D.; Selmi, L. Machine Learning and Data Augmentation Methods for Multispectral Capacitance Images of Nanoparticles with Nanoelectrodes Array Biosensors. *Eng Appl Artif Intell* **2024**, *127*, 107246.
(633) Zhou, Z.; Tian, D.; Yang, Y.; Cui, H.; Li, Y.; Ren, S.; Han, T.; Gao, Z. Machine Learning Assisted Biosensing Technology: An Emerging Powerful Tool for Improving the Intelligence of Food Safety Detection. *Curr Res Food Sci* **2024**, *8*, 100679.
(634) Ahmed Taha, B.; Al-Jubouri, Q.; Chahal, S.; Al Mashhadany, Y.; Rustagi, S.; Chaudhary, V.; Arsad, N. State-of-the-Art Telemodule-Enabled Intelligent Optical Nano-Biosensors for Proficient SARS-CoV-2 Monitoring. *Microchemical Journal* **2024**, *197*, 109774.
(635) Singh, B. Biosensors in Intelligent Healthcare and Integration of Internet of Medical Things (IoMT) for Treatment and Diagnosis. *Indian Journal of Health and Medical Law* **2024**, *7* (1), 1−7.
(636) Alam, Md. M.; Alam, Md. M.; Mirza, H.; Sultana, N.; Sultana, N.; Pasha, A. A.; Khan, A. I.; Zafar, A.; Ahmad, M. T. A Novel COVID-19 Diagnostic System Using Biosensor Incorporated Artificial Intelligence Technique. *Diagnostics* **2023**, *13* (11), 1886.
(637) Lazaro, A.; Villarino, R.; Lazaro, M.; Canellas, N.; Prieto-Simon, B.; Girbau, D. Recent Advances in Batteryless NFC Sensors for Chemical Sensing and Biosensing. *Biosensors (Basel)* **2023**, *13* (8), 775.
(638) Kim, J.; Imani, S.; de Araujo, W. R.; Warchall, J.; Valdés-Ramírez, G.; Paixão, T. R. L. C.; Mercier, P. P.; Wang, J. Wearable Salivary Uric Acid Mouthguard Biosensor with Integrated Wireless Electronics. *Biosens Bioelectron* **2015**, *74*, 1061−1068.

https://doi.org/10.1021/acsomega.4c07991
ACS Omega 2024, 9, 48918−48987